

**COASTAL HYPOXIA ON THE TEXAS SHELF: AN OCEAN OBSERVING AND  
MANAGEMENT APPROACH TO IMPROVING GULF OF MEXICO HYPOXIA  
MONITORING**

A Dissertation

by

RUTH LOUISE MULLINS

Submitted to the Office of Graduate Studies of  
Texas A&M University  
in partial fulfillment of the requirements for the degree of

DOCTOR OF PHILOSOPHY

Approved by:

Chair of Committee,	Steven F. DiMarco
Committee Members,	Piers Chapman
	Norman Guinasso Jr.
	Robert Stickney
	Anthony Filippi
Head of Department,	Piers Chapman

May 2013

Major Subject: Oceanography

Copyright 2013 Ruth Louise Mullins

## ABSTRACT

A combination of *in situ* sampling and real-time ocean observations was used to investigate the processes responsible for the formation and the areal extent of Texas coastal hypoxia from 2002 to 2011. *In situ* sampling, real-time mooring and buoy observations, and multivariate statistical modeling were used to investigate the physical processes driving hypoxia formation. Geostatistical interpolation (ordinary kriging) models were tested to compare the differences in annual hypoxia area on the Texas shelf. Results from these two sections were integrated into recommendations for improving federal hypoxia monitoring and mitigation strategies in the northwestern Gulf of Mexico.

Winds, currents, temperature, salinity, and dissolved oxygen records revealed the annual, seasonal, and daily variability of hypoxia formation on the Texas coast from 2009 to 2011. Hypoxic events occurred from late May to late October lasting from hours to weeks. Hypoxia formation was either the result of salinity stratification, associated with the freshening of surface waters by the advection of Mississippi-Atchafalaya River freshwater westward or the wind- and current-driven upcoast or downcoast flow of Brazos River discharge. Records from 2010 and 2011 showed the variability and frequency of stratification development differs on the north and south Texas shelf. Multivariate linear model results showed contributing factors on the north Texas shelf vary annually and that primary factors for hypoxia development are near-surface current speeds and salinity-driven stratification.

Interpolation models resulted in three size categories for hypoxia area: small ( $100 - 1,000 \text{ km}^2$ ), moderate ( $1,001 - 3,000 \text{ km}^2$ ), and large ( $3,001+ \text{ km}^2$ ). Moderate years include 2002, 2004, and 2007 and a large year was 2008. There was no increase in hypoxic area from years 2002 to 2011, but years 2007 and 2008 resulted in a hypoxic area over  $5,000 \text{ km}^2$ , which is the federally mandated hypoxia reduction target for the northwestern Gulf of Mexico. Geostatistical interpolators represent and predict the structure and spatial extent of the hypoxic area on the Texas shelf by accounting for the anisotropy of physical processes on the Texas shelf. Geostatistical interpolation models are preferred to deterministic models for developing and improving federal hypoxia monitoring and mitigation strategies on the northwestern Gulf of Mexico shelf.

## **DEDICATION**

I would like to dedicate the completion of this work to my family and friends. I would like to especially thank my mother, Louise, my father, Wayman, and my sister, Rachael, for their love, guidance, and support. I would especially like to thank my husband, Houston, for his love, encouragement, and support during the course of this work. Thank you all.

## **ACKNOWLEDGEMENTS**

I would like to thank my committee chair, Dr. Steven DiMarco, and my committee members, Dr. Piers Chapman, Dr. Robert Stickney, Dr. Anthony Filippi, and Dr. Norman Guinasso, for their guidance and support throughout the course of this research. I would like to especially thank Dr. DiMarco for his superb advising over the years, for helping me to find my passion for ocean observing, and for teaching me how to love data. I would also like to thank Dr. Chapman for going above and beyond his role as a committee member and for providing additional support and research guidance during this process. Next, I would like to thank Dr. Filippi for introducing me to GIS and for being an outstanding teacher during my graduate career. I would also like to thank Dr. Guinasso for his valuable comments and intriguing discussions about ocean observing. Finally, I would like to thank Dr. Stickney for helping me to understand the role of managers in oceanography and for his invaluable research and career insights.

I would also like to express my heartfelt thanks to my friends and colleagues and the department faculty and staff for making my time at Texas A&M University a great experience. I have had many colleagues who acted as both friends and mentors during my graduate education. To those colleagues and friends, I cannot thank them enough for their support, love, friendship, and motivation. I could not have done this without them.

I also want to extend my gratitude to Texas Sea Grant, which funded this research. The wonderful group of people at Texas Sea Grant has been a supportive network and a joy to work with during my time at Texas A&M University.

## NOMENCLATURE

ANOVA	Analysis of Variance
AOU	Apparent Oxygen Utilization
ArcGIS 9.3	Environmental Systems Research Institute Arc Geographical Information Systems 9.3
CDOM	Chromophoric Dissolved Organic Matter
CTD	Conductivity Temperature Depth Profiler
EPA	Environmental Protection Agency
FLSD	Fisher's Least Square Differences
LUMCON	Louisiana Universities Marine Consortium
MARS	Mississippi Atchafalaya River Systems
MCH	Texas A&M University Mechanisms Controlling Hypoxia
MCH MS	Texas A&M University Mechanisms Controlling Hypoxia Survey Cruises
MODIS	Moderate Resolution Imaging Spectoradiameter
NAAEAC	North America Albers Equal Area
NDBC	National Data Buoy Center
NOAA	National Oceanographic and Atmospheric Administration
NSF	National Science Foundation
PEER	Texas A&M University Partnership for Environmental and Rural Health

PSU	Practical Salinity Unit
QA/QC	Quality Assurance and Quality Control
RDCP	Recording Doppler Current Profiler
RMS	Root Mean Square
RMPSE	Root Mean Predicted Square Error
RMSE	Root Mean Square Error
SAB	Science Advisory Board
SeaWiFS	Sea-viewing Wide Field-of-view Sensor
SFA	Stephen F. Austin Middle School
SRMSE	Standardized Root Mean Square Error
SSI	Salinity Stratification Index
SEAMAP	NOAA National Marine Fisheries Service Southeast Area Monitoring Assessment Program
TABS	Texas Automated Buoy System
TAMU	Texas A&M University
TEKS	Texas Essential Knowledge and Skills
TPWD	Texas Parks and Wildlife Department
TSI	Temperature Salinity Index
USGS	United States Geological Survey
WF	TAMU Wind Farm Mooring

## TABLE OF CONTENTS

	Page
ABSTRACT .....	ii
DEDICATION .....	iv
ACKNOWLEDGEMENTS .....	v
NOMENCLATURE .....	vi
TABLE OF CONTENTS .....	viii
LIST OF FIGURES .....	x
LIST OF TABLES .....	xiii
1. INTRODUCTION .....	1
1.1 Overview of Coastal Hypoxia .....	1
1.2 Characterizing Gulf of Mexico Hypoxia.....	4
1.3 Hypoxia on the Texas Shelf: A Summary of the Texas Shelf and Potential Physical Factors Driving Hypoxia Formation.....	8
1.4 Study Motivation.....	13
1.5 Organization .....	14
2. INVESTIGATING THE PHYSICAL PROCESSES RESPONSIBLE FOR HYPOXIA FORMATION ON THE TEXAS SHELF .....	17
2.1 Introduction and Organization .....	17
2.2 Data and Methods for Examining Physical Processes Controlling Texas Hypoxia .....	18
2.3 Hypotheses for Analyzing Mooring, Buoy, and Towfish Data .....	24
2.4 Results for Investigating Physical Processes Responsible for Hypoxia Formation on the Texas Shelf .....	29
2.5 Results for Hypotheses A – D .....	38
2.6 Summary and Future Directions.....	47
3. DETERMINING HYPOXIA AREA ON THE TEXAS SHELF.....	53

3.1 Introduction .....	53
3.2 Data and Methods for Determining Texas Hypoxia Area .....	53
3.3 Geostatistical Interpolation Methods .....	56
3.4 Ordinary Kriging Interpolation Outputs and Model Assessment .....	69
3.5 Ordinary Kriging Model Results .....	73
3.6 Surface Results of Ordinary Kriging Models .....	75
3.7 Comparisons of Ordinary Kriging Model Parameters ( <i>Data, Spatial, Lag</i> ) .....	81
3.8 Comparisons of Ordinary Kriging Model Assessments .....	86
3.9 Ordinary Kriging Model Discussions and Future Research Directions .....	90
 4. POLICY AND MANAGEMENT CONSIDERATIONS FOR MONITORING	
TEXAS SHELF HYPOXIA .....	95
4.1 Introduction and Motivation .....	95
4.2 The Development of Management Strategies for Gulf of Mexico Hypoxia .....	97
4.3 Texas Hypoxic Area Contributions to the Gulf of Mexico Shelf .....	101
4.4 Management of Hypoxic Area Discussion .....	103
 5. CONCLUSIONS AND FUTURE RESEARCH DIRECTIONS .....	109
5.1 Conclusions .....	109
5.2 Future Research Directions .....	111
 REFERENCES .....	114
 APPENDIX A .....	124
 APPENDIX B .....	147
 APPENDIX C .....	205
 APPENDIX D .....	235
 APPENDIX E .....	267

## LIST OF FIGURES

FIGURE	Page
1.1 Map of the Northwestern Gulf of Mexico .....	148
1.2 Map of Two Historic Hypoxic Regions in the Northwestern Gulf of Mexico	149
1.3 Brazos River Discharge Hydrograph .....	150
2.1 Ocean Observing Platforms and Acrobat Transects on the Texas Shelf .....	151
2.2 TAMU MACH MS Cruise Plans for MS2, MS3, and MS4 .....	152
2.3 Brazos River Daily Mean Discharge from 2009 to 2011 .....	155
2.4 2009 Low-pass (3-h) Filtered Wind Speeds from NDBC 42035 and TABS B Buoys .....	156
2.5 2010 Low-pass (3-h) Filtered Wind Speeds from NDBC 42035 and TABS B Buoys .....	157
2.6 2011 Low-pass (3-h) Filtered Wind Speeds from NDBC 42035 and TABS B Buoys .....	158
2.7 2009 Low-pass (40-h) Current Velocities from the TAMU WF RDCP .....	159
2.8 2010 Low-pass (40-h) Current Velocities from the TAMU WF RDCP .....	160
2.9 2011 Low-pass (40-h) Current Velocities from the TAMU WF RDCP .....	162
2.10 2009 TAMU WF Array Raw Salinity (PSU) Data.....	164
2.11 2009 TAMU WF Array Temperature (°C) Profile .....	165
2.12 2009 TAMU WF Array SSI and TSI Profiles .....	166
2.13 2009 TAMU WF Array and RDCP Raw Dissolved Oxygen Profiles .....	167
2.14 2010 TAMU WF Array and RDCP Raw Dissolved Oxygen Profiles .....	168
2.15 2011 TAMU WF Array and RDCP Dissolved Oxygen Profile .....	169

2.16	2009 Brazos River, NDBC 42035 Winds, TAMU WF Array and RDCP Daily-averaged Profiles .....	170
2.17	2009 TAMU WF Mid-Depth Daily-Averaged Density, Brunt-Väisälä, and Bottom Dissolved Oxygen Profiles .....	172
2.18	Histograms of Hypoxic Events Observed at the TAMU WF RDCP from 2009 to 2011 .....	173
2.19	TAMU MCH MS Bottom Dissolved Oxygen Concentrations Versus Brunt- Väisälä Frequencies .....	174
2.20	TAMU MCH MS2 North and South Texas Bottom Dissolved Oxygen Concentrations Versus Brunt-Väisälä Frequencies .....	176
2.21	TAMU MCH MS2, MS3, and MS4 Survey Bottom AOU Versus Maximum Brunt-Väisälä Frequencies for North Texas CTD Stations .....	178
2.22	TAMU MCH MS2, MS3, and MS4 Survey Bottom AOU Versus Maximum Brunt-Väisälä Frequencies for South Texas CTD Stations .....	179
2.23	TAMU MCH Selected MS2 CTD Brunt-Väisälä Frequencies and Dissolved Oxygen Water-column Profiles .....	180
2.24	TAMU MCH MS2 Acrobat Towfish Salinity and Dissolved Oxygen Transects .....	183
2.25	TAMU MCH MS4 Acrobat Towfish Salinity and Dissolved Oxygen Transects .....	186
3.1	2002 – 2011 Search Direction Standard Deviation Ellipses .....	189
3.2	2007 Cluster Voronoi Maps .....	190
3.3	2008 Standard Deviation Voronoi Maps .....	191
3.4	2002 SEAMAP ALL Spatial Trend Diagram .....	192
3.5	Ordinary Kriging Parameter <i>Year</i> Box Plots .....	194
3.6	2002 Ordinary Kriging G TX A Adj Map Results .....	195
3.7	2004 Ordinary Kriging G TX A Adj Map Results .....	196

3.8	2007 Ordinary Kriging G TX A Adj Map Results .....	197
3.9	2008 Ordinary Kriging G TX A Adj Map Results .....	198
3.10	2007 Ordinary Kriging G TX I Map Results .....	199
3.11	2007 Ordinary Kriging G TX A Map Results .....	200
3.12	2007 Ordinary Kriging G ALL I Map Results .....	201
3.13	2007 Ordinary Kriging G ALL A Map Results .....	202
3.14	Ordinary Kriging Parameter Comparative Matrices .....	203
3.15	2002, 2007, and 2008 Normalized Gaussian Model Mean Hypoxic Areas Estimates .....	204

## LIST OF TABLES

TABLE	Page
2.1 TAMU WF Operation Dates and Instruments .....	125
2.2 Cruise Dates for TAMU MCH MS Summer Surveys .....	126
2.3 Physical Data Groups and Variable Names, Sources, and Abbreviations ...	127
2.4 Correlation Coefficients and Covariance for Daily Averaged NDBC 42035 and TABS B Buoy Wind Parameters .....	129
2.5 2009 – 2011 Hypoxic Events Recorded by the TAMU WF RDCP .....	130
2.6 2009 10-Term Multivariate Linear Model Determined From Subset Multivariate Linear Models .....	131
2.7 5-Term Multivariate Linear Model for TAMU WF Data in 2009 .....	132
2.8 2009 TAMU WF Multivariate Model Criteria Assessment Results .....	133
2.9 2011 10-Term Multivariate Linear Model Determined From Subset Multivariate Linear Models .....	134
2.10 2011 TAMU WF Multivariate Model Criteria Assessment Results .....	135
2.11 TAMU MCH MS Survey Linear Model Results for Bottom Dissolved Oxygen Versus Maximum Brunt-Väisälä Frequencies .....	136
3.1 NOAA SEAMAP Gulf Hypoxia Watch Summer Survey Dates .....	137
3.2 ESRI ArcGIS Base Map Layers for Area Interpolation Analyses .....	138
3.3 2002 – 2011 Direction Statistics for NOAA SEAMAP Survey Data .....	139
3.4 Ordinary Kriging Models and Abbreviations .....	140
3.5 2002 – 2011 Ordinary Kriging Model Hypoxic Area Estimates .....	141
3.6 One-way ANOVA Results for Ordinary Kriging Parameters .....	142

3.7	One-way ANOVA Results for Ordinary Kriging Standardized RMSE by Parameters .....	143
3.8	Non-parametric Mean Rank Scores for 2002, 2007, and 2008 .....	144
4.1	Comparison of Ordinary Kriging Model Results to the EPA 2008 Action Plan Hypoxia Area Reduction Goal .....	145
4.2	Comparisons of Kriging Parameter <i>Model</i> to EPA 2008 Action Plan Hypoxic Area Reduction Goal .....	146

# **1. INTRODUCTION**

## **1.1 Overview of Coastal Hypoxia**

Hypoxia, a condition of low dissolved oxygen concentrations in bottom waters of the coastal ocean, is a global environmental hazard. According to Diaz (2001), in many coastal waters of the world, hypoxic regions are persistent and occur year-round, whereas other regions may only experience seasonal or short-term (hours to days) hypoxia. Commonly defined as dissolved oxygen concentrations of 1.4 ml/L or below (equivalent to 2.0 mg/L), hypoxia is increasing in global severity and frequency due to anthropogenic inputs of nutrients onto coastal ocean shelves (Diaz and Rosenberg 1995; Diaz and Rosenberg 2008; Rabalais et al. 2001a). Hypoxia results from a combination of multiple biological and physical factors, including anthropogenic sources (e.g. agriculture runoff and pollution), oceanic conditions (e.g. stratified or mixed waters, currents, and upwelling), and weather (e.g. winds, frontal passages, and temperature) (Diaz 2001; Rabalais et al. 2002; Bianchi et al. 2010).

Hypoxia can lead to detrimental effects on marine organisms by threatening coastal ecosystems and local benthic and demersal fisheries (Levin et al. 2009). Impacts on the ecosystem can also lead to negative consequences for local economies that rely on commercial and recreational fisheries (Boesch 2002; Thronson and Quigg 2008, McInnes and Quigg 2011). Many studies document negative effects of hypoxia on ecosystems world-wide, including mortality, stressed benthic communities, decreases

in abundance and diversity, and changes in species feeding and reproductive behaviors (Baden et al. 1990; Boesch and Rabalais 1991; Diaz and Rosenberg 1995; Rabalais and Turner 2001; Rabalais et al. 2002; Thomas and Rahman 2011; Thronson and Quigg 2008). In the Gulf of Mexico, the formation of hypoxia can significantly reduce the population of macrobenthos (Gatson 1985). Declines in species abundances have been noted during times when water conditions changed from oxygenated to hypoxic from spring to summer on the Louisiana and Texas coasts (Rabalais et al. 2001a; Harper et al. 1981).

Many of the world's hypoxic regions, natural or anthropogenic, are formed by a combination of biological and physical drivers, which create unique, often identifiable, seasonal and temporal regional characteristics (Diaz 2001). Hypoxic regions commonly occur in enclosed basins, such as the Black (Karlson et al. 2002) and Baltic Seas (Conley et al. 2009a), or in river-dominated coastal systems, including, but not limited to, the Yangtze (Chung-Chi et al. 2007), Chesapeake Bay (Breitburg 2002), and Mississippi – Atchafalaya River (MARS; Rabalais et al. 2001b; Bianchi et al. 2010) regions.

Natural hypoxic regions occur in upwelling waters. Upwelling moves nutrients from bottom waters up to the surface stimulating phytoplankton growth or blooms. As the blooms die and sink, the addition of organic material to the mid- or bottom waters stimulates microbial degradation resulting in a depletion of dissolved oxygen. If these processes occur in regions of slow moving currents, an oxygen minimum zone (OMZ) forms. OMZs primarily occur at depths of 200 – 1000 m and are found in the eastern boundaries of the Pacific and Atlantic Oceans and the northern Indian Ocean. Coastal

hypoxic regions can also form in regions of coastal upwelling, which provide a regenerated nutrient source to support enhanced primary production on the shelf (Walker and Rabalais 2006, Diaz and Rosenberg 2008; Rabalais et al. 2010).

Anthropogenic hypoxic regions commonly occur in waters near high population densities and rivers. Hypoxia in these regions is generally attributed to increased addition of nutrients resulting from the expansion of agriculture and industry and urbanization (Conley et al. 2009b). Nutrient enrichment resulting in elevated primary production is referred to as eutrophication and anthropogenic hypoxic regions may also be identified as eutrophication-induced hypoxic regions (Gooday et al. 2009). Anthropogenic, or eutrophication-induced, regions are found in waters as shallow as 1 – 2 m (estuaries) to as deep as 600 – 700 m in coastal waters (Diaz and Rosenberg 1995; Diaz 2001). These regions can also be referred to as river-dominated regions, as rivers are the primary source for nutrient additions to the coastal waters (Bianchi et al. 2010).

In river-dominated and seasonally stratified hypoxic systems, eutrophication and stratification are the primary driving factors (Rabalais et al. 2001b; 2002a; Kemp et al. 2009; Bianchi et al. 2010). Coastal river-dominated systems are continuously recharged with nutrients from river discharge. Nutrient additions contribute to increased primary production and the increased production in turn increases the organic matter available for microbial degradation (Bianchi et al. 2010). In turn, microbial respiration consumes oxygen, leading to eutrophication-driven hypoxia in coastal bottom waters.

Stratification is another direct effect within a river-dominated system. Freshwater discharge creates buoyancy-driven stratification in the upper water-column

and inhibits water-column mixing and the transfer of atmospheric dissolved oxygen to bottom layers (Kemp et al. 2009).

Natural and anthropogenic hypoxic regions form in the northwestern Gulf of Mexico (Figure 1.1). The second largest anthropogenic and river-dominated region in the world is commonly found starting from the Mississippi River Bird's Foot delta in the east extending to the Texas-Louisiana border in the west (Rabalais et al. 2001b; Diaz 2001). This hypoxia is hereafter referred to as Louisiana coastal hypoxia. Additional natural and anthropogenic regions have also been recorded in Texas coastal waters (Figure 1.1). These Texas hypoxic regions, including their locations, frequencies of occurrence, and the processes responsible for their formation, are the principal subjects of this dissertation.

## **1.2 Characterizing Gulf of Mexico Hypoxia**

### *1.2.1 Historical Gulf of Mexico Hypoxia*

Coastal hypoxia occurs throughout the northwestern Gulf of Mexico, and has been documented since the 1970s and extensively monitored since 1985. Several federal and state agencies and academic institutions routinely monitor northwestern Gulf of Mexico hypoxia ([www.gulfhypoxia.net](http://www.gulfhypoxia.net)). This summer-seasonal hypoxic region is a highly publicized one of interest to governmental coastal hazard management and mitigation strategists, as this coast is not only susceptible to hypoxia, but also harmful algal blooms, invasive species, hurricanes, and oil spills. The ability to predict coastal

hazards is a high priority for U.S. government agencies, such as the National Oceanographic and Atmospheric Administration (NOAA) and the Environmental Protection Agency (EPA).

Northern Gulf of Mexico hypoxia has been monitored and mapped to determine its areal extent each summer (Figure 1.1). Surveys start west of the Mississippi River delta at Southwest Pass and extend to the northern Texas-Louisiana border. Hypoxia can be found after late February and can last through early October with largest areas occurring from May to early September (Rabalais et al. 2001b). Hypoxia is most severe, continuous, and widely distributed during June to August (Rabalais et al. 2001b). Results of surveys in late July (Rabalais et al. 2001b) show year-to-year spatial variability of Louisiana coastal hypoxia. More importantly, these surveys show this region extending onto the Texas shelf in some years (<http://www.gulfhypoxia.net/>), suggesting a westward extension of Louisiana coastal hypoxia. The surveys are used to calculate a shelf area estimate published in August, which is used as the official metric to guide policy and management efforts to monitor Gulf of Mexico hypoxia and track the progress of reduction efforts.

### *1.2.2 Overview of Processes Controlling Louisiana Coastal Hypoxia*

Gulf of Mexico hypoxia can occur in waters up to 60 m deep, but is commonly only found between depths of 5 - 30 m in the Gulf of Mexico (Rabalais et al. 2001b). Hypoxia in the northern Gulf of Mexico is controlled primarily by the input of freshwater, nutrients, and winds. The Louisiana coastal zone is classified as a seasonally

stratified region under severe hypoxic stress (Kemp et al. 2009; Diaz 2001; Rabalais et al. 2002). In Louisiana coastal waters, the MARS system is the anthropogenic riverine point source for nitrogen and phosphorus (Bianchi et al. 2010). Non-point source Mississippi organic material can also be added from wetlands (Rabalais et al. 2002; 2007; D'Sa and DiMarco 2009; Bianchi et al. 2012). The MARS freshwater discharge is responsible for strong seasonal stratification (Rabalais et al. 2001b; Hetland and DiMarco 2008) as the Mississippi and Atchafalaya Rivers drain 40 % of the contiguous United States watershed (Millman and Meade 1983).

In addition to nutrient inputs and stratification, the physical environment of the Texas-Louisiana shelf favors the formation of a large hypoxic region. The increased insolation and heating during the summer can result in the establishment of a strong pycnocline (Nowlin et al. 1998) and strengthened stratification (Kemp et al. 2009). Winds in the northern Gulf of Mexico exhibit a strong seasonal pattern in which wind is strong and downwelling favorable (from east to west) from September to May. In the summer (June – August), wind speed decreases and shifts to upwelling favorable (from west to east; Cochrane and Kelly 1986; Cho et al. 1998; Nowlin et al. 1998, 2005). The MARS freshwater flux intensifies stratification during weak and upwelling-favorable wind conditions (Hetland and DiMarco 2008; Bianchi et al. 2010). Diurnal wind forcing results in a near-resonant response of surface coastal currents to the wind stress (Zhang et al. 2009, 2010). During the summer, coastal waters flow northward and eastward (upcoast) on the Texas-Louisiana shelf. Flow reverses in the non-summer months with

water moving westward and southward (downcoast) along the Texas and Louisiana shelves (Cho et al. 1998; Nowlin et al. 1998).

Nutrient and freshwater contributions, combined with summer patterns of reversed current flows on the shelf (upcoast to downcoast), maximum solar insolation, and weak or no major atmospheric fronts prime the Louisiana shelf for large-scale hypoxia formation (Bianchi et al. 2010). The resultant Louisiana coastal hypoxia can range from ~50 to 20,000+ km<sup>2</sup> each summer with its area increasing in the past 26 years (Rabalais et al. 2001b).

To address relative biological and physical contributions within this hypoxic region, Hetland and DiMarco (2008) introduced the terms: hypoxic potential and stratification envelope. These terms separate biological and physical drivers responsible for hypoxia formation. The hypoxic potential represents the amount of organic material available in the system for mineralization; the stratification envelope describes areas on the shelf where mixing and ventilation of the bottom water depths occurs. The hypoxic potential and stratification envelope will vary in time and space. From analysis of Texas-Louisiana hydrography, Li et al. (1996, 1997) determined the physical process scales to be order of 15 km in the cross-shelf and 35 km in the along-shelf directions.

### **1.3 Hypoxia on the Texas Shelf: A Summary of the Texas Shelf and Potential Physical Factors Driving Hypoxia Formation**

The Texas shelf is a potential coastal area for additional and independent hypoxic regions. Historical records document not only the extension of Louisiana coastal hypoxia westward, but also the formation of independent persistent and episodic hypoxic areas along the north and south Texas shelf. The physical environment of the Texas shelf, such as the shape of the coastline and hydrographic conditions, differs from that of the Louisiana shelf. Differences in physical environment can be responsible for the possible formation of independent hypoxic events recorded on the Texas shelf.

#### *1.3.1 Historical Texas Shelf Hypoxia*

In a global hypoxia overview, Diaz's (2001) identified moderately severe hypoxia outbreaks on the Texas coast, independent from either Louisiana or Texas bays. Paleoreconstruction using sediment foraminifera abundance confirmed hypoxic events had occurred across the Texas-Louisiana shelf as early as the 1900s (Osterman 2003). Isotopic analyses of benthic foraminifera collected on the Texas-Louisiana shelf identified two independent hypoxic regions (Osterman et al. 2009). The first region is on the Louisiana coast near the Mississippi delta and the second is on the mid-Texas shelf between Galveston and Matagorda Bay (Figure 1.2; Osterman 2003; Osterman et al. 2009). Strauss et al. (2012) conducted isotopic comparisons of benthic foraminifera and found hypoxia occurred at the Brazos River delta during the past 100 years.

Harper et al. (1981) documented the presence of low oxygen waters from June to August 1977 off the Galveston coast and measured the persistence of hypoxic waters on the surrounding benthic communities. Renaud (1986) investigated an event on the Texas shelf, independent from hypoxia formation on the Louisiana coast. Pokryfki and Randall (1987) published data on hypoxic events on the Texas-Louisiana shelf and attributed their development to winds and river discharge. These authors were unable to identify if the events were independent from Louisiana coastal hypoxia or attributed to Brazos River freshwater based on the sampling distance between sites. None of the studies identified the physical or biological processes responsible for the formation of the hypoxic events or regions.

### *1.3.2 Monitoring on the Texas Shelf*

Sampling programs conducted by federal and state agencies since 1985 have measured water quality and bottom dissolved oxygen concentrations year-round at numerous locations on the Texas shelf. Since 2002, the National Oceanographic and Atmospheric Administration National Marine Fisheries Service Southeast Area Monitoring Assessment Program (NOAA NMFS SEAMAP; hereafter referred to as SEAMAP) routinely conducts summer fishery surveys in the Gulf of Mexico. Though not specifically designed to map hypoxia, these surveys routinely measure dissolved oxygen. Data products published at the end of each summer include detailed interpolated near-bottom dissolved oxygen contour maps for the yearly area surveyed (<http://www.ncddc.noaa.gov/hypoxia/>). Surveys are predetermined using a randomized

design to cover a majority of the Texas and Louisiana coastlines, but spatial coverage varies year-to-year based on design, logistics, and weather (<http://www.ncddc.noaa.gov/hypoxia/>).

The Texas Parks and Wildlife Department (TPWD) has systematically collected data at five freshwater inputs along the Texas coast. Those data, collected from 1985 to 2008, measure hydrographic properties and dissolved oxygen to assess water quality from the Sabine River to the Rio Grande. According to those data, hypoxia can occur throughout the year at the five freshwater sources, but is more frequent in the summer (May – August; DiMarco unpublished data).

### *1.3.3 Potential Physical Processes Driving Texas Hypoxia Formation*

The MARS is the primary freshwater source driving the formation and duration of Louisiana coastal hypoxia (Bianchi et al. 2010; Forrest et al. 2011). MARS water can advect onto the Texas shelf. The Brazos River is the only major Texas river that directly flows out onto the northern Texas shelf. The Brazos drains a significantly smaller watershed (north and central Texas) compared to the Mississippi River watershed. The average discharge for the Brazos River since the 1960s is 237.5 cubic m per second compared to approximately 19,000 m<sup>3</sup>/s average for the Mississippi River (Figure 1.3, [tx.usgs.gov](http://tx.usgs.gov); Wiseman et al. 1997). The Brazos River accounts for less than 1 % to 10 % of the total discharge volume of the Mississippi River and introduces approximately 15,000 kg/y of total nitrogen to the coast compared to the approximately 1.5 million kg/y

introduced to the Louisiana coast from the MARS (Dunn 1996; Goolsby et al. 2001; Committee on Environment and Natural Resources 2003, 2010).

Despite lower flow volume than the MARS, the Brazos River watershed does provide enough freshwater to drive hypoxia formation on the northern Texas coast (DiMarco et al. 2012). Flow volumes can be influenced by annual runoff and short-term atmospheric events in central Texas, such as weather, drought, hurricanes, or seasonal storms. As the watershed fills, there is about a 3-week travel time from high rainfall events in central Texas to the coast (DiMarco and Hetland personal communication). The yearly rainfall variability can result in variable flow volumes and discharge onto the Texas shelf (Figure 1.3).

The yearly variability of hypoxia the shelf is also evident in the SEAMAP dissolved oxygen interpolated products ([ncddc.noaa.gov/hypoxia/](http://ncddc.noaa.gov/hypoxia/); Mullins et al. 2011a & 2011b; DiMarco et al. 2012). In 2007, central Texas experienced unusually heavy rainfall and flooding leading to coastal discharge exceeding historical values for June and July (Figure 1.2). Flooding across central Texas resulted in a peak river discharge of  $1,900 \text{ m}^3/\text{s}$ , which is the highest recorded volume since the 1960s and an order of magnitude larger than average discharge volume in July (DiMarco et al. 2012). The abundance of freshwater reaching the coast resulted in freshwater stratification of waters from Galveston south to Freeport (DiMarco et al. 2012). The flooding lasted approximately two months until the stratification dissipated owing to water-column mixing and reventilation of bottom waters as Hurricane Humberto moved over the north Texas shelf. DiMarco et al. (2012) showed that the hypoxia between Galveston and

Freeport was driven by the Brazos River. The analysis of oxygen isotopes in coastal waters allowed DiMarco et al. (2012) to delineate the sources of freshwater on the northwestern Gulf of Mexico shelf to confirm the freshwater driver was the Brazos River.

#### *1.3.4 Texas Shelf Circulation – Winds, Currents, and Upwelling*

Circulation on the Texas shelf is impacted by the change in bathymetry, seasonal winds, atmospheric events, tidal cycles, and river discharge in addition to seasonal northwestern Gulf of Mexico circulation. Nowlin et al. (2005) observed the strongest circulation to occur at the shelf bend due to conservation of mass in the flow as the shelf narrows. Bender et al. (2007) observed short term current reversals lasting days to weeks to occur at any time of the year. Vastano et al. (1995) noted that the central and south Texas coast experiences a different flow regime from the Louisiana coast, where in the summer, south Texas flow is northeast and interacts with the seasonal downcoast currents, causing an area of low to no velocity.

Independent surface currents also occur on the Texas shelf. Barron and Vastano (1994) and Walker (2005) noted an independent current occurring on the Texas shelf that does not occur on the Louisiana shelf - the Texas Current or Texas Jet. The Texas Current is a west-southwest current with velocities ranging from 19 - 59 cm/s on the inner Texas coast (Walker 2005). Walker (2005) showed that 25 % of ocean surface drifters were entrained into and moved offshore by the Texas Current at a recorded average velocity of 39 cm/s. Seasonal fluctuations in velocity can be due to riverine,

estuarine, oceanic, and atmospheric forcing (Barron and Vastano 1994) and can affect the movement of freshwater on the Texas shelf.

Primary production in the western Gulf of Mexico is attributed to coastal upwelling (Walker 2005; Walker and Rabalais 2006). Wind-driven upwelling can be an important physical process that supplies nutrients to surface waters, stimulating primary production in coastal waters in lieu of nutrient loading by river discharge (Rabalais et al. 2010). Walker (2005) showed upwelling to occur in Mexican and south Texas coastal waters during June and July. The upwelling was the result of strong southeasterly wind stress and upcoast currents, which moved cooler, nutrient-rich waters upcoast towards Matagorda Bay. The occurrence of such upwelling events on the Texas coast can potentially supply additional nutrients to the coastal waters and affect the formation of hypoxia.

#### **1.4 Study Motivation**

Coastal hypoxia can have significant implications on Gulf of Mexico marine ecosystems, fisheries, coastal economies, and public health and safety. Federal and regional managers do not currently consider the possibility or influence of independent hypoxic regions on the Texas shelf in monitoring strategies or mitigation efforts for the northwestern Gulf of Mexico despite historical and present-day evidence of hypoxia on the Texas shelf.

The physical environment and seasonal conditions differ on the Louisiana and Texas shelf. Though there is an annual upcoast and downcoast seasonal wind and circulation pattern for the northwestern Gulf of Mexico shelf, there are additional circulation features, such as the Texas Current, that can influence the direction freshwater travels on the Texas coast. Changes in circulation, and ultimately freshwater movement, affect the degree of stratification and formation of hypoxia on the Texas shelf.

This dissertation investigates the distribution of dissolved oxygen on the Texas shelf using historical observations, present-day ocean observing data, and remote sensing to understand:

1. The historical variability of Texas coastal hypoxia, and
2. The processes responsible for Texas coastal hypoxia.

In my dissertation, I also consider current management priorities for monitoring northwestern Gulf of Mexico hypoxia and describe how Texas hypoxia should be included in the mitigation and monitoring strategies for the northwestern Gulf of Mexico. Recommendations are proposed to improve current monitoring strategies and reduction plans implemented by NOAA and the EPA.

## **1.5 Organization**

The dissertation is organized into five sections. Section 1 provided the introduction of Gulf of Mexico and Texas hypoxia and the motivation for this research.

Section 2 results describe the physical environment on the Texas shelf from 2009 to 2011 addressing the following questions relative to physical processes responsible for hypoxia:

1. Does stratification lead to hypoxia formation on the Texas shelf?
2. Is the presence of stratification spatially and temporally uniform on the Texas shelf?
3. Does the stratification envelope vary on the northern and southern Texas shelf?

Section 3 presents results using geostatistical interpolation models to determine hypoxic area on the Texas shelf. Analyses presented include statistical comparisons of each model to answer the following research questions:

1. How do different interpolation models affect annual Texas coastal hypoxic area calculations?
2. Can acceptable standards be developed for interpolating oceanographic data on the Texas and Gulf of Mexico shelf related to monitoring annual hypoxia formation?

In Section 4, I consolidate results from Sections 2 and 3 into considerations and recommendations for management strategies aimed at reducing Gulf of Mexico hypoxia. This chapter focuses specifically on how to integrate hypoxic area on the Texas shelf into current federal policy and management strategies.

Section 5 summarizes results presented in Sections 2, 3, and 4 and provides conclusions and future directions.

There are several appendices for this dissertation. Appendix A includes the tables and Appendix B includes the figures by section. Appendix C is an investigatory study, in which I attempt to use remote sensing to determine potential biological processes contributing to the formation of Texas coastal hypoxia. Appendix E moves from science and policy into education and outreach with the purpose of communicating scientific results to the public. This section will introduce techniques for integrating coastal hypoxia research into K-12 curriculum designed for teaching state science testing standards. Data will show the impacts and results of introducing this curriculum in local classrooms. Appendix E includes supplemental material not included in the area results in Section 3.

## **2. INVESTIGATING THE PHYSICAL PROCESSES RESPONSIBLE FOR HYPOXIA FORMATION ON THE TEXAS SHELF**

### **2.1 Introduction and Organization**

Physical and biological processes drive the formation of hypoxia in the northwestern Gulf of Mexico. Processes impacting the development and breakdown of water-column stratification include freshwater discharge, winds, currents, and hydrography (e.g. salinity and temperature). In this Section, I compare the role of density-driven stratification relative to dissolved oxygen concentrations on the Texas shelf. The results presented in this section provide data in understanding the development and breakdown of stratification in the water-column and how stratification affects hypoxia formation on the Texas coast from 2009 to 2011.

Section 2 is organized into a series of subsections. The data and methods for examining physical processes controlling Texas shelf hypoxia will be outlined in Section 2.1. Section 2.2 introduces a series of hypotheses developed to investigate physical processes relative to one another and to determine the strength of stratification driven by freshwater input, wind, and current patterns on the Texas shelf. Section 2.3 presents a synopsis of the physical conditions and hypoxia on the Texas shelf from 2009 to 2011. Results specific to the hypotheses presented in Section 2.2 will be shown in Section 2.4. Section 2.5 will discuss the results and address future directions for studying physical processes driving hypoxia formation on the Texas shelf.

## **2.2 Data and Methods for Examining Physical Processes Controlling Texas Hypoxia**

### *2.2.1 Description of the TAMU WF Mooring and TAMU TABS and NDBC Buoys Data*

The TAMU environmental mooring mounted a wind turbine test platform in the northern Gulf of Mexico (herein abbreviated as TAMU WF) was deployed during summer 2009 to 2011. The TAMU WF mooring was designed as an environmental water quality mooring with instrumentation to measure temperature ( $^{\circ}\text{C}$ ), salinity (practical salinity unit abbreviated as PSU), dissolved oxygen concentration (mg/L), and nutrient concentration (e.g. nitrate) with two components: cabled water-column array and bottom package with a Recording Doppler Current Profiler (RDCP). Mullins et al. (2009) provide a detailed explanation of the mooring designed and data QA/QC. The yearly record length of the time-series for the TAMU WF mooring varies depending on the deployment and maintenance issues (Table 2.1). Both raw and averaged data were analyzed. The type of data (raw versus averaged) used for the statistical analyses will be discussed in the respective sections.

The current data collected from the RDCP were binned every 1 m starting at 2-m above the bottom and extending down to 13-m in the water-column. The raw data were filtered with a 40-hour low-pass filter to remove the tidal and inertial variability.

Data were compiled from state and federal buoys to compare with the TAMU WF mooring data. The Texas Automated Buoy System (TABS B, state) and the National Data Buoy Center (NDBC 42305, federal) buoys provided surface

measurements of temperature ( $^{\circ}\text{C}$ ), salinity (PSU), winds (m/s), waves, and/or horizontal current velocity for locations north of the Brazos River (Figure 2.1, NDBC 42035) and southwest of the Brazos River (Figure 2.1, TABS B). Data were downloaded from [tabs.gerg.tamu.edu](http://tabs.gerg.tamu.edu) and [www.nodc.noaa.gov/buoy](http://www.nodc.noaa.gov/buoy) respectively. Each data provider completed initial QA/QC. Data from both buoys were used in raw and averaged form similar to the TAMU WF data. The raw wind data was filtered with a 3-hour low pass filter to smooth the high frequency variability. The processing and potential aliasing introduced from data averaging will also be discussed in the appropriate sections.

Analysis in this section additionally combined data from the TAMU WF, TABS B, and NDBC 42035 to estimate stratification in the water-column at the TAMU WF site. A metric for stratification was determined from a salinity and temperature stratification index (SI), which is calculated by subtracting the surface-most value at the TAMU WF mooring from either the lowest instrument on the array (years 2009 and 2010) or values from the RDCP (years 2010 and 2011). In 2009 and 2010, SSI was calculated using surface (7-m) salinity data from the TABS B and bottom (16-m) salinity data from the WF RDCP.

### *2.2.2 Description of the TAMU MCH Data*

The data to investigate the role of physical processes in Texas hypoxia formation were from four TAMU Mechanisms Controlling Hypoxia Surveys (MS) surveys conducted in 2010 and 2011 (Table 2.2). Only August 2010, June 2011, and August

2011 are included in this research. The June 2010 survey was too short for adequate analysis and not used, but is shown for completeness.

Data on these cruises were collected from a conductivity-temperature-depth (CTD) profiler and SeaSciences Acrobat cabled towfish (Acrobat). The type of data collected included vertical depth profiles of salinity (PSU), temperature (°C), dissolved oxygen concentration (mg/L), nutrient concentrations (e.g. nitrate and phosphate), chlorophyll, fluorescence, turbidity, and current velocity. Only salinity temperature, pressure, and bottom dissolved oxygen concentrations are used in this study. Detailed sampling methodology for the CTD and Acrobat will not be discussed in this document, but can be referenced in Mullins et al. (2009, 2010).

The dissolved oxygen from these cruises was measured in ml/L and was not converted to mg/L. If the pressure was not provided in the original QA/QC CTD file, depth (m) was used, as pressure in decibars is approximately equal to depth. For CTD profiles in August 2010, the surface dissolved oxygen value at the surface was removed if values were below zero. These values were not corrected in the final QA/QC processing, which was not within the scope of this research.

The MCH cruise plans are shown in Figure 2.2 for MS2 (August 2010), MS3 (June 2011), and MS4 (August 2011). Cruise plans were slightly adapted year-to-year based on the freshwater inflows of the Mississippi, Atchafalaya, and Brazos Rivers and weather. The Deepwater Horizon oil spill event in 2010 limited the extent of sampling in the northwestern Gulf of Mexico forcing cruise plan to be adapted and include additional sampling along the south Texas coast. Acrobat towfish lines were altered

cruise-to-cruise depending on weather conditions and sea-state. Only stations on the Texas shelf were considered in this study as indicated in Figure 2.2.

### *2.2.3 Description of the TAMU Acrobat Towfish Data*

The CTD casts and towfish surveys were conducted in June and August of 2010 and 2011. Observations were collected along the northern Texas shelf in June and August 2011 and extended southward in June and August 2010 (Mullins et al. 2010, 2011a, b). The parameters measured and descriptions of the data processing and QA/QC can be referenced in detail in Mullins et al. (2010, 2011a, b). Statistical analysis in Section 2.4 was performed on those towfish profiles indicated in Figure 2.2.

### *2.2.4 Description of the Brazos River Data*

In addition to the TAMU WF, TABS, and NDBC data, Brazos River discharge was downloaded from [usgs.gov](http://usgs.gov) for years 2009 and 2011. Raw data were used to examine flow variability from 2009 to 2011. Daily averages for discharge were calculated for the length of the TAMU WF time series in 2009 and 2011.

### *2.2.5 Data Organization*

Data were grouped into the following multivariate categories: hydrography (salinity, temperature), currents, rivers, and winds. Table 2.3 lists the individual data sets in each category. The multivariate categories were not the same for 2009 and 2011, because no array data was available in 2011. Since the TAMU WF array did not record

near-bottom dissolved oxygen data in 2010 and 2011, the RDCP bottom dissolved oxygen data were compared against the three categories. The data were also truncated to the time near-bottom dissolved oxygen was recorded on the array (2009) and bottom dissolved oxygen was recorded from the RDCP (2011).

Each data set was averaged by day to remove the high-frequency variability and to address recording time differences in each data source. Daily averaging was chosen to eliminate the local variability in the systems, to reduce noise in each time-series, and to examine persistent hypoxia (defined as 24 hrs or longer). Averaging the physical parameters did not affect the results, because I was interested primarily in the stability of the water-column relative to persistent hypoxic events rather than episodic events (less than 24 hours).

#### *2.2.6 Calculating Brunt-Väisälä frequency and AOU*

CTD stations on the Texas shelf were selected from the MS surveys in August 2010 and June and August 2011 (Figure 2.1). Temperature, salinity, and pressure were selected for the Brunt-Väisälä calculation. The Brunt-Väisälä frequency was calculated over 1.0 m depth for the MS survey in August 2010 and over 0.5 m depth for MS survey cruises in June and August 2011. The change in interval was a result of a change in QA/QC processing procedures from the first year to the second year of the TAMU MCH MS project. The method used for computing Brunt-Väisälä frequency is given in Millard et al. (1990):

$$N^2 = \rho \cdot g^2 \cdot [-\alpha \cdot (dT/dp - \Gamma) + \beta \cdot (dS/dp)] \text{ (rad/s)}, \quad (2.1)$$

where  $T$  is the temperature ( $^{\circ}\text{C}$ ),

$S$  is the salinity,

$p$  is the pressure (db),

$\rho$  is the density ( $\text{kg/m}^3$ ),

$g$  is the gravity acceleration ( $\text{m/s}^2$ ),

$\alpha$  is the thermal expansion,  $\alpha = - (1/\rho) \cdot (\partial\rho/\partial T)$  ( $^{\circ}\text{C}^{-1}$ ),

$\beta$  is the saline contraction,  $\beta = (1/\rho) \cdot (\partial\rho/\partial S)$ ,

$\Gamma$  is the adiabatic lapse rate,  $\Gamma = -(T_a / C_p) \cdot (\partial\nu/\partial T)$ ,

$\nu$  is the specific volume,  $\nu = 1/\rho$ ,

$T_a$  is the absolute temperature,  $T_a = T + 273.15$  (K)

$C_p$  is the specific heat.

The Brunt-Väisälä frequency was calculated in MATLAB using an adapted script provided for public-use by Phil Morgan (1993) referenced from A.E. Gill (1982). Output from the script provided the square of the Brunt-Väisälä frequency in  $1/\text{s}^2$ , which was converted to cph.

Apparent oxygen utilization (AOU) is a metric representing the sum of the biological activity of the water since the water sample was last in equilibrium with the atmosphere and is a measure of the oxygen utilized by biogeochemical processes in the water-column. AOU is defined as the difference between the saturation of dissolved oxygen and the measured dissolved oxygen in the water-column correction to the salinity, temperature, and pressure where the measurement was taken (Millero 2005):

$$AOU = O_2^{sat} - O_2^{obs}, \quad (2.2)$$

where  $O_2^{sat}$  is the saturated value of dissolved oxygen concentration, and

$O_2^{obs}$  is the measured dissolved oxygen concentration.

The saturated value is the concentration of dissolved oxygen in equilibrium with the atmosphere. The saturated value is corrected to its value at the salinity, temperature, and pressure where the measurement was taken. Coefficients for calculating the saturation value were computed at the potential temperature of water and one atmosphere total pressures are from the data published by Murray and Riley (1969):

$$\begin{aligned} \ln(O_2^{sat}) = & -173.4292 + 249.6339/(T/100) + \\ & 143.3482 \cdot \ln(T/100) - 21.8492 \cdot (T/100) + \\ & S \cdot (-0.033096 + (T/100) \cdot (0.014259 - 0.0017 \cdot (T/100))) \end{aligned} \quad (2.3)$$

where  $T$  is the water temperature (Kelvin),  $S$  is the water salinity. The constants used in the equation result in units of ml/L.

## 2.3 Hypotheses for Analyzing Mooring, Buoy, and Towfish Data

The hypotheses presented here were constructed to investigate the physical processes responsible for hypoxia formation on the Texas shelf. The alternate hypotheses, brief background and justification, and methods are included.

### 2.3.1 Hypothesis A

*H<sub>0</sub>: Hypoxic events at the TAMU WF mooring last longer than 24 hours during the summer and early fall months (May – October).*

Mullins et al. (2009) analyzed real-time mooring data and documented the formation of episodic, short-lived hypoxic events (hours to days) on the Texas shelf. A hypoxic event was determined by calculating a curve crossing at 2.0 mg/L and the time elapsed between each inflection for TAMU WF mooring data. The average time of events was calculated for the length of the mooring time-series. Histograms were made to compare the temporal change of hypoxia duration across the three years.

### 2.3.2 Hypothesis B

*H<sub>0</sub>: Temperature, salinity, SSI, TSI, Brazos River discharge, and wind direction (upwelling-favorable) are not linearly and positively correlated to bottom dissolved oxygen concentration on the northern Texas shelf.*

Hypothesis A compared daily averaged seasonal wind patterns, hydrography, and river discharge to hypoxia formation at the TAMU WF. The hypothesis examined which physical factors were responsible for hypoxia formation on the northern Texas shelf. Results from multivariate regression helped understand which physical processes are more important for hypoxia formation in a given year. Years 2009 and 2011 were only considered, because TAMU WF data was available for summer and non-summer months.

Multivariate linear regression was used for this section. The model used for the multivariate linear regression was (Ott and Longnecker 2008):

$$y_i = \beta_0 + \beta_1 x_{i1} + \beta_2 x_{i2} + \dots + \beta_p x_{ip} + \varepsilon_i \text{ for } i = 1, 2, \dots, n \quad (2.4)$$

where  $\beta_0$  = model intercept,  $\beta_p$  = coefficients of the explanatory variables, and

$\varepsilon_1$  = residuals (deviations of observed from the actual values).

Simple linear regression models include only  $\beta_0 + \beta_1 x_{i1}$ .

Each subgroup of variables was tested in a regression model to identify significant variables within each group. If a significant linear relationship did not exist between dissolved oxygen and a variable, I retested the linear model after log-transforming the data. If the residuals were approximately normal, I consider the log-transformed data into the model. Variables that were significantly linearly correlated with dissolved oxygen (p-value < 0.05) were compiled into a final dataset for each year (Table 2.3). The final multivariate linear regression model was calculated with the significant subgroup variables.

Model parameters and statistics were tabulated for each model. These included the estimated value ( $b_1$ ), the standard error of the estimate ( $SE_{b1}$ ), and p-value. The coefficient of determination ( $r^2$ ) and correlation coefficient ( $r$ ) were also calculated and included for each model. The  $r^2$  term addresses the proportion of variability that is accounted for by the model (e.g. goodness of fit; Ott and Longnecker 2008).

The best subsets of explanatory, or predictor, variables were chosen by considering three assessment criteria – Bayesian information criteria (BIC), adjusted  $r^2$  ( $r^2_{adj}$ ), and  $r^2$  criteria. BIC is a likelihood function and introduces a penalty term for the number of predictors used in the mode. The BIC is an increasing function of the standard error of each estimate model, meaning the unexplained variation in the dependent variable and the number of explanatory variables will increase the value of the BIC for each subset of predictors (Burnham and Anderson 2004). In this analysis,

the change in BIC ( $\delta\text{BIC}$ ) by adding or deleting variables to a linear model was used to select the best subset of variables for explaining dissolved oxygen concentrations at the TAMU WF mooring. The larger the  $\delta\text{BIC}$  value, the more contribution a term has in the overall model.

The second criteria,  $r^2_{\text{adj}}$ , assessed a penalty associated with the removal of variables based on the number of variables in the model. The  $r^2_{\text{adj}}$  is a stricter assessment than the third criteria,  $r^2$ , because this criterion determines the relative contribution of each explanatory variable to the final model rather than selecting the combination of variables providing an  $r^2$  closest to 1. The  $r^2$  criterion provided the best  $r^2$  values, independent of the contribution of each explanatory variable. Using three different criteria allowed a comparison of methodologies and showed which explanatory variables were most important in predicting bottom dissolved oxygen on the northern Texas shelf.

### 2.3.3 Hypothesis C

*H<sub>0</sub>: Hypoxia occurs on the northern Texas shelf when the water-column stratifies, but does not occur at maximum Brunt-Väisälä frequencies less than 40 cph.*

The Brunt-Väisälä frequency quantifies the strength of stratification and is representative of water-column stability, which is the natural frequency of a water parcel's oscillation adiabatically from initial, or rest, position (Brunt, 1927). Typically calculated as cycles per hour (cph), the higher the value, the higher the stability

indicating water-column's resistance to vertical mixing. Belabbassi (2006) found that hypoxia did not occur at Brunt-Väisälä frequencies less than 40 cph. Kiselkova (2008) found a similar relationship, but also the relationship between Brunt-Väisälä frequencies and bottom dissolved oxygen concentrations in Louisiana coastal waters to be non-linear. Brunt-Väisälä frequencies were plotted against the dissolved oxygen concentrations and the Brunt-Väisälä frequency of 40 cph based on Belabbassi (2006) and Kiselkova (2008) to test the hypothesis.

#### 2.3.4 Hypothesis D

*H<sub>0</sub>: There is a non-linear correlation between maximum Brunt-Väisälä frequency and bottom apparent oxygen utilization (AOU) on the Texas shelf based on TAMU MCH MS survey data.*

Hypothesis D combined results from Hypothesis C with values of near-bottom AOU calculated from CTD profiles collected during MS surveys in 2010 and 2011 to determine if a highly stratified water-column facilitates the formation of hypoxia. The maximum Brunt-Väisälä frequency and AOU help to distinguish between physical and biogeochemical processes regarding oxygen depletion in the water-column.

Simple linear regression models (see equation 2.4) were computed in MATLAB for each of the three MS cruises to compare the relationship between near-bottom AOU and Brunt-Väisälä frequencies.

## **2.4 Results for Investigating Physical Processes Responsible for Hypoxia Formation on the Texas Shelf**

### *2.4.1 Freshwater Discharge on the Texas Shelf*

Figure 2.3 shows the Brazos River discharge from 2009 to 2011. In 2009, discharge was low ( $< 100 \text{ m}^3/\text{s}$ ) from January to April and peaked at  $950 \text{ m}^3/\text{s}$  in mid-April to May. In June, the discharge remained less than  $100 \text{ m}^3/\text{s}$ , which continued until September. October had the largest discharge ( $1,350 \text{ m}^3/\text{s}$ ) discharge and remained greater than  $200 \text{ m}^3/\text{s}$  to the end of the year. In 2010, the highest rates ( $\sim 1,200 \text{ m}^3/\text{s}$ ) were in the early part of the year (January to late April) with short-lived peaks occurring during the summer (May – June). In August, discharge dropped to below  $20 \text{ m}^3/\text{s}$ . A short (2-3 day) pulse in September reached  $700 \text{ m}^3/\text{s}$ . In 2011, discharge rates were at the lowest values of all years recorded by USGS (generally below  $75 \text{ m}^3/\text{s}$ ) and the low rates reflected the impact of an extreme drought across Texas ([www.lcra.org](http://www.lcra.org)).

### *2.4.2 Winds on the Northern Texas Shelf*

Freshwater on the shelf, either waters from MARS or the Brazos River, is advected by the wind-driven low-frequency circulation on the Texas-Louisiana shelf. Figures 2.4 to 2.6 show the 3-hour low-pass filtered wind speeds (m/s) recorded from the NDBC 42035 (blue, upper panel) and TABS B buoys (green, lower panel). Wind speeds are plotted in oceanographic convention, i.e. the direction the wind is blowing towards.

Winds in 2009 were upcoast (from southwest to northeast) from late June to late August with speeds ranging from 4 to 9 m/s (Figure 2.4). There were approximately 10 downcoast events during this period with speeds ranging between 1 and 5 m/s. However, these events were short-lived, lasting less than 1 day. Winds changed direction near the end of August, indicating the seasonal shelf upcoast reversal of winds (Section 1). Unlike the summer wind patterns, winds in the non-summer months are more variable with stronger and longer (days to a week) upcoast events, as seen on September 24 to the end of the record.

Winds in 2010 showed a similar summer pattern in direction and speed to 2009 (Figure 2.5). At the start of the record, wind speed was greater than 4 m/s and direction was to the northwest (inshore), except for a 3-day strong southwest event in late June. As the event ended, wind direction returned to a predominant upcoast (north to northeast) flow with small speeds and time lengths (i.e., less than 5 m/s, and a few days) for the remainder of the time-series.

Wind speed and direction in 2011 also resembled a similar seasonal pattern to the winds in 2009 (Figure 2.6). The downcoast winds in the summer months were lesser in magnitude (less than 3 m/s) compared to events in 2009. Winds transition to downcoast in late August, indicated by a strong and longer event ( $> 10$  m/s,  $\sim 1$  week) occurring on August 25.

Correlation coefficients and covariance were calculated for the daily averaged wind parameters in 2009. Table 2.4 shows statistically significant correlations between both buoys ( $> 0.8$ ) with short times scales (3 and 7 days) for speed and the north

components respectively and long time scales (29 and 30 days) for the east and direction components respectively. The p-values for all correlations were less than 0.0001. Because the correlations were strong for all components and the time scale is close to a month for speed, I determined that there was no significance between the buoys. From herein, I only included wind data from NDBC 42035, which is closer in distance to the TAMU WF, for the remainder of the analyses.

#### *2.4.3 Currents at the TAMU WF*

The wind-driven seasonal pattern of circulation directly affects local stratification by advecting freshwater along the Texas shelf. Figures 2.7 to 2.9 shows the TAMU WF RDCP time-series of the 40-hour low-pass current velocities from 2009 to 2011, respectively.

From the beginning of the observations to early August 2009, the currents exhibited a strong upcoast (north-northeast) flow in response to the upwelling favorable wind forcing (Figure 2.4). The strongest surface current velocities ( $> 20$  cm/s) were observed in June. In late August, the current magnitude weakened ( $< 20$  cm/s) and the direction changed to predominantly downcoast (i.e. to the southwest) in the water-column. This non-summer seasonal transition was a response to the shifts in winds (upwelling to downwelling favorable) seen in Figure 2.4 and described in Section 2.4.2. The summer and non-summer seasonal transitions were seen throughout the water-column. Reversals contradictory to the seasonal patterns in flow were evident

throughout the record, but the dynamical causes of the reversals were not further investigated.

In summer 2010, current velocities were observed to be upcoast (north-northeast; Figure 2.8). Velocities ranged between 10 and 25 cm/s in the 2- and 3-m depth bins. There were two 5-day downcoast transitions to the south-southwest recorded on June 15 and July 20. The June downcoast flow was weak in magnitude (less than 10 cm/s) at 2- and 3-m. The July downcoast flow was weaker in the surface bins and increased in velocity in the deeper bins reaching downcoast velocities greater than 20 cm/s. Each downcoast event was strongest ( $> 20$  cm/s) between 4- to 9-m and weakened to less than 10 cm/s from 10- to 13-m.

Velocities in 2011 (Figure 2.9) respond to wind conditions (Figure 2.6); in 2009, the pattern is seasonal (Figures 2.4 and 2.7). Summer conditions show upcoast flow conditions at the start of the time-series in June and persistence through the water-column for the summer months. Unlike 2009, the 2011 upcoast flow was weaker and persistent with less variability in velocity and fewer downcoast reversals. In late August, the non-summer flow started in response to the transition in winds with a strong ( $> 20$  cm/s) downcoast surface flow observed for the remainder of the time-series. As seen in 2009 and 2010, there were also repeated short-lived (2-4 day) upcoast flow observed in the water-column.

#### *2.4.4 Hydrography at the TAMU WF (Temperature and Salinity)*

As discussed in Section 2.1, observations at the TAMU WF showed different environmental conditions during 2009 to 2011 (Table 2.3). Observations for 2009 are used to investigate the formation and breakdown of stratification at the TAMU WF relative to hypoxia forming. Observations in 2009 were recorded at all depths of the TAMU WF cabled array and RDCP for summer and non-summer months. TAMU WF observations for 2011 are included for comparison. Data from 2010 are not included, because of the short time-series of the array data available.

Figures 2.9 and 2.10 show the raw TAMU WF array data for salinity and temperature, respectively. Salinities at the three array depths (7-m, 9-m, and 15-m) ranged approximately from 27 to 36.5 PSU with saltier waters present in the summer months and fresher waters observed in non-summer months starting in late August. A distinct seasonal transition, similar to winds and currents, was evident in the record (Figure 2.10) and began just after August 25. During the summer, salinity was nearly constant at ~36 PSU in the water-column. In late August, salinity decreased rapidly indicating the movement of fresher waters downcoast over the TAMU WF. In the non-summer months, salinity oscillated between ~27 and 36 PSU in the water-column with the lowest salinities observed on September 14 in Figure 2.7. Following this event, salinity again increased in response to a strong upcoast flow between September 15-24. On September 24, salinity began to decrease following the downcoast return of current flows, which last for the remainder of the time-series.

The TAMU WF water-column temperature time-series are plotted in Figure 2.11. Temperatures ranged from approximately 24 °C to 31 °C with the warmest temperatures observed in late August and the coolest temperatures observed around July 1 and in late September. After July 1, water-column temperatures warmed slowly and peaked around August 25 before decreasing near 25 °C at the end of the record. The warming of the water-column reflected the increase in solar insolation transitioning from the spring to summer months.

Stratification indexes were calculated for the 2009 TAMU WF array data (Figure 2.12). The green line shows the salinity stratification index (SSI) and the red line shows the temperature stratification index (TSI).

The SSI began near -2  $\Delta$ PSU and increased to 0  $\Delta$ PSU at the start of the time-series with a very small number of decreases or increases. The small number of changes indicated little to no difference between the near-surface (7-m) and bottom array (15-m). The SSI became strongly negative on August 25 in response to the downcoast wind and currents. The downcoast flow transported fresher water from the east. SSI values remained negative until the end of the time-series, ranging from -1 to -6  $\Delta$ PSU. The strongest negative peak occurred September 1 corresponding to a sharp transition in the currents. Additional strong peaks between -4 and -6  $\Delta$ PSU were observed between September 1 and October 9, again indicating movement of eastern fresher water over the TAMU WF.

The TSI did not show similar trends to the SSI. TSI was greatest at the start of the record in late June and early July with values above zero and peaks around 3  $\Delta$ °C,

indicating a warmer near-surface waters compared to the bottom waters. After July 7, the TSI was near zero for the remainder of the time-series.

#### *2.4.5 Dissolved Oxygen at the TAMU WF*

The 2009 dissolved oxygen concentrations for the TAMU WF array and RDCP are plotted in Figure 2.13. Dissolved oxygen concentrations were depleted (2-4 mg/L), but not hypoxic, at the start of the observations and increased in the water-column (above 4 mg/L) during the summer months. No hypoxic events were observed. Concentrations decreased at the seasonal transition between summer and non-summer with the longest duration of hypoxia observed in the entire water-column between August 25 and September 6. After September 6, shorter hypoxic events were only observed in the bottom depths (15-m array and RDCP). The water-column re-oxygenated there after, except for a short-lived hypoxic event observed at the end of the time-series in the bottom array and RDCP.

In 2010, dissolved oxygen was recorded from the 7 and 9 m array and the RDCP. Dissolved oxygen concentrations at each depth were not correlated compared to the concentrations observed in 2009 (Figure 2.14). No hypoxic events were observed in the near-surface waters (7-m) and concentrations remained above 6 mg/L for the remainder of the time-series. The oscillating pattern observed in mid-June was likely a result of diurnal changes in temperature, which drove oxygen saturation levels. Hypoxia in 2010 was observed in the 9 m and RDCP array at the start of the time-series with events persisting until June 13 (Figure 2.14). On the 9 m array, the lower water-column re-

stratified in response to strong downcoast flow on June 15, resulting in a longer-lived (~3 day) hypoxic event. Low, but not hypoxic, concentrations were observed around June 21 followed by a decrease in dissolved oxygen around June 23 coinciding with a downcoast flow in the water-column. Bottom dissolved oxygen at the 9 m array remained hypoxic until the end of the time-series (June 28).

In 2011, hypoxic events were observed in the RDCP (recall there was no array data). Figure 2.15 shows the bottom dissolved oxygen observations with hypoxia observed only in late May to late June. Following a period of bottom water oxygenation, the bottom water dissolved oxygen was hypoxic again starting around July 1 and then again July 8 and July 25. Each event was persistent, i.e. lasting longer than 24 hours. There was a record gap from late July to early August, in which no hypoxia was observed after late August to the end of the time-series.

#### *2.4.6 Summary of Observations at the TAMU WF*

From the results in the previous sections, it was evident that dissolved oxygen variability and hypoxic events were related to wind-driven processes on the north Texas shelf. To visualize how water-column changes affected the formation of stratification and resultant hypoxia, I calculated daily averages for the Brazos River discharge, wind speed, near-surface current velocities (3-m), SSI, TSI, and TAMU WF RDCP bottom dissolved oxygen for the 2009 (Figure 2.16).

The initial seasonal decrease of bottom dissolved oxygen and hypoxia in late June was coincident with temperature and salinity stratification. Based on the

differences between the two plots, there was a greater change in temperature (+4 °C), then salinity (2 ΔPSU) at the start of the time-series. Bottom dissolved oxygen concentrations decreased, but at this location, no hypoxia formed. Later, the change in temperature (TSI) decreased to near 0 °C and the salinity change increased to – 6 ΔPSU. The drop in dissolved oxygen and hypoxia that formed in early September occurred with a large salinity difference and zero change in temperature. The relationship with the SSI and bottom dissolved oxygen is further supported by correlation analysis. Correlation between the SSI and RDCP bottom dissolved oxygen was significant (p-value < 0.05,  $r = 0.6$ ), whereas the correlation was not significant between TSI and RDCP bottom oxygen (p-value > 0.05,  $r = 0.02$ ).

In the summer and fall, freshwater on the northern Texas shelf did not likely originate from the Brazos River, as the discharge volume was low (Figure 2.16). If there was more Brazos River water discharged onto the shelf, the upcoast currents would have transported the water northward. However, no freshwater signature was present in the SSI during the summer season. The salinity-driven stratification formed in the fall months was also not likely caused by the Brazos River flooding, which moved downcoast in response to the wind and currents. Therefore, the freshwater signature in the SSI potentially resulted from the advection of MARS freshwater westward onto the northern Texas shelf.

To further investigate the strength of the stratification, I compared the mid-depth array (8-m and 12-m) densities and bottom dissolved oxygen to the calculated values of the Brunt-Väisälä frequencies for the fall hypoxic event in 2009 (Figure 2.17). After the

seasonal wind and current reversal on August 25, the densities decreased reaching ~1018 and 1019.5 kg/m<sup>3</sup>. The decrease in density in the water-column on September 4 caused the largest Brunt-Väisälä frequencies (near 60 cph at 8-m depth). The increase in stratification is coincident with the hypoxic event that occurred and persisted for 4 days. Decreases in bottom dissolved oxygen also occurred when the 8-m Brunt-Väisälä frequencies were near or above 40 cph, but hypoxia did not result during all 8-m ~40 cph peaks in the non-summer months.

Stratification and hypoxia formation relationships could not be calculated in 2010 and 2011 because the SSI and TSI could not be calculated. More so, the freshwater source could not be determined from current velocity (Figure 2.8). In 2011, a strong upcoast flow in mid-June potentially forced Brazos River discharge up the northern Texas shelf, but discharge volumes were the lowest recorded since the late 1960's (Figure 2.9). However, with no array data available, the movement of freshwater northward driving stratification formation could not be verified at the TAMU WF.

## **2.5 Results for Hypotheses A – D**

### *2.5.1 Hypothesis A*

Results in Section 2.3 supported a statistically significant relationship between stratification and bottom dissolved oxygen concentrations. Figure 2.18 shows two histograms of TAMU WF RDCP hypoxic events and Table 2.5 shows the length of the individual events in 2009 to 2011. In 2009, there were 8 events averaging

approximately 25 hours with the shortest event observed lasting approximately 30 minutes and the maximum event observed lasting over 125 hours. Four events (50 %) ranged from 10 to 15 hours and only two events (25 %) persisted longer than 24 hours. The longest event observed occurred in early September, which corresponded to SSI values greater than  $-4 \Delta\text{PSU}$  (Section 2.3.4).

In 2010, there were 21 events observed between June 9 and August 25. The shortest event was recorded at 30 minutes and the longest event at 138 hours (approximately 6 days). The average time of hypoxic events in 2010 was approximately 24 hours. Two events persisted longer than 5 days. Five events lasted between 10 and 48 hours and thirteen events ranged from 10 hours to 26 minutes.

Events in 2011 totaled 23 with the shortest event observed less than 30 minutes and the longest event observed at approximately 370 hours. The average of the 2011 events was 30 hours. Five events ranging from one day to 2 weeks and 19 events lasted from approximately 20 minutes to 22 hours.

The raw data showed the number of hypoxic events vary annually (Table 2.5). A greater number of events were observed in the non-summer months in 2009. The number of events was higher in the summer months in 2010 and 2011 compared to 2009, but there were no observations made in the non-summer months to compare against 2009 data. Independent one-sample *t*-tests (assuming unequal variances) did not result in significant differences between the average hypoxic times for any year versus 24 hours (*p*-values > 0.05). Therefore, there was not enough statistical evidence to

determine if hypoxic events were significantly greater than 24 hours in the summer versus non-summer months.

### *2.5.2 Hypothesis B Results*

For this hypothesis, I tested the multivariate relationships between variable subgroups (Table 2.3) in 2009 and 2011. The time-series in these years spanned the summer and non-summer seasonal conditions at the TAMU WF. Table 2.6 shows the 10 variables that individually tested statistically significant ( $p\text{-value} < 0.05$ ) from the subgroups for 2009. The correlation ( $r$ ) of each variable to the TAMU WF RDCP bottom dissolved oxygen is shown in the second column. The correlations and significant variables from the multivariate linear models discussed below supported the existence of linear relationships between each variable and RDCP bottom dissolved oxygen. However, the direction (positive or negative) of the relationship could potentially shift annually from the 2009 observations based on results from Section 2.4.6.

Ten variables from the subgroups were identified to be significantly correlated with bottom dissolved oxygen based on  $p$ -values less than 0.05. Three of the variables (Salt\_WF\_Top\*, Salt\_WF\_Bott, and WF\_SSI) were related to salinity. Only one temperature variable (Temp\_WF\_Bott\*) was significant from the temperature subgroup. The inclusion of salinity and temperature variables indicated that each has an impact of the formation on stratification at the TAMU WF.

Three of the near-surface current subgroup variables were significant (WF\_3\_Spd, WF\_3\_East, and WF\_3\_North). From winds, two variables (NDBC\_Spd, NDBC\_North) were identified as significant.

The Brazos River was selected as the final variable and was the only freshwater source identified as a statistically significant variable from the rivers subgroup. The interactions of these variables, in turn, each can affect the formation and development of stratification at the TAMU WF in 2009.

The significant subgroup variables were combined and reanalyzed in a multivariate linear model. The results are shown in Table 2.6. The parameters of the model (coefficient ( $\beta_1$ ), standard error (SE), and p-value) are also shown. Of the first 10 terms identified, five terms (Table 2.7) were selected based on p-values ( $< 0.05$ ) to estimate bottom dissolved oxygen (Salt\_SSI, Temp\_WF\_Bott\*, WF\_3\_Spd, Brazos, and NDBC\_Spd). Each of the terms included one variable from each subgroup and accounts for a physical process important in controlling stratification. A multivariate linear model using only the five selected terms accounts for ~65 % of the variability; each individual term is determined to be statistically significant to estimate bottom dissolved oxygen (p-values  $< 0.05$ , Table 2.7).

The three criteria assessments ( $\delta\text{BIC}$ ,  $\delta r^2$ , and  $\delta r^2_{\text{adj}}$ ) are shown in Tables 2.8. Each criteria produced different results to which variables were most important in estimating bottom dissolved oxygen at the TAMU WF. In the BIC assessment (Table 2.8), all five terms were considered necessary in determining the best multivariate linear model. The two terms with the greatest change in BIC ( $\delta\text{BIC}$ ) were Salt\_SSI (~40) and

WF\_3\_Spd (~30). The  $\delta r^2_{\text{adj}}$  and  $\delta r^2$  (Table 2.8) assessments resulted in these same two variables contributing to the variability of dissolved oxygen in each model, 59 % and 68% respectively.

To compare fall versus summer hypoxia formation, I conducted the multivariate linear models for the 2011 TAMU WF data to estimate the relationship of non-array terms to bottom dissolved oxygen concentrations. In 2011, seven variables (Table 2.9) were selected: 10 m current velocity (WF\_10\_East, WF\_10\_North), 3-m current velocity (also in 2009), NDBC 42035 wind direction (NDBC\_Dir, NDBC\_East, NDBC\_North), and the Brazos discharge (also in 2009). Recall for this model, there were no array data available and, therefore, no estimates for SSI or TSI. The variability in bottom dissolved oxygen accounted for by this 7-term model was ~20 % lower ( $r^2 = 0.49$ ) than the 5-term model in 2009. The only variable important in all three assessments was NDBC\_North. NDBC\_North had the highest  $\delta\text{BIC}$  (~12) and accounted for ~14 – 15 % of the variability in the  $\delta r^2_{\text{adj}}$  assessment. The  $\delta r^2$  for the three assessments ranged between ~14 % and ~32 %, which were also ~15 – 20 % lower than the  $\delta r^2$  for the criteria in 2009. The  $\delta\text{BIC}$  assessment also included the 10-m and Brazos variables to be important, whereas the  $\delta r^2_{\text{adj}}$  included the 3-m current velocity in addition to these terms.

### *2.5.3 Hypothesis C Results*

This section presents the results of tests for Hypothesis C. Figure 2.19 shows the bottom dissolved oxygen observations versus the maximum Brunt-Väisälä frequencies

for the MCH MS2, MS3, and MS4 surveys. Note in this Sections 2.5.3 and 2.5.4, the units for bottom dissolved oxygen are reported in ml/L and not in mg/L. Data are colored by cruise (recall cruise dates in Table 2.1 and CTD stations in Figure 2.2).

Figure 2.19 shows the bottom dissolved oxygen concentrations collected from CTD stations during MS2, MS3, and MS4 plotted against the maximum Brunt-Väisälä frequencies. Linear regression models calculated for MS surveys (MS2, MS3, and MS4) show the relationships between bottom dissolved oxygen and maximum Brunt-Väisälä frequencies were non-linear (Table 2.11). The p-values for the linear models were not significant for any of the three TAMU MCH MS surveys.

To further investigate changes in stratification on the Texas shelf, I compared stations from MS2 to determine differences in the oxygen and Brunt-Väisälä relationship between the north and south Texas shelf. MS2 was only considered in this analysis, because there was nearly an equal number of stations north and south of the Brazos River delta. MS3 and MS4 did not sample below the Brazos River delta.

Figure 2.20 reemphasizes that hypoxia did not form at maximum Brunt-Väisälä frequencies below 40 cph. The division of MS2 stations into north and south Texas did not show improvement of the linear relationship as shown by the p-values greater than 0.05 in Table 2.12.

Results for this hypothesis show that the relationship between bottom dissolved oxygen and maximum Brunt-Väisälä frequencies is not linear. Additionally, MS data show that hypoxia only forms when stratification was strong as indicated by maximum Brunt-Väisälä frequencies at or greater than 40 cph. There also did not appear to be any

differences in the relationship of bottom dissolved oxygen concentrations and maximum Brunt-Väisälä frequencies north and south of the Brazos River delta. More importantly, these results supported previous results in Section 2.3 that stratification is an important physical driver for hypoxia formation on the Texas shelf.

#### *2.5.4 Hypothesis D Results*

Figures 2.21 and 2.22 show the bottom AOU concentrations versus the maximum Brunt-Väisälä frequency for the north and south Texas stations collected during MS2, MS3, and MS4. The linear regression comparisons by shelf location and cruise are shown in Table 2.12.

The Texas coastal waters are stratified on the northern and southern Texas shelf with the strength of stratification varying by cruise. The largest maximum Brunt-Väisälä frequencies ( $> 100$  cph) were observed across the north Texas shelf during MS3. The maximum Brunt-Väisälä frequencies calculated from MS2 and MS4 surveys, both conducted in August, ranged between  $\sim 10$  and  $80$  cph with frequencies closer to  $80$  cph observed on the north Texas shelf during MS2.

On the north Texas shelf, AOU values ranged between  $-0.25$  and  $\sim 1$  ml/L, indicating no uptake of oxygen. AOU values also were measured above  $2.0$  ml/L, indicating a higher uptake of oxygen at stations in depths between  $10$  to  $25$  m.

The water-column was also stratified below the Brazos River delta (south Texas), however, the degree of stratification was weaker than north of the delta. The south Texas maximum Brunt-Väisälä frequencies (Figure 2.22) were lower ( $< 80$  cph) for MS2

and MS4. For MS3, 75 % of the stations resulted in frequencies greater than 80 cph. South Texas AOU values ranged between -0.25 and ~3.25 ml/L for MS2. For MS3, values were higher for three stations ( $> 0.25$  ml/L), with one station less than 0.5 ml/L. The AOU values for south Texas MS4 stations were less variable ranging between 0 and ~1 ml/L.

Linear regression models did not show a relationship between the Brunt-Väisälä frequency and AOU on the Texas shelf. The linear regression statistics are shown in Table 2.12. When considering individual surveys, the linear relationships were not significant (p-values  $> 0.05$ ) for all cruises, except south MS3 (p-value = 0.028). When combining all the stations from all surveys by shelf location, the north linear relationship was significant (p-value = 0.011) and the south linear relationship was not significant (p-value = 0.215) for bottom AOU versus maximum Brunt-Väisälä frequency. The results indicated the relationship between bottom AOU and maximum Brunt-Väisälä frequency was not linear and exhibited a large degree of variability in time (month and annual) and space (north and south).

Vertical CTD casts north of the Brazos River delta observed strong stratification forming in the near-shore surface waters ( $> 40$  cph) resulting in a strong, thick hypoxic layer (Figure 2.23). For the station further offshore north of the delta, strong stratification ( $> 40$  cph) forms 2-3 m above bottom resulting in a drop in bottom dissolved oxygen. South of the Brazos River delta showed more variability in the stratification with multiple peaks in the Brunt-Väisälä frequency. Peaks were strongest

2-3 meters above the bottom and offshore (20 m depth). The stratification corresponded to lower bottom dissolved oxygen.

To compare all surveys, I conducted independent 2-sample *t*-tests for the mean maximum Brunt-Väisälä frequencies for each survey (Table 2.13). The pairwise matrices showed that the mean maximum Brunt-Väisälä frequencies were significantly different in time and space for ~81 % of the comparisons. The percent significant differences between cruise time and shelf location was 55 % (middle panel) and 67 % for individual cruise locations north or south of the delta. These data continue to support the hypotheses that stratification varies north and south of the Brazos River delta and the location of strong stratification in the water-column impacts the volume of hypoxia formation on the Texas shelf.

The high degree of variability was additionally supported from the examination of Acrobat transects from the MS2 and MS4 surveys. Figures 2.24 and 2.25 show the Acrobat transects north and south of the Brazos River delta. Three distinct salinity layers were observed in MS2 L3 (north of Brazos delta). Salinity in MS2 L3 was near 30 PSU at the bottom and ~21 PSU at the surface with a thin middle layer of ~23 PSU. The strong stratification formed along MS2 L3 resulted in a 2-3 m thick layer of bottom hypoxia.

MS2 transects are shown in Figure 2.24. Spatial variability in stratification was evident from the differences in salinity layers between transects. However, the structure of salinity layering in MS2 L2 (south of delta) was weaker at the ends of the transects. Bottom waters in MS2 L2 were saltier (~35 PSU), but there was less degree of layering

in the water-column. Low, but not hypoxic, dissolved oxygen concentrations were observed near the bottom along MS2 L2 track.

Figure 2.25 shows the temporal variability of stratification on the Texas shelf. MS4 transects, collected in June 2010, show a vertically nearly uniform water-column with little changes in salinity and dissolved oxygen. In the MS4 L2 transect, there were small variations in salinity or oxygen. The water north of the Brazos River delta was slightly fresher (~33-34 PSU) than south of the delta (~35 PSU). A thin, salty band of bottom water was observed in the MS4 L3 track, creating a stratified layer. The thin layer (< 1 m) resulted in a slight decrease of dissolved oxygen.

Strong stratification will inhibit the ventilation of dissolved oxygen down to the bottom waters. Therefore, increases in Brunt-Väisälä frequencies corresponded to increases in AOU and vice versa. The results of these analyses support the Rowe and Chapman (2002) theory of different processes (physical and biogeochemical) control the dissolved oxygen levels in different physical regimes. The MCH MS survey data did show stratification is significantly different in space and time on the Texas shelf.

## **2.6 Summary and Future Directions**

### *2.6.1 Summary*

The mechanisms controlling hypoxia formation on the Texas shelf vary by location (north versus south of the Brazos delta) and during the time of year (summer versus non-summer). Hypoxic duration can increase drastically from year-to-year

depending on wind direction and current magnitude, downwelling and upwelling favorable conditions, and the degree of salinity and/or temperature stratification. During downwelling favorable condition, winds and currents flow down the Texas coast, transporting freshwater from the Louisiana shelf (e.g. 2009). Model results from *Feng* (2011) describe the potential advection of Atchafalaya River water westward, which can account for increases in the salinity-driven stratification. In downwelling conditions, Brazos River water is confined close to shore and flows southwest-ward (DiMarco et al. 2012). Hypoxia on the northern Texas shelf would not be attributed to the Brazos River in downwelling conditions. Upwelling favorable winds will drive Brazos River water upcoast towards Galveston and transport water offshore.

The type of stratification, salinity- or temperature-driven, also impacts the local hypoxic conditions on the Texas shelf. Upwelling and downwelling can occur throughout the year. It is the persistence that leads to the control of hypoxia. In 2009, strong salinity stratification resulted in late summer and early fall hypoxic events on the northern Texas shelf. Temperature stratification occurred in the summer, which resulted in a decrease of bottom dissolved oxygen, but no hypoxia on the northern Texas shelf.

The strength of the interactions between winds, freshwater, and currents is responsible for water-column stability on the Gulf of Mexico shelf. Strong stratification prevents the ventilation of dissolved oxygen from the surface layer down to the bottom waters (Hetland and DiMarco 2008; Bianchi et al. 2010). The horizontal and vertical spatial and temporal structures of hypoxia are influenced by the physical conditions on the Texas shelf. The occurrences of low oxygen waters and hypoxia are related to

vertical stratification on the north and south Texas shelf. Hypoxia was not found in waters with Brunt-Väisälä frequencies less than 40 cph (Belabbassi 2006; Kiselkova 2008). Stronger stability generally occurs on the northern Texas shelf and results in a greater number of hypoxic events relative to the south Texas shelf.

The volume of hypoxia also coincides with the degree of stratification. Strong (> 40 cph) Brunt-Väisälä frequencies in the surface waters form a thicker layer of hypoxia. Strong Brunt-Väisälä frequencies in the mid- and bottom waters results in dissolved oxygen decreases, but not necessarily hypoxia. This is seen in *in situ* CTD profiles and TAMU MCH Acrobat profiles, which provide high-resolution (100 m) observations of the physical water-column variability and hypoxic volume.

Multivariate linear modeling has primarily been used to estimate hypoxic area on the northwestern Gulf of Mexico shelf (Feng 2011; Green et al. 2009). Based on interpolation results from NOAA SEAMAP data, hypoxia area can be patchy and confined either to the north or south Texas shelf. Also, these models incorporate nutrient terms, such as nitrate loading, which are not available from the ocean observing platforms considered here. Instead of considering area, I attempt to use multivariate linear modeling to explain localized hypoxia formation based on physical processes for the north Texas shelf. My models show conditions and degree of mechanisms can change year-to-year and vertical array data is important to account for such changes, as seen with the year 2009 model. Model results from year 2010 and year 2011 demonstrate how spatially constrained hypoxic formation can be on the north Texas

shelf and that nearby buoy data does not accurately represent the degree of stratification at the TAMU WF.

This research is the first study to quantify the spatial and temporal extent of hypoxia and to investigate the degree of annual and seasonal stratification relative to hypoxia formation on the Texas shelf. The number of results presented supports the research of Hetland and DiMarco (2008) that the extent of potential stratification envelope varies spatially and temporally and conclusions by Bianchi et al. (2010) that multiple hypoxic regions can form on the northwestern Gulf of Mexico shelf. Furthermore, the results show the degree of variability in physical processes, especially stratification, that is responsible for a high degree of temporal and spatial variability in hypoxia formation on the Texas shelf and how the processes on the Texas shelf can differ from the processes responsible for Louisiana coastal hypoxia.

### *2.6.2 Future Directions*

The integration of ocean observing data is important in describing the physical coastal ocean environmental conditions for hypoxia formation on the Texas shelf. Mooring array and RDCP data provide invaluable and high resolution information about water-column conditions over a given time period. Buoy data in the vicinity of a mooring is also useful in describing surface atmospheric and oceanographic conditions at the air-sea interface. However, caution must be used as mechanisms responsible for hypoxia formation can be spatially localized as seen with spatial dissimilarity between TABS B surface salinity and temperature and TAMU WF stratification. Correlations

can weaken and in some years there may be no significant correlations between nearby buoys. Array data are also important and necessary to assessing the salinity and temperature stratification on the Texas shelf. An accurate assessment of hypoxia formation on the Texas shelf requires an understanding of the physical conditions, which can only be done with an integration of such platforms.

The temporal deployment of integrated ocean observing systems is important. Temporal scales of Texas hypoxia differ from the summer, persistent Louisiana coastal hypoxia. Each year analyzed in this research showed a different seasonal and annual physical water-column conditions resulting in different temporal time-series of hypoxia formation. Hypoxic events can be short (less than 24 hours) or persistent (greater than 24 hours) depending on water-column conditions, including currents and winds along with temperature and salinity changes. Short-lived events can result from pulses of freshwater creating stratification, e.g. flooding of the Brazos River. Hypoxia can also occur in non-summer months on the Texas shelf. Therefore, platforms must be operational throughout the year to capture annual formation variability.

One mooring is not sufficient to define the Texas shelf environment and physical processes contributing to hypoxia formation, as cruise results have shown conditions suitable for hypoxia formation vary upcoast and downcoast of the Brazos River. Additional moorings further north (near Sabine Pass) and below the Brazos River (near Matagorda) will increase the temporal and spatial resolution necessary to differentiate freshwater sources driving stratification and hypoxia formation. Synoptic analyses from the mooring shows the influence of freshwater, but the source of the freshwater (Brazos

versus MARS systems) cannot be delineated from observational ocean observing data. To do this also requires *in situ* shipboard surveys in conjunction with observing platforms.

The ability to conduct a rapid response cruise is also useful, as shown in DiMarco et al. (2012). Because of the nature of hypoxia formation on the Texas shelf and the influence of Brazos River discharge in persistent formation, such as in year 2007, rapid response cruises are beneficial in responding to isolated events. These types of data are useful in building a long-term hypoxic database for the Texas shelf and are necessary for future efforts in mitigating and predicting hypoxia formation on the Texas shelf.

Future extensions of this research primarily focus on building a longer time-series of physical data and developing an individual monitoring program for the Texas shelf independent of monitoring surveys on the Louisiana coast. Though the data analyzed in this research provided valuable insights into the spatial and temporal scales of hypoxia and the physical processes responsible for hypoxia formation, there was not sufficient data to examine long-term trends in the development and frequency of hypoxic events on the Texas shelf. The best way to improve monitoring and the prediction of hypoxia on the Texas shelf is to build an integrative ocean observing vertical water-column network, which includes *in situ* sampling to effectively monitor physical conditions on the Texas shelf. By collecting more data, the foundations of this research can be expanded into predicting and modeling hypoxic events on the Texas shelf.

### **3. DETERMINING HYPOXIC AREA ON THE TEXAS SHELF**

#### **3.1 Introduction**

A combination of historical data, *in situ* sampling, real-time observations, and interpolation modeling was used to investigate the effects of the physical environment and stratification on the formation of hypoxia and the area of hypoxia on the Texas shelf. The field observations of hydrographic properties from shipboard surveys and real-time ocean observing systems address the evolution and duration of hypoxia on the Texas shelf. Bottom dissolved oxygen collected by NOAA SEAMAP have been used in geostatistical models to determine hypoxia area on the Texas shelf since 2002 and to determine how estimating area on the Texas shelf is impacted by the larger hypoxic area on the Louisiana shelf. The purpose of geostatistical modeling is to investigate how the size and spatial structure of hypoxic area changes annually and to determine which model is most suitable and accurate for estimating hypoxic area on the Texas shelf.

#### **3.2 Data and Methods for Determining Texas Hypoxic Area**

##### *3.2.1 Data*

Since 1985, the current federal management estimate for Gulf of Mexico hypoxia area is determined from a mid-summer annual survey led by LUMCON (Rabalais et al. 2001b). The area estimated is compared to the federally mandate area reduction limit of

5,000 km<sup>2</sup> and is used to gauge progress of mitigation efforts, such as nutrient reductions, in the MARS watershed (Action Plan 2008). LUMCON survey data are collected during the month of July and are primarily focused on measuring the size of the Louisiana coastal hypoxia; the cruise only surveys the northern Texas shelf if Louisiana coastal hypoxia extends far west of the MARS region. Therefore, these cruises are not useful in estimating hypoxic area on the Texas shelf. In this study, I attempt to develop a suitable geostatistical model to estimate hypoxic area and to understand the historic variability of hypoxic area on the Texas shelf.

The data used this study were bottom dissolved oxygen collected by NOAA NMFS surveys from June to August 2002 to 2011 (<http://www.ncddc.noaa.gov/hypoxia/>). A data summary, including the duration of the cruises, is given in Table 3.1.

NOAA NMFS SEAMAP cruises are conducted annually in conjunction with the SEAMAP summer groundfish surveys in the northwestern Gulf of Mexico. Hydrographic data are collected from south Texas to the Mississippi River delta in addition to the fishery surveys. The length of cruises can vary year-to-year and sampling design is randomized and predetermined. Data are publicly available and can be downloaded along with ESRI ArcGIS shapefiles and interpolated maps of bottom dissolved oxygen concentrations (<http://www.ncddc.noaa.gov/hypoxia/>). The published data have undergone federal quality control and assurance (QA/QC) designed by NOAA's Office of Ocean Exploration and Research (<http://www.ncddc.noaa.gov/oer/>).

These procedures will not be discussed in this dissertation, but can be accessed at <http://www.ncddc.noaa.gov/hypoxia/oer>.

The NOAA SEAMAP data also include a published procedure for interpolating bottom dissolved oxygen data, which is not currently provided with the LUMCON area estimates. The method for creating the SEAMAP dissolved oxygen interpolation maps is published at [www.ncddc.noaa.gov/hypoxia](http://www.ncddc.noaa.gov/hypoxia). This procedure, which is common for most NOAA data products (<http://www.ncddc.noaa.gov/oer/>), applies a geostatistical interpolator (ordinary kriging). No hypoxia area is estimated, but contours below 2.0 mg/L are highlighted to indicate hypoxia on the shelf. The method is primarily used for visualization purposes and is not suitable for scientific analyses. Methodology and results in this chapter will address the suitability and the potential bias in this procedure for accurately determining area on the Texas shelf (Sections 3.3 and 3.4).

Data files downloaded directly from NOAA include general cruise logistics, station latitude and longitude, depth, and bottom dissolved oxygen concentrations in milligram per liter (mg/L). The data do not include a projected coordinate system identified in the metadata file, but do include the datum (North American Data 1983).

Before proceeding to the modeling component, I reprojected the original data into a new projection—North American Albers Equal Area (NAAEAC). NAAEAC was selected for its commonality in geographic and oceanographic studies in North America, such as products published by NOAA and USGS ([usgs.gov](http://usgs.gov)). The NAAEAC projection preserves the area of a feature in an east-to-west orientation rather than north-to-south and reduces distortion using two standard parallels versus one standard parallel (Synder

and Steward 1997). Hypoxic area in the northwestern Gulf of Mexico is larger in the east-west direction (along-shelf) than in the north-south direction (across-shelf), which makes NAAEAC a suitable projection for the interpolation modeling.

### *3.2.2 Base Map Design*

After selecting a projection, the next step was to construct a base map in ESRI ArcGIS 9.3 (ArcGIS; <http://www.esri.com/software/arcgis>). I chose this platform for two reasons:

1. To show the versatility of ArcGIS in oceanographic coastal studies and,
2. To investigate different interpolation methods for determining hypoxic area using one program accessible to many types of users.

The basemap was constructed with publically available layers downloaded from federal and state geographical information systems. The layer types and sources used in the basemap are listed in Table 3.2. All layers were reprojected into NAAEAC for QA/QC in the interpolation modeling to ensure accuracy in calculating spatial extent of hypoxia along the Texas coastline and that alignment of coastal features, such as the location of the Brazos River (Figure 1.1), was geographically correct.

## **3.3 Geostatistical Interpolation Methods**

For the interpolation model studies, the NOAA SEAMAP procedures (herein referred to as *Default* model) were recreated and adjusted for comparing the different

types of interpolation models. Calculating area from NOAA SEAMAP methods included the following steps:

1. Importing data files into ArcGIS program,
2. Selecting ‘Geostatistical Analyst’ and running interpolation for dissolved oxygen with ‘Ordinary Kriging’ as the interpolation type,
3. Classifying the resulting interpolation map into 16 equal intervals ranging from 0.00 to 8.00 mg/L,
4. Reclassifying the map output into a vector shapefile,
5. Creating a polygon that outlines the spatial extent of sampling stations for each leg of the NOAA SEAMAP survey cruise,
6. Clipping the vector shapefile created in Step 4 to the polygon created in the previous step and,
7. Recoloring the resultant clipped vector shapefile to show hypoxic levels as red and oxygenated waters as green.

The steps as published consider each leg of a NOAA SEAMAP survey as an independent cruise. To test the interpolation models, the procedures were adjusted to account for one continuous sampling area. First, multiple survey legs were merged into one survey area. Connecting the locations of the outermost stations created a boundary polygon for each year. The interpolation map created from the models was clipped to the respective polygon, resulting in an area estimate dependent on the boundaries of the NOAA SEAMAP surveys. By deviating from the NOAA procedures here, my

interpolation model areas are different from the NOAA SEAMAP published products, even though the model design is the same (Section 3.3).

Interpolating and then clipping the result by year, versus interpolating across a uniform polygon for the entire shelf, was chosen. NOAA SEAMAP sampling sites are selected randomly each year. Because the same locations may not be sampled year-to-year, the survey polygon was created specifically for each year. For this study, it is also not appropriate to extrapolate outside the survey extent, because there are no data to validate the result and extrapolation may result in a biased overestimate of hypoxic area if stations are hypoxic along the polygon boundary.

### *3.3.1 Interpolation Model Selection*

Two types of interpolators were selected for this study – deterministic and geostatistical. Two deterministic models and one geostatistical model were calculated using the ESRI ArcGIS 9.3 Geostatistical Processing toolbox. The specific models were selected to examine the variance between the different types of interpolation categories and the estimated hypoxic areas. The models investigated in this research included: inverse distance weighted (IDW, deterministic), local polynomial interpolation (LPI, deterministic, and ordinary kriging (geostatistical).

Ordinary kriging was selected as the geostatistical model, because NOAA uses this method for visualizing coastal hydrography in the Gulf of Mexico. More so, the published procedure allows a baseline to be set for comparing area results from adjusting components in the current model, such as spatial autocorrelation of bottom dissolved

oxygen. By replicating the NOAA interpolations, I can address if bias exist in the published SEAMAP products and determine if a more accurate model can be developed. Kriging, as a geostatistical interpolator, requires a familiarity of the spatial scales of the dataset interpolated, as the resulting interpolated surface is based on the statistical trends, or the autocorrelation, of the process analyzed. By selecting ordinary kriging, I am also able to model the physical along- and across-shelf scales discussed in Section 1 to compare how spatial statistics vary annually along the shelf and how statistical trends impact accuracy of estimating hypoxic area on the Texas shelf. Furthermore, ordinary kriging is a relatively simple and flexible kriging method applicable for estimating trends in environmental data (discussed further in Section 3.3.2).

Deterministic interpolators are computationally simpler and do not require statistical knowledge about the process being investigated. These two methods create surfaces based exactly on the value of each individual point and not the statistical trends or change between the points. The resultant surface is typically smoother when compared to geostatistical surfaces. The specific deterministic interpolators were selected to test both the accuracy and functionality of a simpler interpolator to estimate hypoxic area for a user, such as a federal manager, who may not understand the across- and along-shelf scales of physical properties in the Gulf of Mexico. I constructed the following hypothesis to statistically compare the two categories of interpolators:

*H<sub>0</sub>: There are not significant differences between Texas hypoxic areas calculated from deterministic and geostatistical interpolation models ( $u_n = 0$ ).*

Area estimates produced by the two deterministic models were not significantly different from area estimates produced by the kriging models based on N-way ANOVA and independent  $t$ -tests. Deterministic methods do not help address why hypoxic area forms on the shelf, because the methods do not require prior knowledge of the statistical environment on the shelf. Therefore, methodology and results for the deterministic interpolations will be discussed in Appendix E. The remainder of this chapter focuses specifically on the ordinary kriging model methodology, which addresses the spatial scales of bottom dissolved oxygen and its changes across and along the Texas shelf.

### *3.3.2 Geostatistical Interpolation and the Ordinary Kriging Model*

Kriging calculates a predicted surface from the statistical properties of the bottom dissolved oxygen concentrations across and along the shelf. Kriging does not require normality in the data and provides an unbiased predictor. The method produces uncertainty (error) surfaces in addition to a predicted (interpolated) surface. Different kriging scenarios can be compared by creating multiple types of statistical surfaces with varying search neighborhoods, such as changing the distance or direction weighting between stations and adjusting for isotropic versus anisotropic (spatial autocorrelation) trends in the data.

Kriging builds a spatial-dependence model quantified from the data (variography) and predicts a new dissolved oxygen value from the variography, the spatial statistics, and the bottom dissolved oxygen levels around the measured sample sites. Kriging assumes zero mean for random errors in the data and the distance and

direction between any pair of random errors influences the covariance between the data pair, rather than the exact location of the pair (Cressie 1993; Lloyd 2010).

The primary method used here is ordinary kriging. Ordinary kriging assumes the linear model with intrinsic stationarity:

$$Z_t(s) = \mu + \varepsilon(s), \quad (3.1)$$

where  $Z_t(s)$  is the  $t^{\text{th}}$  realization at location  $s$ ,  $\mu$  is a constant, but unknown, true mean, and  $\varepsilon(s)$  is the error term, or residuals (Cressie 1988, 1993; Johnston et al. 2004).

One of the constraints of ordinary kriging is the decision-making required for incorporating statistical information into the model. There are a number of important trends, models, and parameters that must be considered in the kriging design (Cressie 1993). To not deviate far from the NOAA SEAMAP procedures and to assess different combinations of ordinary kriging models, an ellipse was selected for the search neighborhood shape (NOAA SEAMAP default). The search neighborhood size was adjusted to include at least 2 to 10 data points to keep consistency with deterministic interpolation model ESRI ArcGIS default. A search neighborhood of 2 data points eliminated a “bulls-eye” effect or non-realistic area around one sampling site.

One of the important objectives of my research is to understand the annual variability of hypoxic area on the Texas shelf, which requires quantifying the spatial structure and statistical trends for each year. The goal is to determine the most appropriate interpolation model for estimating hypoxic area on the Texas shelf. To address the spatial scales, two parameters were selected for importance in modeling the statistical and spatial trends of bottom dissolved oxygen on the Texas shelf: *Anisotropy*

and *Lag*. Adjustments in each parameter accounted for the error, spatial autocorrelation, and directional, spatial, and distance trends in the data.

In addition to the parameters previously listed, two kriging covariance models were compared – *Spherical* and *Gaussian*. *Spherical* is the covariance model used in the NOAA SEAMAP interpolations and *Gaussian* covariance model is utilized in objective analysis, or optimal interpolation, a technique common to studying ocean or atmosphere phenomena (Denman and Freeland 1985). Statistical analysis (one-way and N-way ANOVA, independent *t*-tests) showed no significance differences between yearly hypoxic areas and the covariance models (Appendix E).

An additional dependent variable (*Data*) to investigate if estimating hypoxic area on the Texas shelf is affected by Louisiana coastal hypoxic area estimates (e.g. Is the hypoxic area on the Texas shelf masked in interpolation models applied for the entire northwestern Gulf of Mexico shelf?) was also incorporated. For this variable, *SEAMAP ALL* designated all sampling sites for a given year on the shelf and *SEAMAP TX* represented only the sampling sites on the Texas shelf.

### 3.3.3 Directional Influences (*Anisotropy*) and Spatial Trends

Anisotropy, a property where autocorrelation changes with both distance and direction between two locations, can influence the kriging model results. Anisotropy, rather than isotropy (change only with distance) should be considered if there is a known directional trend in the data analyzed. Anisotropy impacts the covariance model and the interpolated values (Cressie 1993, 1988). The directional trend is usually not known, as

with a global trend that can be explained and modeled by a mathematical formula (Cressie 1993). Since the direction trend is not initially known, it is modeled as random error and quantified in the kriging model by estimating the spatial relationship of a search, such as a trend in the north to south direction (Cressie 1993, 1988). Five exploratory statistical techniques were tested to determine if distance and directional trends exist in the NOAA SEAMAP data.

The first method, average nearest neighbor, determines the average distance (km) between NOAA SEAMAP stations on the Louisiana-Texas (*SEAMAP ALL*) and Texas (*SEAMAP TX*) shelf. All possible differences are measured between pairs of sites and averaged. Results are shown in Table 3.3. For *SEAMAP ALL*, values ranged approximately from 9.4 to 12.6 km and from approximately 9.6 to 12.8 km for *SEAMAP TX*. There were small, but not significant (independent *t*-test,  $p\text{-value} > 0.05$ ) differences, ranging from approximately 0.1 to 0.6, between the two datasets.

Moran's Index was computed for each year to examine the spatial autocorrelation (Table 3.3) and measures the similarity in the data based on location and bottom dissolved oxygen concentrations. The resultant test statistic, Moran's *I*, provides a measure describing the distribution (cluster, disperse, or random) of sites (Mitchell 2005). Values near +1 represent dispersion and near -1 represent clustering. The null hypothesis test for Moran's *I* test was no spatial clustering exists in either *SEAMAP ALL* or *SEAMAP TX* data (Mitchell 2005). The *p*-values for the Moran's *I* test are reported in Table 3.3 and showed no significance for any year ( $p\text{-value} > 0.05$ ).

Direction distribution, the third method, examined if a direction trend exists and estimated an ellipse based on the standard deviation of the data. Directional values are shown in the Table 3.3 and the shape of the standard deviational ellipses are shown Figure 3.1 for each year and *Data* variable. One standard deviation ellipses (68 % cover of sampling sites) are shown. The ellipses change annually based on the area covered in the NOAA SEAMAP survey. For *SEAMAP ALL*, the average direction distribution was approximately 70 degrees and for *SEAMAP TX* was approximately 45 degrees.

The fourth method, Voronoi mapping, was implemented to examine the local variability within the *SEAMAP* datasets for each year. Two types of Voronoi maps were examined – cluster and standard deviation (Figure 3.2 and 3.3). Voronoi maps are a series of polygons, in which the polygon size represents the distance between sampling sites. The boundaries of the polygon are drawn so that the sampling site is at the centroid of each and closest to the boundary than any surrounding sampling site (Johnston et al. 2004). Voronoi maps are another visualization to determine how clustered or dispersed sampling sites are on the Texas shelf. For this research, each map provided initial observations about the error associated with the interpolation estimate based on the size of the polygons. Voronoi mapping also allowed me to investigate the variation in bottom dissolved oxygen across different years and with changing the dataset from including all sites versus isolating only sites on the Texas shelf.

The cluster Voronoi map identifies local outliers (Johnston et al. 2004) and was used here to verify if hypoxia was measured on the Texas shelf in order to compare data from sites against the interpolation results. An estimate of the hypoxic structure can also

be estimated from a cluster Voronoi map. An example of Voronoi outputs for bottom dissolved oxygen concentrations on the Texas shelf in years 2007 and 2008 is shown in Figure 3.2. In year 2007, the output indicated a large and narrow hypoxic area (dark red) off the northern Texas coast originating near the Brazos River delta. There was also a large and wide hypoxic area on the Louisiana shelf, indicating that interpolation results should produce large area estimates for both *SEAMAP ALL* and *SEAMAP TX*.

The bottom two panels of Figure 3.3 show the results for the standard deviation Voronoi map for 2008, a year with a large mid-summer Louisiana coastal hypoxic area. Standard deviation Voronoi maps estimate the local variation in the interpolation surface. In this year, variation was low at the edges of the region, because bottom oxygen values are high and do not fluctuate between sites. Variation was higher near sites with low bottom dissolved oxygen, which occur north and south of the Brazos River delta.

The final tool implemented was a trend analysis diagram. Trend analysis diagrams provide a three-dimensional perspective of the data and help to identify potential spatial trends by fitting polynomials on axes representing the bottom dissolved oxygen across and along the Louisiana-Texas shelf (Johnston et al. 2004). Trend analysis diagrams are used here to determine if the trends are linear or nonlinear. The diagrams are not used to quantify the trend, because I am only interested in the results for developing the different kriging models, such as if anisotropic conditions should be included and if the across- and along-shelf distances vary.

Figure 3.4 shows the data for 2002 with the x-axis representing sites from east (Louisiana) to west (south Texas) and the z-axis representing the along-shelf concentration (low to high moving east to west). The y-axis is the across-shelf bottom dissolved oxygen concentrations (inshore to offshore). The data are spaced on the axes by bottom dissolved oxygen with the graph origins representing low (near 0 mg/L) and to high (8 mg/L) concentrations.

The across- and along-shelf trends were nonlinear in 2002 with lower values of bottom dissolved oxygen occurring inshore and starting from the Mississippi River delta extending over to the mid-Texas shelf (near the Brazos River delta). Similar analysis was performed for 2003 to 2011 and similar trends were evident in 2004, 2007, and 2008. However, trends were varied and became more linear in 2003, 2005, 2009, and 2011 indicating higher bottom dissolved oxygen values on the Texas shelf. Since the trends were not similar for all years, I did not consider a global trend to exist in the dataset, which required no trend removal in the dataset before use in the ordinary kriging models.

Observations from these five methods showed that directional influences and spatial trends exist on the northwestern Gulf of Mexico shelf. More importantly, anisotropy changes when considering *SEAMAP ALL* versus *SEAMAP TX*. The results from these tests indicate that the parameter, *Spatial*, is important to include in the model design and that anisotropic versus isotropic model conditions can affect the final interpolated result.

### 3.3.4 Lag

The sampling autocorrelation lag for *SEAMAP ALL* and *SEAMAP TX* was examined to accurately model annual anisotropic conditions on the Texas shelf. In ArcGIS, the lag is spatial determination defined as a vector with a distance and direction representing how a particular phenomenon changes in the space investigated (e.g. northwest Gulf of Mexico moving from Louisiana to south Texas). All possible lags between sample sites are classified into bins of similar distance and direction (Johnston et al. 2004). The size of the lag can be modeled by the software (NOAA SEAMAP *Default*) or user-defined based on the statistical trends of the phenomenon modeled. If the lag size is too small, it can mask local variability. If too large, it can not capture the correlation between any distance and direction in the system.

For this research, 12 bins were preselected to keep consistent with the NOAA SEAMAP interpolation standard, which is also the ArcGIS Geostatistical Analyst default size. To set-up the *Lag* variable, two types of lags were tested – *Default* and Adjusted Lag (*Adj Lag*). *Default* lag was calculated automatically in ArcGIS Geostatistical Analyst using Cressie's (1985) weighted least squares normalized algorithm to estimate a range estimate for the lag size based on the empirical covariance (Johnston et al. 2004). The *Adj Lag* is calculated as follows:

$$(\frac{1}{2} (D_{ij})) \div \text{Bin\#} \quad (3.2)$$

where  $D_{ij}$  is the length of the largest distance between two sample sites (km), and Bin# is the number of bins (Johnston et al. 2004). The *Adj Lag* for *SEAMAP ALL* and *SEAMAP TX* are shown by year in the ordinary kriging model statistics in Appendix E.

The lag size for the shelf-wide data (*SEAMAP ALL*) ranged between 30 to 70 km and 20 to 30 km for the Texas shelf (*SEAMAP TX*). The lags grouped by dataset show a larger spatial correlation between bottom dissolved oxygen values when considering the entire northwestern Gulf of Mexico shelf versus a smaller correlation between sites on the Texas shelf. The calculated lags only support the idea that spatial statistics on the shelf can differ and lag size should be adjusted in the ordinary kriging model to avoid potential bias in the interpolated area.

### 3.3.5 Ordinary Kriging Model Development

The following models were developed to compare how different ordinary kriging parameters affect estimating hypoxic area based on the spatial patterns and statistical trends described previously:

- a. Ordinary Kriging, *Spherical, Anisotropy, Default Lag*
- b. Ordinary Kriging, *Spherical, Isotropy, Default Lag*  
(NOAA SEAMAP Default)
- c. Ordinary Kriging, *Spherical, Anisotropy, Adjusted Lag*
- d. Ordinary Kriging, *Gaussian, Anisotropy, Default Lag*
- e. Ordinary Kriging, *Gaussian, Isotropy, Default Lag*
- f. Ordinary Kriging, *Gaussian, Isotropy, Adjusted Lag*

Each model was tested using *SEAMAP ALL* and *SEAMAP TX* datasets for years 2002 to 2011, excluding 2010 since the sample site data were not available from NOAA

SEAMAP. Herein, the kriging models and results are referred to by the abbreviations in Table 3.4.

### **3.4 Ordinary Kriging Interpolation Outputs and Model Assessment**

Each kriging model produced four output surface maps:

1. Bottom dissolved oxygen values for each sample site (raw data)
2. Predicted values of bottom dissolved oxygen
3. Prediction standard error
4. Probability threshold for occurrence of hypoxia

Examples for each of the output surfaces are shown in Section 3.5. The prediction standard error was calculated from the model variance, which is calculated from the differences between the interpolated and actual data results. The error represented the uncertainty of the model prediction. The probability surface map shows the probability that areas on the Texas shelf exceed a user-defined threshold, which in this case is 2.0 mg/L. To calculate this surface, data values are assigned a 0 if bottom dissolved oxygen concentrations are 2.0 mg/L and below. Values are assigned a 1 if concentrations exceed 2.0 mg/L. The individual ordinary kriging model was recalculated with this transformed dataset to produce the probability surface.

Hypoxic area was quantified by creating a polygon shapefile from the predicted map output by extracting the 2.0 mg/L contours for each year. For *SEAMAP TX* outputs, hypoxic area was clipped at the state line, in order to not include hypoxic area on the

Louisiana coast in the estimate. Area polygons were used to assess the structure of the hypoxic area to describe if events are independent over the Texas shelf or an extension of Louisiana coastal hypoxia westward. Area estimated from the size of the polygons were compiled and analyzed with simple linear regression to determine if the hypoxic area over the Texas shelf increased since 2002.

Methodology for testing the hypothesis and analyzing hypoxic area estimates included summary statistics (mean, standard deviation), linear regression, independent *t*-tests, and one-way and N-way Analysis of Variance (ANOVA) to determine if a correlation exists in area estimates by year and/or if similarities exist between the different ordinary kriging models. Parametric and nonparametric tests were applied to evaluate the variation across the different models to determine which ordinary kriging parameters (*Data*, *Spatial*, and *Lag*) are most critical in designing one model suitable for estimating area for any year.

New data were produced from each model and included statistics from each individual model, such as the covariance model and anisotropic parameters. The data were exported from ArcGIS as text files and assimilated into yearly model results (Appendix E). Statistical data collected are described in Appendix E and are not included in results section (Section 3.5) because only selected statistics were used to assess model performance.

Each model was subjectively assessed based on a particular set of statistical data produced, the cross-validation statistics. The selected subsets of cross-validation statistics were used to assess the model's individual and group performance: mean, root-

mean-square (RMSE), average standard error, standardized mean, and standardized root-mean-square (SRMSE). The combination of these prediction error terms describes how effectively the model predicts unknown values of bottom dissolved oxygen and allows the user to make an informed decision about which model produces more accurate predictions.

There were five criteria for assessing model performance and diagnostics based on the results of the summary statistics (Johnston et al. 2004) used:

1. *Predictions should be centered on the measured bottom dissolved oxygen concentrations (unbiased).*
  - a. Mean prediction errors will be near zero if the prediction errors are unbiased (1<sup>st</sup> criteria).
  - b. The standardized mean prediction errors, calculated by dividing the prediction errors by the standard errors, will also be near zero (2<sup>nd</sup> criteria).
2. *Predicted bottom dissolved oxygen concentrations should be close to the true (sample site) values.*
  - a. The RMSE, calculated from the square root of the averaged squared distances between predicted and actual bottom dissolved oxygen values, are small (3<sup>rd</sup> criteria).
3. *To assess the uncertainty, the predicted standard errors should be valid, which means the variability in the model is correct.*

- a. The average standard errors are close to the RMSE values. If the average standard errors are greater than the RMSE, the variability is overestimated in the model. If average standard errors are smaller than the RMSE, the variability is underestimated in the model (4<sup>th</sup> criteria).
- b. The SRMSE (prediction error divided by prediction standard error) should be close to 1. Values greater than 1 are underestimating the variability and less than 1 are overestimating the variability in the bottom dissolved oxygen predictions (5<sup>th</sup> criteria).

For these criteria, non-parametric rank matrices were created (1 = nearest to suitable criteria value and 6 = farthest from suitable criteria value) for each model by year. The mean and standard errors of the rankings were calculated to compare against model results for each year. Next, the top three lowest ranked models were selected for each criterion to determine which is the most accurate ordinary kriging model for estimating Texas shelf hypoxic area.

In addition to quantitative assessments, qualitative criteria for model performance were also investigated to compare the ranks given above to the hypoxic structures interpolated in each model. Qualitative assessment is important for evaluating whether the interpolated hypoxic structure is realistic based on the actual data and physical environment of the shelf. Assessments include examining the predicted surfaces for unrealistic areas, such as bull-eyes, or if the model resolves independent events, such as an event caused by increased freshwater discharge on shelf (e.g. Brazos flooding hypoxic event documented in DiMarco et al. (2012). Additional assessments

include examining the areas calculated by each model within a given year and how the area structure varies for the different models in relationship to the actual data. The qualitative analysis supplements the quantitative assessments as regards deciding upon one suitable ordinary kriging model applicable to the Texas shelf in any given year.

### **3.5 Ordinary Kriging Model Results**

#### *3.5.1 Area Estimates Produced by Ordinary Kriging Models*

The area estimates produced from the 12 models by year is shown in Table 3.5 (Recall the model abbreviations in Table 3.4). Hypoxia was only present in four of the nine years analyzed. The hypoxic areas estimated in the four years (2002, 2004, 2007, and 2008) tested significantly different from zero area using a 1-way ANOVA (p-values  $< 0.05$ ). The estimates ranged from 15 (2004 – *Sp All A*) to approximately 7,000 km<sup>2</sup> (2007 – *G TX A Adj*). Fisher's Least Squared Difference (FLSD) test showed that all years, except 2002 and 2007, are significantly different from one another (p-value  $< 0.05$ ).

Not all models in 2002, 2004, and 2007 estimated an area (Table 3.5). The only year in which all models estimated hypoxia was in 2008. The means were recalculated removing models with zero area estimates and herein are referred to in the analysis as *Excl Years*. Independent 2-sample *t*-tests comparing original and *Excl Years* (Table 3.5) for a given hypoxic year (e.g. 2004) did not show significant differences (p-value  $< 0.05$ ) for mean comparisons for *Year*, *Model*, *Data*, *Spatial*, and *Lag* parameters.

An ANOVA (1-way) test and box plot for *Year* shows significant differences in area estimates ( $p\text{-value} < 0.05$ ) by year (Table 3.5 and 3.6, Figure 3.5). The greatest range in model area estimates was seen in the 2007 data with areas from 0 to approximately 7,000 km<sup>2</sup>. However, the 2008 data showed the largest estimates ranging from 4,700 to 6,200 km<sup>2</sup>. The smallest range in area estimate occurred in 2004 (0 to ~ 450 km<sup>2</sup>). The range in estimates for 2002 was approximately 0 to 4,700 km<sup>2</sup>.

Based on yearly means and the range of area estimates, the years with hypoxia can be classified into three categories: Small (1 – 1,000 km<sup>2</sup>), Moderate (1,001 – 3,000 km<sup>2</sup>), and Large (3,001 – 5,000+ km<sup>2</sup>). The mean areas are shown in Table 3.5 and classifications by years are:

Small: 2004

Moderate: 2002, 2007 (including zero estimates)

Large: 2007 (excluding zero estimates), 2008

Year 2007 overlaps two categories depending on which mean (*All Years* versus *Excl Years*) is considered. The area range in 2007 model estimates is discussed in Section 3.7. The remainder of this chapter will emphasize the four hypoxic years and the classifications by first examining the hypoxic structure for each category and then investigating how the adjustments in *Data*, *Lag*, and *Spatial* parameters affect the ordinary kriging model results (recall parameter descriptions in Section 3.4).

### 3.6 Surface Results of Ordinary Kriging Models

Prediction, standard deviations, and probability threshold surfaces were created for each of the 12 ordinary kriging surfaces from 2002 to 2009 and 2011. Surfaces were not created for 2010, because of insufficient data available from the NOAA SEAMAP website. All surface results are included in Appendix E. Only surface results for 2002, 2004, 2007 and 2008 *G TX A Adj* model are discussed here, as this model includes all possible spatial parameter adjustments. The *G TX A Adj* model resulted in area estimates for each year in the respective categories and includes significant results for the variables analyzed in later sections. The significance of these results is discussed in Section 3.7.

#### 3.6.1 *G TX A Adj* Surface Results for Years 2002, 2004, 2007, and 2008

The distribution of hypoxia varied by year. Sample sites from NOAA SEAMAP surveys are shown in panel A (upper left) and hypoxic sites are colored dark red. Not all sites in a given year were hypoxic. In 2002, the southernmost locations for hypoxia on the Texas shelf were near Matagorda Bay (Figure 3.6) as well as south of Galveston Bay. In 2004, hypoxia was only measured north of the Brazos River delta off Galveston Bay (Figure 3.7). Hypoxia was concentrated near and directly south of the Brazos River delta in 2007 (Figure 3.8). In 2008, hypoxia was concentrated north and south of the Brazos River delta and near the Texas-Louisiana state line coinciding with large number of hypoxic sites in Louisiana waters (Figure 3.9).

Panel B (upper right) shows the predicted bottom dissolved oxygen surface for all years of the *G TX A Adj* scenario. Hypoxic area is indicated by the dark red color. The predicted hypoxia area varied by year. In the *G TX A Adj* models, predicted area coincided with hypoxic sites and the shape of the hypoxic regions vary by year. The structure shows independent regions in 2002, 2004, and 2007 from Louisiana coastal hypoxia (figures 3.6, 3.7 and 3.8). The structure in 2002 extends from Galveston Bay down to Matagorda (Figure 3.6). In 2004, the estimate area is smaller and located directly off Galveston Bay (Figure 3.7). In 2007, the large predicted area started on the north Texas shelf and continued down the mid- to south Texas shelf (Figure 3.8). Structure differed in 2008 with the predicted area on the Texas shelf connected to Louisiana coastal hypoxia (Figure 3.9).

The predicted standard error surface (mg/L) for the selected model and years is shown in Panel C (lower left). Low errors ( $< 1$  sd) range from dark blue (lowest) to light blue ( $\sim 1$ ), which indicates the *G TX A Adj* model accurately estimates bottom dissolved oxygen on the Texas shelf. Large errors ( $< 1$  sd) range from light pink ( $\sim 1$ ) to dark red ( $= 3$ ). Large errors indicate an inaccurate depiction of bottom dissolved oxygen by the interpolation models. The predicted standard errors were patchy for all years with low values correlating to larger density of sample sites (e.g. near Galveston Bay). Errors increased in regions on the shelf with a low sample site density, such as the south Texas shelf near Mexico. For this particular model, the predicted standard areas were below 1.0 in most years, with overall lowest values for year 2007 (Figure 3.8).

The predicted standard error was larger for years when hypoxia comes from the Louisiana shelf, such as 2008 (Figure 3.9).

The final panel (Panel D – lower right, Figure 3.6 – 3.9) maps the probability surfaces that an area on the shelf will exceed the threshold of 2.0 mg/L. The probability threshold surfaces do not necessarily match predicted hypoxic areas in panel B, which is especially true for 2002, 2004, and 2008 (Figure 3.6). Yellow to light green colors in Panel D indicate areas of low probability that measurements collected in an area on the shelf will exceed 2.0 mg/L. The lowest probability, or likeness for hypoxia, was seen for a small area in 2002 (Figure 3.6) and for the Brazos River event in 2007 (Figure 3.8). The probability surfaces changed annually for the *G TX A Adj* models (figures 3.6 – 3.9) and within other models (Appendix E). Areas with no hypoxia showed a higher probability ( $> 0.60$ ) that bottom dissolved oxygen exceed the hypoxic threshold. These areas commonly occurred in years with no hypoxia on the Texas shelf and areas where sample sites were far from hypoxia, such as south of the Brazos River delta and near the Texas-Mexico border. The areas that show low probability ( $< 0.3$ ) coincided with the hypoxia areas estimated in the prediction surfaces for *G TX A Adj* models and models in Appendix E.

Overall, in all models, the probabilities reflected the certainty hypoxia is present based on the pattern in sampling sites combined with the estimated area. This means the probability surfaces more accurately represent the true area by the occurrence of a lower probability when hypoxia actually occurs and higher probability in areas with increased distance between sample sites, as seen in the higher resolution of probabilities on the

northern Texas shelf in 2002 (Figure 3.6). Probability threshold estimates also indicate issues, such as underestimation of anisotropy, that potentially exist in a given ordinary kriging model, as the calculation depends strongly on the actual, raw data values.

### 3.6.2 Year 2007 Ordinary Kriging Model Surface Results

Due to the variation ( $\sim 7,000 \text{ km}^2$ ) in model results for 2007, I decided to also examine the interpolation results for *Gaussian* kriging models to compare surfaces resulting from adjustments of the *Data* and *Spatial* variables. Recall that only *Gaussian* results are shown because no significant differences between *Model* (*Spherical* versus *Gaussian*) were found (Section 3.1).

In Panel A (Figure 3.10), hypoxic sites in 2007 are found predominantly at and south of the Brazos River delta. These sites correlate with the Brazos River flooding event described in DiMarco et al. (2012) and are seen in the Brazos River discharge profiles shown in Figure 2.1. There is also one hypoxic station near Galveston Bay and north of the delta, indicating the possibility of a second independent region or an extension of hypoxia from the Louisiana coast.

The interpolated surfaces for each model differ based on the significant differences in area estimates (Figure 3.5). The first comparison of spatial structure is between *Data* (*SEAMAP ALL* and *SEAMAP TX*) and *Spatial* (*Aniso* versus *Iso*) models (Figures 3.10 – 3.13). The structure and origin of the areas change between the *Aniso* and *Iso* models for *SEAMAP TX* and *SEAMAP ALL*. For both *Spatial* models for *SEAMAP ALL*, there are no hypoxic regions interpolated on the Texas shelf (Figures

3.12 and 3.13). The hypoxic area is predicted to be the same for both *SEAMAP TX Iso* and *Aniso* model results (Figures 3.10 and 3.11).

The predicted standard error surfaces also reflect the variations among the interpolated surfaces for *Data* and *Spatial*. The standard error is large ( $< 1.1$  mg/L) for *SEAMAP ALL* surfaces (Figures 3.12 and 3.13). Larger errors are also calculated in south Texas corresponding to gaps in the NOAA SEAMAP surveys for both *Data* surfaces. The predicted standard error is lower ( $< 1.0$  mg/L) for the *Aniso* surfaces compared to *Iso* surfaces, which range between 1.0 and 1.5 mg/L. For the *SEAMAP TX*, the errors differ for the *Iso* and *Aniso* results with more variability in the predicted errors occurring in the *Iso* results (Figure 3.10). The errors are below 1.0 mg/L in the mid shelf at the hypoxic region and the south Texas shelf in the *Iso* results (Figure 3.10). The same shelf locations in the *Aniso* results are at 1.0 mg/L and above with less variability across the modeled surface (Figure 3.11).

There are noticeable differences between model variables in the probability surfaces. For *SEAMAP ALL* surfaces, the threshold probability for exceeding 2.0 mg/L is low ( $< 0.2$ ) for Louisiana coast and high ( $> 0.6$ ) on the Texas shelf (Figures 3.12 and 3.13). For *SEAMAP TX* surfaces, the probability surfaces correspond to the similar hypoxic area structures in the *Iso* and *Aniso* results (Figures 3.10 and 3.11). The probabilities are the lowest in the hypoxic area originating from the Brazos flooding event ( $< 0.3$ ), but are larger ( $> 0.4$ ) for the smaller hypoxic region north of the Brazos River delta.

### 3.6.3 Summary of Ordinary Kriging Model Surface Results

Based on the qualitative analysis of the model surfaces, hypoxic structure varies between years in addition to the amount of area estimated. In any given year, hypoxic structure can result in small or large independent areas (e.g. 2004 and 2007) or in an extension of Louisiana coastal hypoxia westward (e.g. 2008). The structure can also vary across different ordinary kriging scenarios as a result of adjusting variables. Considering both *Data* and *Spatial* results in different estimated areas and structures of hypoxia on the Texas shelf in a given year. *SEAMAP TX* models with *Lag* overestimate area in moderate-large ( $> 2,000 \text{ km}^2$ ) and large ( $> 3,001 \text{ km}^2$ ) years (e.g. 2007). However, models with *Lag* perform better than models without in estimating independent regions on the Texas shelf and in small and small-moderate ( $< 2,000 \text{ km}^2$ ) years (e.g. 2002 and 2004).

Interpolated surfaces using *SEAMAP ALL* can mask the formation of hypoxia on the Texas shelf even though hypoxia was measured at sample sites and there was evidence of the 2007 Brazos flooding event responsible for hypoxia forming (DiMarco et al. 2012). When comparing *Spatial* variable, isotropic (*Iso*) conditions in the model created circular, and often separated, hypoxic regions as seen in 2002 and 2007. Anisotropic (*Aniso*) conditions in the model result in more elongated areas in the north-south direction and narrower areas in the east-west direction reflecting the results of spatial trend analysis in Section 3.1 and the along- (20 – 35 km) and across-shelf (10 – 20 km) physical scales on the Texas shelf discussed in Section 1 and earlier in this section.

### 3.7 Comparisons of Ordinary Kriging Model Parameters (*Data*, *Spatial*, *Lag*)

Based on the area estimates and qualitative surface analysis, *Data* and *Spatial* ordinary kriging model variables result in different hypoxic area estimates on the Texas shelf. In addition, *Lag* is related to the anisotropy and affects the interpolation search distance and correlation between sites (recall Section 3.3.4). In this section, I quantitatively assess the differences in area estimates for hypoxic years based on the adjustments for *Data*, *Spatial*, and *Lag* parameters.

#### 3.7.1 Comparisons of Ordinary Kriging Model Parameters

Figure 3.14 shows the results from a series of ANOVA and FLSD tests between hypoxic years and the model parameters. Each matrix highlights significant differences (p-value < 0.05) in dark red. Estimates in 2008 were significantly different from all other years for each parameter, which is indicated in blue (Figure 3.14). Differences between all years and 2008 were due to the large hypoxic area on the Louisiana coast, which influenced interpolation results on the north Texas shelf seen in the area estimates (Tables 3.5 and 3.6) and interpolated surfaces (Appendix E).

Beginning with *Data* comparisons, moderate hypoxic years show an interesting result compared to other hypoxic years. For *SEAMAP ALL*, 2002 is significantly different from all years, whereas considering only *SEAMAP TX*, 2007 is significantly different from all years except 2008 (p-values < 0.05). The location of hypoxia formation on the Texas shelf accounts for the differences between the moderate years, in

that the structure of the hypoxic area was different. In 2002, the area estimate is a result of the influential and large hypoxic area on the Louisiana coast extending westward. In 2007, the origin of the hypoxic area starts at the Brazos River delta and extends south as a long, narrow band along the Texas coast, with little or no apparent connection to the Louisiana shelf.

The *SEAMAP ALL* results can underestimate or mask out separated regions of hypoxia on the Texas shelf that occur at or south of the Brazos River delta (e.g. Figure 3.8). Potential masking is supported by no significant difference between 2004 (small year) and 2007 (moderate-to-large year) in *SEAMAP ALL* comparisons. *SEAMAP TX* estimates capture independent regions on the Texas shelf above and below the Brazos River delta, but can potentially over exaggerate the area. Overestimation is statistically supported by there being no significant difference between 2007 and 2008 (p-value < 0.05, Figure 3.14). The change in moderate-year significance also supports the theory that another parameter(s) may be necessary for more accurately estimating hypoxia on the Texas shelf.

### *3.7.2 Lag and Spatial Ordinary Kriging Model Results*

Parameters that can influence the hypoxic area estimates are *Lag* and *Spatial*, in which both terms address the statistical scales of bottom dissolved oxygen changes across and along the shelf. I have compared the area estimates for models with both parameters to investigate which parameter related to autocorrelation is more important in

estimating an accurate hypoxia structure each year and which parameter accounts for the range of area estimates across all models and years.

*Lag* results show no significance difference in the *Default* conditions between years, except for 2008. No difference is likely attributed to using the same autocorrelation length for all years. *Default* option in the models does not consider spatial changes in the along- or across-shelf distances. When adjusting the model for lag size by year, significant differences in area estimates exist between all combinations of years except 2007 and 2008 and 2002 and 2007 (p-value < 0.05, Figure 3.14). No significant differences suggest that distances between sites relative to the change in bottom dissolved oxygen on the shelf may be similar in each year in the NOAA SEAMAP surveys independent of the *Data* parameter.

When comparing the *Spatial* parameter, 2008 is the only year significantly different from the other hypoxic years (Figure 3.14) for *Iso*. The result indicates that no direction or distance differences exist in the across- and along-shelf scales for the other years analyzed. When including anisotropy (*Aniso*) in the kriging models, all years significantly differ from one another indicating that spatial trends are important to estimating hypoxic area regardless of the other model parameters. Anisotropy in bottom dissolved oxygen on the Texas shelf affects the interpolated estimate, which further supports the idea that changing the physical conditions on the shelf impacts the spatial structure of hypoxia on the shelf (Section 2). Considering an isotropic (*Iso*) environment is not accurate for estimating area and does not allow delineation between years and the size of the hypoxic area.

Hypoxic area estimates for moderate and large hypoxic years were normalized to the respective yearly means and plotted in Figure 3.15 to further examine the influence of combinations of parameters to estimating area. Normalizing each model provided insight into selective combinations of parameters resulting in under- or overestimating area. The panels are organized by year and each model category abbreviation is organized by *Data* on the x-axis. The units for the y-axis represent normalized mean with units of 1,000 km<sup>2</sup> with 0 representing the yearly mean of all models.

In 2002, *SEAMAP TX* scenarios all underestimate area by 100 to 1500 km<sup>2</sup> with largest underestimate calculated by the *G TX A Adj* model. Two *SEAMAP ALL* estimates slightly underestimate area by approximately 100 km<sup>2</sup>. The *G All A Adj* model overestimates area by a factor greater than 1.5 (> 1,500 km<sup>2</sup>) relative to the mean of all models. The three *SEAMAP ALL* models underestimate mean area by 1,000 km<sup>2</sup> in 2007 whereas the three *SEAMAP TX* models overestimate mean area by approximately 250 to 1750 km<sup>2</sup>, with *G TX A Adj* accounting for the largest overestimate. In 2008, both *A Adj* models overestimate area by approximately 100 to 1,000 km<sup>2</sup>. All other models underestimate area by approximately 100 to 1,750 km<sup>2</sup> with lowest area estimated with the *G All I* model.

When considering all models in the three years, approximately ~44 % of the *SEAMAP ALL* models underestimate area by more than 1,000 km<sup>2</sup> compared to only one *SEAMAP TX* model, which further supports how *Data* parameter affects area estimate accuracy for the Texas shelf. Approximately 22 % of the *SEAMAP ALL* models overestimate area by greater than 500 km<sup>2</sup> compared to only one *SEAMAP TX* model (*G*

*TX A Adj*). Normalizing the model estimates the importance of *Data* in model design, specifically the improvements in estimating area on the Texas shelf when the data sites are limited to the Texas shelf. Isolating the sites reduces a potential masking effect (underestimation of Texas area) and/or overestimation on the northern Texas shelf given a large Louisiana coastal hypoxic area (e.g. 2008).

### 3.7.3 Summary of Ordinary Kriging Parameter Results

Statistical test results and the comparisons of normalized model means for moderate to large hypoxic years (2002, 2007, and 2008) show three parameters are responsible for the range of area estimates – *Data*, *Lag*, and *Spatial*. *SEAMAP TX* models better estimate hypoxic area and structure on the Texas shelf, but certain models can underestimate or overestimate area within 250 to 1,750 km<sup>2</sup> within a moderate (25 – 58 % area estimate difference) or large year (8 – 35 % area estimate difference). However, despite the estimation error, *SEAMAP TX* does not mask area on the Texas shelf as seen in *SEAMAP ALL* models.

Comparing *Lag* settings reveals that the distance and direction between sites is important in accurately calculating and representing hypoxic area on the Texas shelf. Not including any estimate of a lag assumes these length and directional distances are similar across the entire northwestern Gulf of Mexico, which is further supported in the *Spatial* results.

*Spatial* parameter is the most important of the three parameters analyzed. If only isotropic conditions on the Texas shelf are considered, there is no difference in distance

and directional changes of bottom dissolved oxygen along the shelf in any given year. The across- and along-shelf physical scales are important to understanding changes in bottom dissolved oxygen on the Texas shelf. Statistical results support the inclusion of anisotropy, above the other two parameters, into ordinary kriging models to accurately estimate hypoxic area and assess the hypoxic structure in any given year on the Texas shelf.

Finally, simple linear regressions computed for the mean areas by year do not show an increase in hypoxic area over time on the Texas shelf. The regression results were not included in this Section, but are included in Appendix E. With only 8 years available for analysis, the variance in the regression was too large to estimate a trend. Linear trend estimation was further complicated with having four hypoxic years in the dataset, with two of years categorized as small (2002, 2004), one year as moderate (2007), and one year as large (2008).

### **3.8 Comparisons of Ordinary Kriging Model Assessments**

It is not practical to run each individual model every year. To meet the research objectives outlined in Section 1 and to determine the most accurate ordinary kriging model for changing the current Gulf of Mexico hypoxia monitoring and management practices (Section 4), it is only necessary to assess model performance for moderate and large hypoxic years (2002, 2007, and 2008).

### 3.8.1 Ordinary Kriging Model Assessment Statistics

The individual model assessment statistics are included in Appendix E and will not be discussed here. Summary points regarding the assessment statistics from the Appendix E tables are:

- a. All values are near zero with no deviations greater than 0.05 in the mean and standardized means.
- b. The RMSE and standardized RMSE are close to 1 for all models in all hypoxic years.
- c. The largest deviations in the accuracy of the estimates occurred in 2007 (models *G TX A* and *G TX A Adj*), because of underestimating the variability (negative SRMSE) of the bottom dissolved oxygen and thus overestimating the hypoxic area. However, in 2002 and 2008, these two models more accurately estimate the variability and area on the Texas shelf.

### 3.8.2 Ordinary Kriging Model Assessment Methods

Rather than focusing on individual models, I attempted to determine model success by testing the SRMSE for all years versus hypoxic years and conducted a nonparametric rank comparison to evaluate all *Gaussian* models (recall there was no significance between *Gaussian* and *Spherical* models, Section 3.2) based on the six criteria outlined in Section 3.4.

To support the overall observations from all criteria, I conducted 1-way ANOVA and 2-sample independent *t*-tests for the parameters versus the SRMSE, which validated

whether the model was correctly estimating the variability in bottom dissolved oxygen on the Texas shelf.

### 3.8.3 Ordinary Kriging Model Assessment Results

Table 3.7 shows the results for both ANOVA comparisons for all years (2002 to 2011, excluding 2010) and hypoxic years (2002, 2004, 2007, and 2008). The 1-way ANOVA results showed all three parameters to be significantly different in SRMSE values for all years and only *Data* and *Spatial* to be important in hypoxic years. If each variable were not important in predicting area, there would be no significant differences in the SRMSE values. A N-way ANOVA with the three variables against *Year* also proved all possible combinations to be significantly different ( $p\text{-value} < 0.001$ ).

ANOVA tests of the parameters in only hypoxic years resulted in only *Data* and *Spatial* being significantly different ( $p\text{-value} < 0.05$ ) and *Lag* not significantly different in the SRMSE comparisons (Table 3.7). Results based on SRMSE assessment show that the interpolated shelf area, as well as the anisotropic trends, was critical to estimate the hypoxic area on the Texas shelf. Manually adjusting the lag distance in the model was important for examining changes in bottom dissolved oxygen across the shelf, but was not crucial to estimating area in hypoxic years.

I used non-parametric ranked assessments for the model criteria (recall Section 3.4) to reduce the number of suitable models down to 1 per year that best predicted bottom dissolved oxygen and estimate hypoxic area on the Texas shelf. Table 3.8 shows the non-parametric mean rank score results from ranking all *Gaussian* models to

the criteria outline in Section 3.4. The first column of the Table lists the models considered for the three years (2002, 2007, and 2008), which were selected to represent one year in each size category (small-2002, moderate-2007, and large-2008). One hypoxic year, 2004, was excluded because four of six *Gaussian* models did not estimate a hypoxic area on the Texas shelf. The second column orders the mean rank score for each of the models based on the average calculated from assessment criteria and the third column includes the hypoxic area estimated by each of the models.

Based on the mean rank ordering, one model has the lowest, or best score, of the six models considered – *Gaussian SEAMAP TX Anisotropic (G TX A)*. In each year, the average rank was 2.6 and below with the lowest rank in 2002. This meant *G TX A* yearly models estimate most accurately the true bottom dissolved oxygen on the Texas shelf. The lowest performing model was the *Gaussian SEAMAP ALL Isotropic (G All I)* model in 2002 and the *Gaussian SEAMAP TX Isotropic (G TX I)* model in 2007 and 2008. Both models resulted in mean rank scores above 4.4 indicating that model poorly performed in the lower rankings for the assessment criteria.

Examining how the *Data* parameter performed was also important, since earlier results showed more accuracy in in area estimates on the Texas shelf for *SEAMAP TX* models. In 2007 and 2008, *SEAMAP ALL* models performed better than *SEAMAP TX* models ranking in the 2<sup>nd</sup> to 4<sup>th</sup> positions. The *Data* models alternated positions in 2002 with 2 of 3 *SEAMAP ALL* models ranking in the lower 50 % of the assessment ranking. No one model received a ranking below 5, indicating that no one particular model received consistent lowest rankings of 6. On the other hand, no particular model ranked

lower than a 2, likewise indicating that no particular model performed in the top scores for assessment criteria ranking.

#### *3.8.4 Summary of Model Parameters & Assessment*

The analysis of assessment criteria, both with the ANOVA and non-parametric ranking, further supported that two parameters were more important in ordinary kriging model design – *Spatial* and *Data*. In the first assessment comparing SRMSE, *Data* and *Spatial* were most important for all years, not just hypoxic years as seen with the *Lag* parameter. In the rank comparisons, the model with the best performance in categorical hypoxic years was *Gaussian SEAMAP TX Anisotropic*. The consistency of this model in estimating bottom dissolved oxygen in the three years considered further supported the importance of only considering data on the Texas shelf to prevent masking of hypoxic area by the Louisiana shelf. Furthermore, this model showed the importance of considering the along- and across-shelf spatial autocorrelation in bottom dissolved oxygen across the Texas shelf and the importance of including anisotropy in model design to accurately estimate and categorize hypoxic area on the Texas shelf.

### **3.9 Ordinary Kriging Model Discussions and Future Research Directions**

#### *3.9.1 Discussion*

Accurately estimating hypoxic on the Texas is not a simple process. Results from the geostatistical interpolation modeling have shown that the spatial statistics on

the Louisiana and Texas shelf differ and these differences can greatly affect the hypoxic area estimated on the Texas shelf. Area estimates change depending on whether sample sites are included from the Louisiana shelf, which can overestimate area if there is a large Louisiana coastal hypoxia year. A large hypoxic area on the Louisiana shelf can potentially mask independent regions on the northern and mid-Texas shelf as seen with model estimates in 2007.

Geostatistical modeling assessment is also a subjective process, which further complicates trying to design one model appropriate for estimating Texas shelf area. Over 50 % of the ordinary kriging models performed reasonably solid based on assessment criteria. However, the statistical accuracy of a model is not the only consideration. Performance was also based on the model's capability to spatially resolve independent hypoxic regions on the Texas shelf as seen with the *G TX A Adj* and *G ALL A Adj* models in 2007.

An additional complication to spatially resolving area is seen in models with lag adjustments. Though *Lag* was not statistically significant in variable and assessment comparisons, the affect of adjusting lag is seen in *SEAMAP TX* models estimating small hypoxic areas ( $< 2,000 \text{ km}^2$ , e.g. 2002 and 2004 in Table 3.5 and Appendix E) and/or independent hypoxic regions on the Texas shelf. Model performance, based on assessment criteria, improves slightly when adjusting for spatial lag for small hypoxic years. However, in moderate-large ( $> 2,000 \text{ km}^2$ ) and large hypoxic years (e.g. 2007 and 2008), models with lag adjustments can overestimate hypoxic area on the Texas shelf (e.g. 2007 *G TX A Adj*, Table 3.5). Though estimating any hypoxia on the Texas shelf is

critical, moderate and large years are more important to estimating northwestern Gulf of Mexico hypoxia from a federal management perspective (Section 4).

Including the appropriate spatial scales in the interpolation model is necessary to accurately estimate area. Results from Section 3.5 show the two most important parameters to include in a geostatistical model are dataset and anisotropy. The largest improvements in model performance resulted from adjusting for anisotropy and the limiting the number of stations to only the Texas shelf. The isolation of the *Gaussian SEAMAP TX Aniso* model, which does not include lag, as the best performing in hypoxic years, supports this conclusion. This model provided the most accurate representation of hypoxic area on the Texas shelf for 2002 to 2011. Only considering sampling sites on the Texas shelf and not sites on the northwestern GOM shelf resolves potentially large hypoxic regions on the Texas shelf that result from Brazos River discharge and independent regions that may form on the north Texas shelf (e.g. 2002) independent of hypoxic conditions in Louisiana. Modeling the spatial autocorrelation distance and direction on the shelf accurately will best help to delineate between independent areas on the Texas shelf versus extension of hypoxic area from the Louisiana shelf.

### *3.9.2 Future Research Directions*

Categorizing the hypoxic area size and calculating the area is crucial in analyzing trends in hypoxia over time (e.g. Is hypoxic area increasing on the Texas shelf?) and is necessary for federal managers to design and implement monitoring and mitigation strategies for reducing hypoxic area in the northwestern Gulf of Mexico (Section 4).

This study addresses only one type of geostatistical model – ordinary kriging. Based on the results and conclusions in this study, the current ordinary kriging model implemented by NOAA SEAMAP does not accurately represent the spatial scales of bottom dissolved oxygen on the northwestern GOM shelf and does not provide an accurate estimate of hypoxic area on the Texas shelf. A simple improvement to the NOAA ordinary kriging model is to include anisotropy and to interpolate bottom dissolved oxygen on the Texas shelf independently from the Louisiana shelf to better determine the hypoxic area in the northwestern GOM. However, ordinary kriging may not be the best model and future efforts should look into different types of geostatistical models and techniques, such as geostatistical simulation modeling.

Additional efforts include conducting similar analysis with different types of kriging models, such as universal or indicator kriging. For instance, universal kriging applies a deterministic function, which may be obtained from a long time-series trend average of bottom dissolved oxygen across- and along-shelf changes on the Texas shelf. Indicator kriging is a binary method that considers a threshold for continuous data. In this case, the threshold could be designated based on the frequency of occurrence on hypoxia on the Texas shelf relative to hypoxia measured in a given year.

Regardless of method choice, future directions need to continue to consider different types of models to compare the accuracy of different kriging models to one another to improve accuracy in estimating area on not only the Texas shelf, but also the entire northwestern GOM shelf. Adding more years of data will improve the kriging models for estimating area on the shelf, in addition to comparing different kriging

models. The NOAA SEAMAP data analyzed in this research covers only years 2002 to 2011. Continuing to include additional years as the data becomes available will continue to improve hypoxic area estimates, as well as help to establish long-term trends and frequency of occurrence for hypoxic area on the Texas shelf.

## **4. POLICY AND MANAGEMENT CONSIDERATIONS FOR MONITORING TEXAS SHELF HYPOXIA**

### **4.1 Introduction and Motivation**

Hypoxia monitoring and mitigation policies have been a federal priority since 1997 with the establishment of the Mississippi River Gulf of Mexico Watershed Nutrient Task Force ([water.epa.gov](http://water.epa.gov)). This Task Force, managed by the Environmental Protection Agency (EPA), is tasked with understanding the effects of eutrophication on hypoxia formation in the Gulf of Mexico ([water.epa.gov](http://water.epa.gov)). Those efforts initiated a large stakeholder effort to design nutrient and water quality strategies to reduce Gulf of Mexico hypoxia (EPA Task Force 2008), and have directed millions of dollars of funding and resources to studying Gulf of Mexico hypoxia. The resulting strategies continue to guide funding opportunities. One of the major metrics for the Task Force is the reduction of hypoxic area on the Gulf of Mexico shelf. The management goal is to reduce the Gulf of Mexico hypoxic area to 5,000 km<sup>2</sup> by 2015 (EPA Task Force 2008). Reduction in the size of the hypoxic area is the primary indicator of success driving the mitigation policies outlined by the Action Plan (2008). However, to focus only on the Louisiana shelf in the Task Force's efforts does not accurately assess hypoxia in the northern Gulf of Mexico.

Current management and monitoring strategies acknowledge hypoxia primarily on the Louisiana shelf, with occasional occurrences of Louisiana hypoxia extending

westward on the northern Texas shelf. The Action Plan strategies often attribute those hypoxic events to the westward downcoast extension of the Louisiana coastal hypoxia and do not consider local processes responsible for formation of hypoxia on the Texas shelf or how hypoxic on the Texas shelf can significantly influence the yearly Gulf of Mexico area estimates.

Based on my estimates of hypoxic area on the Texas shelf, an area metric may not be the best metric for monitoring hypoxia on the northwestern Gulf of Mexico. The official survey estimates from the LUMCON cruises are not designed for sampling hypoxia on the Texas shelf and these cruises typically do not routinely sample west of Galveston Bay. My analysis of physical processes on the Texas coast shows conditions suitable for hypoxia formation and duration differ from conditions on the Louisiana shelf. Changing conditions also affects the hypoxic area that forms on Texas shelf, since events can be extensions of Louisiana hypoxia westward (e.g. 2008) or large independent events (e.g. 2007).

In addition to using area as the official metric, the assessment of hypoxic structure and controls and the capacity to reduce hypoxia to less than 5,000 km<sup>2</sup> needs to be reassessed. Interpolation results presented in Section 3 show that the hypoxic area on the Texas shelf can exceed the target goal, both for dependent (Louisiana coastal hypoxia) and independent (Texas shelf) regions. In this Section, I present considerations to improve the current management strategies for monitoring Gulf of Mexico hypoxia.

In addition to area-centric focus, strategies developed by the Task Force are also nutrient-centric, meaning recommendations focus on the voluntary reduction of nutrient

loads, and do not consider the role of physical processes in controlling Gulf of Mexico hypoxia formation (Bianchi et al. 2010). The primary management reductions and mitigations are focused on the Mississippi and Atchafalaya River systems and the large hypoxic area forming on the Louisiana shelf each summer. Even if the Louisiana hypoxic zone approaches the western shelf, the implemented governmental strategy of monitoring lacks accurate spatial and temporal observational resolution or coverage to adequately assess the extent of the hypoxic zone.

Current monitoring and reductions strategies may not be as effective as previously believed for the Gulf of Mexico. To address the role of Texas hypoxia from a management perspective, it is first necessary to understand the motivation behind federal policy development and then to discuss temporal and spatial occurrences of the Louisiana coastal hypoxia westward on the Texas shelf. Next, it is necessary to determine if independent hypoxic events occur on the Texas shelf and if so, policy and monitoring efforts need to be redirected to manage that coastal hazard.

#### **4.2 The Development of Management Strategies for Gulf of Mexico Hypoxia**

The need to monitor hypoxia in coastal waters originated from approval of the Clean Water Act in 1972, which is regulated by the EPA ([www.epa.gov](http://www.epa.gov)). Every five years, a taskforce is convened to reassess current hypoxia strategies in the Gulf of Mexico in an effort to complete three goals, focused on mitigating hypoxia in coastal waters, restoring parts of the basin impacted by hypoxia, and improving the quality of

life and the surrounding economy impacted by Gulf of Mexico hypoxia (EPA Task Force 2008). Hypoxia monitoring started by investigating the impact and increase of coastal eutrophication on the Gulf of Mexico shelf water quality (Rabalais et al. 2002). Three main topics resulted in political efforts to develop resource management strategies for the Gulf of Mexico (Rabalais et al. 2007):

1. Increased interest in understanding eutrophication in the MARS,
2. Assessing the sensitivity of the hypoxic area to nutrient loading from agricultural states, and
3. Growth of scientific knowledge in the area, including mapping and studies of the Louisiana coastal hypoxia.

These three aims resulted in large-scale political efforts to develop resource management strategies for the Gulf of Mexico (Rabalais et al. 2007).

Detailed information and supporting documents, including national strategies (Action Plans), were drafted by the EPA and disseminated to the Gulf of Mexico community. Past and current documents can be found at [water.epa.gov/watersheds/named/msbasin/index.cfm](http://water.epa.gov/watersheds/named/msbasin/index.cfm). The first Action Plan, published in 2001 by the Task Force, was the national strategy and included monitoring and mitigation strategies for coastal eutrophication and hypoxia. The Action Plan represented the national strategy based on a four-year assessment of Gulf of Mexico hypoxia science. The strategy detailed reports published by researchers, institutes, and the National Research Council to develop the first attempt to reduce the frequency, size,

and duration of Louisiana coastal hypoxia. Key points, which also have been maintained through the years, originating from Action Plan include:

- Improved coordination among federal, state, academic, and private efforts,
- Reduction of nutrient loading from point sources and urban runoff,
- Improved monitoring and research in the watershed and coastal ocean environments to understand processes responsible for hypoxia and,
- Coastal, basin and quality of life goals addressing the reduction of Louisiana hypoxic zone to below 5,000 km<sup>2</sup> by 2015, including the restoration of environmental areas impacted by nutrient loading, reduction of nitrogen loading to Gulf of Mexico, and improving local communities and economies impacted by hypoxia.

The Action Plan serves as the federal policy foundation for directing future efforts to reduce and mitigate hypoxia and implement adaptive management strategies to accomplish these goals.

In 2006, the EPA requested a Science Advisory Board (SAB) to evaluate the science and research pertaining to the Louisiana coastal hypoxia. The SAB was to review scientific assessments used by the Task Force in the development of hypoxia monitoring and nutrient criteria. The SAB also reviewed water quality in the MARS and quantified costs associated with attempts to reduce hypoxia in the northern Gulf of Mexico. This effort took more than a year and included a 21-person panel comprised of scientists from academia, industry, and government with experts from various fields such as oceanography, agronomy, and economics.

Findings from the SAB support the hypothesis that Louisiana coastal hypoxia is related to nutrient loading from MARS and reduction of the system requires a nutrient reduction strategy with an adaptive management plan for continuous monitoring. Though the SAB agreed on nutrient reduction strategies, the panel did not agree with the hypoxic area size reduction to less than 5,000 km<sup>2</sup> by 2015 (US EPA 2007). The SAB concluded the reduction was not feasible because of the time lag between nutrient input reductions and ecological response. The feasibility was also limited by complications in policy, program, and strategy efforts to reduce nutrients, as many of the nitrate reductions proposed at the federal level were voluntary. The SAB suggested that efforts be focused on managing the factors responsible for hypoxia rather than emphasizing a precise, time-sensitive areal reduction.

Revising the 2005 Action Plan led to a reassessment of the 2008 Action Plan, which included the final SAB report ([www.epa.gov/sab/panels/hypoxia\\_adv\\_panel.htm](http://www.epa.gov/sab/panels/hypoxia_adv_panel.htm)). The Task Force response to SAB recommendations included revisions to the original Action Plan to include five-year assessments of nutrient load reduction and hypoxia science, but did not include adjustments to the area reduction target or timeline ([water.epa.gov/watersheds/named/msbasin/index.cfm](http://water.epa.gov/watersheds/named/msbasin/index.cfm)). The 2008 Action Plan additionally addressed monitoring of Gulf of Mexico hypoxia by identifying actions, progress, and reassessment criteria (EPA Task Force 2008). Major actions continued to focus on reducing the extent of the Gulf of Mexico hypoxic zone to less than 5,000 km<sup>2</sup> by 2015. That goal has driven the monitoring and research funding priorities. It has also led to a focus only on the Louisiana shelf and not the entire northern Gulf of Mexico

shelf system. The 2008 Action Plan is currently used by federal and state agencies responsible for drafting and implementing mandates set to reduce nutrients in the Gulf of Mexico coastal environment. Additions to the 2008 Action Plan included the release of Annual Reports to track progress on actions to reduce nutrient loading and hypoxic area size ([water.epa.gov/watersheds/named/msbasin/index.cfm](http://water.epa.gov/watersheds/named/msbasin/index.cfm)). Annual Reports are also used to document federal, state, and local efforts and gauge the effectiveness in meeting the goals set forth in the 2008 Action Plan ([water.epa.gov/watersheds/named/msbasin/index.cfm](http://water.epa.gov/watersheds/named/msbasin/index.cfm)).

National assessments have also been conducted since the release of the 2008 Action Plan. The *Scientific Assessment of Hypoxia in U.S. Coastal Waters* was a federal interagency effort published in 2010 to update and assess the problem of coastal and estuarine hypoxia in U.S. waters. That report included a case study on northern Gulf of Mexico hypoxia and progress made by the EPA Task Force. The most recent publication is the 2011 Task Force Annual Report, which summarizes management nutrient mitigation efforts and Gulf of Mexico seasonal hypoxia monitoring results. Future management assessments include a 2012 yearly report and reassessment and updates to the 2008 Action Plan in 2013.

#### **4.3 Texas Hypoxic Area Contributions to the Gulf of Mexico Shelf**

In this section, I have developed independent hypotheses to test the contribution of hypoxic area on the Texas shelf to the federally mandated target goal. I have also

included results from Section 3 and Appendix E that help to address the redirection of federal mitigation and monitoring strategies that I proposed in Section 4.1.

#### *4.3.1 Interpolation and Management Reduction Methods*

The first hypothesis compares hypoxic areas from different interpolation models tested in Section 3 and Appendix E to the federal target reduction goal.

*H<sub>0</sub>: The summer Texas hypoxic area is not significantly different from 5,000 km<sup>2</sup>, the nationally accepted management target goal for the total Louisiana-Texas shelf.*

The calculated areas from the deterministic and statistical interpolators were tested using a series of *t*-tests and ANOVAs to compare against the target reduction goal of less than 5,000 km<sup>2</sup> by 2015 set forth the Task Force Action Plan 2008.

#### *4.3.2 Geostatistical Interpolation Methods and Results*

To identify years that potentially have hypoxic area greater than 5,000 km<sup>2</sup>, I grouped the ordinary kriging scenarios by *Model* and tested by year to compare differences between mean area estimates and 5,000 km<sup>2</sup>. Table 4.1 shows the results of 2-sample independent *t*-tests for *Model* with all years and excluding years where a scenario did not estimate any hypoxia. The results show 2002 and 2007 to be significantly different from the 5,000 km<sup>2</sup> for both conditions and 2008 to not be significantly different.

The next step was to isolate and test each *Model* scenario independently to determine which areas differed significantly from the Action Plan goal. Table 4.2 shows results for years and scenarios estimating hypoxia (2002, 2007, and 2008). *Model* estimates significantly different from 5,000 km<sup>2</sup> are highlighted in blue – 2008 *Spherical All* and *Gaussian TX*. The two scenarios have two of the smallest variances for all models tested and confidence intervals including 5,000 km<sup>2</sup>. The respective p-values are 0.0422 and 0.0372.

Three scenarios have confidence interval ranges including 5,000 km<sup>2</sup> (highlighted in dark red). Note that the ranges for these scenarios, based on *Model* groups, include zero and/or low area estimates. Even when these estimates are included, results for years with large hypoxic area still result in a significant test ( $> 5,000 \text{ km}^2$ ,  $p\text{-value} < 0.05$ ). Different interpolation models can produce areas statistically near to the federal target goal, which implies that area on the Texas shelf can exceed 5,000 km<sup>2</sup> in 33 % of years analyzed (2002, 2007, and 2008). When considering the ordinary kriging model suggested as the most suitable model in Section 3 (*Gaussian SEAMAP TX Anisotropic, G TX A*), these three years can exceed the target reduction goal.

#### **4.4 Management of Hypoxic Area Discussion**

If one of every three years monitored can exceed a target reduction without hypoxic area contribution from the Louisiana shelf, federal managers are not accurately assessing successes in reduction strategies in the northwestern Gulf of Mexico. In years

such as 2008, the area estimate can exceed 5,000 km<sup>2</sup> as an extension of Louisiana hypoxia westward. In other years, such as 2007, the hypoxic area can be independent, or confined to only the Texas shelf. Large hypoxic areas on the Texas shelf impact both monitoring and the success of federal mitigation efforts, including nutrient reduction strategies. The processes responsible for maintaining and extending hypoxic area are not entirely nutrient-driven based on results presented in Section 2 and Appendix C. Therefore, federal and state managers may consider two options when developing management plans for Gulf of Mexico hypoxia:

1. Do not separately consider any hypoxic area contribution on the Texas shelf,  
or
2. Consider hypoxic area contribution on the Texas shelf as a separate entity.

The first option represents the current management plan. Hypoxia on the Texas shelf is either included with Louisiana mid-summer estimates if occurring on the northern shelf or is disregarded if independent events occur during the year. If we are to consider the Texas contribution, then strategies need to be revised to address the physical drivers responsible on the Texas and Louisiana shelves in addition to the MARS nutrient loading on the Louisiana shelf.

The second consideration is recommended if the focus for developing hypoxia criteria is based on adaptive management. Results in this work have supported the ideas expressed by many in the Gulf of Mexico community that area estimate as the official metric and the current level of 5,000 km<sup>2</sup> is an arbitrary success measure with no substantive links to ecology, ecosystems, or other hypoxic zones in the world (Cowan et

al. 2008; Bianchi et al. 2010). Results from area determinations with different interpolation models provide significant evidence that hypoxia on the Texas shelf alone can exceed this reduction target despite the size and/or processes responsible for Louisiana coastal hypoxia.

If management plans retain area as the standard metric, then special consideration needs to be given to the type of interpolation used to calculate the official area estimate. Deterministic interpolators, such as inverse distance weighting and local polynomial interpolation, provide smooth surfaces fitted to the data values, but can provide underestimations in the actual area or potentially violate model assumptions, such as assuming an equal grid spacing. Regardless of interpolation model choice, managers need to address model assumptions when relying on a single area estimate produced by a particular method to represent the northern Gulf of Mexico shelf. Failure to address assumptions or design elements of an interpolator can lead to under- and overestimates in area results.

Data selection is also important in calculating hypoxic area on the Gulf of Mexico shelf. By including all shelf sample sites, areas on the Texas shelf can be masked, resulting in no area calculated in different scenarios, whereas scenarios using only Texas shelf data predict a moderate to large area as seen in 2007 (Table 3.5). By selecting for only sites on the Texas shelf, smaller and moderate independent areas can be resolved.

Deterministic interpolators are computationally simple (few user decisions) and such fast methods are useful for investigating the presence and initial size of hypoxia on

the Texas shelf relative to the Louisiana shelf. For a more rigorous determination of Texas shelf hypoxic area and in determining whether the area is an extension of Louisiana coastal hypoxia or independent, a kriging model should be used to account for the annual statistical trends in the data.

Managers who use kriging must consider and include the spatial scales for physical processes in the northwestern Gulf of Mexico in the model. This may require additional investigation of statistical patterns in the dissolved oxygen concentrations on the shelf, which can vary annually. Managers must also consider separating the northwestern Gulf of Mexico shelf into regions (e.g. Texas and Louisiana) and adjust the kriging model parameters (*Model*, *Anis*, *Lag*, etc.) accordingly to interpolate within each region independently. Site selection (entire northern Gulf of Mexico shelf versus Texas shelf) is another important consideration in kriging models. Area estimates will differ depending on the number of stations included in the interpolation model. Separating stations by shelf location can also be a key factor in identifying independent hypoxic areas on the Texas shelf as shown in Section 3 and Appendix E. Failure to address these considerations can result in inaccurate estimates of area on the entire Gulf of Mexico shelf.

The same is true when considering spatial dependence. According to the results in Section 3, the lag and anisotropy should be adjusted accordingly to reflect spatial scales of physical processes on the Texas shelf and to avoid producing inaccurate areas, such as bulls-eyes around single hypoxic stations or overestimates of independent areas for too small a lag distance, such as shown in the scenario results for 2007 (figures 3.10

– 3.13, Appendix E). Bottom dissolved oxygen values on the Texas-Louisiana shelf do show spatial dependence as seen in exploratory data analysis in Section 3.2. Bottom dissolved oxygen values are low near freshwater sources and increase away from the source and moving into deeper waters. Not considering spatial dependence in bottom dissolved oxygen data can potentially mask hypoxic areas, producing estimates with low or no area.

Based on results in Section 3 and the potential impact Texas hypoxic areas have in Gulf of Mexico hypoxic area estimates, I suggest that management policies and strategies should be adapted to address hypoxic events on the Texas shelf independently of hypoxia on the Louisiana shelf. Areas from isolated river events, as evident in the 2007 Brazos River flooding, and large Texas-Louisiana shelf areas measured in 2008 will hinder progress towards the reduction goal of less than 5,000 km<sup>2</sup> as mandated in the 2008 Action Plan. Federal and state management plans should be redrafted to include independent hypoxic areas on the Texas shelf and revisions should be considered to adjusting the projected running average and reduction limit of 5,000 km<sup>2</sup>. The 5,000 km<sup>2</sup> estimate is unattainable if the Texas shelf is included and is not representative of the total northern Gulf of Mexico hypoxic area. The limit is too large for considering reduction efforts on the Texas shelf and it might not be appropriate to set such a limit given the tendency for Texas hypoxia formation to be driven by physical processes rather than river nutrient loading. The current Action Plan target is better represented as an estimate for only the Louisiana shelf, not the entire northwestern Gulf of Mexico.

In conclusion, Texas shelf hypoxia is an important contributor to the overall hypoxic area in the Gulf of Mexico. Limiting management to nutrient-centric strategies will result in failure to accurately assess Gulf of Mexico hypoxia. Federal and state managers should consider Texas hypoxic areas and the processes responsible for formation and duration of Texas hypoxia in developing federal standards for reducing Gulf of Mexico hypoxia. Not including Texas hypoxia dynamics will complicate managers' efforts to accurately calculate Gulf of Mexico hypoxic area and assess reduction efforts in response to changes in nutrient and water quality criteria implemented for the Gulf of Mexico.

## **5. CONCLUSIONS AND FUTURE RESEARCH DIRECTIONS**

### **5.1 Conclusions**

Coastal hypoxia on the Texas shelf exhibits different temporal and spatial scales compared to Louisiana coastal hypoxia. In any given year, the physical conditions on the Texas shelf can vary and affect hypoxia formation. The physical processes responsible for Texas hypoxia formation are temporally and spatially variable by season and year. Coastal hypoxia can form as episodic ( $< 24$  hours) or persistent ( $> 24$  hours) events in summer and non-summer months on the Texas shelf. The primary physical factor driving the formation of hypoxic events is stratification. Stratification results from changes in salinity ( $\Delta\text{PSU} > 4$ ). Changes in temperature stratification can potentially lead to hypoxia forming as increased temperature stratification leads to decrease in bottom dissolved oxygen.

The primary sources of freshwater responsible for changing the salinity stratification are the Brazos River and the Mississippi-Atchafalaya River system. Seasonal downwelling favorable conditions advect freshwater from the Louisiana shelf onto the northern Texas shelf. During downwelling conditions, Brazos River water is transported south on the Texas shelf, potentially increase salinity stratification and the occurrence of hypoxia. Upwelling favorable conditions can transport Brazos River water upcoast and increase the salinity stratification in the water-column. During years of low Brazos River discharge onto the Texas shelf, increased stratification and hypoxia

formation on the northern Texas shelf is driven primarily by the advection of Louisiana freshwater westward.

Annual variability of hypoxia formation includes the extension of Louisiana coastal hypoxia westward and/or individual hypoxic regions on the Texas shelf. In a given year, hypoxic area on the Texas shelf can range from 0 to 7,000 km<sup>2</sup>. The area is dependent on the physical conditions of the shelf and the hypoxia formation on the Louisiana shelf. Estimating hypoxic area and structure requires a knowledge of the statistical spatial scales of processes on the Texas shelf. Spatial scales associated with autocorrelation (e.g. anisotropy) and sampling design (e.g. interpolated dataset) can under- or overestimate hypoxic area. Interpolating over the entire northwestern Gulf of Mexico can lead to underestimates and/or masking of independent hypoxic regions on the Texas shelf. Underestimates and masking effects or overestimations occur when anisotropy of bottom dissolved oxygen across the northwestern Gulf of Mexico is not correctly modeled.

The difference in spatial statistics between Louisiana and Texas requires a geostatistical interpolation model designed for only the Texas shelf to be used for accurately estimating area. The spatial extent of Texas shelf hypoxia varies year-to-year and in some years, can provide a significant contribution (up to 20 %) of the total hypoxic area in the northwestern Gulf of Mexico. In addition to area, long-term monitoring is necessary to establish a hypoxic climatology (e.g. its frequency of occurrence and long-term trends in area) for the Texas shelf. Detailed recommendations for addressing these area contributions and future monitoring, including methods for

interpolating bottom dissolved oxygen data on the Texas shelf specific to goals of federal policy managers were provided in an effort to improve the current federal hypoxia management practices.

## **5.2 Future Research Directions**

The integration of ocean observing platforms and *in situ* survey data helps to provide a thorough understanding of the temporal and spatial variability of hypoxia formation on the Texas shelf. Accurately estimating hypoxic area from surveys and combining estimates with real-time monitoring of physical conditions on the shelf helps to understand when and why independent hypoxic regions form in Texas coastal waters. Although this study addresses multiple interdisciplinary facets of Texas coastal hypoxia and provides an understanding of the physical processes responsible for controlling hypoxic area, further investigations can be carried to advance our knowledge of the system. Suggestions for future work include expanded observations, modeling, and outreach components:

### *Observational component*

- Additional prolonged time-series observations at several sites north and south of the Brazos River delta and at the Texas-Louisiana border, including the additional of new moorings and supplemental water-column instrumentation to existing moorings and buoys (e.g. TABS) to estimate stratification.

- Incorporation of high-resolution data, (e.g. Acrobat towfish and coastal gliders) and additional *in situ* shipboard surveys to develop longer annual time-series of hypoxia and physical conditions on the Texas shelf.
- Continue, but expand spatially and temporally, existing hypoxia monitoring programs conducted by NOAA, TAMU, and LUMCON in the northwestern Gulf of Mexico.

#### *Modeling component*

- Analysis of physical time-series data provided by TAMU-operated biogeophysical model simulations to hindcast and forecast hypoxia events on the Texas shelf and to further investigate the role of MARS freshwater in hypoxia formation on the Texas shelf.
- Construct statistical models incorporating physical shelf conditions to predict the annual area extent of Texas hypoxia.
- Continue to investigate different types of geostatistical models to improve the federal estimates of annual northwestern Gulf of Mexico hypoxia, including models to accurately estimate Texas shelf hypoxic area.

#### *Outreach component*

- Continue to work with federal, regional, and state managers to improve current policies and management strategies for monitoring and mitigating northwestern Gulf of Mexico hypoxia.

- Work with federal, regional, and state data providers to increase the collection of physical data and bottom dissolved oxygen monitoring on the Texas coast.

## REFERENCES

Baden, S. P., L. O. Loo, L. Pihl, and R. Rosenberg. 1990. "Effects of eutrophication on benthic communities including fish: Swedish west coast." *Ambio. Stockholm.*, 19 (3): 113–122.

Barron, C. N. and A. C. Vastano. 1994. "Satellite observations of surface circulation in the northwestern Gulf of Mexico during March and April 1989." *Cont. Shelf Res.*, 14: 607-628.

Belabbassi, L. 2006. Examination of the relationship of river water to occurrences of bottom water with reduced oxygen concentrations in the northern Gulf of Mexico, Ph.D. dissertation, Texas A&M University, College Station.

Bender, L. C., N. L. Guinasso, J. N. Walpert, J. N. Lee III, L. Linwood, R. D. Martin, R. Hetland, S. K. Baum, M. K. Howard. 2007. "Development, operation, and results from the Texas Automated Buoy System." *Gulf of Mexico Science*, 25(1): 33-60.

Bianchi, T. S., S. F. DiMarco, J. H. Cowan Jr., R. D. Hetland, P. Chapman, J. W. Day, and M. A. Allison. 2010. "The science of hypoxia in the northern Gulf of Mexico: A review." *Sci. Tot. Environ.*, 408: 1474–1484. doi:10.1016/j.scitotenv.2009.11.047.

Biggs, D. C. and L. L. Sanchez. 1997. "Nutrient-enhanced primary productivity of the Texas-Louisiana continental shelf." *J. Mar. Sys.*, 11: 237-247.

Boesch, D. F. 2002. "Challenges and opportunities for science in reducing nutrient over-enrichment of coastal ecosystems." *Estuaries*, 25: 886-900.

Boesch, D. F., and N. N. Rabalais. 1991. "Effects of hypoxia on continental shelf benthos; comparisons between the New York Bight and the northern Gulf of Mexico." in *Modern and Ancient Continental Shelf Anoxia*, edited by R. V. Tyson and T. H. Pearson, Geological Society Special Publication 58, London. pp. 27-34.

Breitburg, D. L. 2002. "Near-shore hypoxia in the Chesapeake Bay: patterns and relationships among physical factors." *Estuar. Coast. Shelf Sci.*, 30: 593–609.

Brunt, D. 1927. "The period of simple vertical oscillations in the atmosphere." *Q. J. Roy. Meteorol. Soc.*, 53: 30-32.

Chung-Chi, C., G. Gon, and F. Shiah. 2007. "Hypoxia in the East China Sea: one of the largest coastal low-oxygen areas in the world." *Mar. Env. Res.*, 64: 399–408.

Cho, K., R. O. Reid, and W. D. Nowlin Jr. 1998. "Objectively mapped stream function fields on the Texas-Louisiana shelf based on 32 months of moored current m data." *J. Geophys. Res.*, 103: 10377–10390.

Coble, P., H. Chuanmin, R. W. Gould Jr., G. Chang, and A. M. Wood. 2003. "Colored dissolved organic matter in the coastal ocean: an optical tool for coastal zone environmental assessment and management." *Ocean. Soc.*, 17(2): 51-59.

Cochrane, J. D., F. J. Kelly. 1986. "Low-frequency circulation on the Texas-Louisiana continental shelf." *J. Geophys. Res.*, 91(C9): 10645–10659.

Committee on Environment and Natural Resources. 2003. Assessment of coastal hypoxia in U. S. waters, *National Science and Technology Council*, Washington, D.C., 82 pp.

Committee on Environment and Natural Resources. 2010. Scientific assessment of hypoxia in U. S. coastal waters, *Interagency working group on harmful algal blooms, hypoxia, and human health of the Joint Subcommittee on Ocean Science and Technology*, Washington D. C., 47 pp.

Conley, D. J, S. Bjorck, E. Bonsdorff, J. Carstensen, G. Destouni, B. G. Gustafsson, et al. 2009a. "Hypoxia-related processes in the Baltic Sea." *Environ. Sci. Tech.*, 43(10): 3412–3420.

Conley, D. J., H. W. Paerl, R. W. Howarth, D. F. Boesch, S. P. Seitzinger, et al. 2009b. "Controlling eutrophication: Nitrogen and phosphorus." *Science*, 323: 1014-1015. doi:10.1126/science.1167755.

Cowan Jr., J. H., C. B. Grimes, and R. F. Shaw. 2008. "Life history, hysteresis, and habitat changes in Louisiana's coastal ecosystem." *Bull. Mar. Sci.*, 83: 197-215.

Cressie, N. 1985. "Fitting variogram models by weighted least squares." *J. Int. Assoc. Math. Geol.*, 17: 653-702.

Cressie, N. 1988. "Spatial prediction and ordinary kriging." *J. Int. Associ. Math. Geol.*, 20: 405-421.

Cressie, N. 1993. *Statistics for spatial data*. Wiley Series in Probability and Statistics, New York. 900 pp. ISBN-10:0471002550.

D'Sa, E. J. and S. F. DiMarco. 2009. "Seasonal variability and controls on chromophoric dissolved organic matter in a river-dominated coastal margin." *Limn. Ocean.*, 54: 2233-2242.

Denman, K. L. and H. J. Freeland. 1985. "Correlation scales, objective mapping, and a statistical test of geostrophy over the continental shelf." *J. Mar. Res.*, 43: 517-539.

Diaz, R. J. 2001. "Overview of hypoxia around the world." *J. Environ. Qual.*, 30(2): 275-281.

Diaz, R. J. and R. Rosenberg. 1995. "Marine benthic hypoxia: A review of its ecological effects and the behavioural responses of benthic macrofauna." *Oceanogr. Mar. Biol. Ann. Rev.*, 33: 245-303.

Diaz, R.J. and R. Rosenberg. 2008. "Spreading coastal hypoxias and consequences for marine ecosystems." *Science*, 321: 926-929.

DiMarco, S. F., J. Strauss, N. May, R. L. Mullins-Perry, E. L. Grossman, and D. Shormann. 2012. "Texas coastal hypoxia linked to Brazos River discharge as revealed by oxygen isotopes." *Aquat. Geo.*, 18(2): 159-181.

Dinnel, S. P. and W. J. Wiseman. 1986. "Freshwater on the Louisiana and Texas shelf." *Cont. Shelf Res.*, 6(6): 765-784.

Dunn, D. D. 1996. "Trends in nutrient inflows to the Gulf of Mexico from streams draining the conterminous United States 1972-1993." *Department of the Interior, U. S. Geological Survey, Water-Resources Investigations Report 96-4113*.

Gardner, W. D., A. V. Mishonov, and M. J. Richardson. 2006. "Global POC concentrations from in-situ and satellite data." *Deep-Sea Res. II*, 53: 718-740.

Gatson, G. R. 1985. "Effects of hypoxia on macrobenthos of the inner shelf off Cameron, Louisiana." *Estuar. Coast. Shelf Sci.*, 20: 603-613.

Gonzales, L. and C. Keane. 2010. "Status of the geoscience workforce 2010." *Amer. Geol. Instit.*, ISBN 978-0-922152-86-5. <http://www.agiweb.org/workforce>.

Gooday, A. J., F. Jorissen, L. A. Levin, J. J. Middleburg, S. W. A. Naqvi, N. N. Rabalais, M. Scranton, and J. Zhang. 2009. "Historical records of coastal eutrophication-induced hypoxia." *Biogeo.*, 6: 1707-1745.

Goolsby, D. A., W. A. Battaglin, B. T. Aulenbach, and R. P. Hooper. 2001. "Nitrogen input to the Gulf of Mexico." *J. Environ. Qual.*, 30(2): 329-336. doi:10.2134/jeq2001.302329.

Harper Jr., D. E., R. R. Salazar, R. J. Case. 1981. "The occurrence of hypoxic bottom water off the upper Texas coast and its effect on the benthic biota." *Contrib. Mar. Sci.*, 24: 53-79.

Hetland, R. D., and S. F. DiMarco. 2008. "How does the character of oxygen demand control the structure of hypoxia on the Texas-Louisiana continental shelf?" *J. Mar. Sys.*, 70: 49-62. doi:10.1016/j.jmarsys.2007.03.002.

Jensen, J. R. 2005. *Introductory digital image processing 3<sup>rd</sup> Ed.* Prentice Hall, New Jersey. 526 pp.

Jensen, J. R. 2007. *Remote sensing of the environment: an earth resource perspective, 2<sup>nd</sup> Ed.* Prentice Hall, New Jersey, 592 pp.

Johnston, K., J. M. Ver Hoef, K. Krivoruchko, and N. Lucas. 2004. *ArcGIS 9: Using ArcGIS geostatistical analyst.* ESRI, California. 299 pp.

Jonassen, D. H. 1999. "Designing constructivist learning environments." in *Instructional design theories and models: a new paradigm of instructional theory, vol. II*, edited by C. M. Reigeluth. Lawrence Erlbaum Associates, New Jersey. pp. 215-239.

Karlson, K., R. Rosenberg, and E. Bonsdorff. 2002. "Temporal and spatial large-scale effects of eutrophication and oxygen deficiency on benthic fauna in Scandinavian and Baltic waters – a review." *Ocean. Mar. Bio.*, 40: 427-489.

Kemp, W. M., J. M. Test, D. J. Conley, D. Gilbert, and J. D. Hagy. 2009. "Temporal responses of coastal hypoxia to nutrient loading and physical controls." *Biogeo.*, 6: 2985-3008.

Kimmons, R., M. Liu, J. Kang, L. Santana. 2011. "Attitude, achievement, and gender in a middle school science-based ludic simulation for learning." *J. Edu. Tech. Sys.*, 40(4): 341-370.

Kiselkova, V. 2008. "Effect of instabilities in the buoyancy-driven flow on the bottom oxygen: applications to the Louisiana shelf." Ph.D. dissertation, Texas A&M University, College Station.

Levin, L. A., W. Ekau, A. J. Gooday, F. Jorissen, J. Middleburg, J. Naqvi, C. Neira, N. Rabalais, and J. Zhang. 2009. "Effects of natural and human-induced hypoxia on coastal benthos." *Biogeo.* 6: 1707-1745.

Lewis, E. B. and D. R. Baker. 2010. "A call for a new geoscience education research agenda." *J. Res. Sci. Teaching*, 47(2): 121-129. doi:10.1002/tea20320

Li, Y., W. D. Nowlin Jr., and R. O. Reid. 1996. "Spatial-scale analysis of hydrographic data over the Texas-Louisiana continental shelf." *J. Geophys. Res.*, 101(C9): 20595-20605.

Li, Y., W. D. Nowlin Jr., and R. O. Reid. 1997. "Mean hydrographic fields and their interannual variability over the Texas-Louisiana continental shelf in spring, summer, and fall." *J. Geophys. Res.*, 102(C9): 1027-1049.

Lloyd, C. 2010. *Spatial data analysis: an introduction for GIS users*. Oxford University Press. London. 272 pp. ISBN-10:0199554323.

Lohrenz, S. E., G. L. Fahnenstiel, D. G. Redalje, G. A. Lang, M. J. Dagg, T. E. Whitledge, Q. Dortch. 1999. "Nutrients, irradiance, and mixing as factors regulating primary production in coastal waters impacted by the Mississippi river plume." *Cont. Shelf Res.*, 19(9): 1113-1141.

McInnes, A. and A. S. Quigg. 2011. "Near-annual fish kills in small embayments: casual vs. causal factors." *J. Coastal Res.*, 26: 957-966.

Millard, R. C., W. B. Owens, and N. P. Fofonoff. 1990. "On the calculation of the Brunt-Väisälä frequency." *Deep Sea Res.*, 37: 167-181.

Millero, F. J. 2005. *Chemical Oceanography*, CRC Press Taylor and Francis Group, Florida. 496 pp.

Mississippi River/Gulf of Mexico Watershed Nutrient Task Force (EPA Task Force) (2008), Gulf hypoxia action plan 2008 for reducing, mitigating, and controlling hypoxia in the northern Gulf of Mexico and improving water quality in the Mississippi River basin, *Environmental Protection Agency* (<http://water.epa.gov>).

Mitchell, A. 2005. *The ESRI guide to GIS analysis Vol. 2*. ESRI, California. 299 pp.

Muller-Karger, F. E., J. J. Walsh, R. H. Evans, and M. B. Meyers. 1991. "On the seasonal phytoplankton concentration and sea surface temperature cycles of the Gulf of Mexico as determined by satellites." *J. Geophys. Res.*, 96: 12,645-12,665.

Mullins, R. L., S. F. DiMarco, J. Walpert, and N. L. Guinasso Jr. 2009. "Real-time environmental monitoring from a wind farm platform in the Texas hypoxic zone." *Proc. OCEANS 2009 Mar. Tech. Soc.*

Mullins, R. L., S. F. DiMarco, and N. L. Guinasso Jr. 2010. "Innovative environmental sampling during the summer of 2010 in the western Gulf of Mexico." *Proc. OCEANS 2010 Mar. Tech. Soc.*

Mullins, R. L., S. F. DiMarco, X. Zhang, and N. L. Guinasso Jr. 2011a. "Interdisciplinary ocean observing applications for investigating coastal hypoxia in the Gulf of Mexico." *Proc. OCEANS 2011 Mar. Tech. Soc.*

Mullins, R. L., S. F. DiMarco, J. Walpert, and N. L. Guinasso Jr. 2011b. "Interdisciplinary ocean observing on the Texas coast." *Mar. Tech. Soc.*, 45(1): 98 – 111.

Murray, C. N., and J. P. Riley. 1969. "The solubility of gases in distilled water and seawater." *Deep Sea Res.*, 16: 311-320.

Myint, S. W. and N. D. Walker. 2002. "Quantification of surface suspended sediments along a river dominated coast with NOAA AVHRR and SeaWiFS measurements: Louisiana, U.S.A." *Inter. J. Remote Sensing*, 23: 3229-3249.

Nowlin, W. D., A. E. Jochens, R. O. Reid, and S. F. DiMarco. 1998. "Texas-Louisiana shelf circulation and transport processes study – synthesis report.vol.i and ii." *OCS Study MMS 98-0035 and MMS 98-0036*, US Department of the Interior, Minerals Management Service, Gulf of Mexico OCS Regional Office, New Orleans, LA.

Nowlin, W. D., A. E. Jochens, S. F. DiMarco, R. O. Reid, and M. K. Howard. 2005. "Low-frequency circulation over the Texas-Louisiana continental shelf, in Circulation in the Gulf of Mexico: Observations and models." edited by Wilton Sturges and Alexis Lugo-Fernandez, *AGU Geophysical Monograph*, 161: 219-240.

Osterman, L. E. 2003. "Benthic foraminifers from the continental shelf and slope of the Gulf of Mexico: An indicator of shelf hypoxia." *Estuar. Coast.*, 58: 17-35.

Osterman, L. E., R. Z. Poore, P. W. Swarzenski, D. B. Senn, and S. F. DiMarco. 2009. "The 20<sup>th</sup>-century development and expansion of Louisiana shelf hypoxia, Gulf of Mexico." *Geo-Mar. Lett.*, 29(6): 405-414. doi:10.1007/s00367-009-0158-2.

Pokryfki, L., and R. E. Randall. 1987. "Nearshore hypoxia in the bottom water of the Northwestern Gulf of Mexico from 1981 to 1984." *Mar. Env. Res.*, 22: 75-90.

Rabalais, N. N. and R. E. Turner. 2001. *Coastal Hypoxia: Consequences for Living Resources and Ecosystems*, American Geophysical Union, Washington, D. C. 464 pp.

Rabalais, N. N., D. E. Harper Jr., and R. E. Turner. 2001a. "Responses of nekton and demersal and benthic fauna to decreasing oxygen concentrations." in *Coastal hypoxia consequences for living resources and ecosystems*, edited by N. N. Rabalais and R. E. Turner, American Geophysical Union, Washington, D.C. 464 pp.

Rabalais, N. N., R. E. Turner, W. J. Wiseman Jr. 2001b. "Hypoxia in the Gulf of Mexico." *J. Environ. Qual.* 30: 320–329.

Rabalais, N. N., R. E. Turner, and W. Wiseman. 2002. "Gulf of Mexico hypoxia, aka 'the dead zone'." *Annu. Rev. Ecol. Syst.*, 33: 235–263. doi:10.1146/annurev.ecolsys.33.010802.150513.

Rabalais, N. N., R. E. Turner, B. K. Sen Gupta, D. F. Boesch, P. Chapman, and M. C. Murrell. 2007. "Hypoxia in the northern Gulf of Mexico: Does the science support the plan to reduce, mitigate, and control hypoxia?" *Estuar. Coast*, 30: 753-772. doi:10.1007/BF02841332.

Rabalais, N. N., R. J. Diaz, L. A. Levin, R. E. Turner, D. Gilbert, and J. Zhang. 2010. "Dynamics and distribution of natural and human-caused hypoxia." *Biogeo.*, 7: 585-619.

Renaud, M. L. 1986. "Hypoxia in the Louisiana coastal waters during 1983: Implications for fisheries." *Fish. Bull.*, 84(1): 19-26.

Rowe, G. T. and P. Chapman. 2002. "Hypoxia in the northern Gulf of Mexico: some nagging questions." *Gulf Mex. Sci.*, 20: 153-160.

Salisbury, J. E., J. W. Campbell, E. Linder, L. D. Meeker, F. E. Muller-Karger, C. J. Vorosmarty. 2004. "On the seasonal correlation of surface particle fields with wind stress and Mississippi discharge in the northern Gulf of Mexico." *Deep-Sea Res. II*, 51: 1187-1203.

Snyder, J. P. and H. Steward. 1997. "Bibliography of map projections." *U.S. Geol. Survey Bull.*, 200 pp.

Strauss, J., E. L. Grossman, J. A. Carlin, and T. M. Dellapenna. 2012. "100 years of benthic foraminiferal history on the inner Texas shelf inferred from fauna and stable isotopes: preliminary results from two cores." *Cont. Shelf Res.*, 38: 89 – 97. doi:10.1016/j.csr.2012.03.004.

Stumpf, R. P., M. E. Culver, P. A. Tester, M. Tomlinson, G. J. Kirkpatrick, B. A. Pederson, E. Truby, V. Ransibrahmanukul, and M. Soracco. 2003. "Monitoring *Karenia brevis* blooms in the Gulf of Mexico using satellite ocean color imagery and other data." *Harmful Algae*, 2: 147-160.

Thomas, P. and M. S. Rahman. 2011. "Extensive reproductive disruption, ovarian masculinization and aromatase suppression in Atlantic croaker in the northern Gulf of Mexico hypoxic zone." *Proc. R. Soc. Biol. Sci.*, 1:1-12. doi:10.1098/rspb.2011.0529.

Thronson, A. and A. S. Quigg. 2008. Fifty-five years of fish kills in coastal Texas." *Estuar. Coasts*, 31: 802-813.

United States Environmental Protection Agency (US EPA). 2007. "Hypoxia in the northern Gulf of Mexico: an update by the EPA Science Advisory Board." *EPA*, EPA-SAB-08-003.

Vastano, A. C., C. N. Barron Jr., and E. W. Shaar Jr. 1995. "Satellite observations of the Texas Current." *Cont. Shelf Res.*, 15(6): 729-754.

Walker N. D. 2005. "Wind and eddy-related shelf/slope circulation processes and coastal upwelling in the northwestern Gulf of Mexico." in *Circulation in the Gulf of Mexico: observations and models*, edited by Wilton Sturges and Alexis Lugo-Fernandez, *AGU Geophysical Monograph*, 161: 295-313.

Walker, N. D., W. J. Wiseman, L. J. Rouse, and A. Babin. 2005. "Effects of river discharge, wind stress, and slope eddies on circulation and satellite-observed structure of the Mississippi River plume." *J. Coast. Res.*, 21: 1228-1244.

Walker, N. D., N. N. Rabalais. 2006. "Relationships among satellite chlorophyll a, river inputs, and hypoxia on the Louisiana continental shelf, Gulf of Mexico." *Estuar. Coasts*, 29: 1081–1093.

Wiseman, W. J., N. N. Rabalais, R. E. Turner, S. P. Dinnel, and A. MacNaughton. 1997. "Seasonal and interannual variability within the Louisiana coastal current: Stratification and hypoxia." *J. Mar. Sys.*, 12: 237-248. doi:10.1016/S0924-7963(96)00100-5.

## **APPENDIX A**

### **TABLES**

Table 2.1 TAMU WF Operation Dates and Instruments

<b>Year</b>	<b>Date</b>	<b>Instrumentation Depths</b>
<i>2009</i>	<i>June 23 - October 9</i>	<i>7-, 9-, 15-meter array, RDCP</i>
2010	June 9 - August 25	7-, 9-meter array, RDCP
<i>2011</i>	<i>May 27 - November 11</i>	<i>RDCP</i>

\* 2009 and 2011 (in italics) were only consider for statistical analysis in Section 2.5, because data recorded covered summer and non-summer months

Table 2.2 Cruise Dates for TAMU MCH MS Summer Surveys

<i>Year</i>	<i>Date</i>	<i>Abbreviation</i>
2010	June 14 - June 19	MS1
<b>2010</b>	<b>Aug 2 - Aug 7</b>	<b>MS2</b>
<b>2011</b>	<b>June 23 - July 1</b>	<b>MS3</b>
<b>2011</b>	<b>Aug 7 - 15</b>	<b>MS4</b>

Table 2.3 Physical Data Groups and Variables Names, Data Sources, and Abbreviations

Group	Parameter	Source	Abbreviations	Units
Salinity	Bottom Salinity	RDCP	RDCP_Salt	PSU
	Surface Salinity	TABS B	TABS_Salt	PSU
	Salinity Stratification Index	TABSB & RDCP	TABSRDCP_Salt	PSU
	Surface Salinity	TAMU WF	<i>WF_Salt_Top*</i>	PSU
	Bottom Salinity	TAMU WF	WF_Salt_Bott	PSU
	Salinity Stratification Index	TAMU WF	WF_SSI	PSU
Temperature	Bottom Temperature	RDCP	RDCP_Temp	°C
	Surface Temperature	TABS B	TABS_Temp	°C
	Temperature Stratification Index	TABSB & RDCP	TABSRDCP_Temp	°C
	Bottom Temperature	TAMU WF	WF_Temp_Top	°C
	Surface Temperature	TAMU WF	<i>WF_Temp_Bott*</i>	°C
	Temperature Stratification Index	TAMU WF	WF_TSI	°C
Currents	3-meter Speed	TAMU RDCP	WF_3_Spd	cm s <sup>-1</sup>
	3-meter Direction	TAMU RDCP	WF_3_Dir	°N
	3-meter East Component	TAMU RDCP	WF_3_East	cm s <sup>-1</sup>
	3-meter North Component	TAMU RDCP	WF_3_North	cm s <sup>-1</sup>
	10-meter Speed	TAMU RDCP	WF_10_Spd	cm s <sup>-1</sup>
	10-meter Direction	TAMU RDCP	WF_10_Dir	°N
	10-meter East Component	TAMU RDCP	WF_10_East	cm s <sup>-1</sup>
	10-meter North Component	TAMU RDCP	WF_10_North	cm s <sup>-1</sup>

Table 2.3 Continued

Group	Parameter	Source	Abbreviations	Units
<b>Winds</b>	Direction	TABS B	TABS_Dir	°N
	Speed	TABS B	TABS_Spd	cm s <sup>-1</sup>
	East Component	TABS B	TABS_East	cm s <sup>-1</sup>
	North Component	TABS B	TABS_North	cm s <sup>-1</sup>
	Direction	NDBC 42035	NDBC_Dir	°N
	Speed	NDBC 42035	NDBC_Spd	cm s <sup>-1</sup>
	East Component	NDBC 42035	NDBC_North	cm s <sup>-1</sup>
	North Component	NDBC 42035	NDBC_East	cm s <sup>-1</sup>
<b>Rivers</b>	Mississippi River Discharge	USGS	Miss	m <sup>3</sup> sec <sup>-1</sup>
	Atchafalaya River Discharge	USGS	Atch	m <sup>3</sup> sec <sup>-1</sup>
	Brazos River Discharge	USGS	Brazos	m <sup>3</sup> sec <sup>-1</sup>

Variable abbreviations in *italic* indicate variables with log-based data transformations in multivariate linear modeling (Section 2.2 and 2.4).

Table 2.4 Correlation Coefficients and Covariance for Daily Averaged NDBC 42035 and TABS B Buoy Wind Parameters

Year 2009	Parameter	Correlation	Covariance Zero Crossing (Days)
NDBC 42035 vs. TABS B Buoy	East	<b>0.95</b>	29
	North	<b>0.88</b>	7
	Direction	<b>0.95</b>	30
	Speed	<b>0.83</b>	4

Significant correlations ( $r$ ;  $p$ -values  $< 0.001$ ) between parameters by instrument depth are in bold

Table 2.5 2009 – 2011 Hypoxic Events Recorded by the TAMU WF RDCP

<b>EVENTS</b>	<b>2009</b>	<b>2010</b>	<b>2011</b>
<b>June</b>	0	3	12
<b>July</b>	0	8	11
<b>August</b>	1	10	n/a
<b>September</b>	5	n/a	n/a
<b>October</b>	2	n/a	n/a
<b>Shortest</b>	22 mins	26 mins	9 mins
<b>Longest</b>	5 days	6 days	15 days
<b>Average</b>	25 hours	24 hours	30 hours

Table 2.6 10-Term Multivariate Linear Model Determined From Subset Multivariate Linear Models

Variable	Correlation (r)	Estimate ( $\beta_1$ )	Standard Error	p-value
Intercept	n/a	79.430	195.020	0.685
Salt_WF_Top*	0.4	-37.635	76.796	0.625
Salt_WF_Bott	0.19	1.147	2.307	0.620
WF_SSI	0.6	1.968	2.301	0.039
Temp_WF_Bott*	-0.03	5.839	2.740	0.036
WF_3_Spd	-0.57	-0.054	0.011	0.000
WF_3_East	0.39	-0.002	0.011	0.826
WF_3_North	0.49	0.015	0.016	0.347
Brazos	-0.18	-0.004	0.002	0.048
NDBC_Spd	0.37	0.264	0.087	0.003
NDBC_North	0.45	0.010	0.054	0.850

Rows in blue indicate statistically significant terms (p-values < 0.05).

\* indicates a log-transformed variable.

Table 2.7 5-Term Multivariate Linear Model for TAMU WF Data in 2009

Variable	Estimate ( $\beta_1$ )	Standard Error	p-value
Intercept	-13.990	6.084	0.023
WF_SSI	0.960	0.133	< 0.001
Temp_WF_Bott*	5.793	1.814	0.002
WF_3_Spd	-0.058	0.009	< 0.001
Brazos	-0.004	0.002	0.017
NDBC_Spd	0.300	0.072	< 0.001

\* indicates a log-transformed variable

The  $r^2$  for the multivariate linear model is 0.651.

Table 2.8 2009 TAMU WF Multivariate Model Criteria Assessment Results

Variable	$\delta\text{BIC}$	$\delta r^2_{\text{adj}}$	$\delta r^2$
WF_SSI	40.08	-0.26	-0.20
Temp_WF_Bott*	5.55	-0.02	0.04
WF_3_Spd	29.78	-0.13	-0.16
Brazos	1.31	-0.01	0.02
NDBC_Spd	12.14	-0.05	0.06

\* indicates a log-transformed variable

Blue cells indicate important terms in each criteria for estimating model variance. The  $\delta\text{BIC}$  model  $r^2$  is 0.651. The  $r^2$  for  $\delta r^2_{\text{adj}}$  and  $\delta r^2$  models is 0.634 and 0.521 respectively.

Table 2.9 2011 10-Term Multivariate Linear Model Determined From Subset Multivariate Linear Models

Variable	Correlation (r)	Estimate ( $\beta_1$ )	Standard Error	p-value
Intercept	n/a	7.876	1.379	< 0.0001
WF_10_East	-0.33	-0.076	0.025	0.003
WF_10_North	-0.17	0.055	0.027	0.047
WF_3_Spd	-0.3	-0.029	0.015	0.049
NDBC_Dir	-0.12	-0.026	0.008	0.0007
NDBC_East	0.03	0.429	0.107	0.0001
NDBC_North	-0.18	-0.152	0.048	0.002
Brazos	0.27	0.125	0.042	0.004

The  $r^2$  of the 7-term model is 0.494.

Table 2.10 2011 TAMU WF Multivariate Model Criteria Assessment Results

Variable	$\delta\text{BIC}$	$\delta r^2_{\text{adj}}$	$\delta r^2$
Intercept	n/a	n/a	n/a
WF_10_East	7.780	n/a	0.0690
WF_10_North	2.569	n/a	0.0121
WF_3_Spd	2.174	n/a	0.0424
NDBC_Dir	4.669	-0.0059	0.0043
NDBC_East	2.054	-0.0037	0.0037
NDBC_North	11.769	-0.1506	n/a
Brazos	2.175	n/a	0.0786

Blue cells indicate important terms in each criteria for estimating model variance.

The  $\delta\text{BIC}$  model  $r^2$  is 0.322. The  $r^2$  for  $\delta r^2_{\text{adj}}$  and  $\delta r^2$  models is 0.434 and 0.1504 respectively.

Table 2.11 TAMU MCH MS Survey Linear Model Results for Bottom Dissolved Oxygen versus Maximum Brunt-Väisälä Frequencies

Cruise	$r^2$	p-values
MS2	0.0905	0.0704
MS3	0.254	0.114
MS4	0.0572	0.41
MS2 South	0.0652	0.307
MS2 North	0.0699	0.274

Table 3.1 NOAA SEAMAP Gulf Hypoxia Watch Summer Survey Dates

<b>NOAA SEAMAP Gulf Hypoxia Watch Surveys</b>	
<i>Year</i>	<i>Date</i>
2002	June 11 - July 18
2003	June 10 - July 17
2004	June 17 - July 16
2005	June 15 - Aug 1
2006	June 14 - July 16
2007	June 6 - Aug 3
2008	June 11 - July 16
2009	June 8 - July 18
2010	June 8 - July 17
2011	June 25 - July 17

Table 3.2 ESRI ArcGIS Base Map Layers for Area Interpolation Analyses

<i>Layer</i>	<i>Source</i>	<i>Location</i>
United States state boundaries	USGS	<a href="http://coastalmap.marine.usgs.gov">http://coastalmap.marine.usgs.gov</a>
Mexico boundary	USGS	<a href="http://coastalmap.marine.usgs.gov">http://coastalmap.marine.usgs.gov</a>
Coastal bathymetry	TNRIS	<a href="http://www.tnris.org/get-data">www.tnris.org/get-data</a>
Shoreline	NOAA	<a href="http://www.coastalgeospatial.noaa.gov">www.coastalgeospatial.noaa.gov</a>
Texas rivers	Texas Water Development Board (TWDB)	<a href="http://www.twdb.state.tx.us/mapping/gisdata.asp">www.twdb.state.tx.us/mapping/gisdata.asp</a>
SEAMAP data	NOAA	<a href="http://www.ncddc.gov/hypoxia">www.ncddc.gov/hypoxia</a>

Table 3.3 2002 – 2011 Directional Statistics for NOAA SEAMAP Survey Data

<i>Year</i>	<i>Direction Distribution (degrees)</i>		<i>Average Nearest Neighbor (km)</i>		<i>Moran's I Spatial Index</i>	
	<i>ALL</i>	<i>TX</i>	<i>ALL</i>	<i>TX</i>	<i>ALL</i>	<i>TX</i>
2002	70.2430	44.8163	12.4798	11.5899	0.6434	0.4989
2003	n/a	46.7282	n/a	12.4798	n/a	0.7368
2004	71.0930	45.7892	11.3640	11.8848	0.7403	0.5359
2005	69.1573	44.0220	11.4070	11.3462	0.7018	0.3955
2006	72.3419	47.6836	11.9348	12.7630	0.5939	0.4707
2007	69.2262	41.6014	13.1298	13.8210	0.6377	0.4408
2008	70.0340	44.5168	12.6098	12.1208	0.9408	0.5788
2009	70.6322	44.1199	9.4058	9.5975	0.7119	0.5791
2011	69.9840	47.9091	13.5089	12.9419	0.5314	0.5094
* Moran's Spatial Autocorrelation p-values reported						
** All p-values for Direction Distribution and Average Nearest Neighbor <i>ALL</i> versus <i>TX</i> are less than 0.01, except for 2003						
*** Two-sample independent <i>t</i> -tests results conclude significant differences (p-values < 0.05) between year and dataset for all comparisons, except 2003 (red), which did not have sample sites available for analysis on the Louisiana shelf.						

Table 3.4 Ordinary Kriging Models and Abbreviations

Model	Data	Spatial	Lag	Abbreviation
Spherical	All	Iso	Default	S All I
Spherical	All	Aniso	Default	S All A
Spherical	All	Aniso	Lag Adj	S All A Adj
Spherical	TX	Iso	Default	S TX I
Spherical	TX	Aniso	Default	S TX A
Spherical	TX	Aniso	Lag Adj	S TX A Adj
Gaussian	All	Iso	Default	G All I
Gaussian	All	Aniso	Default	G All A
Gaussian	All	Aniso	Lag Adj	G All A Adj
Gaussian	TX	Iso	Default	G TX I
Gaussian	TX	Aniso	Default	G TX A
Gaussian	TX	Aniso	Lag Adj	G TX A Adj

Table 3.5 2002 – 2011 Ordinary Kriging Model Hypoxic Area Estimates

Model	Data	Spatial	Lag	Hypoxic Area (km <sup>2</sup> )								
				2002	2003	2004	2005	2006	2007	2008	2009	2011
Spherical	All	Iso	Default	856	0	0	0	0	0	6047	0	0
Spherical	All	Aniso	Default	3258	0	15	0	0	0	5565	0	0
Spherical	All	Aniso	Lag Adj	4704	0	332	0	0	55	6247	0	0
Spherical	TX	Iso	Default	1519	0	301	0	0	3056	5116	0	0
Spherical	TX	Aniso	Default	813	0	0	0	0	5733	4763	0	0
Spherical	TX	Aniso	Lag Adj	1667	0	0	0	0	5696	5115	0	0
Gaussian	All	Iso	Default	2017	0	0	0	0	0	4379	0	0
Gaussian	All	Aniso	Default	1981	0	0	0	0	0	5010	0	0
Gaussian	All	Aniso	Lag Adj	4525	0	0	0	0	0	5616	0	0
Gaussian	TX	Iso	Default	2018	0	358	0	0	2716	5265	0	0
Gaussian	TX	Aniso	Default	0	0	0	0	0	2716	5164	0	0
Gaussian	TX	Aniso	Lag Adj	1427	0	451	0	0	7058	5340	0	0
<i>Mean*</i>				2065	0	121	0	0	2252	5302	0	0
<i>Standard Error*</i>				414	0	52	0	0	770	149	0	0
<i>Mean**</i>				2253	0	291	0	0	3861	5302	0	0
<i>Standard Error**</i>				404	0	74	0	0	911	149	0	0
<i>p-value</i>				<b>0.75</b>	<i>n/a</i>	<b>0.09</b>	<i>n/a</i>	<i>n/a</i>	<b>0.21</b>	<b>n/a</b>	<i>n/a</i>	<i>n/a</i>
<p>* Means computed for all years (no zeros were excluded)</p> <p>** Means computed excluding years with no hypoxic area estimated (e.g. 2002 Gaussian TX Aniso Default)</p> <p>*** p-values are for 2-sample t-test comparisons between Mean* and Mean** (<math>H_0: \mu_1 = \mu_2</math>)</p>												

Table 3.6 One-way ANOVA Results for Ordinary Kriging Parameters

Year	Variable	F-Statistic	p-value
All Years	Model	0.05	0.8178
All Years	Data	0.57	0.4527
All Years	Spatial	0.29	0.5893
All Years	Lag	0.9	0.3463
<i>All Years</i>	<i>Year</i>	<i>38.36</i>	<i>&lt;.001</i>
Excl Yrs	Model	0.08	0.7749
Excl Yrs	Data	0.89	0.3496
Excl Yrs	Spatial	0.46	0.5021
Excl Yrs	Lag	1.42	0.2398
<i>Excl Yrs</i>	<i>Year</i>	<i>23.21</i>	<i>&lt;.001</i>

\* Red indicates statistically significant variables (p-value < 0.05).

Table 3.7 One-way ANOVA Results for Ordinary Kriging Standardized RMSE by Parameters

ALL YEARS			YEARS 2002, 2004, 2007, & 2008		
Parameter	F-Statistic	p-value	Parameter	F-Statistic	p-value
Year	1.98	0.0579	Year	2.17	0.105
Model	1.54	0.2172	Model	1.79	0.1869
Data	6.37	0.0132	Data	4.9	0.0319
Spatial	7.31	0.0081	Spatial	4.3	0.0436
Lag	5.31	0.0233	Lag	2.85	0.098

Red indicates statistically significant variables (p-values < 0.05).

Table 3.8 Non-parametric Mean Rank Scores for 2002, 2007, and 2008

	Model	Mean Rank Score	Estimated Area (km <sup>2</sup> )
2002	<b>G TX A</b>	2	0
	G All A Adj	3.2	4525
	G TX A Adj	3.4	1427
	G All A	3.6	1981
	G TX I	4.2	2018
	G All I	4.6	2017
2007	<b>G TX A</b>	2.6	2716
	G All A Adj	2.6	0
	G All A	2.8	0
	G All I	3.6	0
	G TX A Adj	4.4	7058
	G TX I	5	2716
2008	<b>G TX A</b>	2.4	5265
	G All A Adj	3.2	5616
	G All I	3.2	4379
	G All A	3.8	5010
	G TX A Adj	4	5340
	G TX I	4.4	5164

Red indicates the model with the lowest mean rank score.

Table 4.1 Comparison of Ordinary Kriging Model Results to the EPA 2008 Action Plan Hypoxic Area Reduction Goal

<i>Year</i>	<i>Models</i>	<i>Std. Deviation (km<sup>2</sup>)</i>	<i>Degrees of Freedom</i>	<i>Test Statistic</i>	<i>C.I. Lower</i>	<i>C.I. Upper</i>	<i>p-value</i>
2002	All Models	1433.600	11	-7.0909	1154.6	2976.3	0.00002
2002	Models*	1339.900	10	-6.799	1353.1	3153.4	0.00005
2007	All Models	2668.600	11	-3.5666	557.0	3948.0	0.00440
2007	Models*	2409.900	6	-1.2501	1632.7	6090.1	0.25780
2008	All Models	516.614	11	2.0266	4974.0	5630.5	0.06760
2008	Models*	Not applicable - data for all models					
Models* excludes models with 0 area							

\* indicates model comparisons with the removal of individual models estimating zero hypoxic area

Red designates statistically significant relationships between mean area and 5,000 km<sup>2</sup> (p-values < 0.05).

Blue designates results not statistically significant relationships between mean area and 5,000 km<sup>2</sup> (p-values > 0.05).

Table 4.2 Comparisons of Kriging Parameter *Model* to the EPA 2008 Action Plan Hypoxic Area Reduction Goal

<i>Year</i>	<i>Models</i>	<i>Std. Deviation (km<sup>2</sup>)</i>	<i>Test Statistic</i>	<i>C.I. Lower</i>	<i>C.I. Upper</i>	<i>p-value <math>\alpha = 0.05</math></i>
2002	Spherical All	1943.700	-1.8635	0.0	7767.6	0.2077
2002	Gaussian All	1458.500	-2.5635	0.0	6464.5	0.1244
2007	Spherical TX	1535.000	-0.1983	1015.1	8641.4	0.8642
2007	Gaussian TX	2506.800	-0.5782	0.0	10391.0	0.6216
2008	Spherical All	350.438	4.71	5082.4	6823.5	0.0422
2008	Gaussian All	618.853	0.0042	3464.2	6538.8	0.997
2008	Spherical TX	203.959	-0.0165	4491.4	5504.7	0.9883
2008	Gaussian TX	88.165	5.037	5037.4	5475.4	0.0372

Blue indicates kriging model scenarios significantly different from 5,000 km<sup>2</sup> at the  $\alpha = 0.05$  level.

Dark red values highlight upper confidence intervals bounds that exceed the 2008 Action Plan area reduction goal.

## **APPENDIX B**

### **FIGURES**



Figure 1.1 Map of the Northwestern Gulf of Mexico. Map shows the northwestern Gulf of Mexico and shows the location of the Brazos River and its tributaries, which is the primary freshwater source to the Texas shelf. The north Texas shelf is indicated by the location of Galveston Bay with the Brazos River delta considered the mid-Texas shelf. The south Texas shelf starts at Corpus Christi Bay to Mexico. The 10 to 60 m isobaths are shown in light to dark blue respectively.

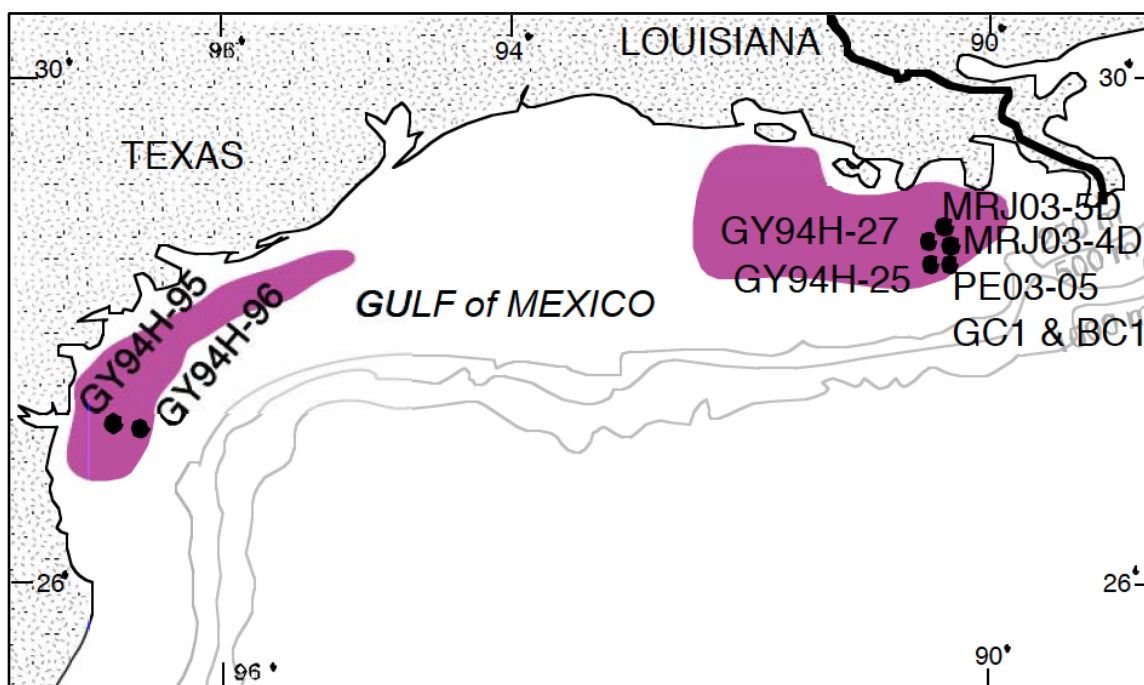


Figure 1.2 Map of Two Historic Hypoxic Regions Based on Benthic Foraminifera Abundance. Benthic foraminifera were analyzed to determine a microfaunal indicator for hypoxic conditions on the northwestern Gulf of Mexico shelf. The areas in dark pink indicate two regions of hypoxia that have occurred in the last century. (Source data and figure based on Osterman et al. 2003, 2009)

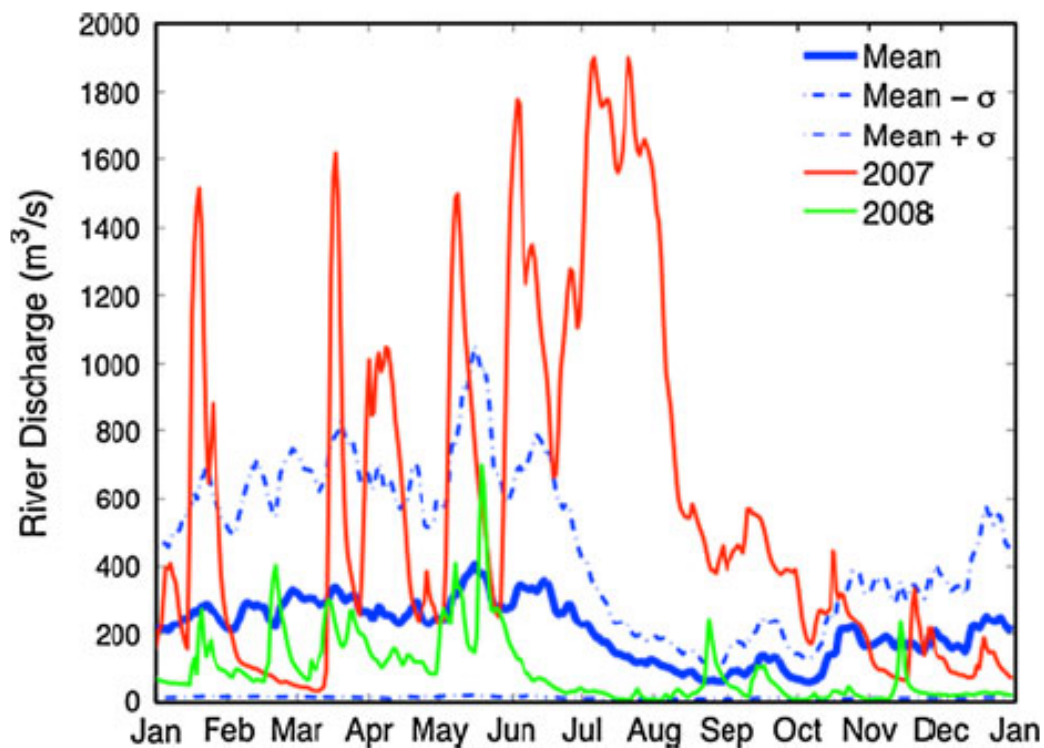


Figure 1.3 Brazos River Discharge Hydrograph. The mean Brazos River discharge is shown for years 1967 to 2010 by the solid blue line. Yearly discharge is shown for 2007 (solid red) and 2008 (solid green). Throughout the year, there are multiple peaks with higher volumes occurring in the early spring to early summer. Discharge volumes were the highest in 2007 reaching a peak discharge near 1,900 m<sup>3</sup>/s. The summer flooding resulted in a two-month independent hypoxic event on the Texas shelf. (Source: DiMarco et al. 2012)

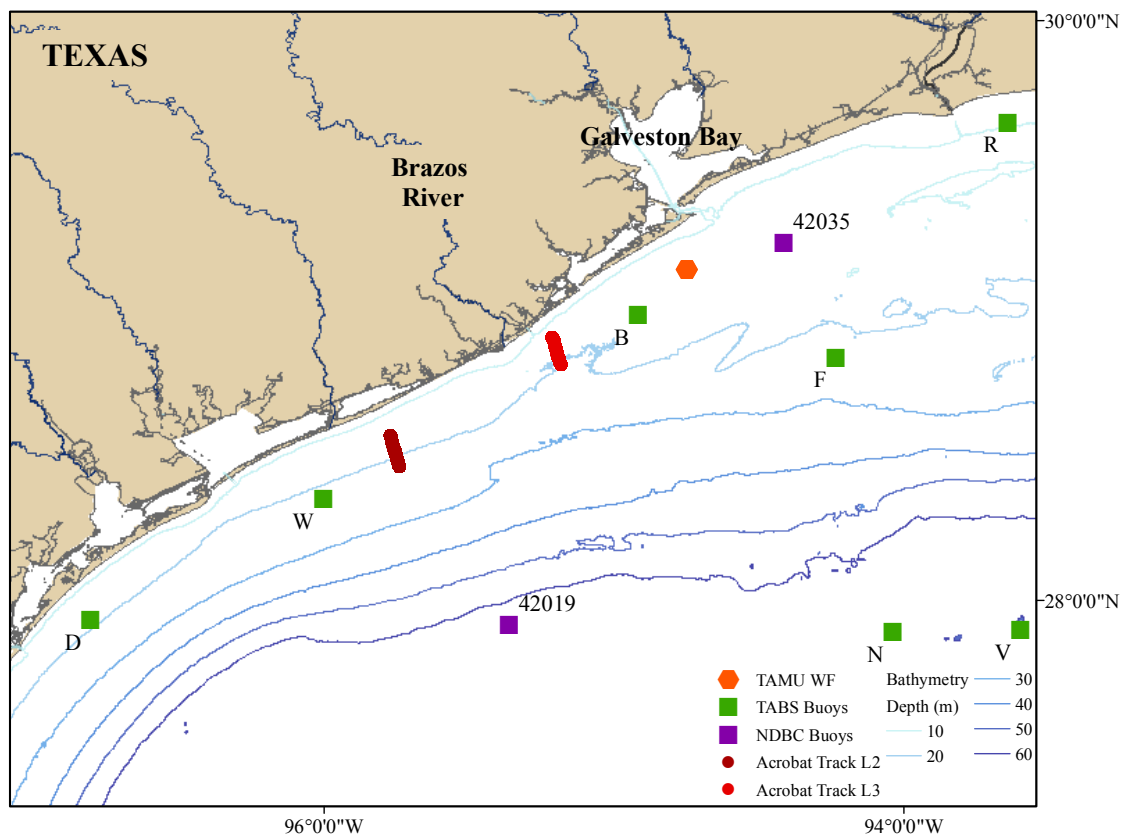
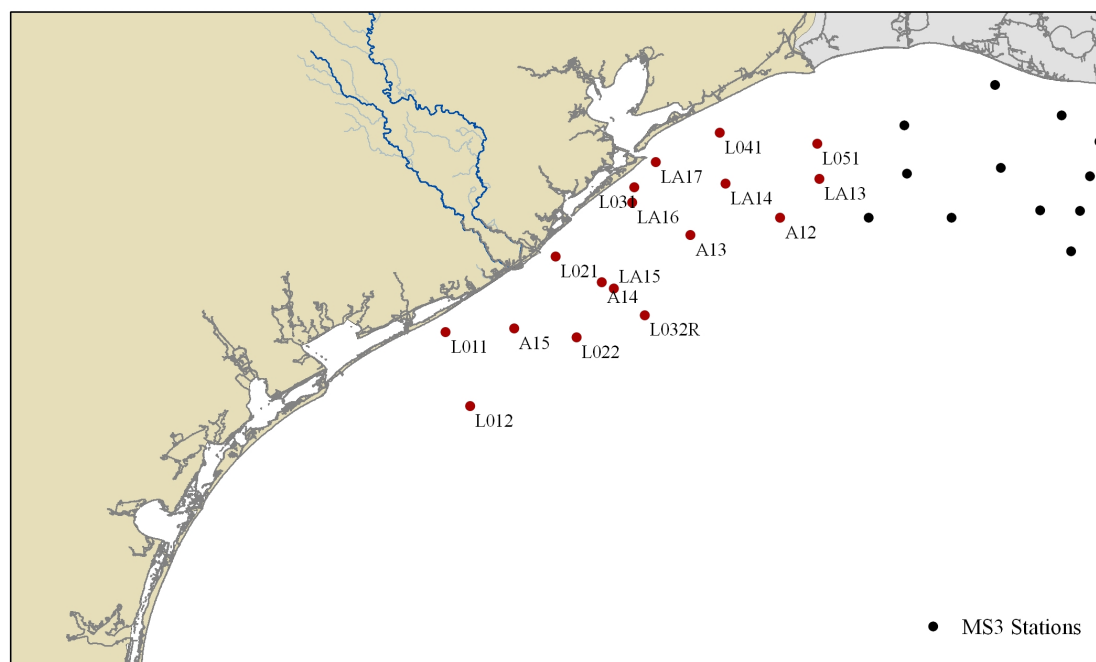
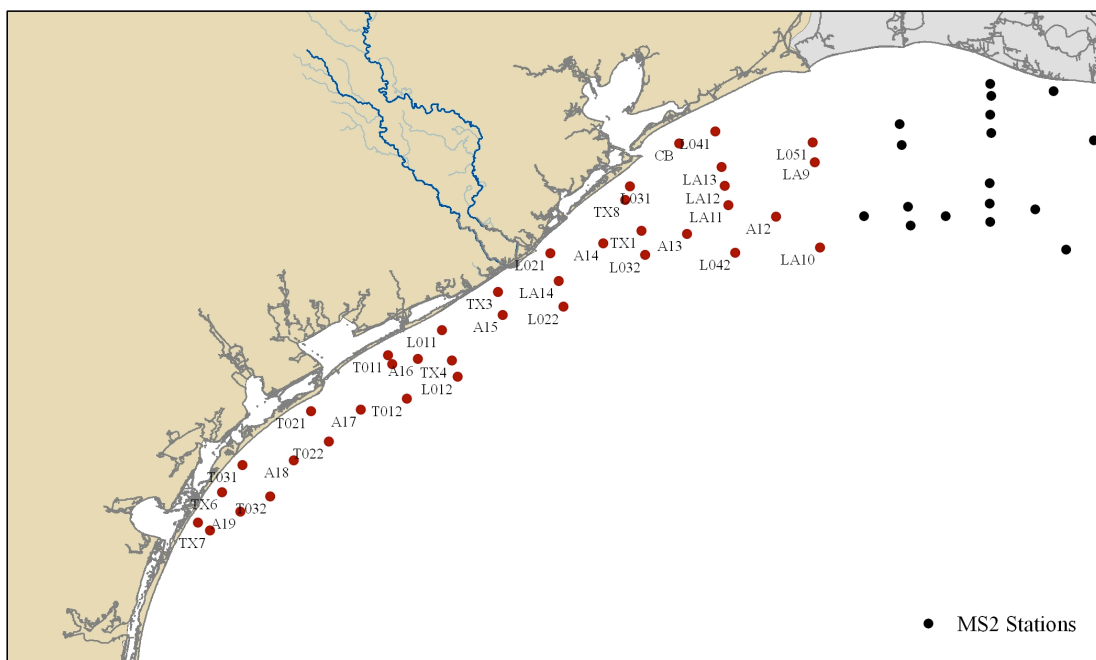


Figure 2.1 Ocean Observing Platforms and Acrobat Tracks on the Texas Shelf. The map above shows the locations of the TAMU mooring and towfish tracks, and TABS and NDBC buoys analyzed in Section 2. TABS B and NDBC 42035 buoys data were analyzed for this research and are indicated by the orange circle. The two dark red lines indicate the TAMU Acrobat towfish tracks (L2 and L3) analyzed in Section 2. The 10 to 60 m isobaths are shown.

Figure 2.2 TAMU MCH MS Cruise Plans for MS2, MS3, and MS4. CTD stations labeled and colored red are stations considered for statistical analyses in Section 2. The stations in black are sampled during each cruise, but are on the Louisiana shelf and not considered in this research.



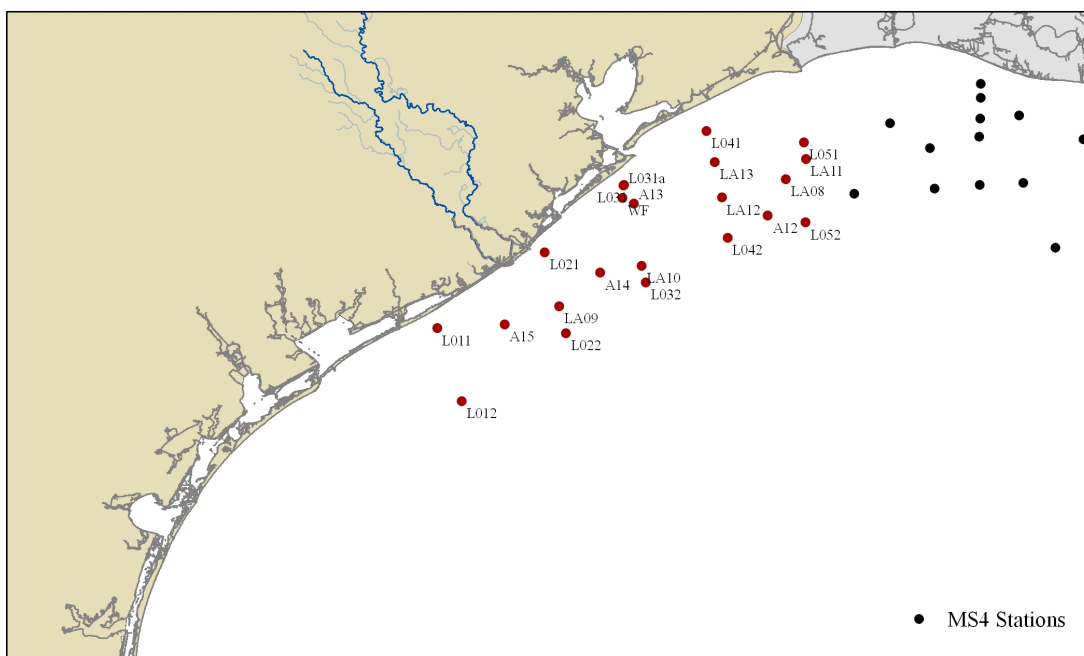


Figure 2.2 Continued

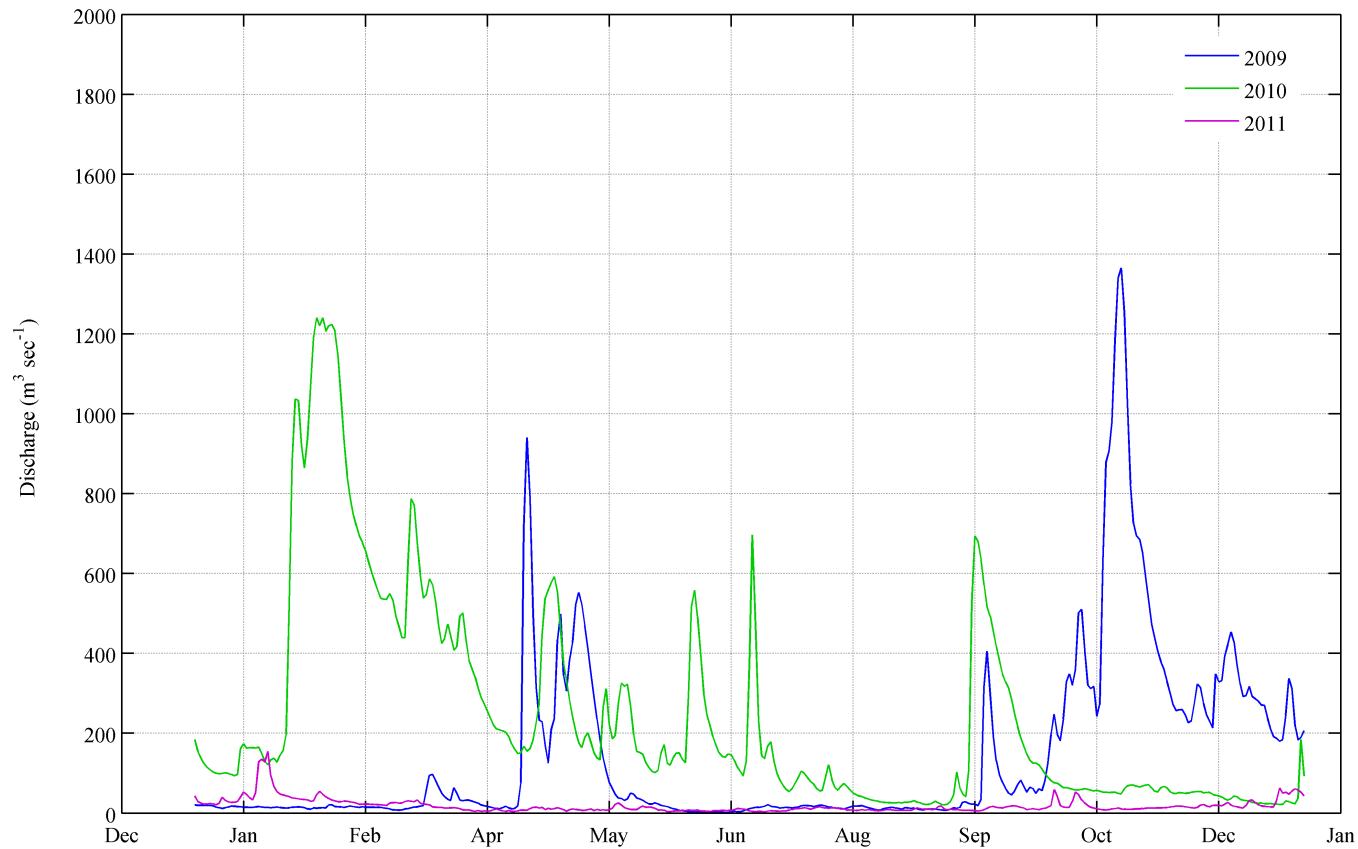


Figure 2.3 Brazos River Daily Mean Discharges from 2009 to 2011. The plot above shows the individual daily mean discharge volumes ( $\text{m}^3 \text{sec}^{-1}$ ) for 2009 to 2011. The blue line shows discharge for 2009, in which two high volume ( $> 900 \text{ m}^3 \text{sec}^{-1}$ ) peaks were seen in April and October. The green line is the discharge for 2010 with the highest peak occurring at the beginning of the year and volume falling below  $700 \text{ m}^3 \text{sec}^{-1}$  for the remainder of the year. The pink line shows discharge for 2011, which was an extreme drought year for Texas with discharge not increasing greater than  $200 \text{ m}^3 \text{sec}^{-1}$  at any time of the year.

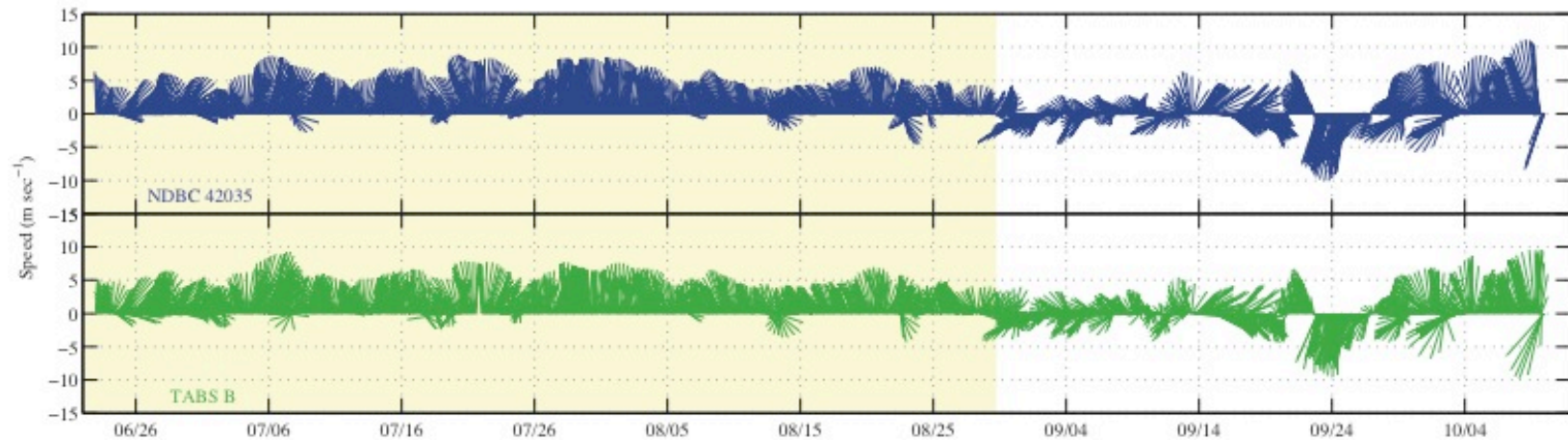


Figure 2.4 Low-pass (3-h) Filtered Wind Speeds in 2009 from NDBC 42035 and TABS B Buoys. Wind speeds (m/s) are plotted for NDBC 42035 (top panel, blue) and TABS B (lower panel, green) buoys for 2009 for the duration of the TAMU WF deployment (June 23 – October 9). The vectors are oriented to show the direction the wind is going (oceanographic convention) with northerly directions indicating upcoast flows and southerly directions indicating downcoast flows. The yellow box highlights the summer months. Winds were predominantly upcoast in the summer months (late June to late August) and reverse in the non-summer months (beginning of September to October 9). The non-summer months were also more variable with a number of strong reversals between up- and downcoast flow occurring that lasting for days to a week. NDBC 42035 and TABS B buoy wind speeds were strongly correlated ( $r > 0.8$ ,  $p\text{-value} < 0.0001$ ) with a covariance time scale of 30 days.

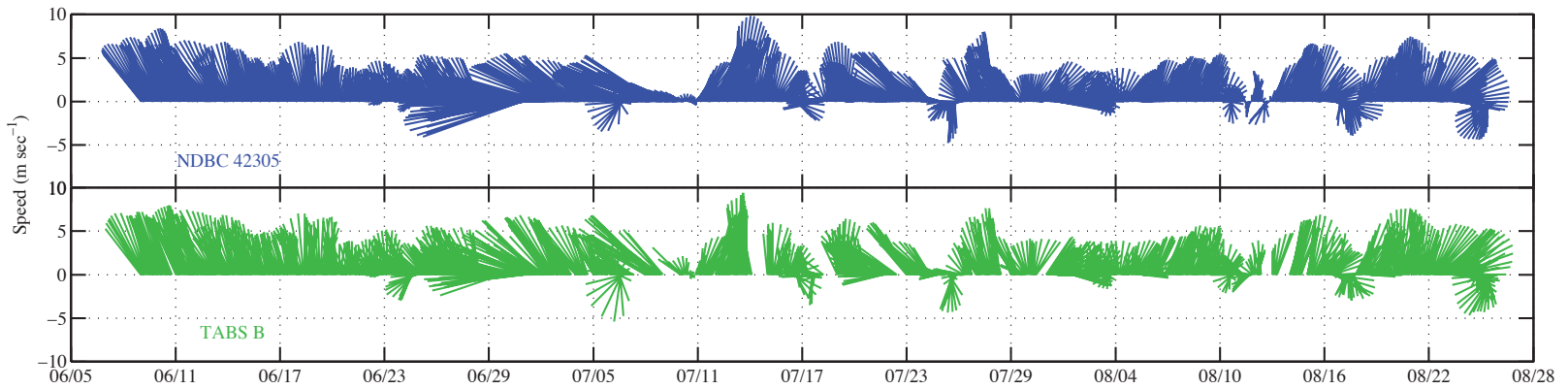


Figure 2.5 Low-pass (3-h) Filtered Wind Speeds in 2010 from NDBC 42035 and TABS B Buoys. Wind speeds (m/s) are plotted for NDBC 42035 (top panel, blue) and TABS B (lower panel, green) buoys for 2010 for the duration of the TAMU WF deployment (June 9 – August 25). Only the summer months were considered, due to TAMU WF deployment complications. Winds reflected summer conditions with strong upcoast flows ranging between 5 and 10 m/s for most of the record with short-lived downcoast reversals also occurring. NDBC 42035 and TABS B buoy wind speeds were strongly correlated ( $r > 0.8$ ,  $p\text{-value} < 0.0001$ ) with a covariance time scale of 30 days.

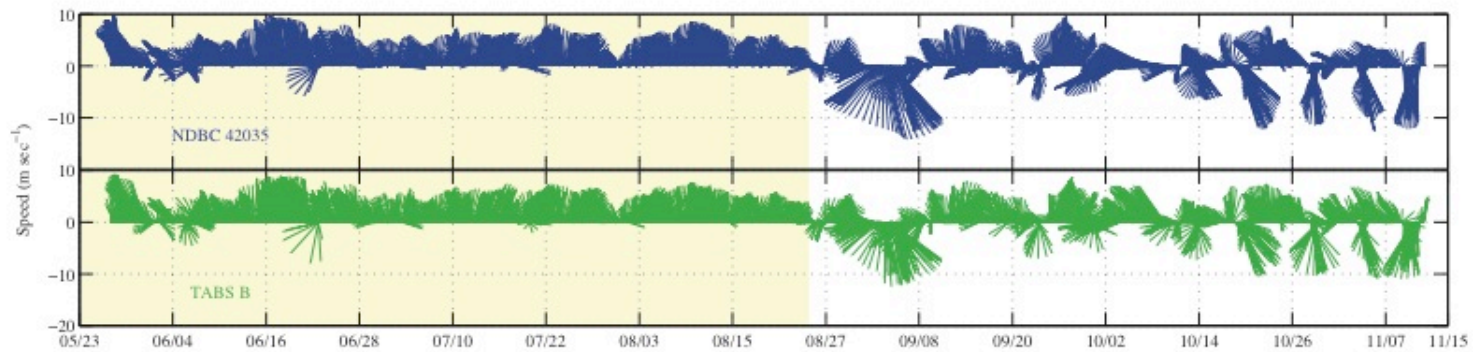


Figure 2.6 Low-pass (3-h) Filtered Wind Speeds in 2010 from NDBC 42035 and TABS B Buoys. Wind speeds (m/s) are plotted for NDBC 42035 (top panel, blue) and TABS B (lower panel, green) buoys for 2011 for the duration of the TAMU WF deployment (May 27 to November 11). The vectors are oriented to show the direction the wind is going (oceanographic convention) with northerly directions indicating upcoast flows and southerly directions indicating downcoast flows. The yellow box highlights the summer months. Winds were predominantly upcoast in the summer months (late June to late August) and reversed in the non-summer months (beginning of September to October 9). The non-summer months were also more variable with a number of strong reversals between up- and downcoast flow. The reversals lasted for days to a week. NDBC 42035 and TABS B buoy wind speeds were strongly correlated ( $r > 0.8$ ,  $p\text{-value} < 0.0001$ ) with a covariance time scale of 30 days.

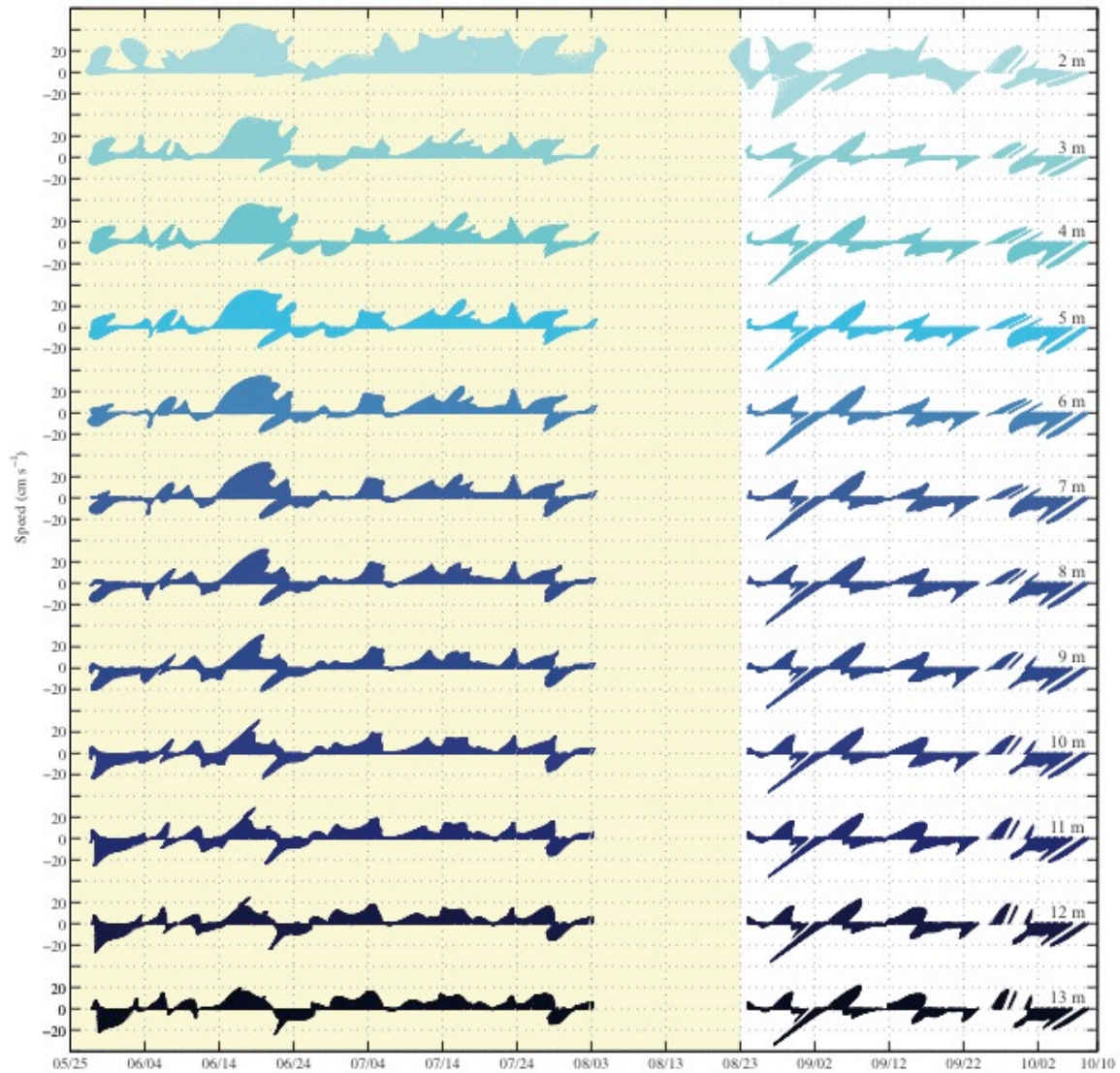


Figure 2.7 Low-pass (40-h) Current Velocities in 2009 from the TAMU WF RDCP. Wind velocities (cm/s) are plotted for depths bins from the TAMU WF RDCP in 2009. Depth bins start and 3 m and continue down to 13 m. The shading of blue indicates the depth bin with the lightest blue representing 3 m bin and the darkest blue indicating the 13 m bin. The yellow box highlights the summer month corresponding to the wind speeds in Figure 2.4. The surface currents (2 and 3 m) were upcoast for a majority of the summer and transition to downcoast flow in the non-summer months. Reversals in seasonal direction in the deeper bins were short-lived rotations (e.g. waves), but were not explored further.

Figure 2.8 Low-pass (40-h) Current Velocities in 2010 from the TAMU WF RDCP. Wind velocities (cm/s) were plotted for depths bins from the TAMU WF RDCP in 2010. Depth bins start and 3 m and continue down to 13 m. The shading of blue indicates the depth bin with the lightest blue representing 3 m bin and the darkest blue indicating the 13 m bin. The gap in the record was due to instrument maintenance. The surface currents (2 and 3 m) were upcoast for a majority of the summer and range between 10 and 25 cm/s. Short-lived reversals (1 – 5 days) in the deeper bins were short-lived rotations (e.g. waves), but were not explored further.

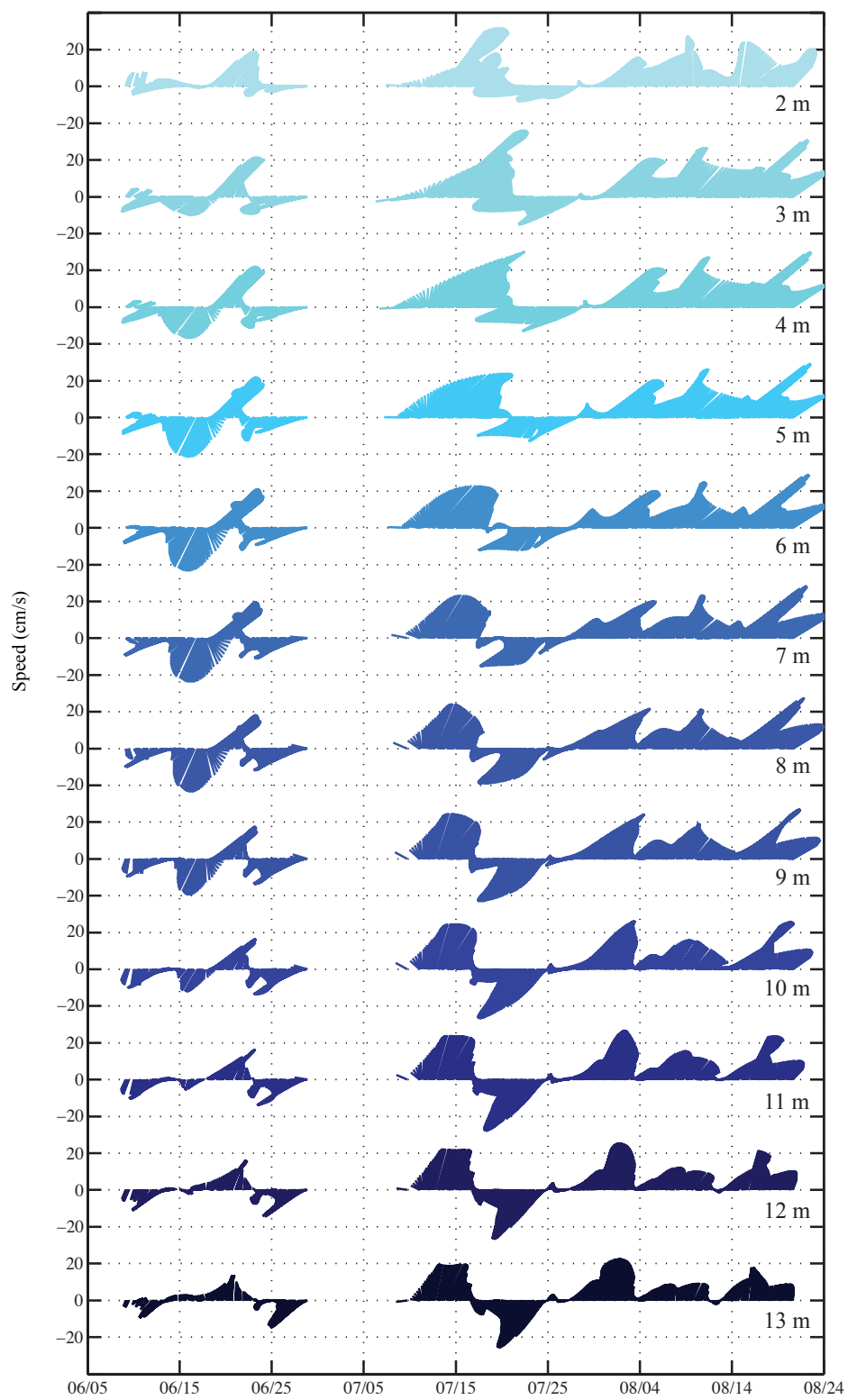
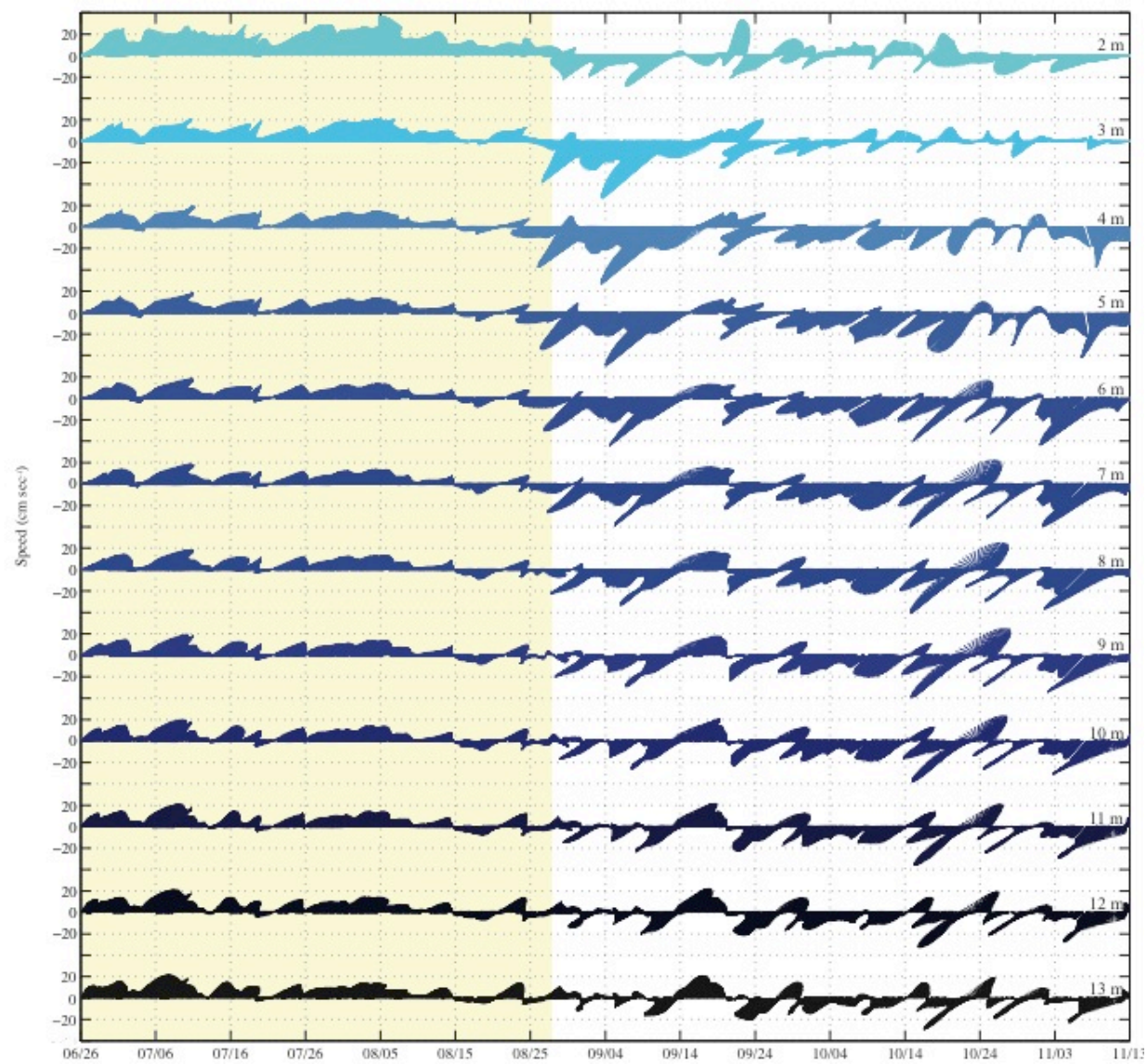


Figure 2.9 Low-pass (40-h) Current Velocities in 2011 from the TAMU WF RDCP. Wind velocities (cm/s) are plotted for depths bins from the TAMU WF RDCP in 2009. Depth bins start and 3 m and continue down to 13 m. The shading of blue indicates the depth bin with the lightest blue representing 3 m bin and the darkest blue indicating the 13 m bin. The yellow box highlights the summer month corresponding to the wind speeds in Figure 2.6. The surface currents (2 and 3 m) were upcoast for a majority of the summer and transitioned to stronger downcoast flow in the non-summer months. Velocities ranged from 10 to 25 cm/s in the top depth bins and weakened to below 20 cm/s down in the water-column. Reversals in seasonal direction in the deeper bins were short-lived rotations (e.g. waves), which were not further explored.



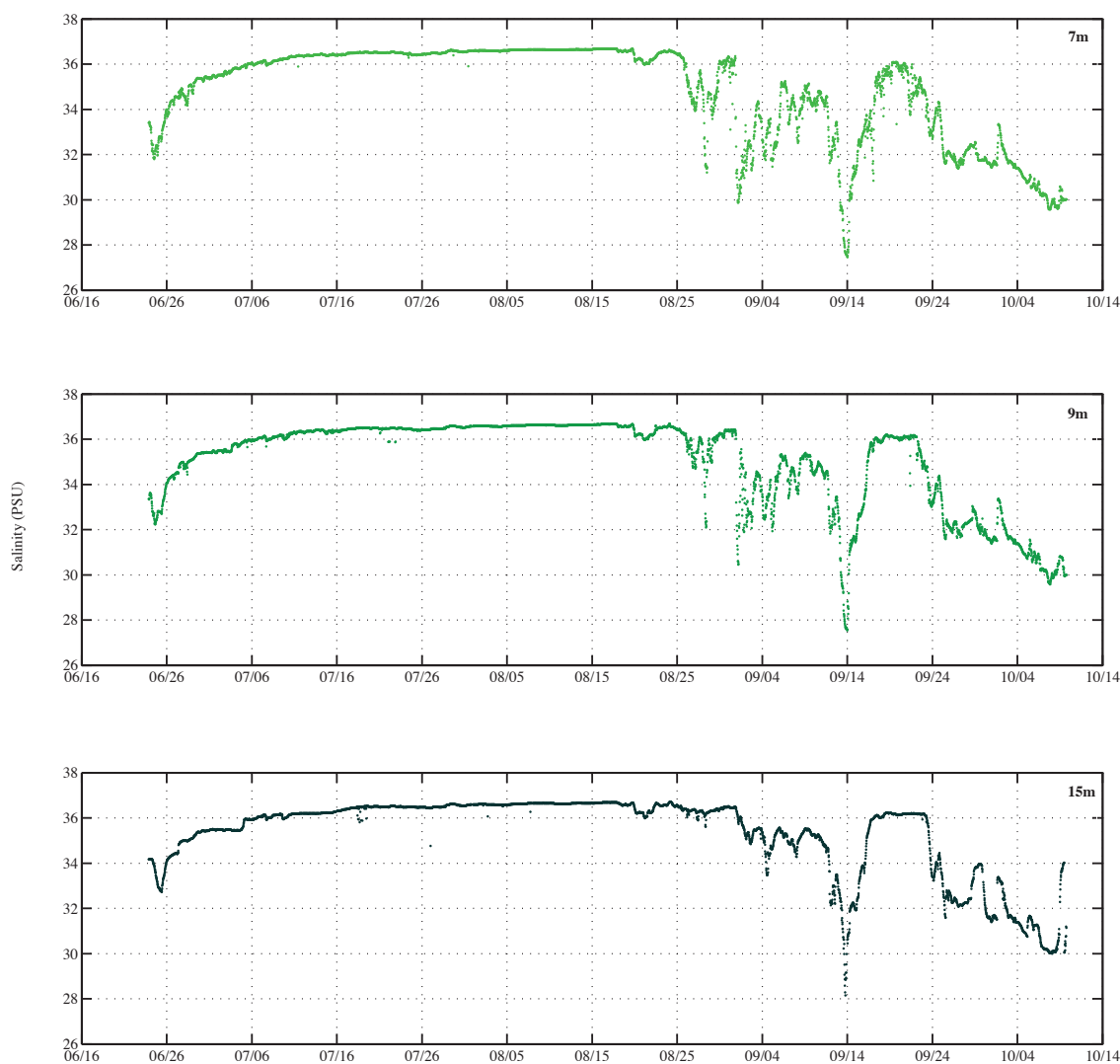


Figure 2.10 2009 TAMU WF Array Raw Salinity (PSU) Data. The three panels show the 2009 TAMU WF array salinities starting with the 7 m array on the top panel and the 15 m on the lowest panel. Salinities at the three depths ranged from ~28 to 36.5 PSU. After the initial array deployment, salinity increased and remained nearly constant at 36 PSU for the summer months. At the seasonal transition (August 25) to non-summer conditions, water-column salinity oscillated between 28 and 36 PSU for the remainder of the time series. The freshest salinity occurred on September 14, indicating a movement of freshwater over the TAMU WF.

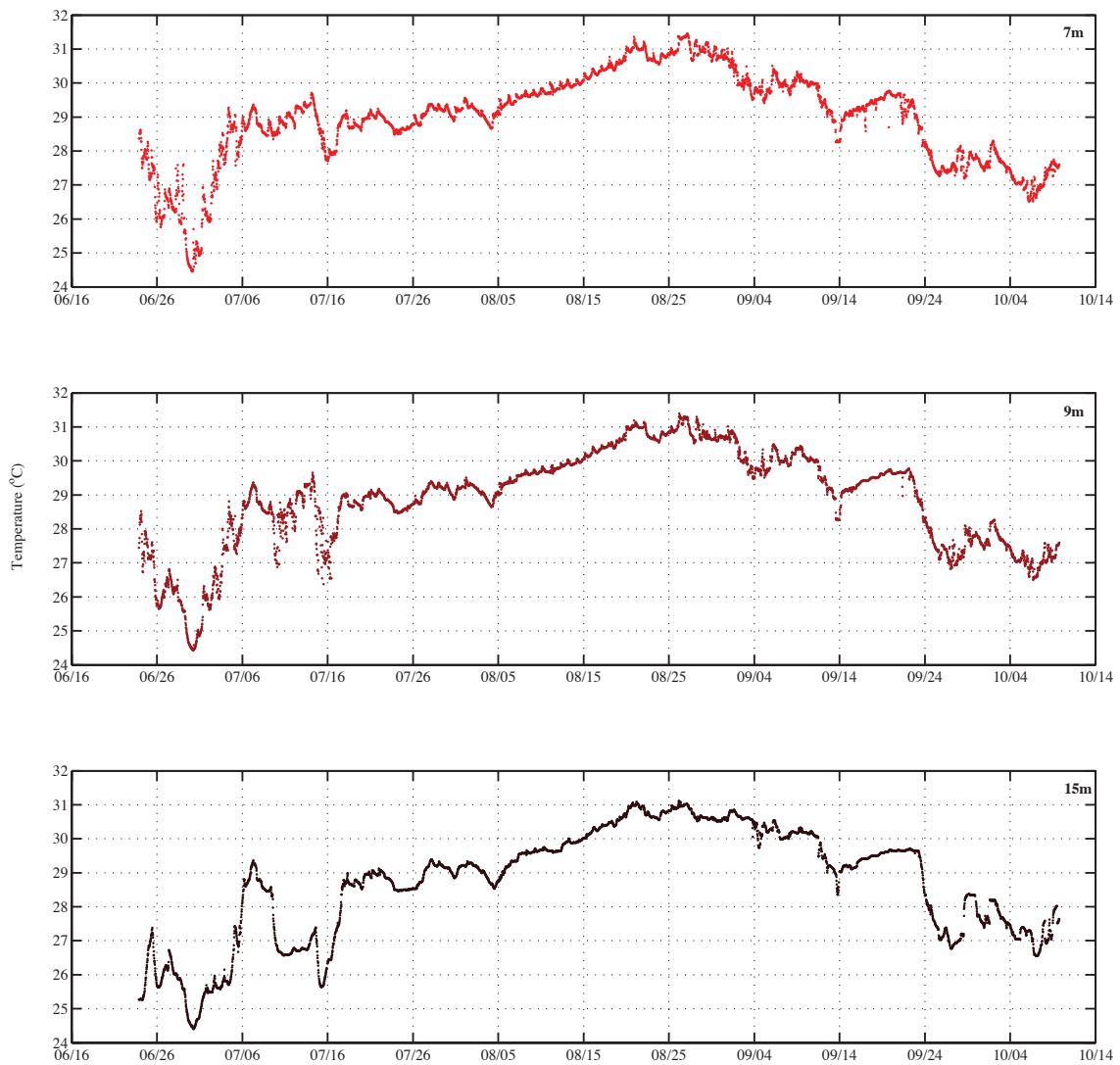


Figure 2.11 2009 TAMU WF Array Temperature Profile. The three panels show the 2009 TAMU WF array temperatures starting with the 7 m array on the top panel and the 15 m on the lowest panel. Temperatures ranged from ~31.5 to 24.5 °C. The seasonal trend between summer and non-summer months was not as apparent as seen in Figures 2.4, 2.7, and 2.10. Temperatures were the coolest (less than 29 °C) at the start of the time series and increased during the summer months in response to increased insolation. Water column temperatures started to decrease on August 25 and continued to decrease for the remainder of the record.

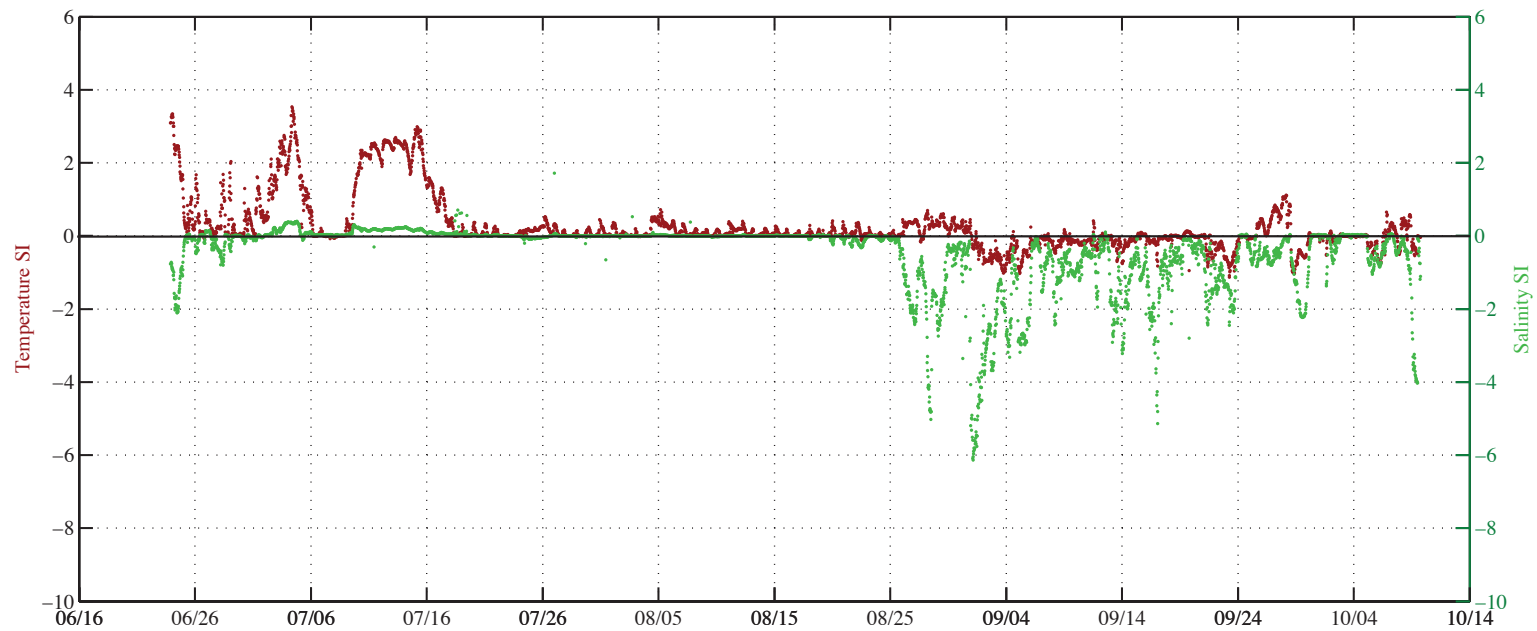


Figure 2.12 2009 TAMU WF Array SSI and TSI Data. The 2009 TAMU WF array SSI (units of  $\Delta$ PSU) and TSI (units of  $^{\circ}$ C) are plotted above and were calculated from the raw TAMU WF array data. The red line represents the TSI and the green line indicates the SSI. The black line designates 0, which means the surface (7 m) and bottom (15 m) salinity or temperature observations are equal. The SSI was nearly 0 for the summer months with the largest range being the negative peak at the start of the record. The SSI decreased rapidly on August 25, which is the seasonal transition between summer and non-summer on the Texas coast. In late August and early September, SSI reached negative values between -4 and -6. The TSI was stronger in the beginning of the summer ranging between  $\sim$ 2 and 3.5  $^{\circ}$ C. After July 16, the TSI decreased to near zero for the remainder of the time series and then decreased slightly ( $< 1$   $^{\circ}$ C) after August 25. The TSI stayed negative for most of the non-summer period with only two increases in late September and mid-October.

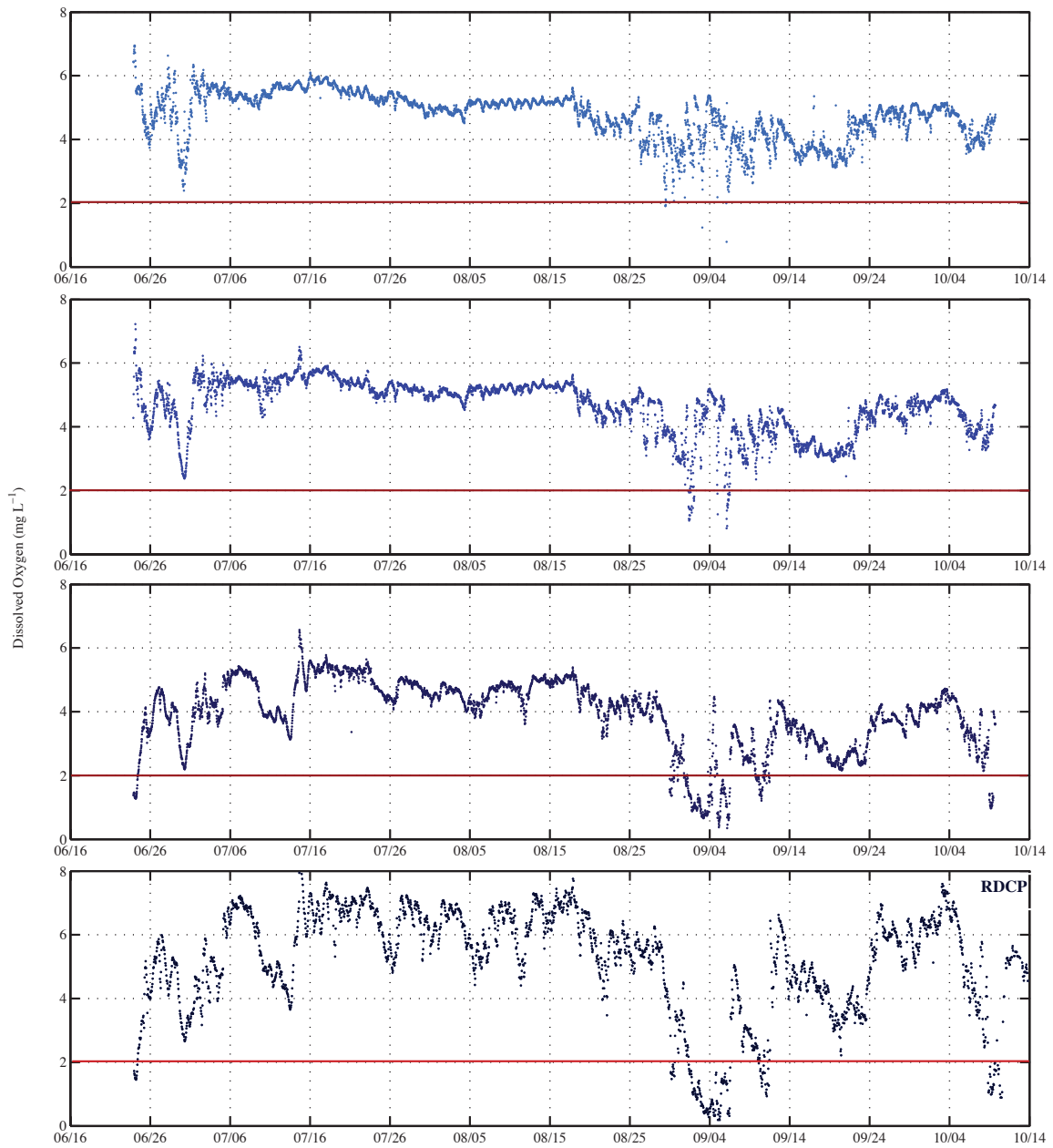


Figure 2.13 2009 TAMU WF Array and RDCP Raw Dissolved Oxygen Data. The four panels show the 2009 TAMU WF array (top three panels) and RDCP (bottom panel) dissolved oxygen concentrations (mg/L). The red line indicates the hypoxic boundary at 2.0 mg/L. Hypoxia was only observed at the 15 m (3<sup>rd</sup> panel) and the RDCP (4<sup>th</sup> panel) at the start of the time series and the summer season. Bottom dissolved oxygen concentrations dropped after the seasonal transition starting August 25 in the entire water-column with the most persistent event occurring around September 4. Oxygen values increased above hypoxic levels after September 14 before dropping below 2.0 mg/L at the end of the time series.

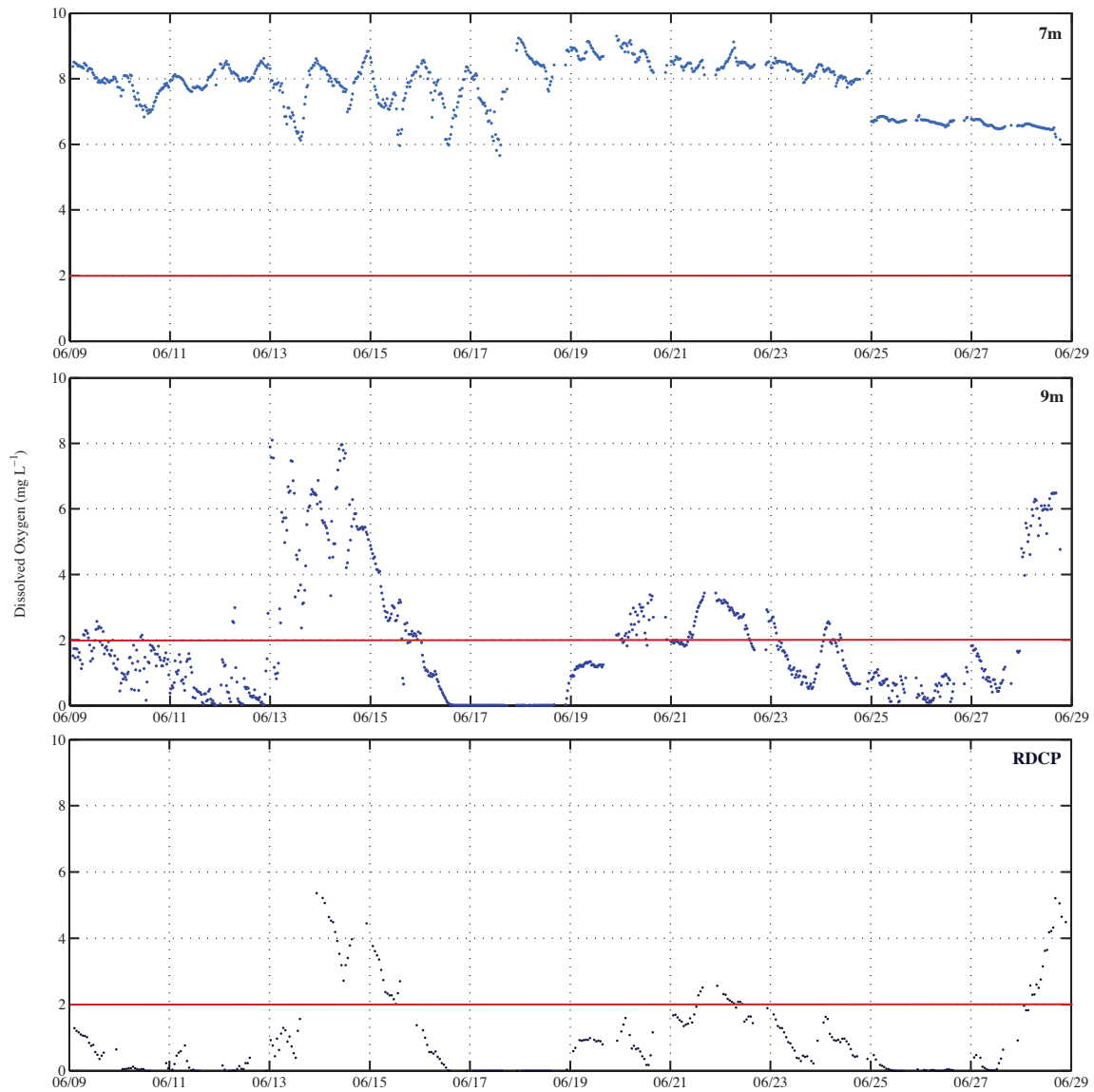


Figure 2.14 2010 TAMU WF Array and RDCP Raw Dissolved Oxygen Profiles. The four panels show the 2010 TAMU WF array (top two panels) and RDCP (bottom panel) dissolved oxygen concentrations (mg/L). The red line indicates the hypoxic boundary at 2.0 mg/L. Hypoxia was observed at the start of the time series and persisted through June 14 at the RDCP and 9 m array. Following a short period of water-column oxygenation, hypoxia formed again on June 16 and persisted longer to June 21 at both depths. Another short oxygenation occurred on June 22, before persistent hypoxia was observed again for another 6 days (June 28). Hypoxia was not observed in the 7 m depth.

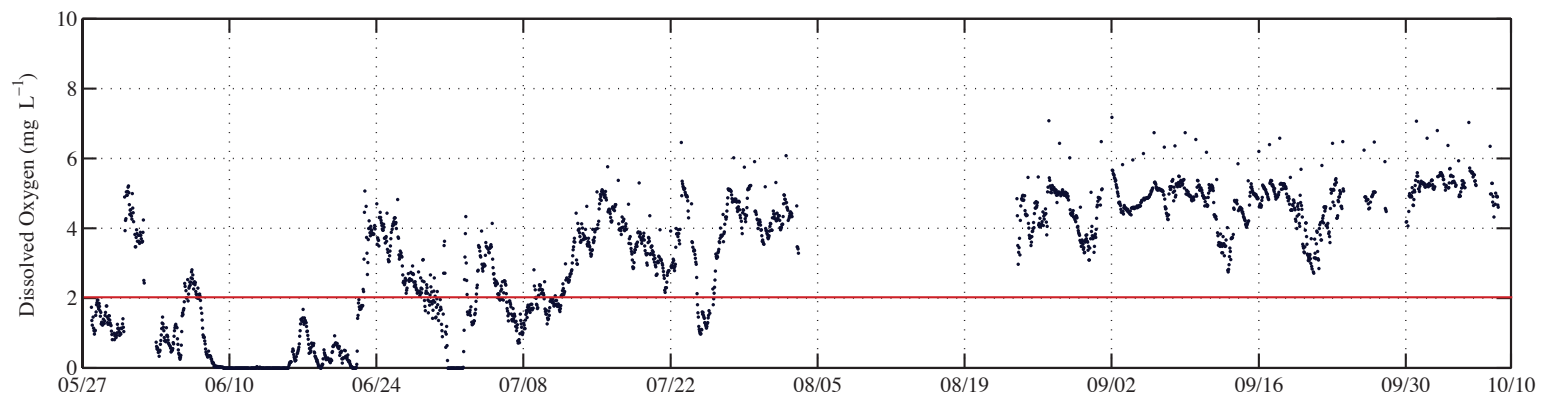
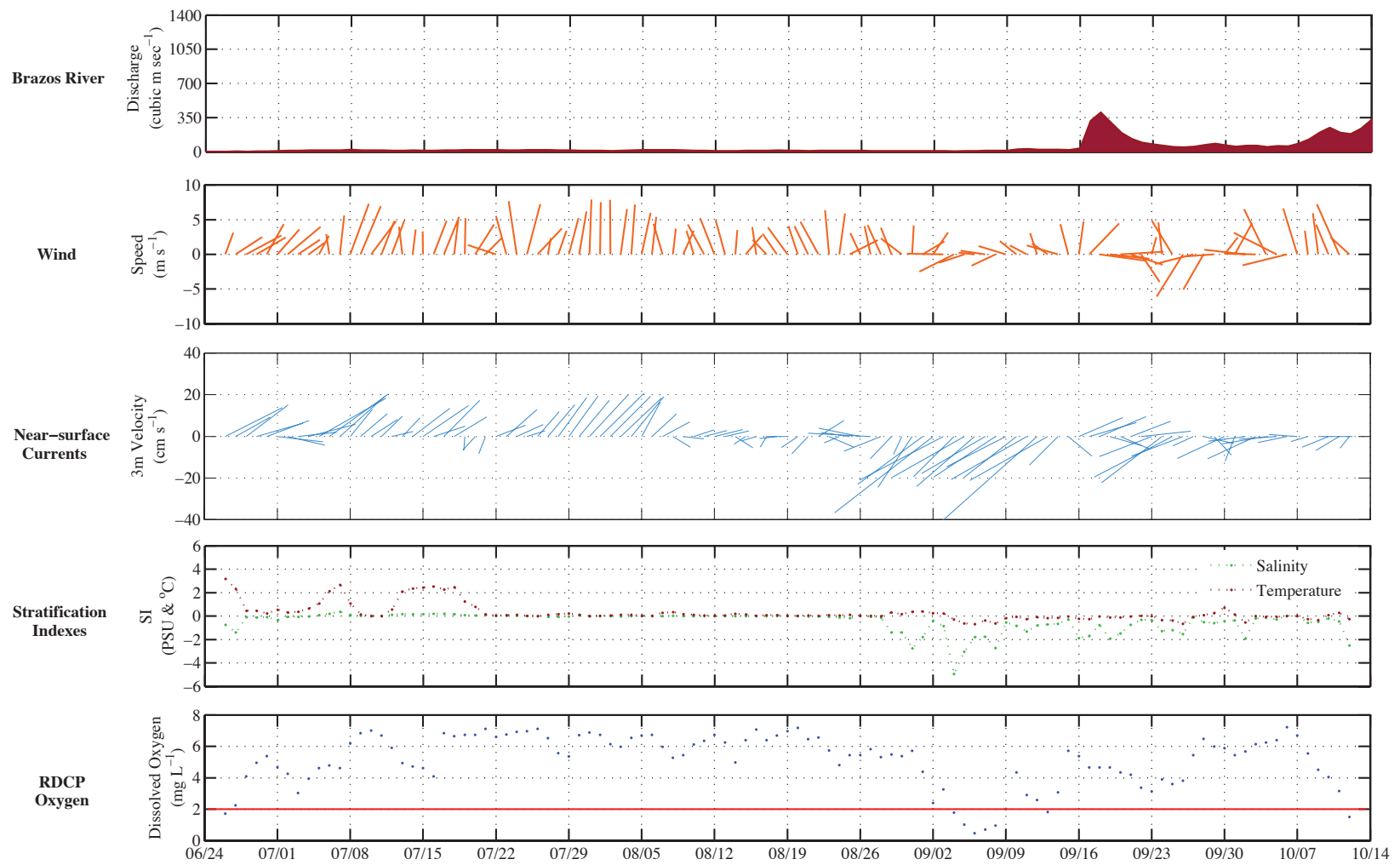


Figure 2.15 2011 TAMU WF Array and RDCP Dissolved Oxygen Profile. The plot shows the 2011 TAMU WF RDCP raw dissolved oxygen data. There was no array data for 2011. The red line indicates the hypoxic boundary at 2.0 mg/L. The gap in the time series is due to instrument maintenance in the late summer. Hypoxia was observed at the start of the record and throughout the summer months. Events were episodic (< 24 h) or persistent (> 24 h). After redeployment of the RDCP, hypoxia was not observed again for the remainder of the time series.

Figure 2.16 2009 Brazos River, NDBC 42035 Winds, TAMU WF Array and RDCP Daily-averaged Profiles. The five panels show the 2009 daily-averaged data for the Brazos River discharge (source: USGS), NDBC 42035 wind speed, TAMU WF RDCP 3 m current velocities, SSI, and TSI, and bottom dissolved oxygen. There is very small amount of Brazos River discharge in the summer during the duration of the TAMU WF. The upcoast wind direction and current velocities do not transport freshwater to the north Texas shelf as indicated by the weak SSI. The TSI was stronger at the start of the time series, which was potentially driving the decrease of dissolved oxygen. However, the TSI did not cause stratification strong enough to result in hypoxia formation. Water conditions changed following the coastal transition between summer and non-summer. Hypoxia occurred as a result of a strengthening the SSI, which was most likely due to the advection of MARS water westward onto the northern Texas shelf. The fall hypoxic event (September 4) was not the cause of Brazos River water advecting northward, which was supported by the non-summer downcoast flow and variable winds.



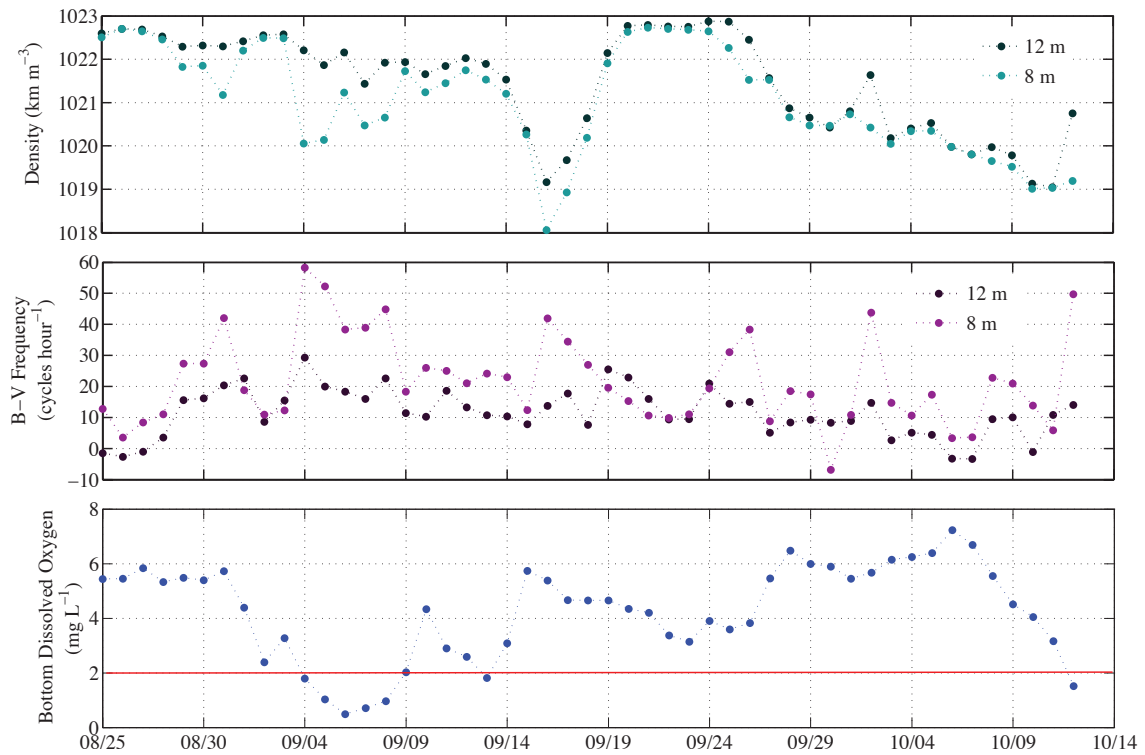


Figure 2.17 2009 Mid-Depth Daily-Averaged Density, Brunt-Väisälä, and Bottom Dissolved Oxygen Data from the TAMU WF. The three panels show the density (top panel) and Brunt-Väisälä frequencies calculated from the daily-averaged TAMU WF array data. The 8 m mid-depth, determined from the conditions between the 7- and 9 m array are shown in light teal (density, top panel) and light purple (Brunt-Väisälä, middle panel). The 12 m mid-depth, determined from the conditions between the 9 and 15 m array instruments are shown in dark teal (density, top panel) and dark purple (top panel). The daily-averaged TAMU WF RDCP bottom dissolved oxygen was plotted in the bottom panel with the red line indicating the hypoxic boundary. The surface-most layer (8 m) was fresher and more stratified than the lower layer (12 m). The fall hypoxic event observed in 2009 coincided with the strongest Brunt-Väisälä frequencies peaking near 60 cph. Although only one hypoxic event was observed, bottom dissolved oxygen did drop as result of increased Brunt-Väisälä frequencies in the fall, as seen mid- to late September and on October 11.

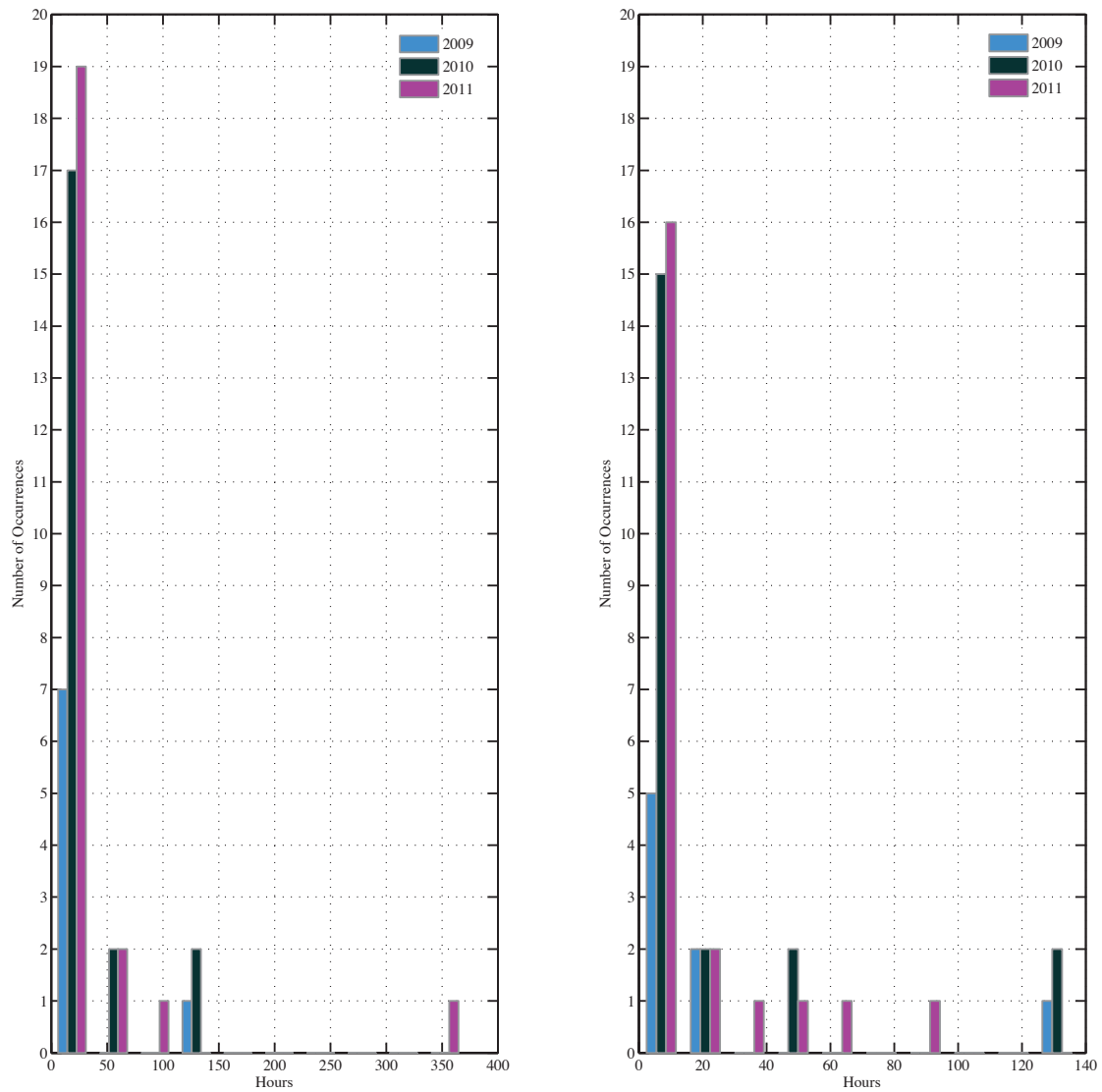


Figure 2.18 Histograms of Hypoxic Events Observed at the TAMU WF RDCP from 2009 to 2011. The histogram on the right shows the hypoxic events observed from the raw TAMU WF RDCP data from 2009 to 2011. The greatest numbers of occurrences were less than 25 h for all three years. The longest event was observed in 2011 lasting longer than 350 h. The histogram on the right removes the event outlier in 2011. The distribution of events showed most events to occur at and less than 10 h. Events were more persistent in 2009 and 2011 than 2010 with 4 events each year lasting more than 24 h. The average hypoxic event in the three years was approximately 24 h for 2009, 25 h for 2010, and 30 h for 2011.

Figure 2.19 TAMU MCH MS Bottom Dissolved Oxygen Concentrations Versus Brunt-Väisälä Frequencies. The scatterplot shows data for all three TAMU MCH MS cruises (MS2 – blue, MS3 – pink, and MS4 – green). The red line indicates the hypoxic boundary (note the unit change to ml/L) and the black line marks 40 cph. The black line is the threshold determined by Belabassi (2006) and Kiselkova (2008) as the maximum Brunt-Väisälä frequency in which no hypoxia occurs for values below 40 cph. As seen in the plot, the TAMU MCH MS data fell above the Brunt-Väisälä threshold with hypoxic CTD stations exhibiting maximum Brunt-Väisälä frequencies above 40 cph.

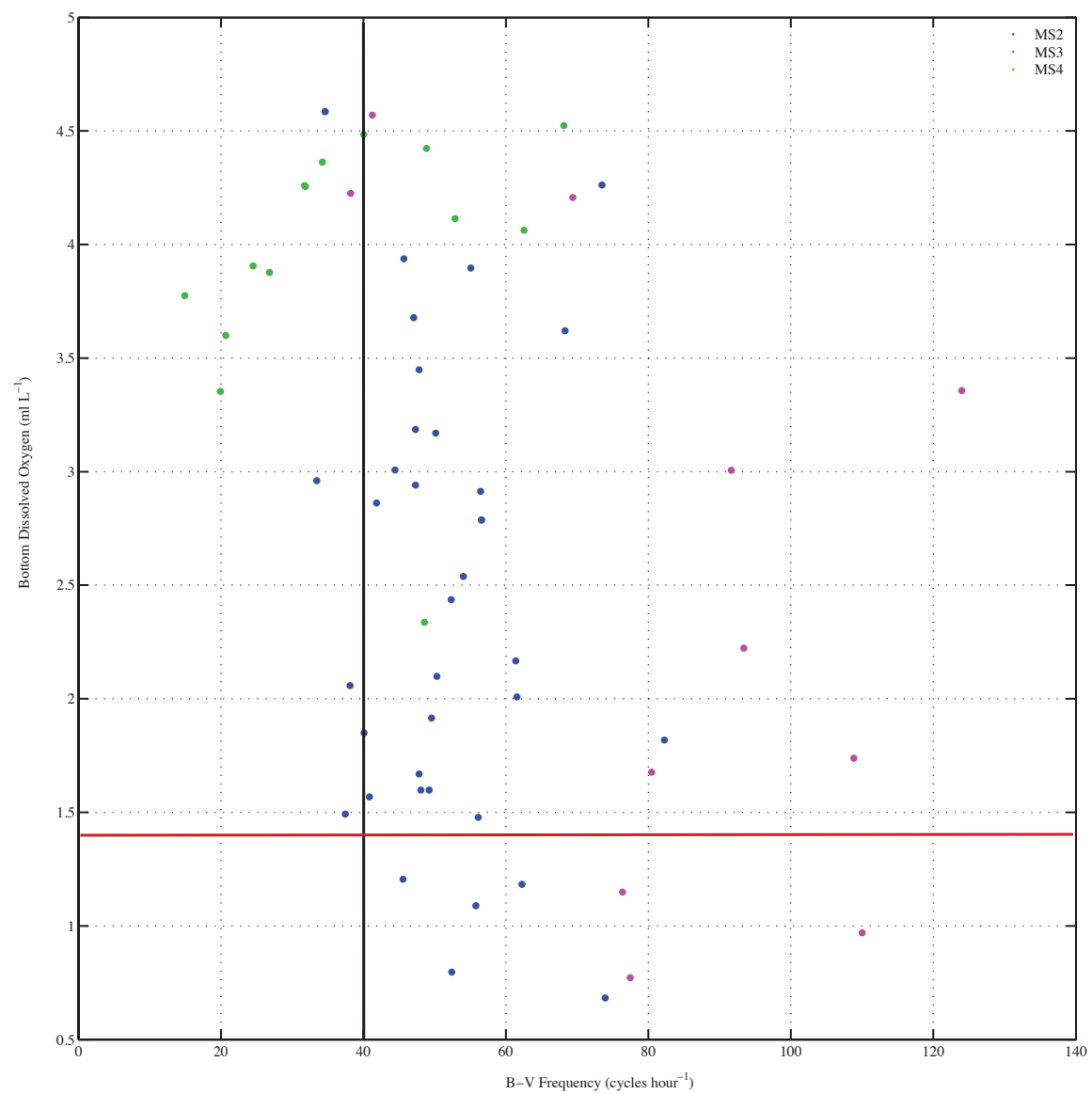
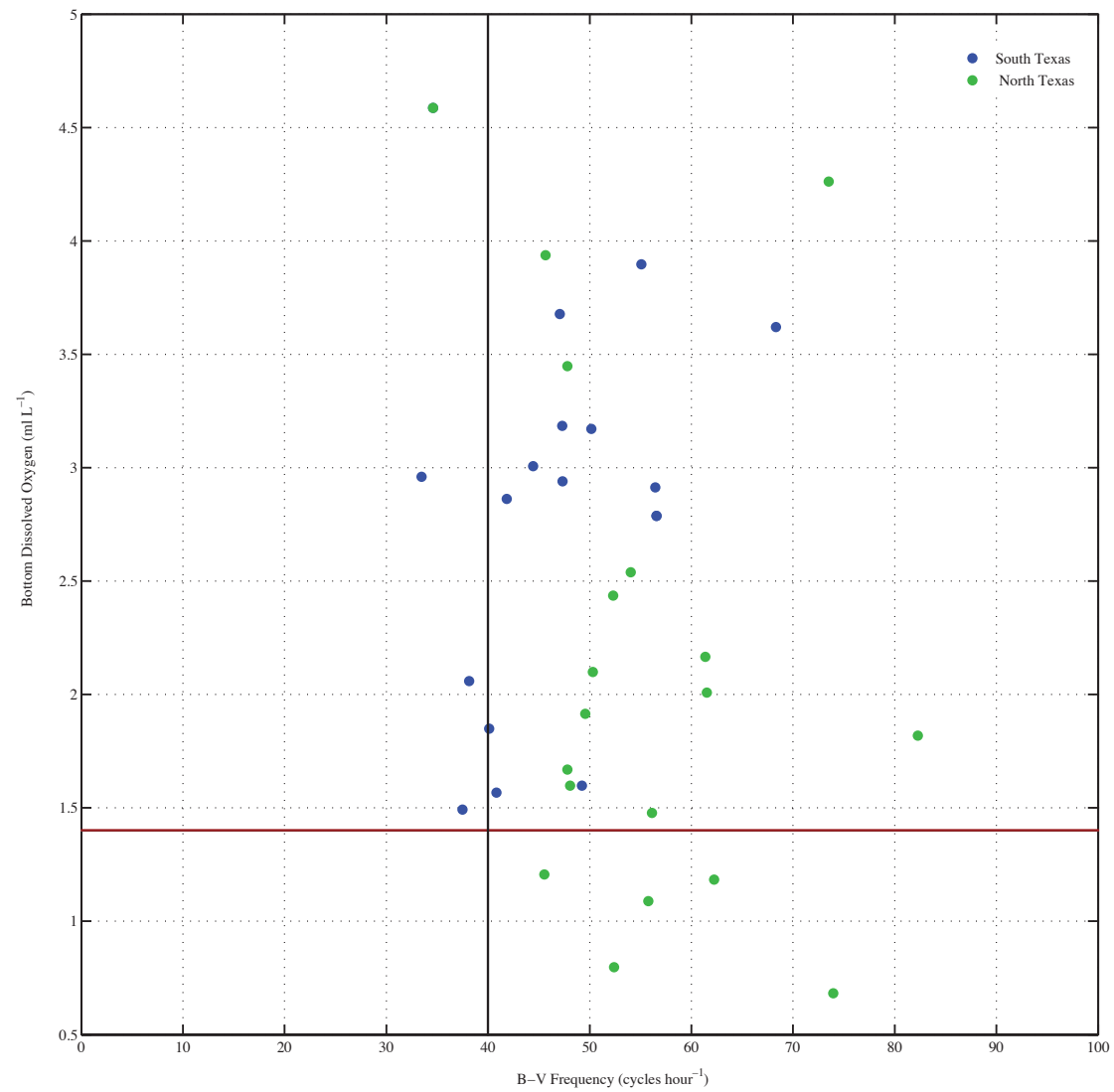


Figure 2.20 TAMU MCH MS2 North and South Texas Bottom Dissolved Oxygen Concentrations Versus Brunt-Väisälä Frequencies. The scatterplot shows data for TAMU MCH MS2 divided into north (green) and south (blue) Texas stations. The red line indicates the hypoxic boundary (note the unit change to ml/L) and the black line marks 40 cph. The black line is the threshold determined by Belabassi (2006) and Kiselkova (2008) as the maximum Brunt-Väisälä frequency in which no hypoxia occurs for values below 40 cph. As seen in the plot, the TAMU MCH MS data were above the Brunt-Väisälä threshold with hypoxic CTD stations exhibiting maximum Brunt-Väisälä frequencies above 40 cph.



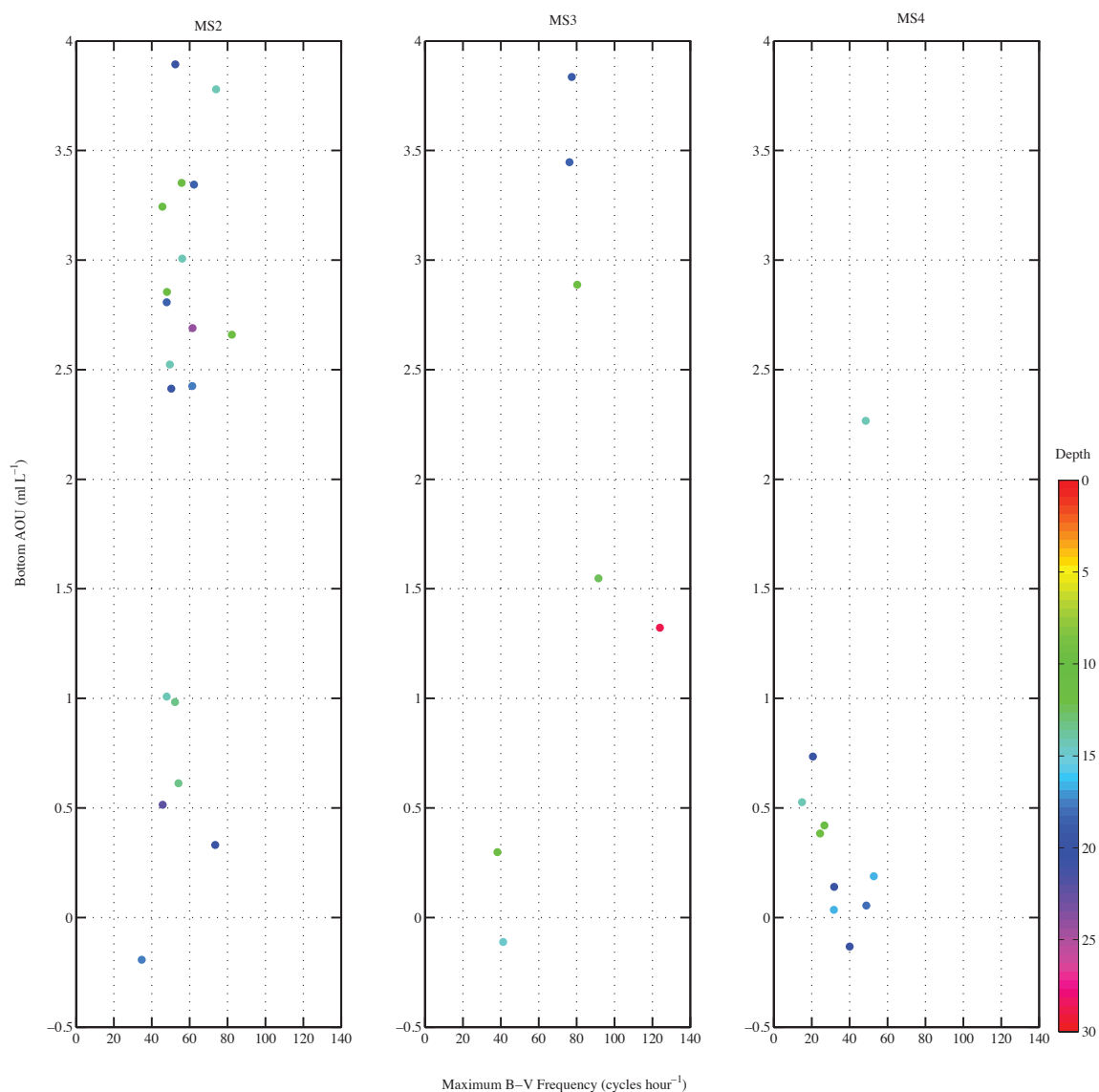


Figure 2.21 TAMU MCH MS2, MS3, and MS4 Survey Bottom AOU Versus Maximum Brunt-Väisälä Frequencies for North Texas CTD Stations. The three panels are ordered left to right by TAMU MCH MS survey with MS2 on the far left, MS3 in the middle, and MS4 on the far right. The data points are scaled by depth (m) with red indicating values at the shallow depths and blues to purples indicating deeper depths. Note there is a unit change for the dissolved oxygen concentrations from mg/L to ml/L.

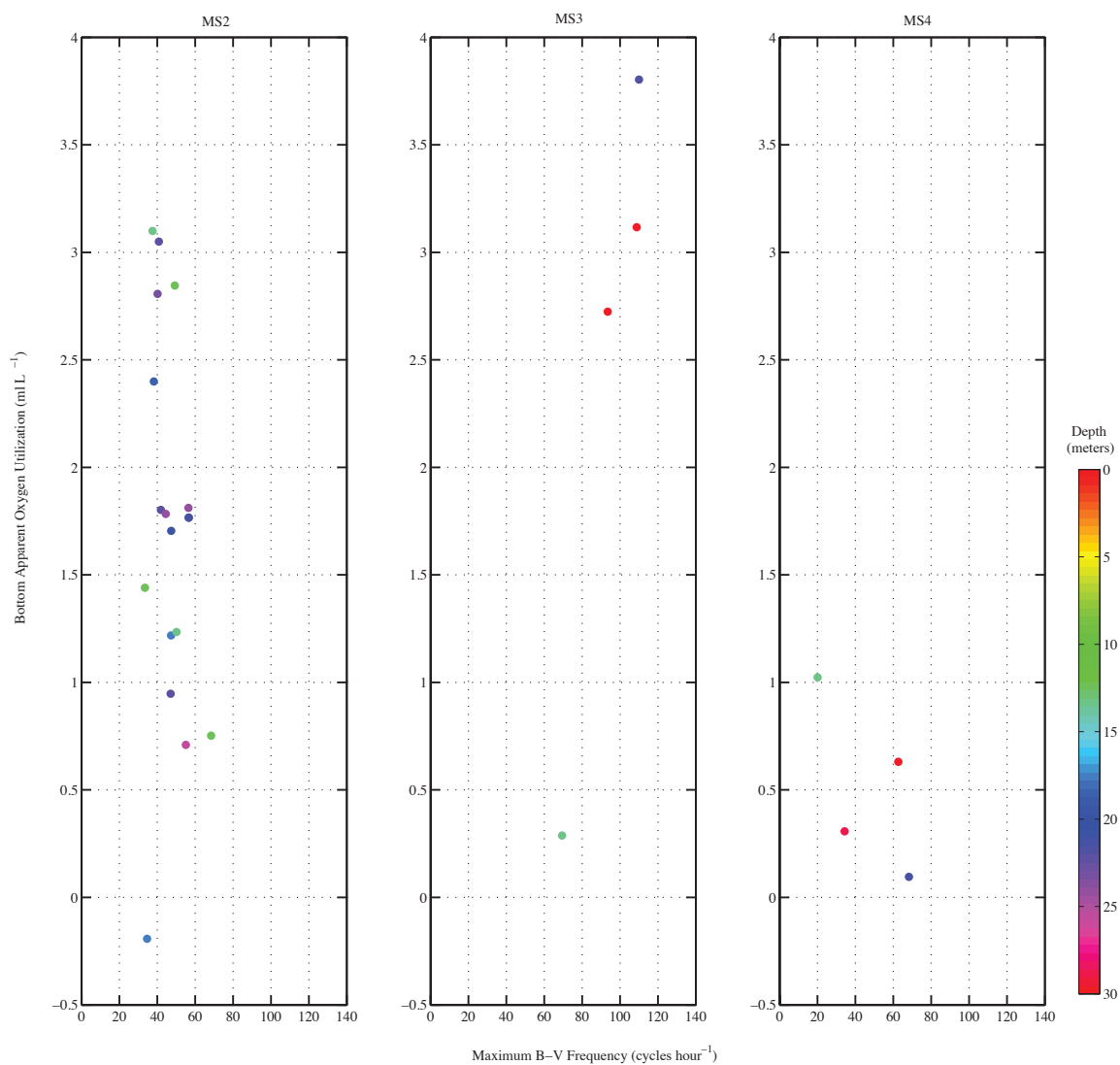
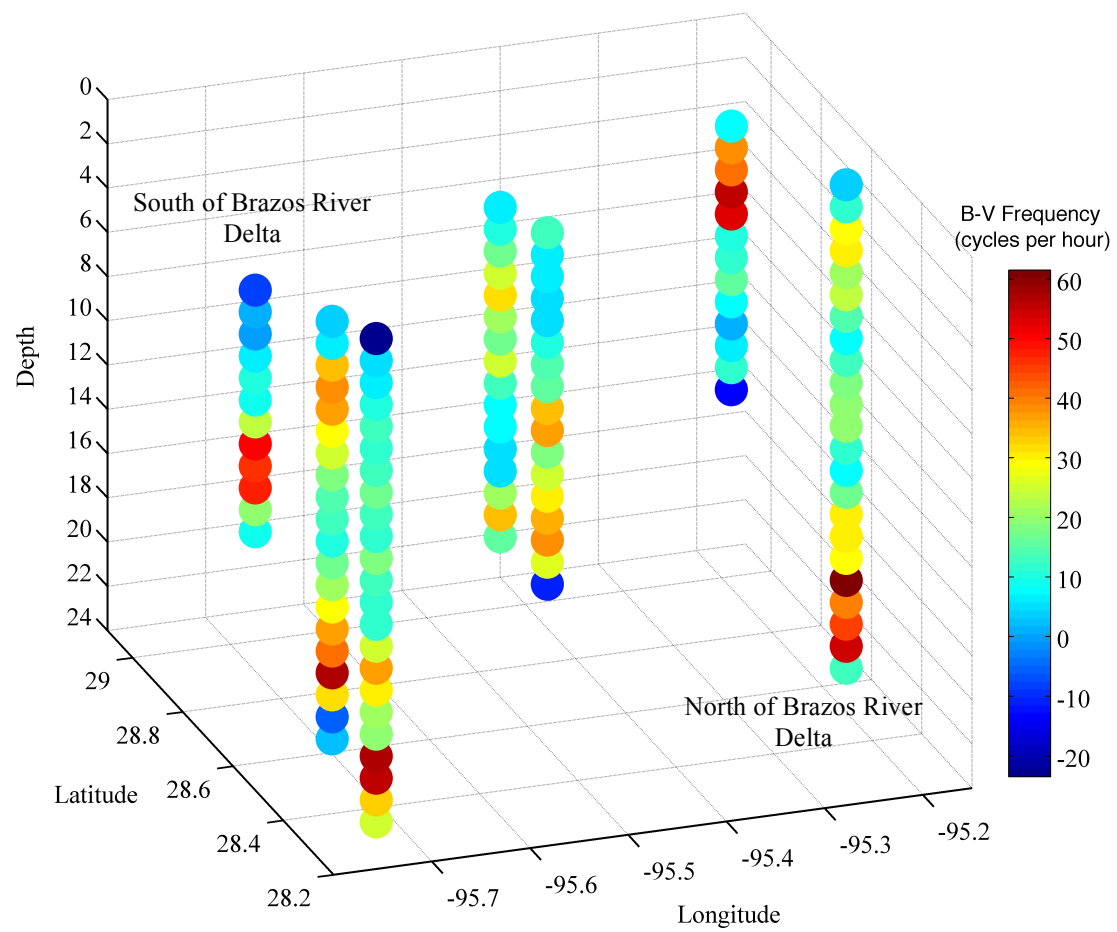


Figure 2.22 TAMU MCH MS2, MS3, and MS4 Survey Bottom AOU Versus Maximum Brunt-Väisälä Frequencies for South Texas CTD Stations. The three panels are ordered left to right by TAMU MCH MS survey with MS2 on the far left, MS3 in the middle, and MS4 on the far right. The data points are scaled by depth (m) with red indicating values at the shallow depths and blues to purples indicating deeper depths. Note there is a unit change for the dissolved oxygen concentrations from mg/L to ml/L.

Figure 2.23 TAMU MCH Selected MS2 CTD Brunt-Väisälä Frequencies and Dissolved Oxygen Water Column Profiles. The two panels show CTD profiles for stations north, at, and south of the Brazos River delta. The depth bins (1 m) in the top panel are colored by Brunt-Väisälä frequencies (cph) and the lower panel depth bins are colored by dissolved oxygen concentration (ml/L). The right of each panel are stations north of the delta and left of each panel are stations south of the delta. The profiles in the background are near-shore and the profiles in the foreground are further offshore. Dark red circles in the bottom panel indicate hypoxic bins. Strong stratification the surface bins resulted in hypoxia formation north of the Brazos River delta. Strong stratification in the mid- and bottom depth bins resulted in a decrease of dissolved oxygen, but no hypoxia formation.



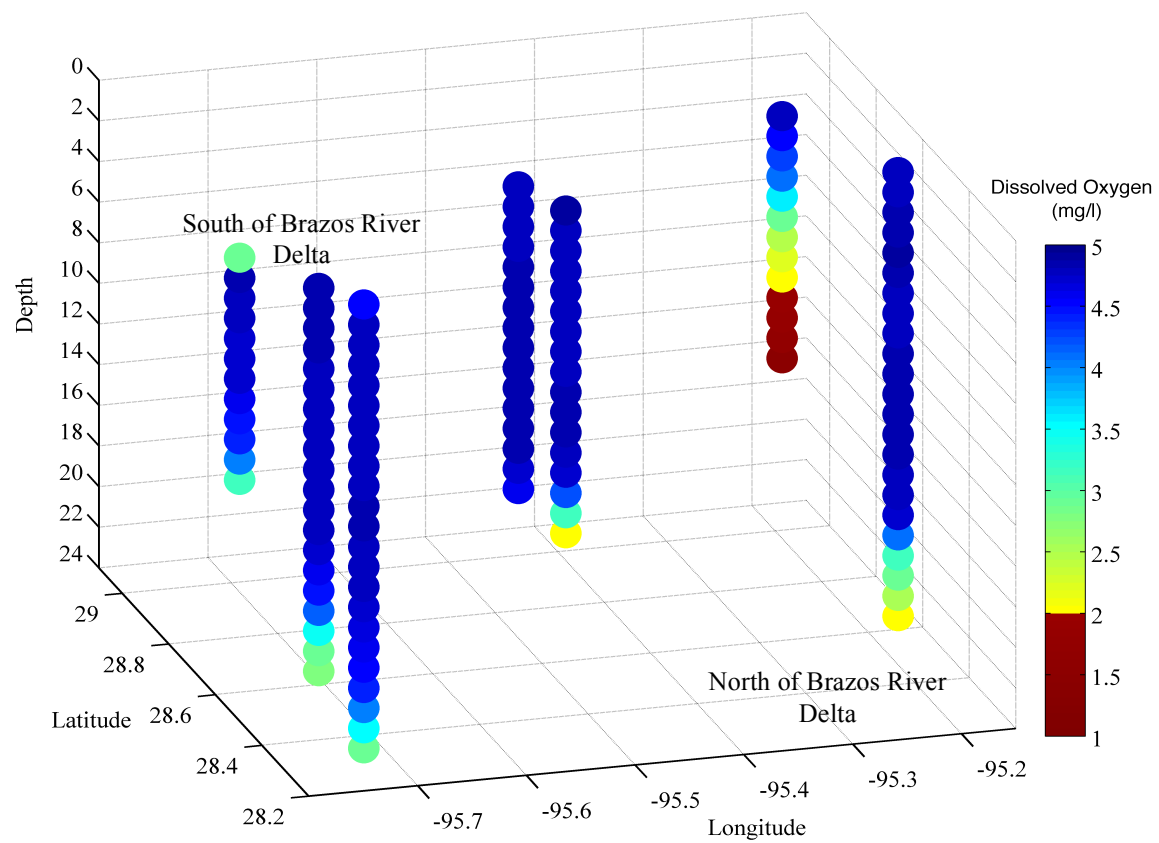
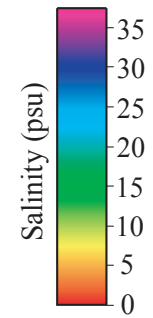
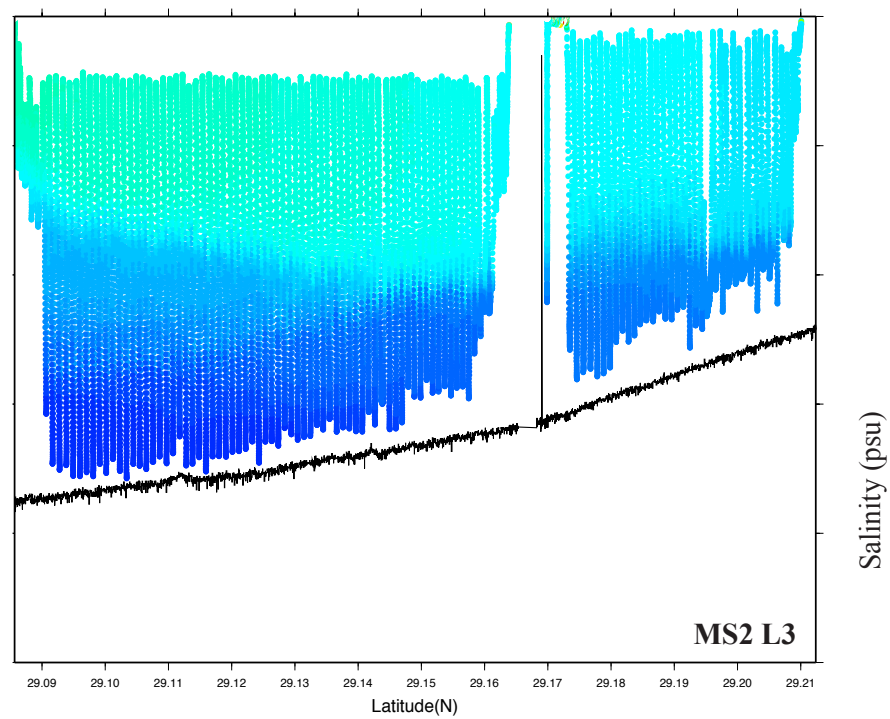
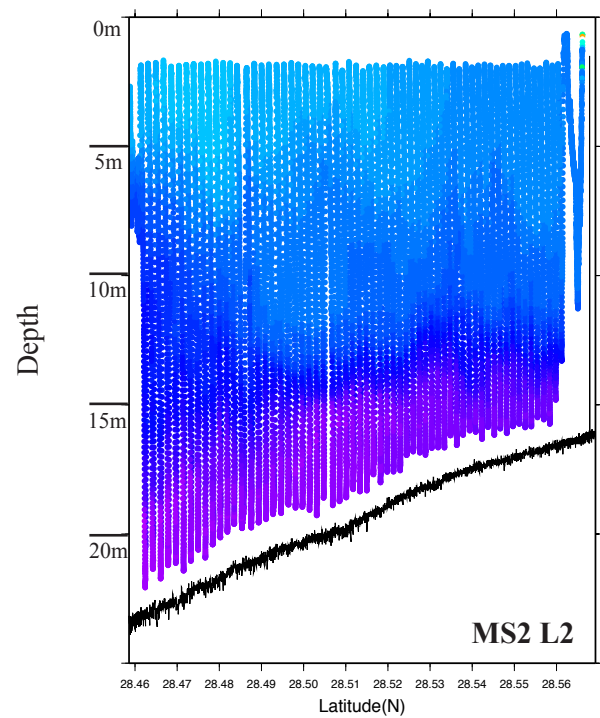


Figure 2.23 Continued

Figure 2.24 TAMU MCH MS2 Acrobat Towfish Salinity and Dissolved Oxygen Tracks. The four panels show the TAMU Acrobat towfish profiles collected north (L3, right) and south (L2, left) of the Brazos River delta. The top panels show the vertical salinity and the bottom two panels show the vertical dissolved oxygen (mg/L) concentrations. There was a distinct and strong layering in the salinity north of the Brazos delta seen in MS L3, which resulted in strong stratification causing thick layer (2 – 3 m) of hypoxia in the bottom waters. The layering in MS L2 was not as strong with vertical intrusions of salty and fresher waters. The layers were less defined and there was a greater range of salinity observed, which did not result in stratification strong enough to prevent the diffusion of oxygen to the bottom layers.



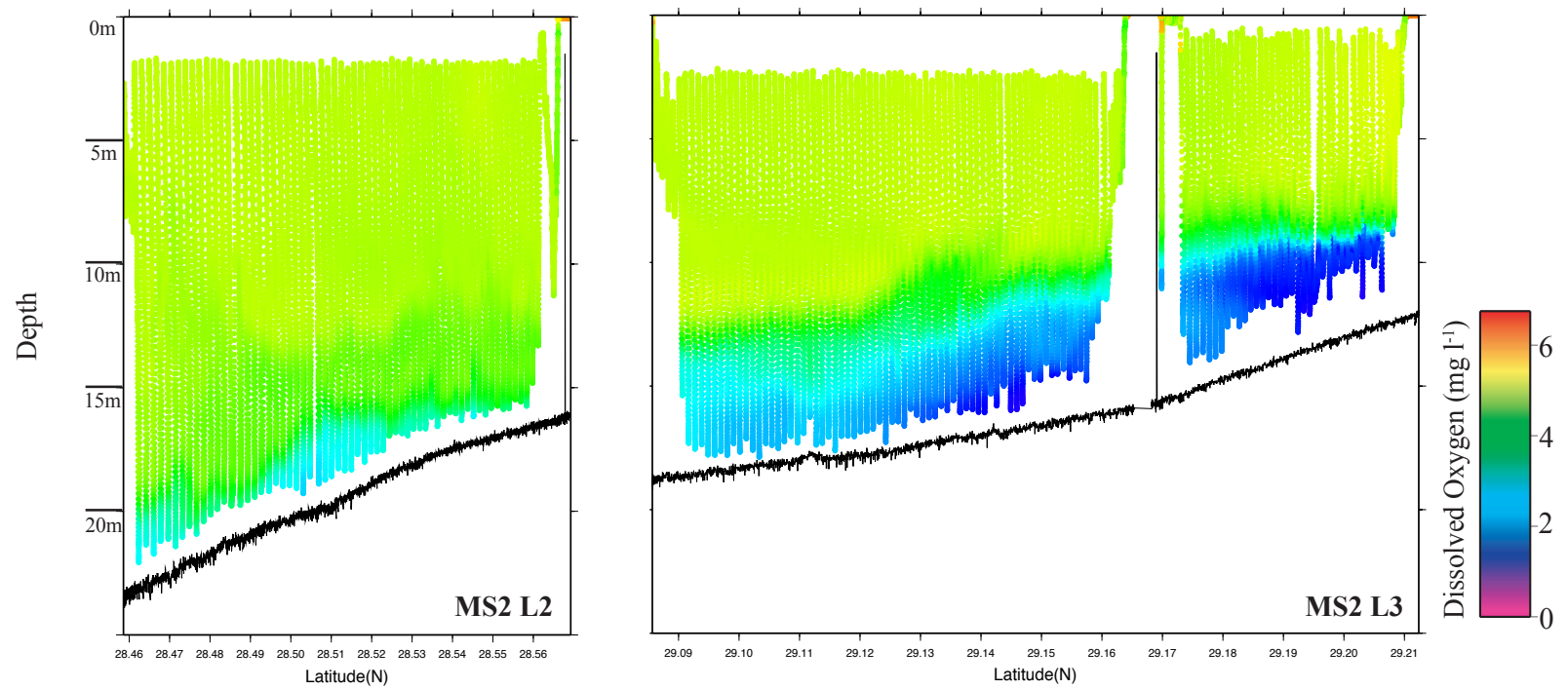
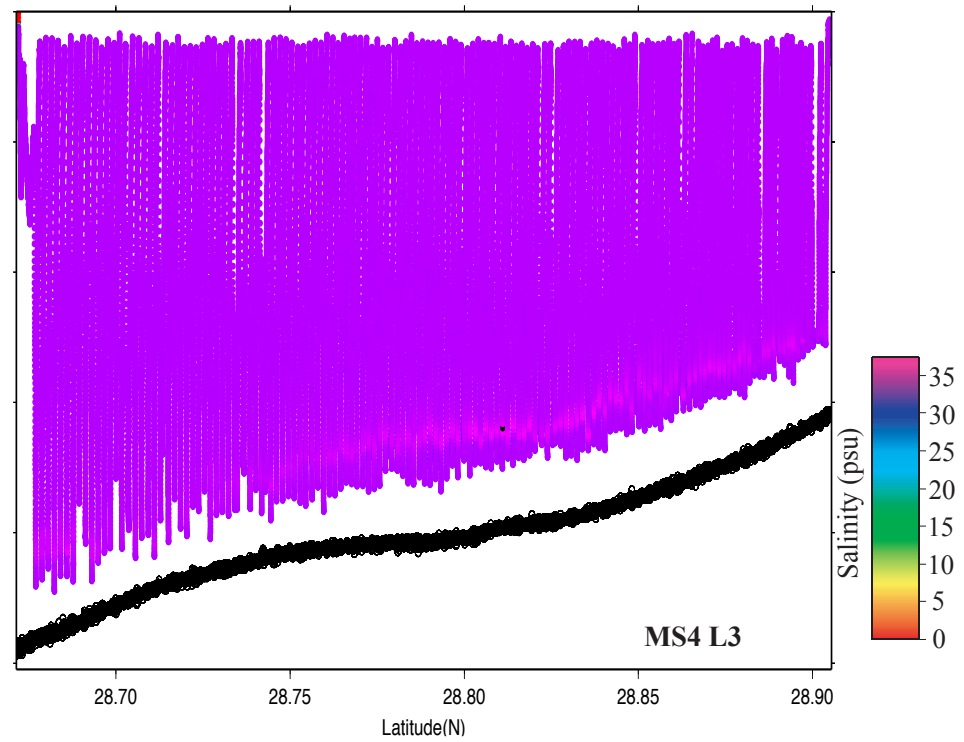
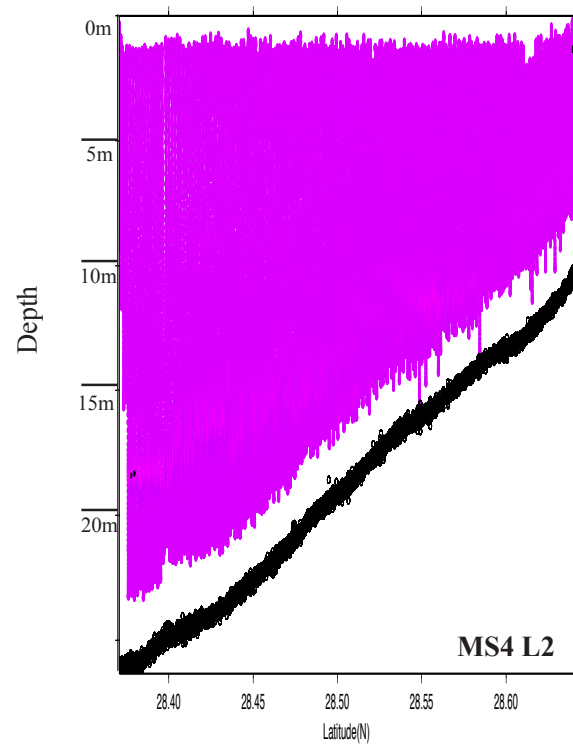


Figure 2.24 Continued

Figure 2.25 2011 TAMU MCH MS2 Acrobat Towfish Salinity and Dissolved Oxygen Tracks. The four panels show the TAMU Acrobat towfish profiles collected north (L3, right) and south (L2, left) of the Brazos River delta. The top panels show the vertical salinity and the bottom two panels show the vertical dissolved oxygen (mg/L) concentrations. The salinity and dissolved oxygen was uniform for a majority of the track. The only change in salinity was observed in a thin ( $< 1$  m) layer at the bottom in the MS4 L3 track, which caused stratification. However, the increase in stratification only resulted in an  $\sim 1.0$  mg/L drop in dissolved oxygen concentration and no hypoxia.



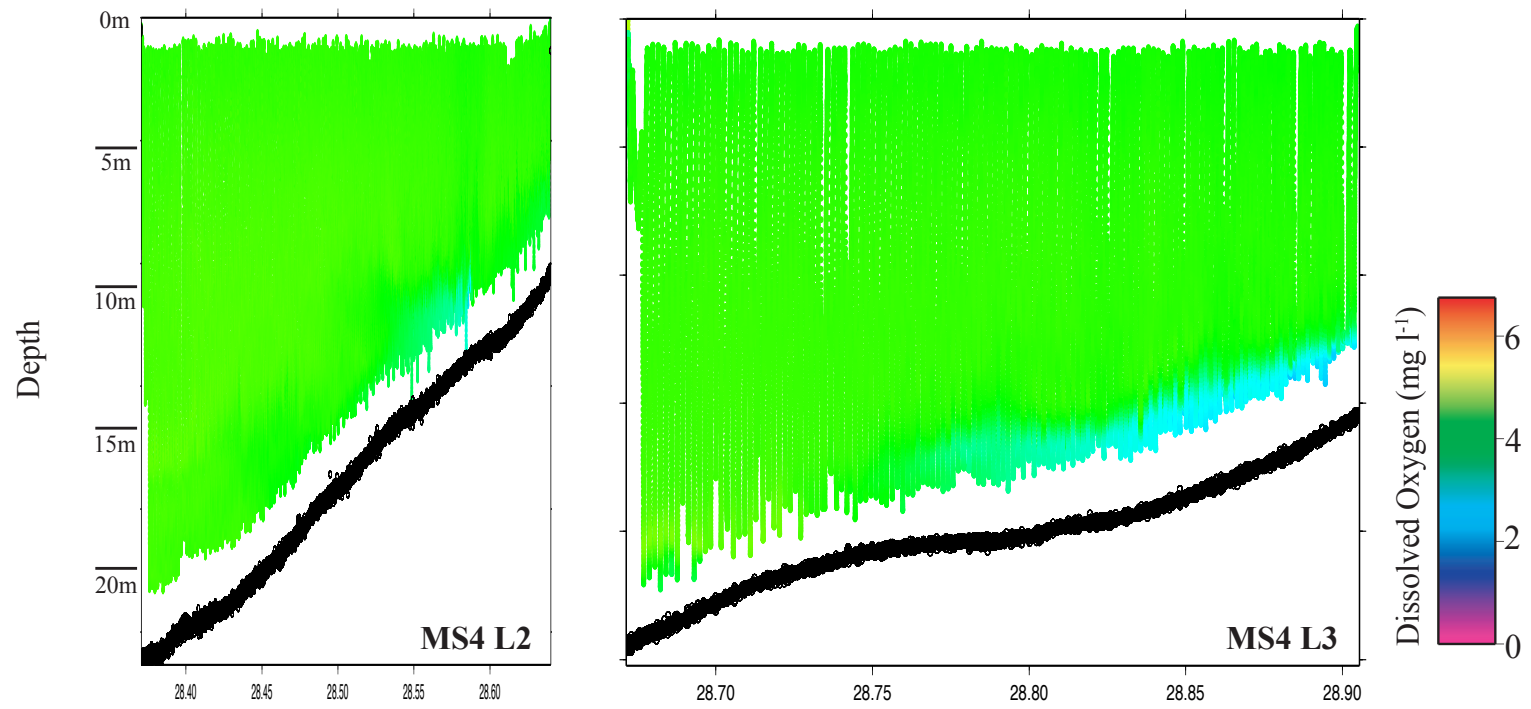


Figure 2.25 Continued

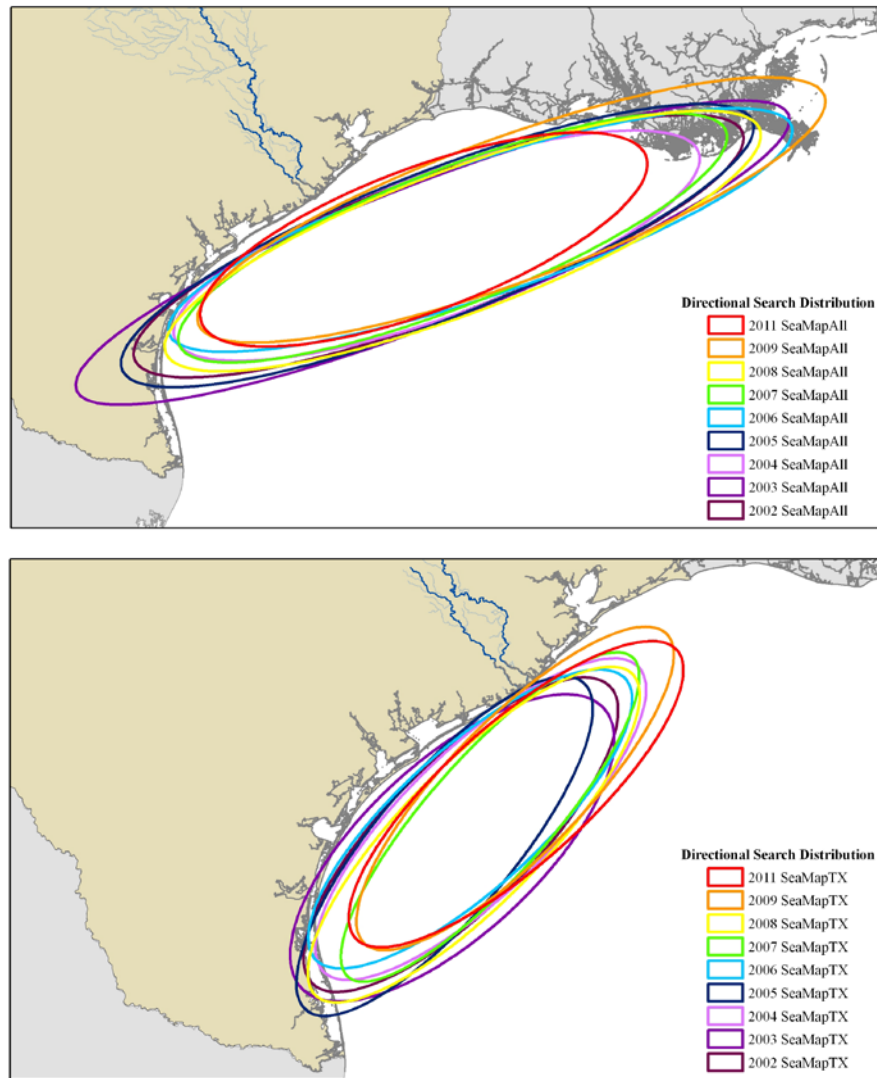


Figure 3.1 2002 - 2011 Search Direction Standard Deviation Ellipses. The two maps show a 1-standard deviation ellipse for the directional trend in the *SEAMAP All* (top) and *SEAMAP TX* (bottom) datasets. Each year is plotted showing a directional trend of approximately 70 degrees for *SEAMAP All* data and approximately 45 degrees for *TX SEAMAP* data. There is no ellipse included for 2010, because the original data was not available from NOAA SEAMAP.

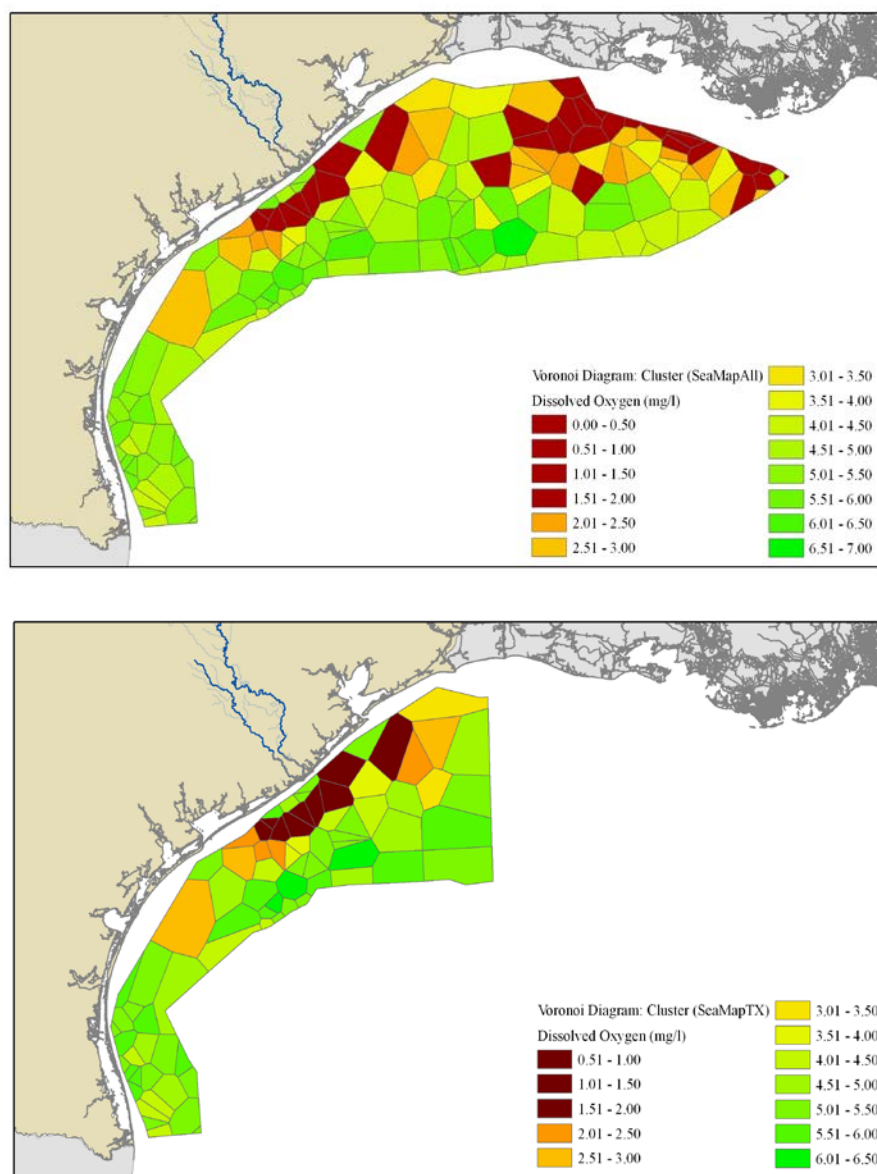


Figure 3.2 2007 Cluster Voronoi Maps. The two map panels show Voronoi cluster analysis for 2007 *SEAMAP ALL* (top) and *SEAMAP TX* (bottom) data. The dark red color indicates bottom dissolved oxygen below 2.0 mg/L. The cluster method identifies outliers (regions of hypoxia) in the data by identifying bottom dissolved oxygen polygons that differ from surrounding polygons by greater than 0.5 mg/L. In both datasets, the hypoxic region associated with the Brazos River flooding is seen, which indicates this region should be identified in the ordinary kriging model results as an independent region from Louisiana coastal hypoxia.

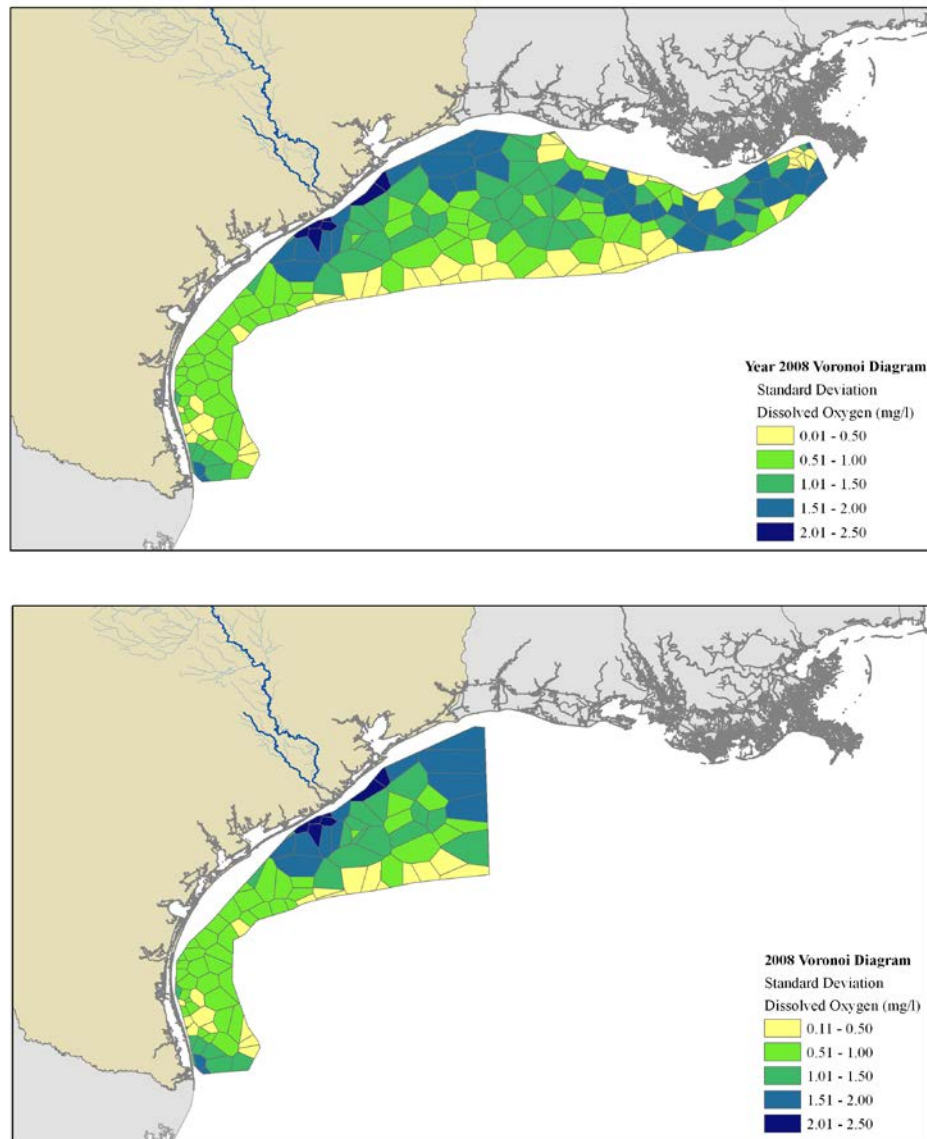
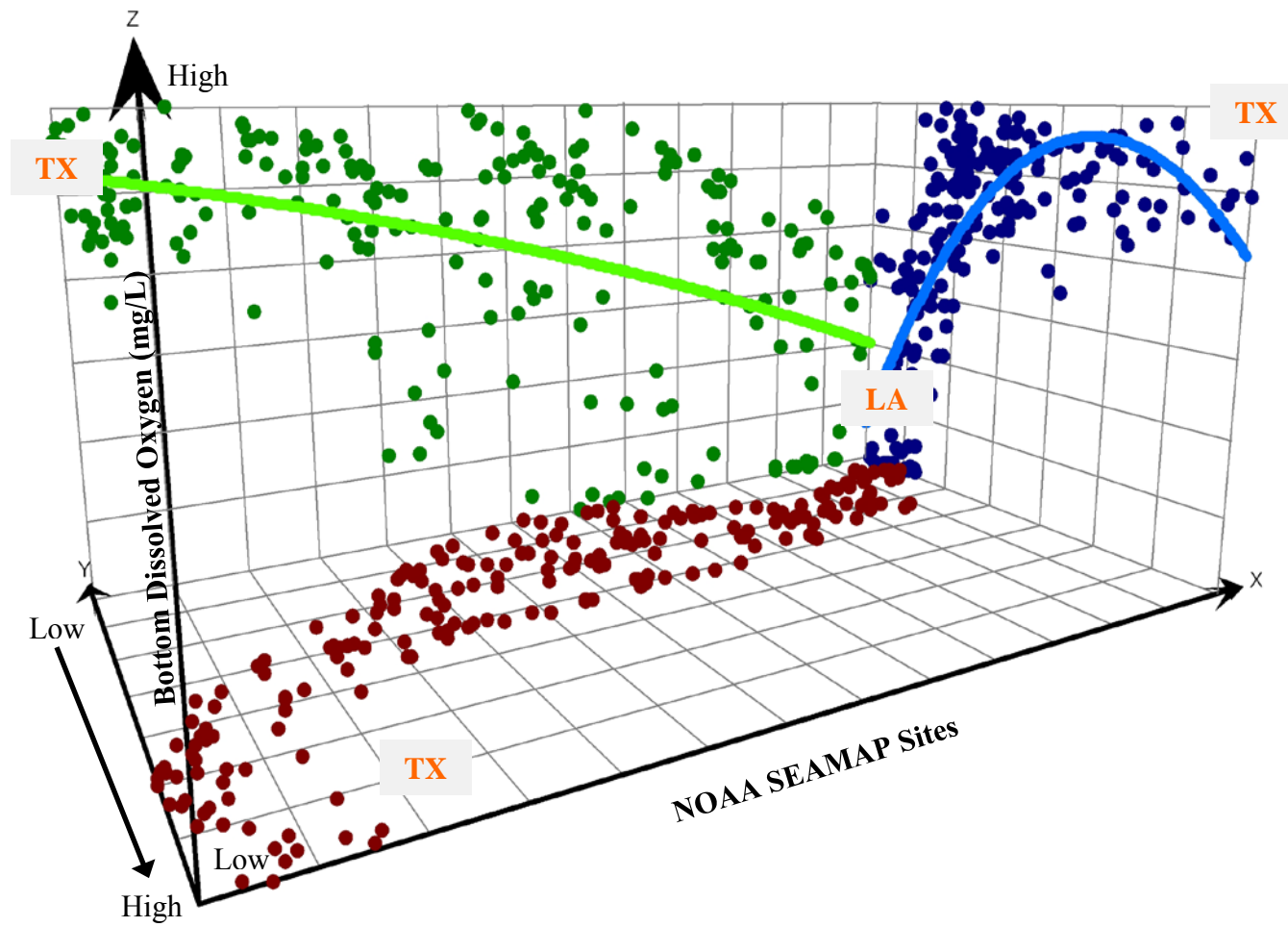


Figure 3.3 2008 Standard Deviation Voronoi Maps. The two map panels show Voronoi standard deviation analysis for 2008 *SEAMAP ALL* (top) and *SEAMAP TX* (bottom) data. The blue and dark blue colors indicate high standard deviation ( $> 1.5$  mg/L) in bottom dissolved oxygen. The standard deviation method identifies potential regions of hypoxia in the data by identifying bottom dissolved oxygen polygons that deviate from the mean bottom dissolved oxygen in a given polygon. In both datasets, potentially low bottom dissolved oxygen is measured near the Brazos River and there is a larger influence from Louisiana coastal hypoxia on the northern Texas shelf. The standard deviations also differ at the Texas-Louisiana boundary for the parameter *Data*, indicating potential local error in the ordinary kriging model results.

Figure 3.4 2002 SEAMAP ALL Spatial Trend Diagram. The diagram plot provides a visualization of how bottom dissolved oxygen in 2002 changes across and along the shelf. The dark red circles represent the actual sampling sites moving from Louisiana to Texas (right to left). The green circles represent the along-shelf bottom dissolved oxygen values with lower values at the plot intersection to higher values at the top of the z-axis. The blue circles represent how bottom dissolved oxygen values change across the shelf from inshore (y-axis, back origin) to offshore (y-axis, top right corner). The green (along-shelf) and blue (across-shelf) trend lines indicate the nonlinear relationship in both directions. There is a higher degree of variability (lower bottom dissolved oxygen) near the Texas-Louisiana border in the along-shelf component and a clustering of higher bottom dissolved oxygen values in the mid to south Texas shelf (y-axis, back right corner). Only 2002 is shown here, but similar trends are seen in all NOAA SEAMAP years analyzed.



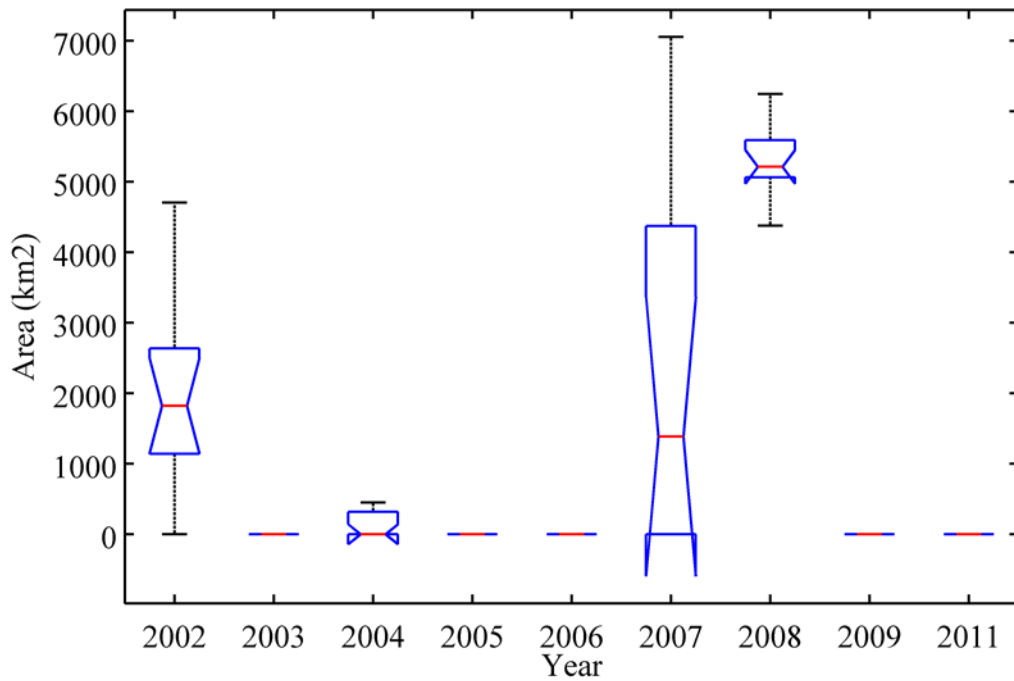


Figure 3.5 Ordinary Kriging Parameter *Year* Box Plots. The box plots for each year show the variability within Texas hypoxic area estimates for all years analyzed. The box length characterizes the differences among all years when considering all kriging scenarios. The red line indicates the mean value. The upper and lower edges (blue) represent the first and third quartile range of the dataset. The black lines extend to the most extreme data points that are not considered outliers and outliers are indicated by '+'. Year 2007 has the most spread with estimates of zero area to above 5,000 km<sup>2</sup>. Year 2008 has large estimates, but narrow spread between scenario results compared to years 2002, 2004, and 2008. The five years with flat lines represent years with no area calculated in any model.

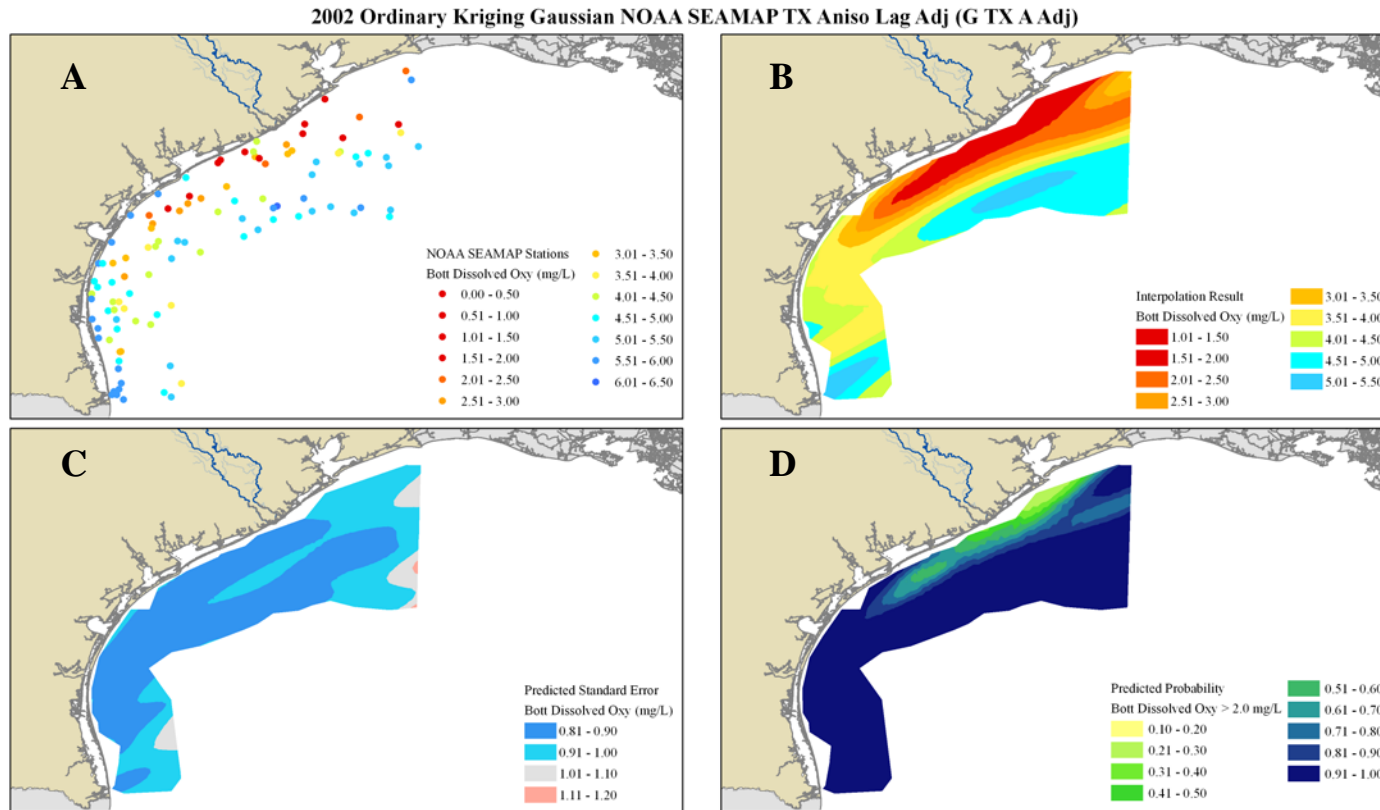


Figure 3.6 2002 Ordinary Kriging *G TX A Adj* Map Results. The map shows the output for the *Gaussian NOAA SEAMAP TX Aniso Adj Lag* model. The four panels show bottom dissolved oxygen values by site (A), interpolated surface (B), predicted standard error for the interpolation (C) and predicted probability threshold for values greater than 2.0 mg/L (D).

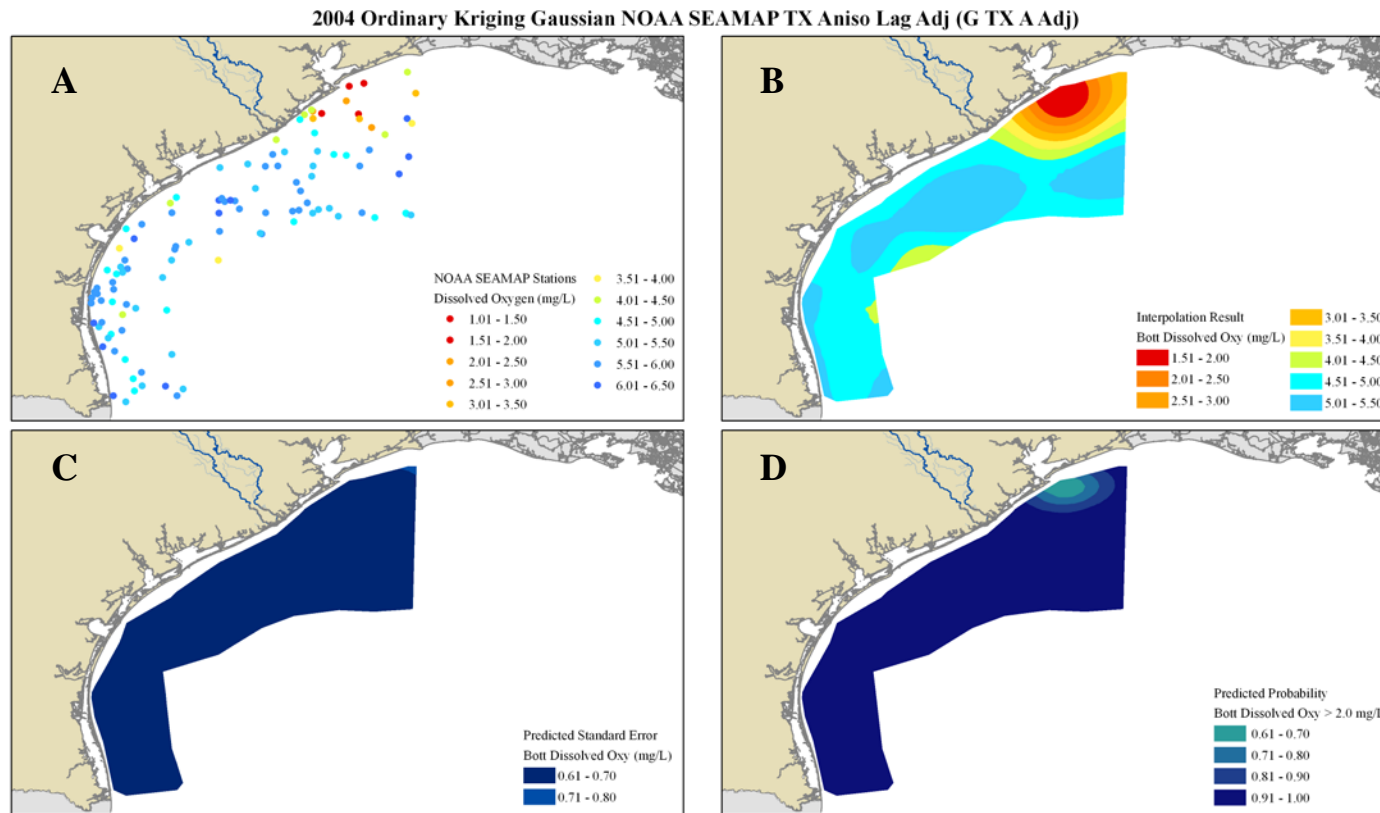


Figure 3.7 2004 Ordinary Kriging *G TX A Adj* Map Results. The map shows the output for the *Gaussian NOAA SEAMAP TX Aniso Adj Lag* model. The four panels show bottom dissolved oxygen values by site (A), interpolated surface (B), predicted standard error for the interpolation (C) and predicted probability threshold for values greater than 2.0 mg/L (D).

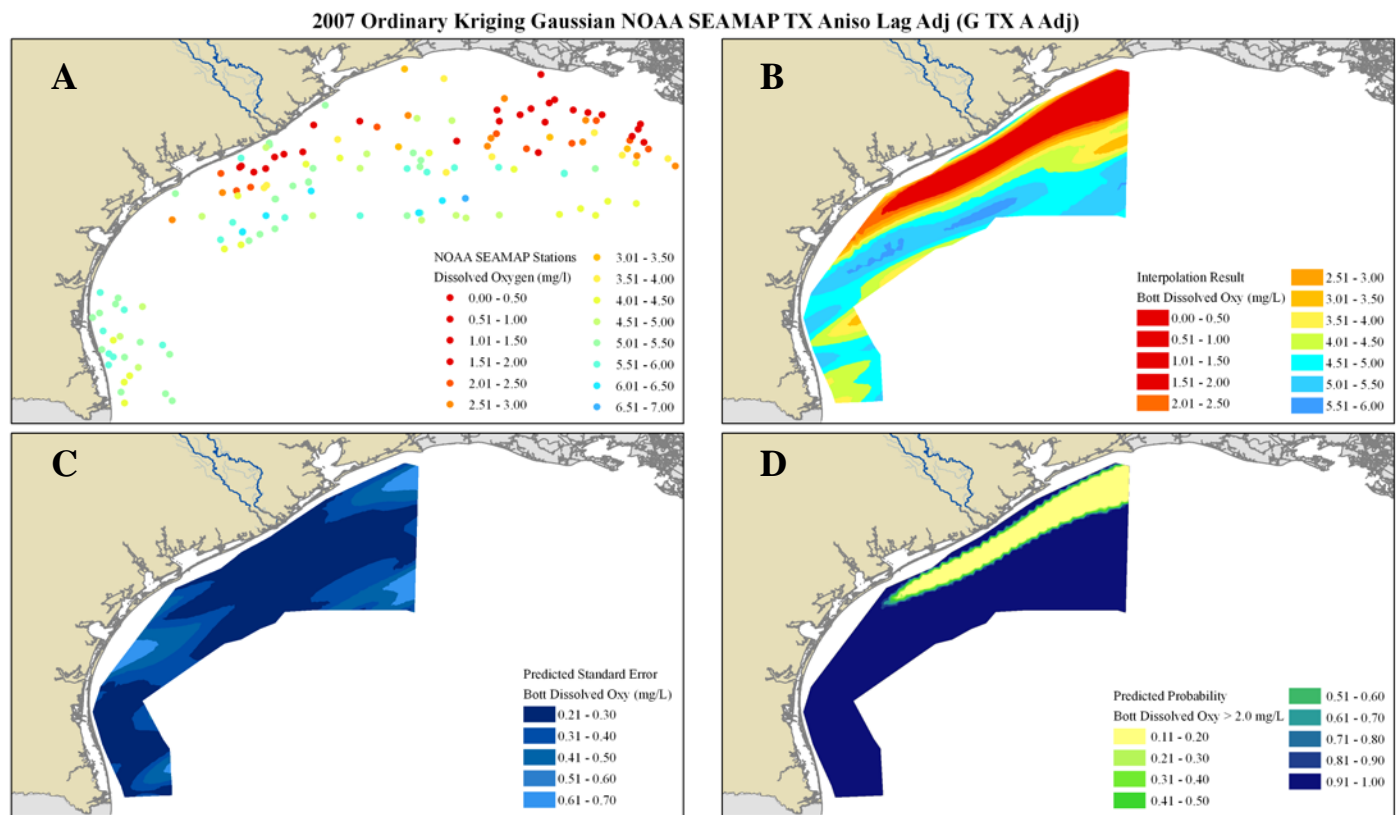


Figure 3.8 2007 Ordinary Kriging *G TX A Adj* Map Results. The map shows the output for the *Gaussian NOAA SEAMAP TX Aniso Adj Lag* model. The four panels show bottom dissolved oxygen values by site (A), interpolated surface (B), predicted standard error for the interpolation (C) and predicted probability threshold for values greater than 2.0 mg/L (D).

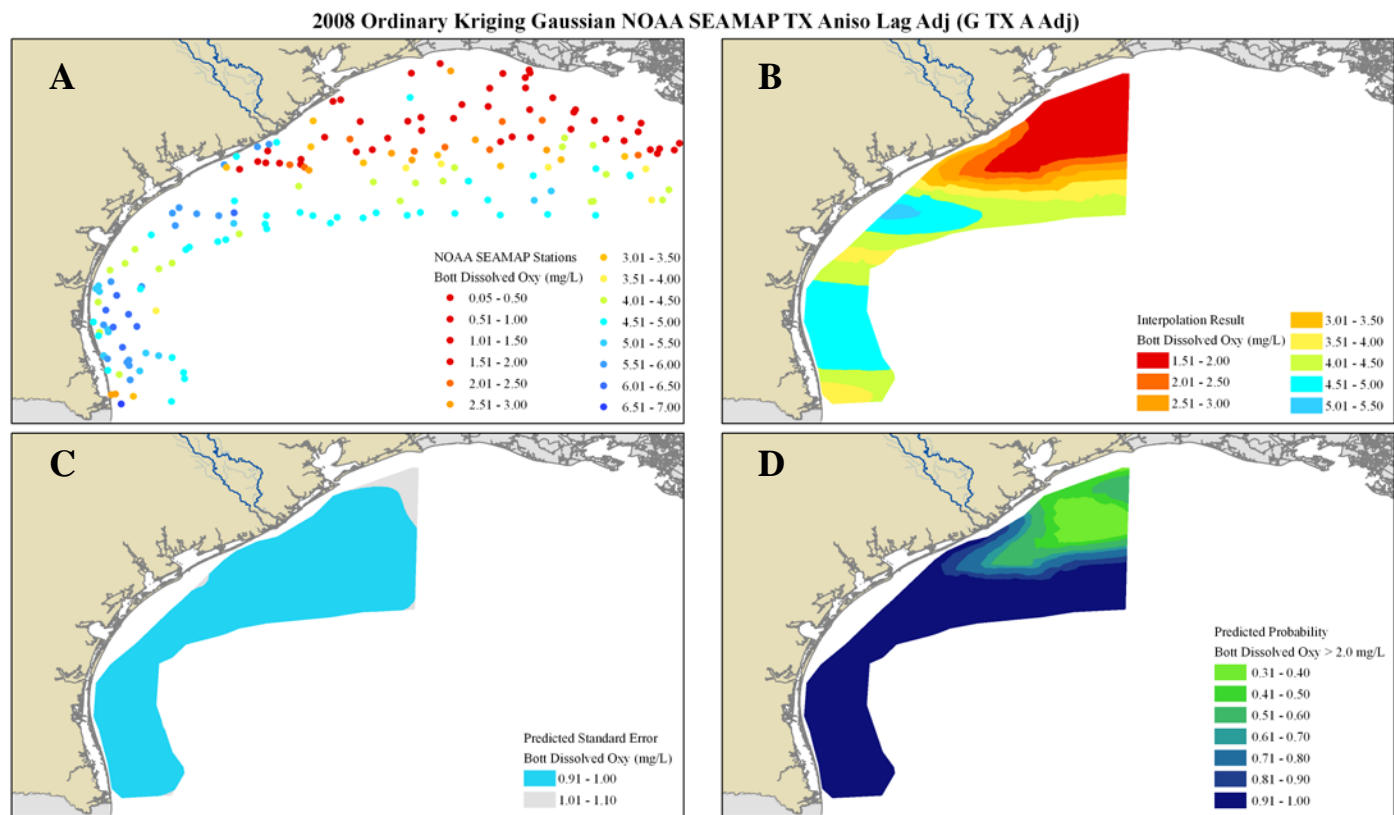


Figure 3.9 2008 Ordinary Kriging *G TX A Adj* Map Results. The map shows the output for the *Gaussian NOAA SEAMAP TX Aniso Adj Lag* model. The four panels show bottom dissolved oxygen values by site (A), interpolated surface (B), predicted standard error for the interpolation (C) and predicted probability threshold for values greater than 2.0 mg/L (D).

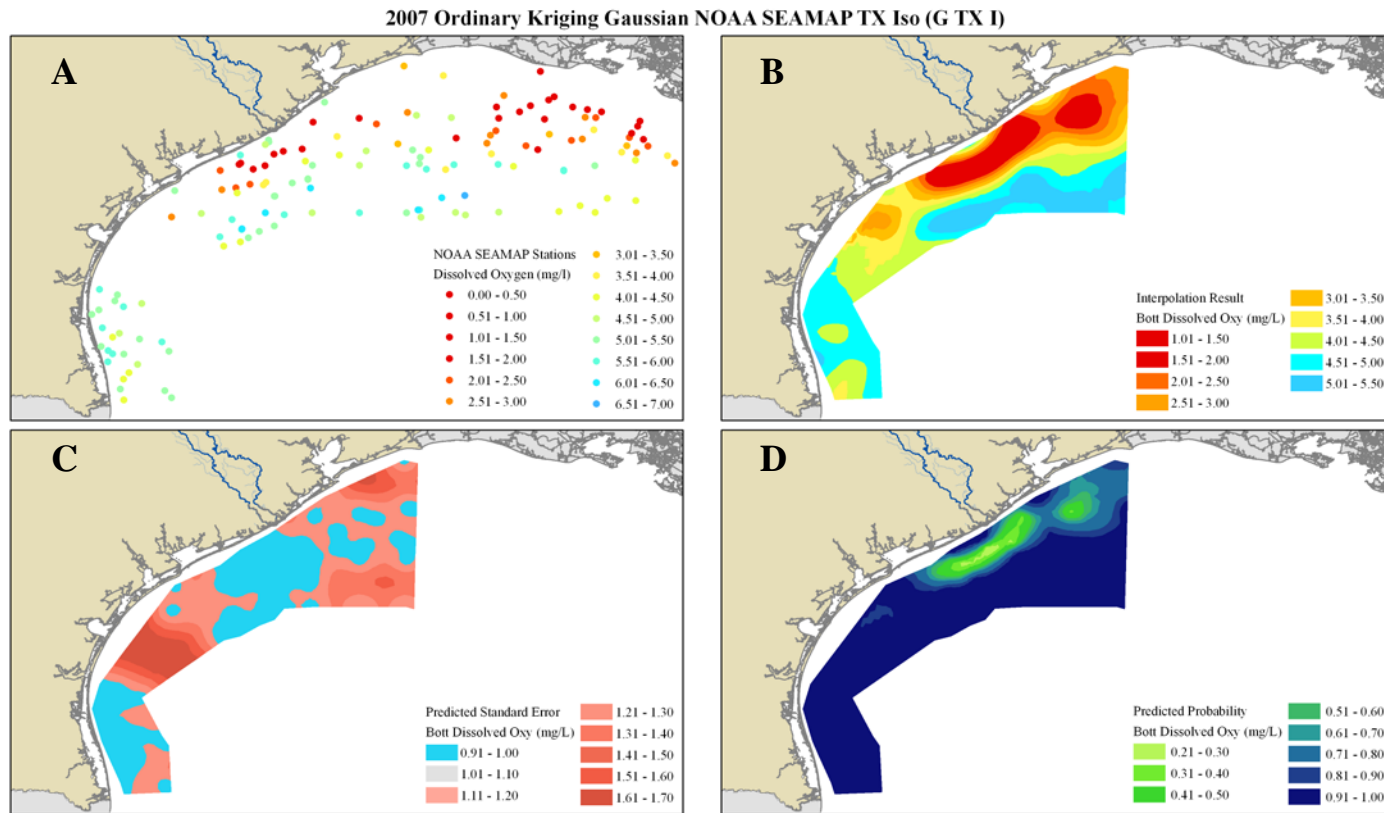


Figure 3.10 2007 Ordinary Kriging *G TX I* Map Results. The map shows the output for the *Gaussian NOAA SEAMAP TX Iso* model. The four panels in each result represents actual bottom dissolved oxygen values by site (A), interpolated surface (B), predicted standard error for the interpolation (C) and predicted probability threshold for values greater than 2.0 mg/L (D).

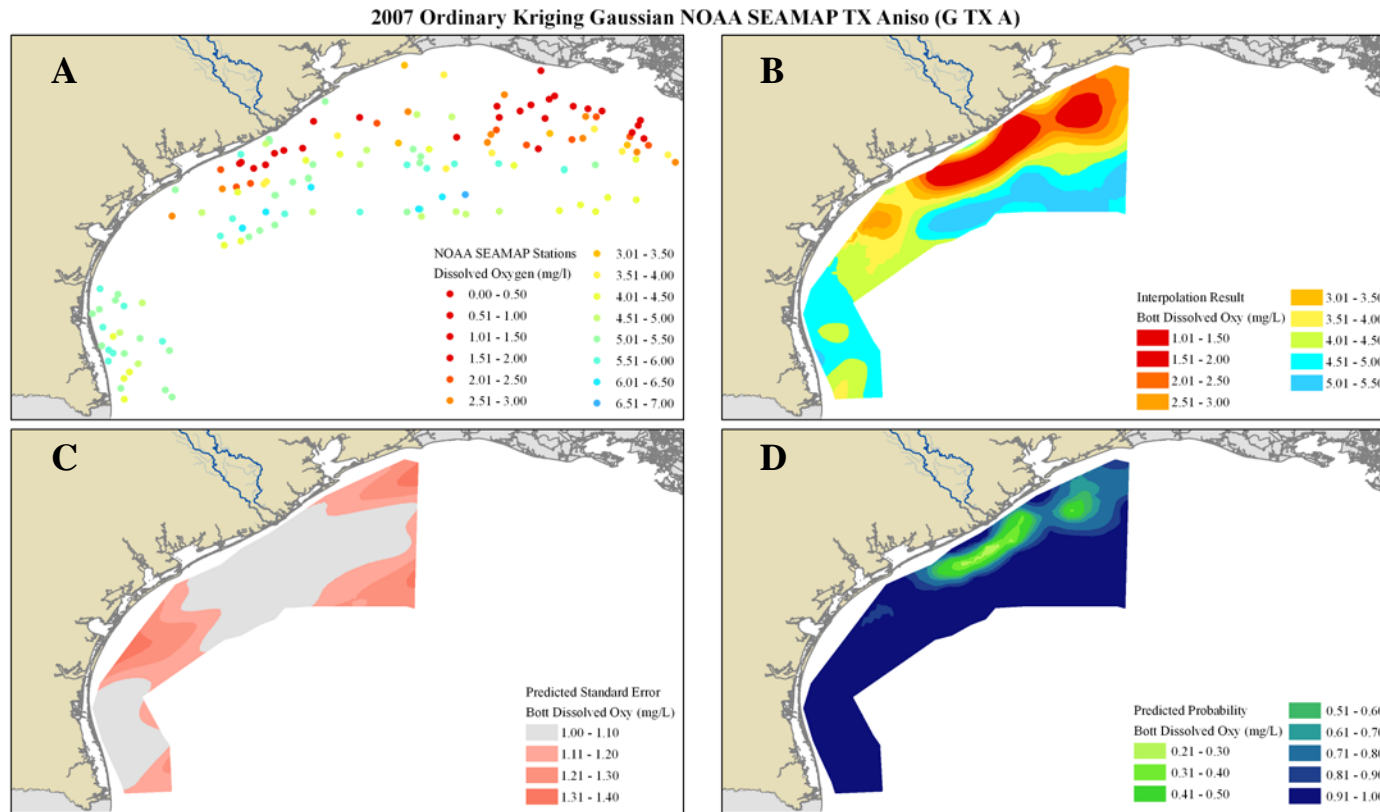


Figure 3.11 2007 Ordinary Kriging *G TX A* Map Results. The map shows the output for the *Gaussian NOAA SEAMAP TX Aniso* model. The four panels show bottom dissolved oxygen values by site (A), interpolated surface (B), predicted standard error for the interpolation (C) and predicted probability threshold for values greater than 2.0 mg/L (D).

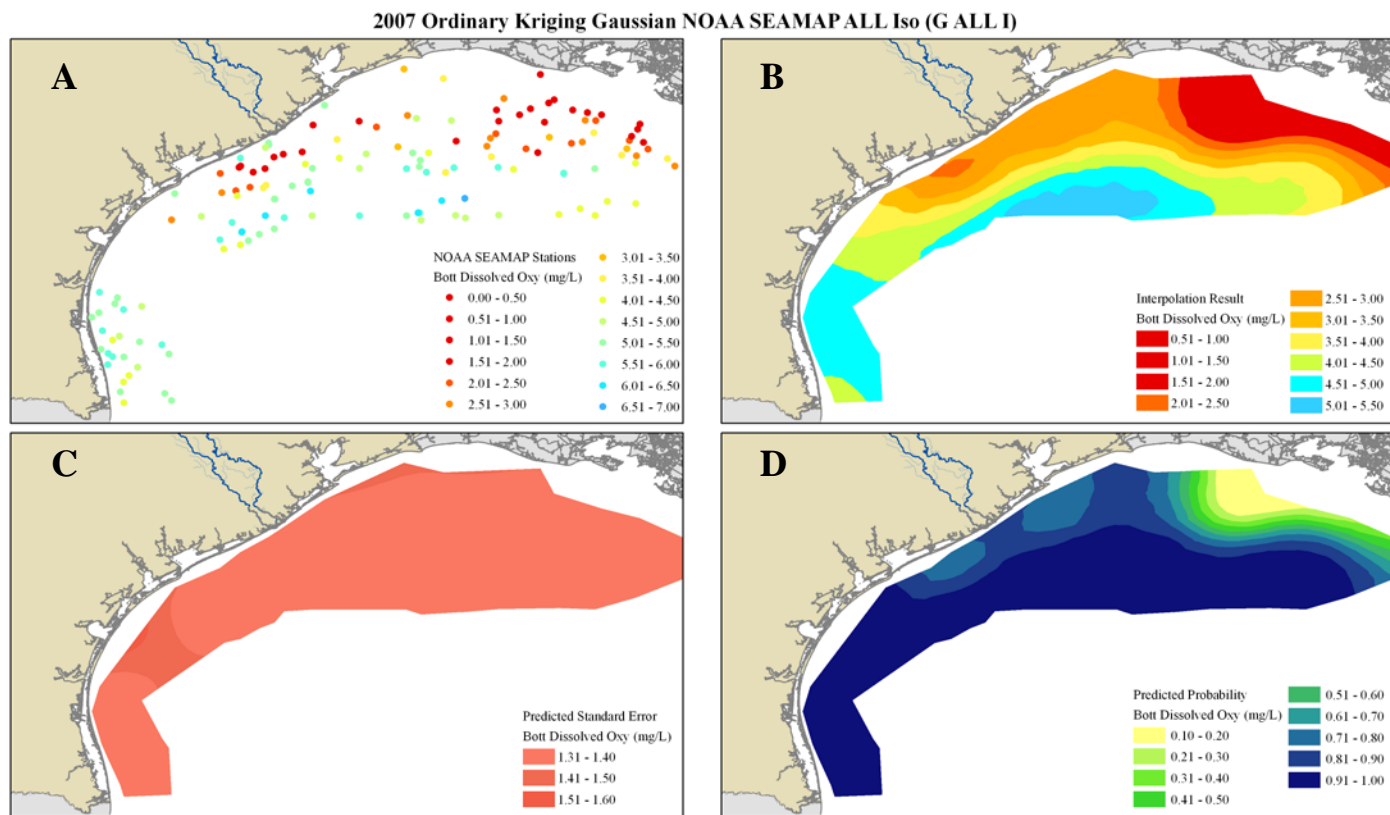


Figure 3.12 2007 Ordinary Kriging *G ALL I* Map Results. The map shows the output for the *Gaussian NOAA SEAMAP ALL Iso* model. The four panels show bottom dissolved oxygen values by site (A), interpolated surface (B), predicted standard error for the interpolation (C) and predicted probability threshold for values greater than 2.0 mg/L (D).

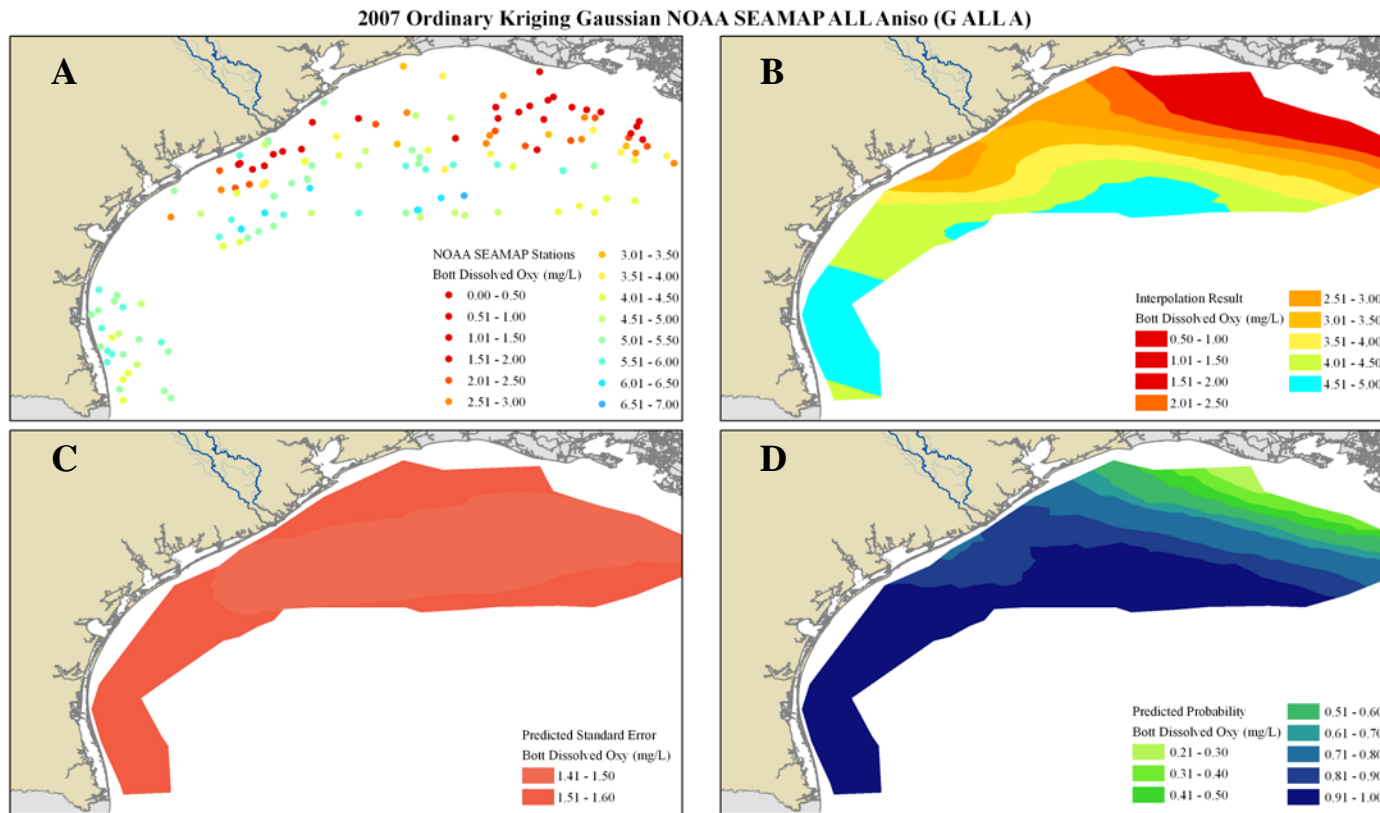


Figure 3.13 2007 Ordinary Kriging *G ALL A* Map Results. The map shows the output for the *Gaussian NOAA SEAMAP ALL Aniso* model. The four panels show actual bottom dissolved oxygen values by site (A), interpolated surface (B), predicted standard error for the interpolation (C) and predicted probability threshold for values greater than 2.0 mg/L (D).

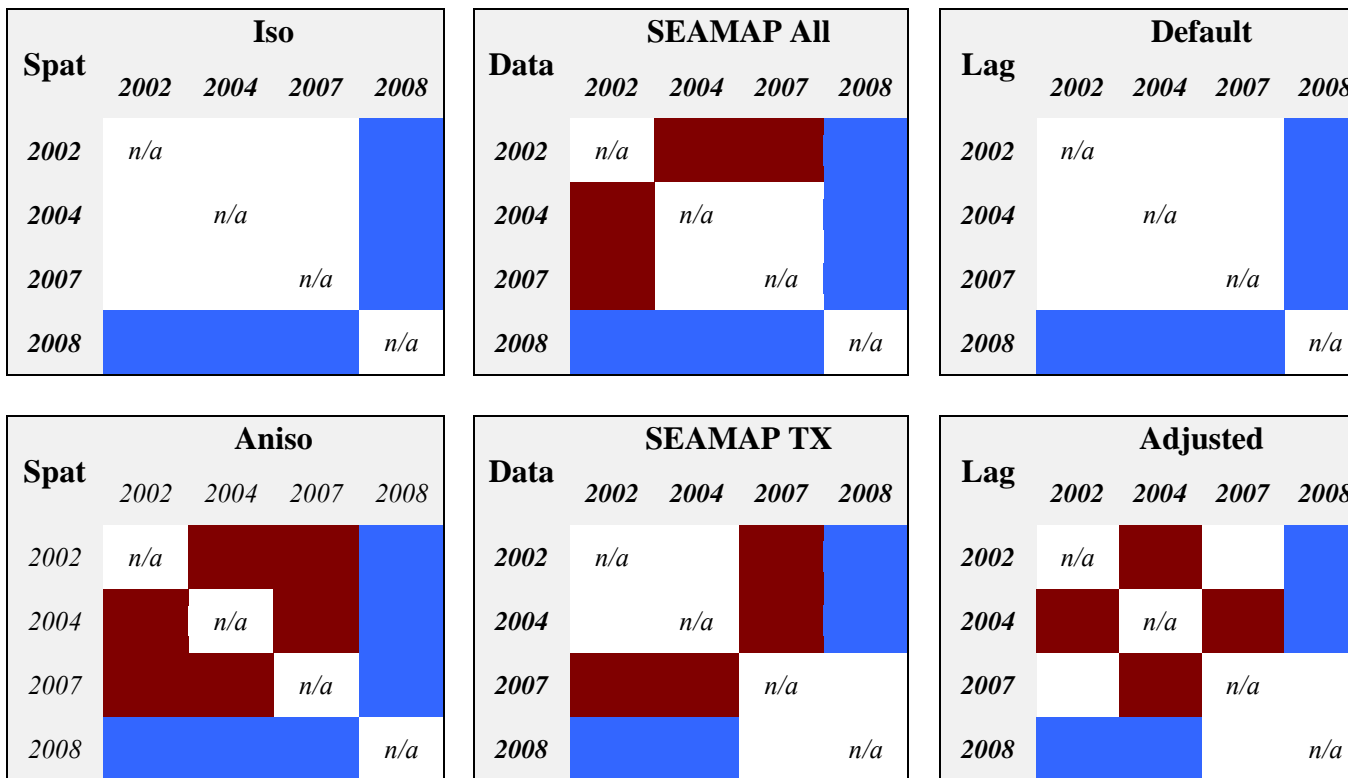


Figure 3.14 Ordinary Kriging Parameter Comparative Matrices. The matrices compare two different ordinary kriging scenario variables: *Spatial*, *Data*, and *Lag* against *Year*. Significantly different relationships (p-value < 0.05) between each variable and *Year* are colored maroon or blue. Blue emphasizes differences among years specifically to year 2008, which is designated as a large hypoxic year on the Texas shelf. In most variable comparisons, year 2008 is significantly different from all years except for *SEAMAP TX* and *Adjusted Lag*. In *Iso* and *Default Lag* comparisons to *Year*, there are no additional significant relationships among other years. Both *Spherical* (Appendix E) and *Gaussian* models considering *SEAMAP TX* and *Adj Lag* account for the Brazos River flooding causing a large hypoxic region on the Texas shelf, which makes area estimate comparisons in 2007 similar to 2008 area estimates.

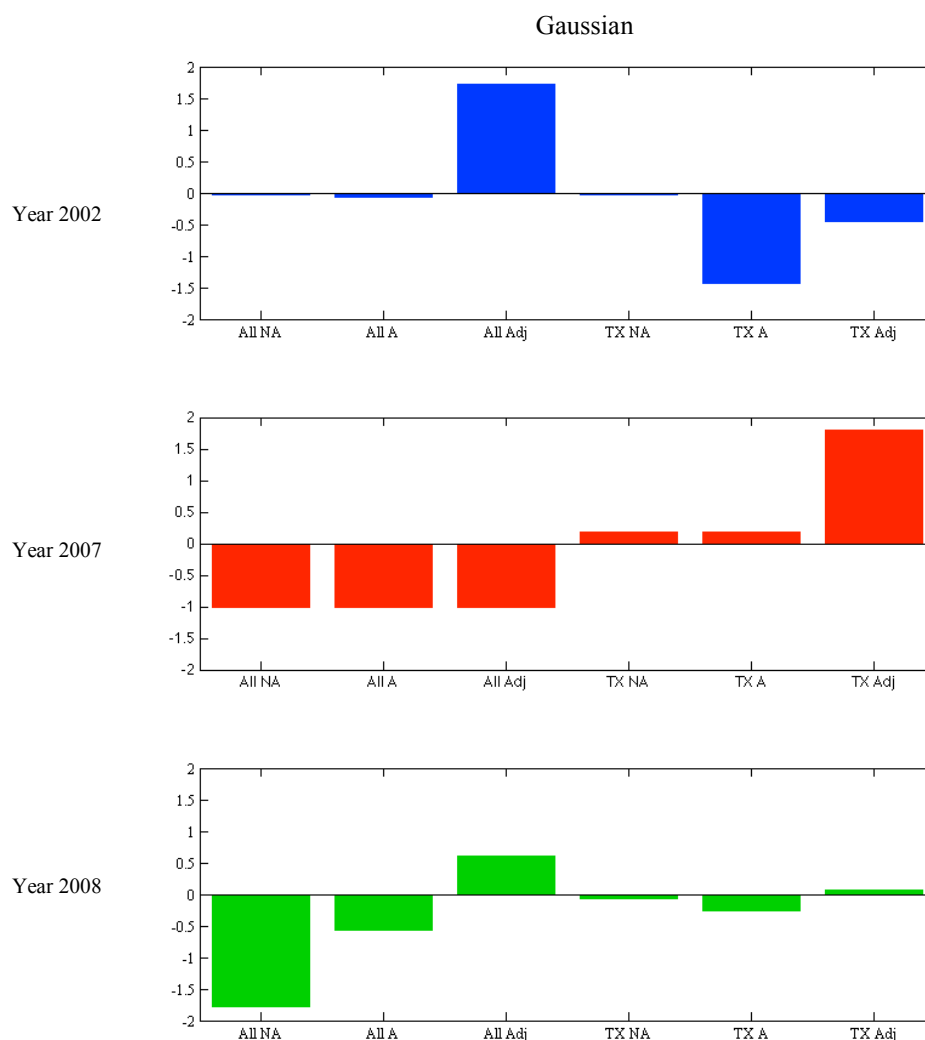


Figure 3.15 2002, 2007, and 2008 Normalized Gaussian Model Mean Hypoxic Areas Estimates. The three panels of bar graphs show the normalized mean hypoxic area estimates for Gaussian ordinary kriging models for 2002, 2007, and 2008. Each of the years is selected to specifically represent one year in each of the three size designations (small, moderate, and large respectively). Each Gaussian ordinary kriging scenario is normalized to the mean hypoxic area estimate for each year determined from all estimates within the year. The y-axis in each plot is in units of 1,000 km<sup>2</sup>. *SEAMAP ALL* models, except for *Adj Lag*, underestimate hypoxic area on the Texas shelf. *Adj Lag* models for *SEAMAP All* and *SEAMAP TX* more likely strongly over- or underestimate area by 500 – 1,750 km<sup>2</sup>. The most consistency in model area estimates occurs in 2007, in which *SEAMAP ALL* underestimate area on the Texas shelf and *SEAMAP TX* overestimates area on the Texas shelf.

**APPENDIX C**

**A REMOTE SENSING APPROACH TO INVESTIGATING  
BIOGEOCHEMICAL PROCESSES RELATIVE TO HYPOXIA FORMATION  
ON THE TEXAS SHELF**

## **C.1 Remote Sensing Applications for Monitoring Texas Hypoxia**

### *C.1.1 Remote Sensing in the Gulf of Mexico*

Large rivers, such as the MARS, have an integral role in delivering nutrients to the Louisiana coast. This directly impacts the formation of hypoxia in the western Gulf of Mexico. Along with nutrients, river systems can also introduce suspended sediments and organic material to the coastal ocean. Suspended sediment is an important factor in regulating coastal productivity, as the amount of sediment in the water alters light availability in the water column (Lohrenz et al. 1999). Dissolved organic matter similarly plays an important role in carbon cycling on the shelf (Salisbury et al., 2004). Nutrients, suspended sediments, and dissolved organic loading to the Louisiana shelf affect hypoxia formation as shown by the Rowe and Chapman (2002) across-shelf model of three distinct zones of hypoxia based on the amounts and types of particulate loading to the Louisiana shelf. The along-shelf (or east to west) hypoxic controls (nutrients/organic material versus freshwater input) from MARS have been documented by Hetland and DiMarco (2008) and Bianchi et al. (2010).

There is no high-volume freshwater nutrient source fueling biological production on the Texas shelf similar to the MARS discharge on the Louisiana shelf, as shown in Chapter 1 (Rabalais et al. 2002; Bianchi et al. 2010). The input from the MARS discharge more regularly contributes to biological processes affecting hypoxia formation, despite occasional large-scale freshwater inputs on the Texas shelf (e.g. 2007, DiMarco et al. 2012). Salisbury et al. (2004) investigated suspended particulate matter

using satellite imagery to compare shelf inputs by Gulf of Mexico rivers to the coast. Their results showed weak correlations between the magnitude of the MARS or Brazos River freshwater inputs and influx of particulate matter to the Gulf of Mexico shelf, but rather found concentrations of particulate matter to be more correlated with wind mixing. Salisbury et al. (2004) were unable to differentiate whether particles were river-derived sediments or organic detrital matter from phytoplankton. Furthermore, the authors did not find a significant correlation between satellite chlorophyll estimates and suspended particulate matter calculated from their algorithms. These results further confirmed earlier data from the mid-1960s in a study published by Dinnel and Wiseman (1986) tracking the extent of MARS water and sediment concentrations 1000 km west of the Mississippi delta onto the north Texas coast from April to June.

Apart from river loading, additional biological processes may contribute to hypoxia formation on the northern Gulf of Mexico shelf and should be considered when investigating Texas hypoxia formation. The nutrient inputs from rivers fuel phytoplankton production and the microbial decomposition of the associated biomass is one cause of hypoxia on the shelf (Rabalais et al. 2001; Bianchi et al. 2010). Remotely sensed biomass from blooms can be a potential indicator of a nutrient source on the shelf, as blooms can contribute a significant amount of organic matter, in addition to river organic matter, to fuel microbial respiration and do occur on the Texas shelf (Stumpf et al. 2003).

Tracking phytoplankton blooms and organic matter with remote sensing is common in oceanography, including in the Gulf of Mexico. For example, Walker and

Rabalais (2006) demonstrated how satellite imagery is an effective technique for estimating phytoplankton biomass on the coastal Louisiana shelf. Biggs and Sanchez (1997), followed by Walker and Rabalais (2006) provided satellite data showing how Atchafalaya River outflows support increases in primary production and chlorophyll  $\alpha$  (Chl  $\alpha$ ) concentrations. In the Gulf of Mexico, Muller-Karger et al. (1991) showed highest levels of satellite-derived Chl  $\alpha$  occurred on the Louisiana shelf, due to freshwater discharges and nutrient fluxes of the Mississippi and Atchafalaya Rivers.

Other investigations (Myint and Walker 2002; Walker 2005) used NOAA AVHRR, SeaWiFS, and MODIS imagery to estimate near-surface suspended sediment and suspended solids, phytoplankton concentrations, and chlorophyll  $\alpha$ . D'Sa and DiMarco (2009) noted that high chromophoric dissolved organic matter (CDOM) in surface waters is associated with high biomass values and high dissolved oxygen concentrations; in bottom waters, high CDOM is associated with low dissolved oxygen concentrations.

In addition to using Chl  $\alpha$  as an indicator for estimating biomass, satellite imagery also allows researchers to identify regions of coastal upwelling. Upwelling can recycle dissolved organic matter and nutrients, which may lead to nutrient-driven hypoxia formation (Walker et al. 2005; Bianchi et al. 2010).

The cited studies combined different parameters estimated from satellite observations to investigate the role and/or temporal variability of phytoplankton biomass or upwelling on the Gulf of Mexico shelf. The studies demonstrated the ability of remote sensing to measure phytoplankton biomass and organic matter in coastal Gulf of

Mexico waters and to estimate possible biological controls influencing hypoxia formation on the Texas shelf. Combining remote sensing techniques with mooring and cruise data can increase the spatial and temporal resolution for examining the relationship between Brazos River discharge, nutrient concentrations, and hypoxia formation on the Texas shelf. Additionally, recent advances in satellite imagery processing and improvements in algorithms allow separation of particulate matter that was not addressed in Salisbury et al. (2004).

In this study, I attempted to quantify that relationship by analyzing satellite-derived Chl  $\alpha$ , CDOM, and euphotic depth on the Texas shelf during year 2008. I selected 2008 because this year produced one of the largest hypoxic areas (see Section 3), which guarantees a larger sample size for statistical analysis. The hypoxia off Texas in 2008 was an extension of Louisiana coastal hypoxia, as a result of high freshwater discharge from MARS.

#### *C.1.2 Introduction to Giovanni – A Web-Based Remote Sensing Data Repository*

The web-based application, **GES-DISC Interactive Online Visualization And aNalysis Infrastructure** (Giovanni) is a interactive web-based tool that compresses the amount of pre-processing required to analyze or incorporate satellite remote sensing data into research. Imagery for this Chapter was downloaded from the Giovanni website for two different satellites (<http://disc.sci.gsfc.nasa.gov/giovanni/overview/index.html>).

### *C.1.3 Data Level and Instrument Selection*

Satellite data are classified into four major groups representing the level of processing. Classification begins with the original instrument measurements (Level 0). Level 1 includes adjusting unprocessed data for sensor calibrations and adding time-references and ancillary information (i.e. metadata). Level 2 starts basic temporal, spatial, and spectral quality control with progression to levels with algorithm post-processing (Level 3) and assimilation (Level 4) into models (Jensen 2005; 2007). Level 3 data were used for this research. Post-processing at Level 3 includes atmospheric and radiometric corrections (e.g. haze reduction and scaling and converting pixel values to radiance values). Quality control also includes averaging and mosaicing daily swaths to minimize cloud cover and sun glint, which are common problems when using satellite imagery.

Data used for this study were from the Moderate Resolution Imaging Spectroradiometer (MODIS) and Sea-viewing Wide Field-of-view Sensor (SeaWiFS) satellites. The MODIS satellite has 36 spectral bands with Bands 8 – 16 collecting ocean data and observes Earth's entire surface in one to two days. MODIS Terra passes from north to south during the morning hours across the equator and MODIS Aqua crosses south to north passing the equator during the afternoon ([modis.gsfc.nasa.gov](http://modis.gsfc.nasa.gov)). The differential timing improves effects caused by atmospheric factors, such as cloud cover and aerosol scattering. With two satellites sensing, MODIS provides images with a spatial resolution at 250, 500, and 1,000 m resampled to 4 – and 9 km. For this study, I only used 250 m pixels subsampled at 4- and 9 km resolution.

SeaWiFS was launched in 1997. This satellite was one of the earlier sensing instruments, designed primarily to provide quantitative ocean data, and operated until December 2010. A major design priority for SeaWiFS was to provide information about oceanic biology, particularly phytoplankton and ocean color at a sensor resolution of 1.1 km, using eight spectral bands ranging from 402 to 885 nanometers and a survey time of approximately 24 hours to cover the Earth (Jensen 2007). Post-processing algorithms used to derive biological information can be found at [oceancolor.gsfc.nasa.gov/cgi/algorithms.cgi](http://oceancolor.gsfc.nasa.gov/cgi/algorithms.cgi).

#### *C.1.4 Satellite Biological Parameters*

Three biological parameters derived from satellites are considered: Chl *a*, CDOM, and euphotic depth. Those three may provide a starting estimate for examining the biogeochemical contribution to hypoxia formation and duration on the Texas shelf. The amount of Chl *a* in the water is assumed to be directly related to phytoplankton biomass and abundance (Jensen 2005). However, many *in situ* studies have shown bulk carbon to Chl *a* ratios can vary 10-40 fold due to changes in phytoplankton biochemistry and physiology (Gardner et al. 2006).

CDOM is partly responsible for the color of coastal seawater. It is composed of dissolved and particulate organic matter and is detectable in the blue to ultraviolet range of the spectrum (Jensen 2005). CDOM can fuel coastal biological activity, such as phytoplankton growth and concentrations can be higher in lower salinity regions, making CDOM useful for tracking freshwater flows into the coastal oceans (Coble et al. 2003).

The spatial extent of organic matter on the shelf does not depend only on the magnitude of the MARS discharge, but rather is a function of wind speed and direction and the buoyancy of the MARS plume on the northwestern GOM shelf (Salisbury et al. 2004). At certain times in the year, primarily April to June, organic matter originating from MARS can extend far west (~400 km) and onto the Texas shelf (Salisbury et al. 2004).

The third parameter analyzed was euphotic depth. The euphotic depth is the depth below which photosynthesis cannot be supported due to light attenuation, generally accepted as the depth at which light transmission is 1% of the light available at the surface. The euphotic depth can be affected by high concentrations of organic and inorganic matter, such as phytoplankton or by suspended sediments from rivers flowing onto the shelf.

#### *C.1.5 Data Selection and Methods*

Datasets were queried within *Giovanni* for the following parameters: Chl *a*, CDOM, and euphotic depth. If the imagery at Level 3 was available, daily images were averaged to build monthly composites for June 2008. That month was chosen to overlap with the 2008 NOAA SEAMAP cruise, during which the hypoxic area extended from Louisiana onto the northern Texas shelf. As discussed in Chapter 4, each of the interpolation scenarios for 2008 calculated the largest values for hypoxic area on the Texas shelf. Therefore, 2008 provided a large sample size ( $N \sim 140$  site locations) with a majority of the sample sites being hypoxic.

Once downloaded from *Giovanni*, the data were saved as netCDF files with a cylindrical equidistant projection and imported into ESRI ArcGIS 9.3. Each dataset was reprojected into NAAEAC and mapped with the same base layers used to create the maps presented in Chapter 4. The processing steps to analyze data in ArcGIS were as follows:

1. Projection was first defined for satellite rasters (Equidistant Cylindrical) and rasters were then reprojected in NAAEAC,
2. Rasters were georectified to the NOAA coastline shapefile,
3. Rasters were converted from floating point to integer and multiplied by 10,000,
4. Values from the raster were extracted for each point of the NOAA SEAMAP Texas locations,
5. Extracted values were divided by 10,000 to convert back to true data values, and
6. Missing data values (labeled as NaN) were removed before exporting the data to ArcGIS.

After data extraction in ArcGIS, the data files were imported into MATLAB and linear regression models were computed to determine if any correlations existed between variables and near-bottom dissolved oxygen concentrations on the Texas shelf.

## C.2 MODIS 4km and SeaWiFS 9km Parameter Results

### *C.2.1 MODIS and SeaWiFS Rasters*

Chl *a*, CDOM, and euphotic depth for June 2008 at 4 and 9km resolution were plotted against bottom dissolved oxygen concentrations for the NOAA SEAMAP TX sites. The rasters are shown in Figure C.1. The first two panels are the MODIS 4km Chl *a* and CDOM. Chl *a* near the coast was high ( $\sim 100$  mg/m<sup>3</sup>) compared to waters in the central Gulf with higher values of productivity extending far offshore on the Louisiana and northern Texas shelf. Higher concentrations in the south, near Mexico, are confined to the southern Texas shelf. This pattern indicates a distinction between Chl *a* concentrations north and south of the Brazos River as productivity is defined by changes in the shelf width. The third panel shows the SeaWiFS 9km Chl *a* concentrations. The range of concentration is the same between sensor resolutions; however, the extent of the high concentrations is wider across the Texas shelf with less of a transition between coastal and offshore waters. The expansion of higher concentrations offshore appears to also be related to the larger resolution cell size.

CDOM (no units) shows higher concentrations ( $\sim 10$ ) on the continental shelf with patches of lower concentrations near Galveston and the Texas-Louisiana border, although values were still higher when compared to deep, central Gulf of Mexico waters ( $\sim 0.1$ ). There is also less variation of CDOM on the northern and southern Texas shelf than is seen with the Chl *a* data. The SeaWiFS 9 km CDOM map has more data gaps on the shelf and a large area of low CDOM concentrations on the northern Texas shelf.

There is also increased variability in concentrations starting on the Louisiana shelf and moving south along the Texas shelf with values ranging between 0.1 and 10. The larger resolution size also accounts for a portion of the variability as seen in the SeaWiFS 9 km Chl *a* as more CDOM values are averaged within the given cell size.

The euphotic depth, mapped in the fifth panel, shows shallow depths extending out to 100 m on the continental shelf on the Louisiana and northern Texas shelves, with the shallowest depths ( $\sim 2$  m) on the Louisiana shelf near the MARS region. The euphotic depth on the southern Texas shelf (west of the Brazos River) is shallow near the coast and deepens offshore with a sharper transition from shallow to deep water compared to the northern Texas shelf. The euphotic depths in June 2008 follow the same along- and across-shelf pattern as the MODIS 4 km Chl *a* image.

#### *C.2.2 MODIS and SeaWiFS Compared to NOAA SEAMAP TX Bottom Dissolved Oxygen*

Figure C.2 shows three-dimensional representations of MODIS Chl *a* and bottom dissolved oxygen variability across the Texas shelf in June 2008. The hypoxic concentrations on the northern Texas shelf are colored maroon and occupy much of the shelf down to approximately 40 m. Chl *a* concentrations collected from the MODIS satellite exhibit similar spatial pattern to the hypoxia, but there are a few points in each dataset with very high ( $>5$  mg/m<sup>3</sup>) concentrations. The highest concentrations occur in the surface waters near the northeastern part of the Texas shelf reaching concentrations as high as 7.5 mg/m<sup>3</sup> indicating that there is a high amount of pigment in the surface waters.

### *C.2.3 Linear Regression Results for MODIS and SeaWiFS Parameters*

Figure C.3 shows MODIS and SeaWiFS Chl *a* and CDOM (4 km and 9 km) plotted against bottom dissolved oxygen concentrations. The results of the linear regression are in Table C.1.

Both Chl *a* graphs show a weak ( $r^2 < 0.2$ ), negative ( $r \sim -0.3$ ) correlation with bottom dissolved oxygen. The MODIS 4 km Chl *a* graph shows low dissolved oxygen coinciding with high Chl *a* values and two possible outliers of low bottom dissolved oxygen with extremely high concentrations. A similar relationship is seen in the graph of SeaWiFS 9 km Chl *a* and bottom dissolved oxygen. There is one potential outlier in the lower range of the bottom dissolved oxygen corresponding to higher values of Chl *a*.

CDOM and bottom dissolved oxygen have a weak ( $r^2 \sim 0.03$  and  $0.1$ ) and positive ( $r \sim 0.2$  and  $0.3$ ) correlation for both the MODIS 4 km and SeaWiFS 9 km data respectively. When examining the SeaWiFS 9 km CDOM, there is an increase in CDOM as bottom dissolved oxygen values increase. There are smaller concentrations of CDOM at low bottom dissolved oxygen values. At the higher end of the bottom dissolved oxygen values, there are higher concentrations of CDOM ( $>5$ ).

The last graph in Figure C.4 (euphotic depth versus bottom dissolved oxygen) shows hypoxic samples and lower dissolved oxygen values between 20 and 40 m of the euphotic depth. Bottom dissolved oxygen values increase as the euphotic depth decreases supporting previous research that hypoxia is generally confined to these shelf depths (Rabalais 2002a). The range of euphotic depths versus dissolved oxygen also starts to significantly increase representing a fan-type spread or more variance in the

scatterplot (Figure C.4). The relationship is weak ( $r = 0.131$ ), but is statistically significant.

The correlation coefficients for each factor are weak ( $<0.5$ ), but significantly different from a slope of 0, and the coefficients of determination are also small ( $<0.2$ ). The correlation coefficients are significant ( $H_0: r = 0$ ), indicating that the relationship between Chl  $a$ , CDOM, and bottom dissolved oxygen is linear.

### **C.3 Discussion and Future Directions for Remote Sensing**

#### *C.3.1 Discussion*

Remotely sensed data have been used to examine the relationship between surface Chl  $a$ , CDOM, and euphotic depth versus bottom dissolved oxygen in the Texas coastal hypoxic zone. The exploratory research presented here examines if satellite imagery has the potential for investigating biogeochemical processes relative to hypoxia formation on the Texas shelf. Data from 2008 show weak, but significant, linear relationships between parameters of interest and bottom dissolved oxygen values. Each linear model was unable to resolve model variability (low  $r^2$ ), indicating that the relationships between Chl  $a$ , CDOM, euphotic depth and bottom dissolved oxygen are not strongly linear (low  $r$ ). Attempts to isolate a smaller range of dissolved oxygen values, such as hypoxic locations or data above 40 m, did not improve the regressions. I expect the correlations might improve when comparing surface Chl  $a$ , CDOM, and euphotic depth to large, independent hypoxic regions on the Texas shelf seen in 2002.

The hypoxic area in 2008 is primarily driven by physical and biogeochemical processes on the Louisiana shelf, not processes on the Texas shelf, which could account for the weak correlation and variability in this study.

Despite the Louisiana shelf influence in 2008, Salisbury et al. (2004) found no significant correlation between satellite Chl *a* and suspended particulate matter. D'Sa and DiMarco (2009) found that high CDOM and high biomass in surface waters was correlated with high bottom dissolved oxygen. My results coincide with their findings based on the different  $r^2$  calculated for the individual parameters, with high Chl *a*, or biomass ( $> 70 \text{ mg/m}^3$ ) being correlated with high CDOM ( $> 7$ ) in the surface waters. There does not appear to be a relationship between nearshore Chl *a* and CDOM for any of the satellite data for June 2008. The low values for CDOM measured by the satellite do not necessarily represent the movement of the MARS discharge westward. The higher values for Chl *a* indicate that the enhanced production is a result of the MARS discharge. Nutrients introduced to the system from MARS can enhance productivity at the edges of the plume (Lohrenz et al. 1999). The resulting production, if high, can interfere with the satellite signal and algorithm determination of surface water constituents leading to an inaccurate interpretation that waters on the western GOM shelf are not influenced by MARS discharge (Salisbury et al. 2004).

There are a number of considerations in using remote sensing data to investigate biogeochemical processes affecting Texas hypoxia. The first is data availability. Most remote sensing data products are averages or composites over space and time. In this study, the spatial resolution of 4 km and 9 km likely did not have a strong impact on the

correlation strengths, as the raster cell resolutions were smaller than the physical and biological scales of coastal ocean processes.

A second consideration is data averaging. Because clouds cover much of the Gulf of Mexico, an average satellite composite product was used. Weekly composites were not available for some of the parameters and if available, had too many data gaps on the Texas shelf lowering the sample size for analysis. Compositing imagery could have masked local variability in the coastal system, which could account for a portion of the variability in the linear regressions. An example of this are the data gaps (indicated by white squares) in the CDOM imagery. There are areas on the Texas shelf with no CDOM data available in either the 4 km or 9 km imagery. However, this was not true of all parameters analyzed. Euphotic depth and Chl *a* have very few gaps on the Texas shelf, providing a large dataset for statistical analysis for June 2008.

The third consideration for addressing variability is spatial averaging within raster cell size and validation of satellite products against *in situ* data. The remote sensing data products were not quality assured or calibrated against *in situ* data, which is outside the scope of this research, but this must be considered when interpreting linear regression results. Each parameter can be impacted by local environmental conditions, such as an algal bloom or river flooding. If an algal bloom occurs, the resulting increased biomass can impact the averaging of the composite product and linear model results, emphasizing higher concentrations of Chl *a* that may not be present under non-bloom conditions. In performing a linear regression, the increased biomass may account for the variability (low  $r^2$ ) in the results. Such impacts can add a bias, or influential

clustering, in the dataset and affect the regression model by additionally increasing the variability. CDOM is directly related to terrestrial organic matter and river flooding could contribute more organic matter to the coastal ocean system, also leading to anomalies in the remotely sensed data that could influence statistical results. As shown in D'Sa and DiMarco (2009), surface CDOM is not a particularly good indicator of low dissolved oxygen at the bottom, as supported by linear regression results. Another consideration for the weak linearity could be attributed to the time lags existing between surface Chl *a* production, decomposition as the algal biomass dies and sinks to the bottom, and microbial respiration of the decayed matter which consumes oxygen. The rates can be driven by nutrient availability and physical processes and vary along and across the shelf from days to weeks (Rabalais et al. 2010; Bianchi et al. 2010).

### *C.3.2 Future Directions*

The next steps in investigating the practicality of using remote sensing data in Texas hypoxia investigations are to first expand the temporal resolution by examining additional years. Year 2008 was an anomaly for hypoxic area on the Texas shelf, having the largest area calculated relative to all other NOAA SEAMAP years. To improve incorporation of remote sensing data, years with no to little hypoxia should be used to establish baselines for the remote sensing parameters of interest. After establishing baselines, comparisons can be made between no, low, moderate, and high hypoxic years.

Another consideration is to compare hypoxia areas rather than individual sampling sites. By combining the results from Section 3 with the results here,

comparisons can be made between hypoxic area and satellite parameters. The sampling sites are *in situ* data and cover a smaller area than the cell resolutions in the satellite imagery. However, the spatial scales of physical conditions on the shelf (Section 1) can help to minimize this constraint and help to improve the relationships. Considering an area as opposed to an *in situ* site may account for the variability in the linear relationships between satellite parameters and bottom dissolved oxygen. Averaging data over a hypoxic area may improve correlations by comparing different regions on the shelf, rather than individual locations with smaller resolution than the imagery. Also, by isolating areas of interest, such as the narrow and large hypoxic area associated with the Brazos River in 2007, might help isolate local variability in the datasets.

Finally, it is recommended that remote sensing parameters on the Texas and Louisiana shelves should be compared to develop baselines and investigate differences in biogeochemical processes over a larger shelf area for no, small, moderate, and large hypoxic years. Studies referred to previously and background information presented in Section 1 show that the physical and biogeochemical processes differ between the Louisiana and Texas shelves (Bianchi et al. 2010; Hetland and DiMarco 2008). Running comparisons with shipboard *in situ* data and remote sensing products will also help to determine the role of remote sensing in coastal ocean studies.

This study has shown that remote sensing has potential to contribute to the overall understanding of hypoxia formation on the Texas shelf. This study has also provided statistical support that significant linear correlations may exist between remote sensing parameters and bottom dissolved oxygen and addresses how correlations might

be improved between surface and *in situ* cruise data. Incorporating these types of interdisciplinary data into this type of research provides a more global view of the entire shelf and provides general insight into the biogeochemical processes that impact hypoxia formation and duration alongside the physical processes. Remote sensing assimilation repositories, such as *Giovanni*, provide accessible, processed remote sensing imagery that does not require extensive pre- and post-processing, allowing faster access, manipulation, and visualization of shelf-wide processes that can contribute to our understanding of hypoxia dynamics on the Texas shelf.

Table C.1 Linear Regression Model Statistics for Remote Sensing Parameters versus NOAA SEAMAP Bottom Dissolved Oxygen in 2008 on the Texas Shelf.

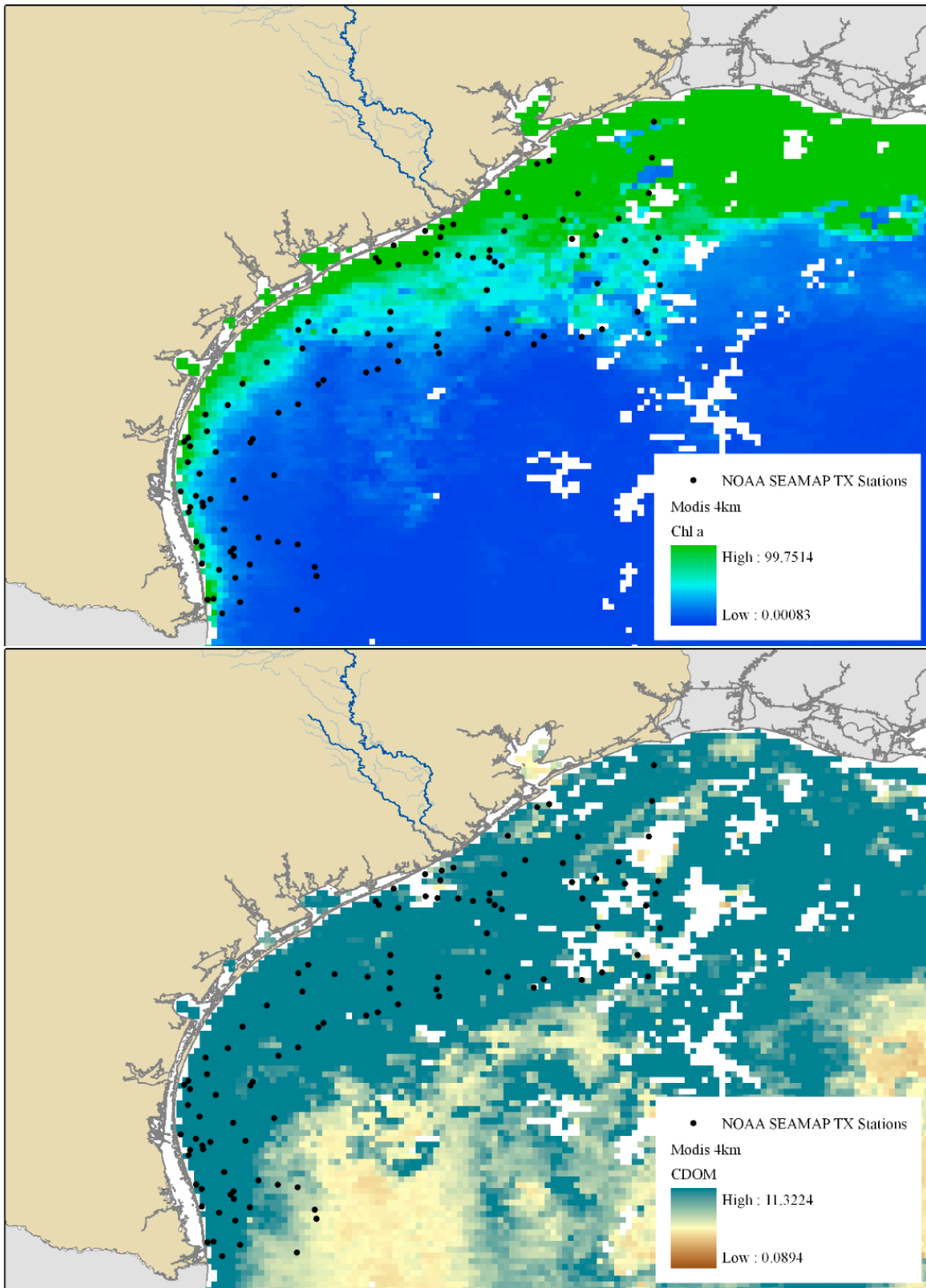
<i>Data</i>	<i>Slope (<math>b_1</math>)</i>	<i>Intercept</i>	<i>Degrees of Freedom (<math>N-1</math>)</i>	<i>Correlation Coefficient (<math>r</math>)</i>	<i>Coefficient of Determination (<math>r^2</math>)</i>	<i>p-value (<math>H_0: b_1 = 0</math>)</i>	<i>Confidence Intervals</i>	
							<i>Lower</i>	<i>Upper</i>
Modis 4km Chl a	-0.33	2.69	100	-0.37	0.14	<b>0.0001</b>	-0.53	-0.16
Modis 4km CDOM	-0.34	4.52	95	0.19	0.04	0.0603	-0.01	0.38
SeaWiFS 9km Chl a	-0.77	2.05	85	-0.38	0.14	<b>0.0003</b>	-0.55	-0.18
SeaWiFS 9km CDOM	0.60	3.17	76	0.31	0.10	<b>0.0052</b>	0.10	0.50
Modis 4km Euphotic Depth	-8.32	-44.21	100	-0.44	0.19	<b>0.0001</b>	-0.26	-0.58

Significant test results showing a linear relationship between parameter and bottom dissolved oxygen are indicated in red (p-value < 0.05).

The correlation coefficient ( $r$ ) shows the strength and direction of the linear relationship, either positive or negative.

The coefficient of determination ( $r^2$ ) shows the proportion of variance explained within each model.

Figure C.1 Year 2008 MODIS and SeaWiFS Chl *a*, CDOM, and Euphotic Depth on Texas Shelf. The first two panels plot the MODIS 4km data products and the second two panels plot the SeaWiFS 9 km data products. The fifth panel is map of the MODIS 4km euphotic depth. White areas in the images represent cells where data was not available due to cloud cover for the month. The black circles mark the locations of the NOAA SEAMAP TX stations.



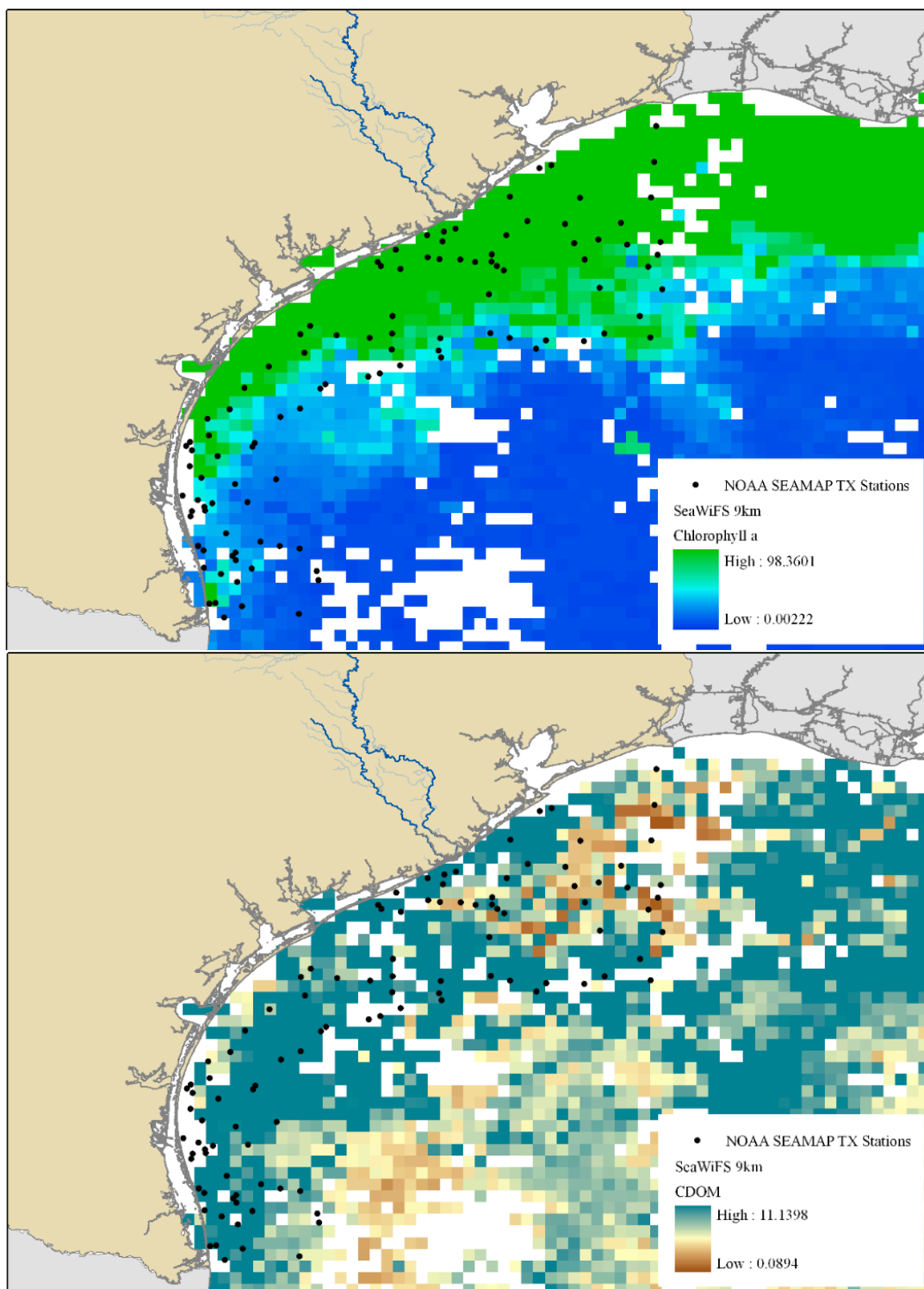


Figure C.1 Continued

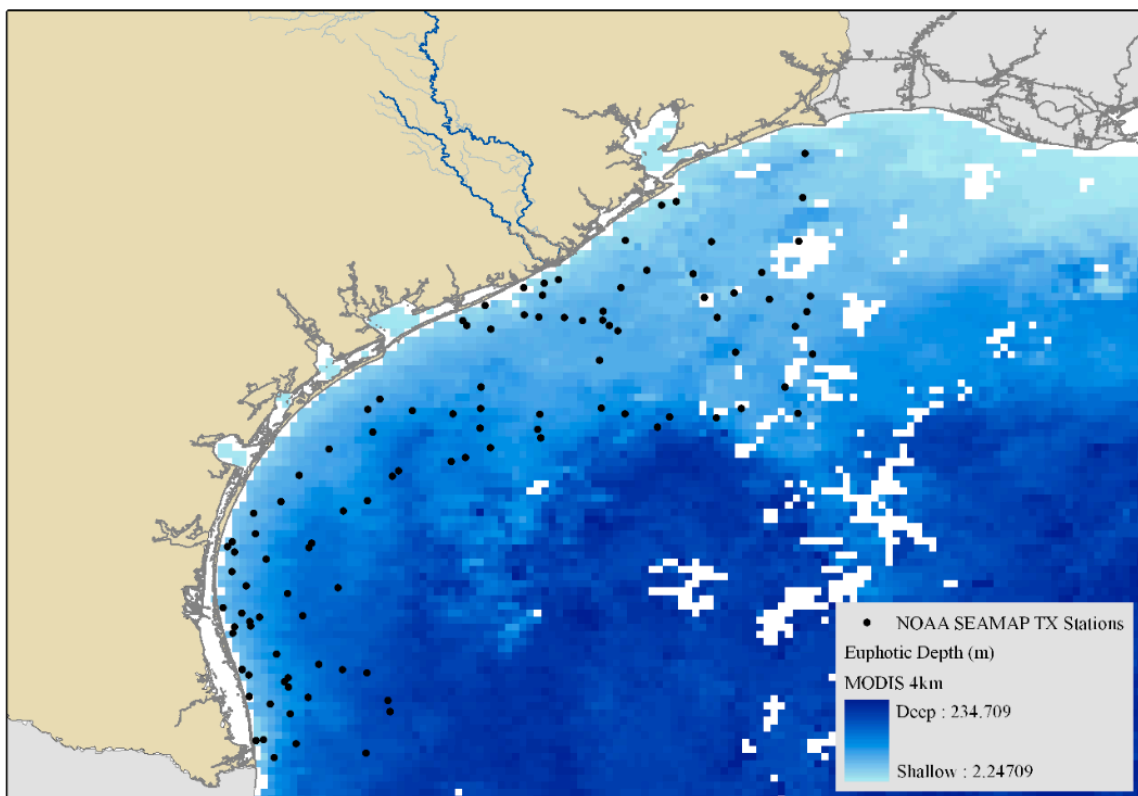
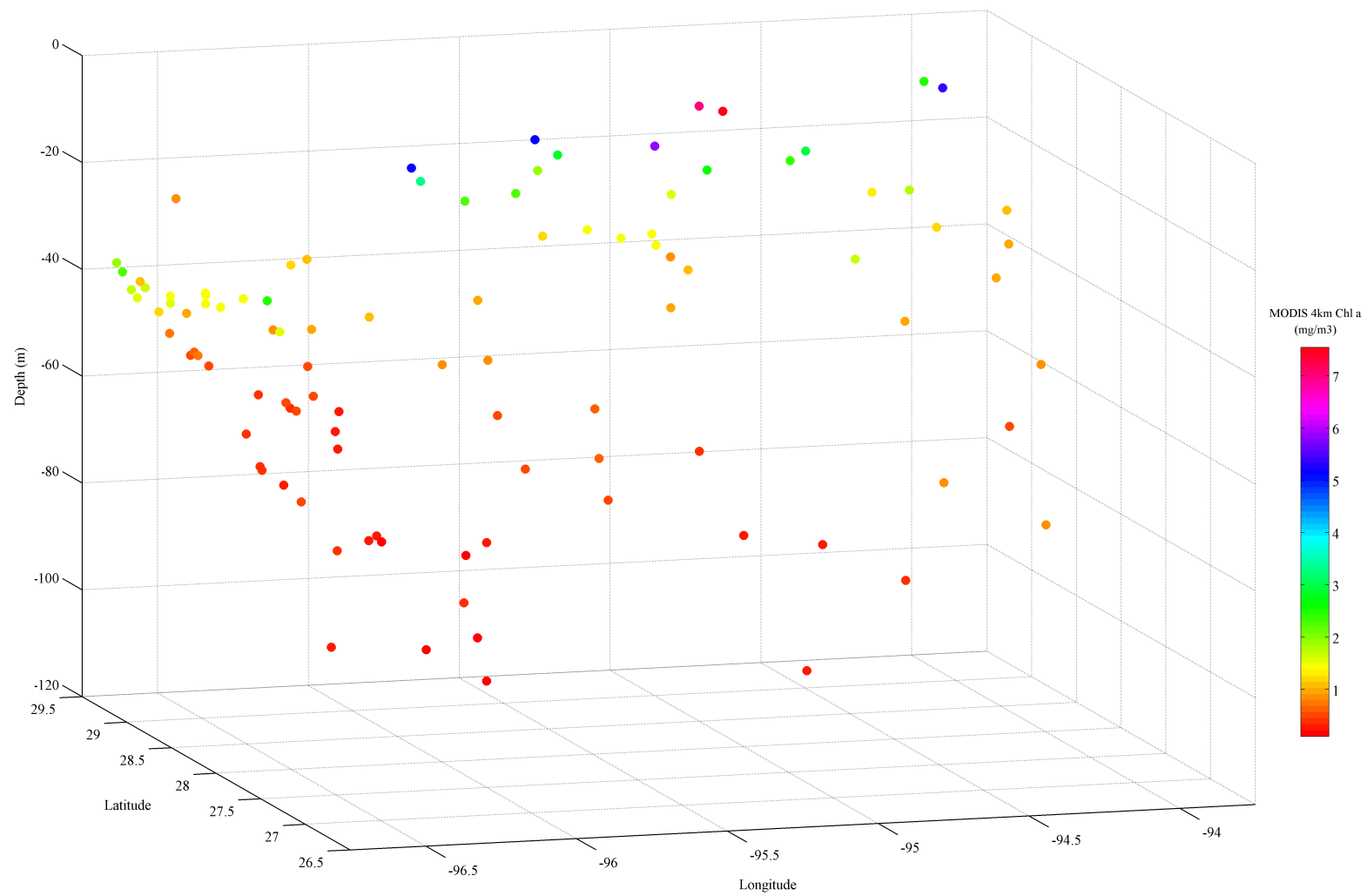


Figure C.1 Continued

Figure C.2 Dissolved Oxygen and Chlorophyll *a* Concentrations in 2008 on the Texas Shelf. The top 3-D plot shows the bottom dissolved oxygen concentrations ( $\text{mg L}^{-1}$ ) as sampled during the NOAA SEAMAP summer survey in 2008. Hypoxic samples are colored maroon and are found near the northeastern side of the Texas shelf between approximately 10 and 35 m water depth. The lower panel plots the Chl *a* concentrations collected from MODIS satellite imagery (4 km resolution) for each SEAMAP location.



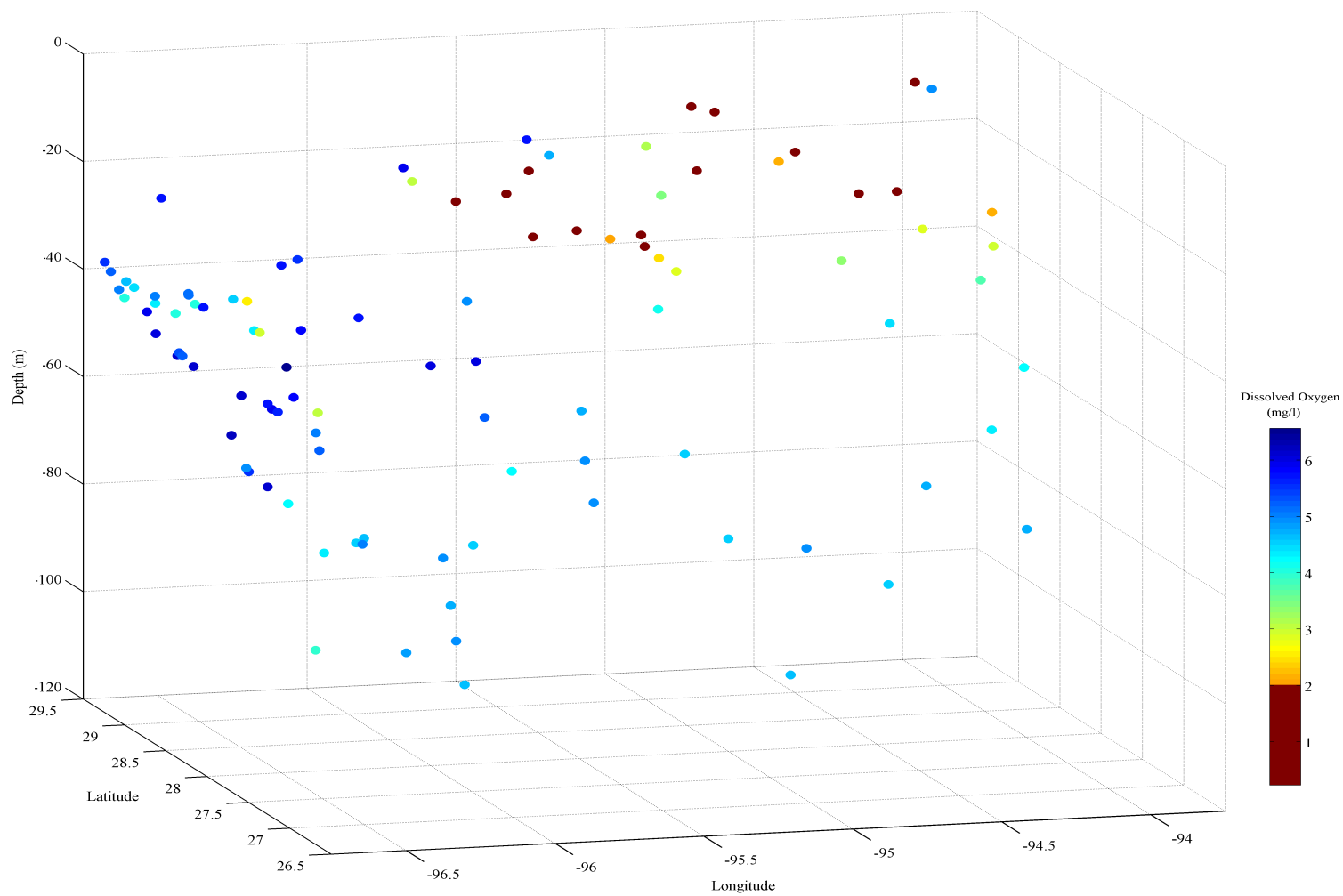
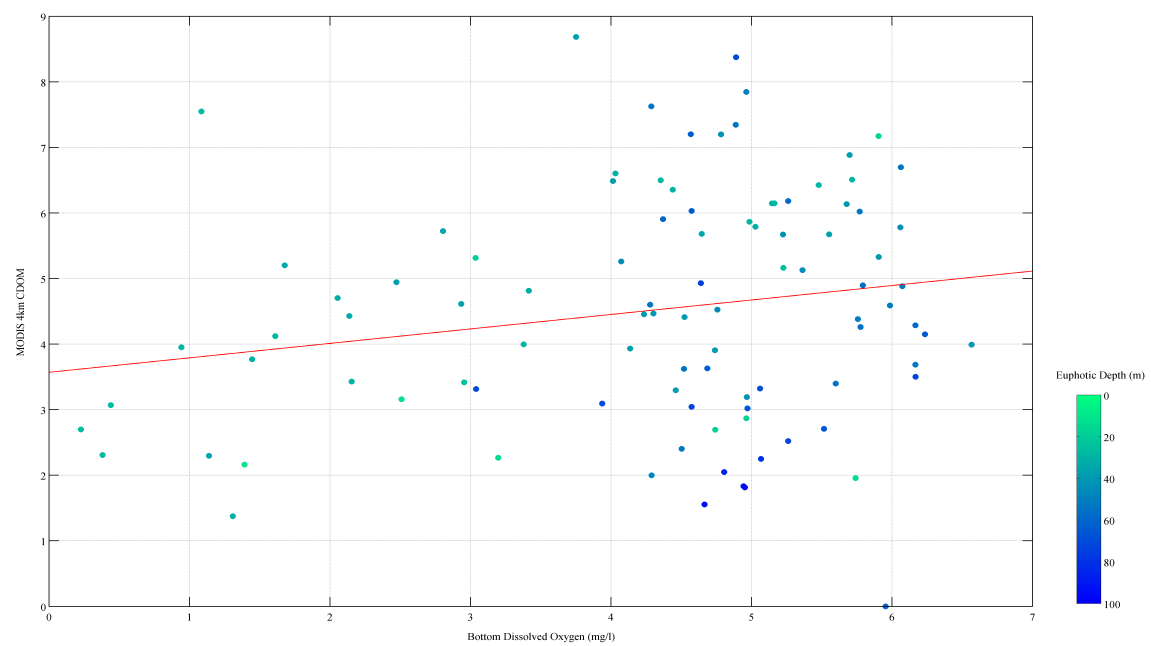
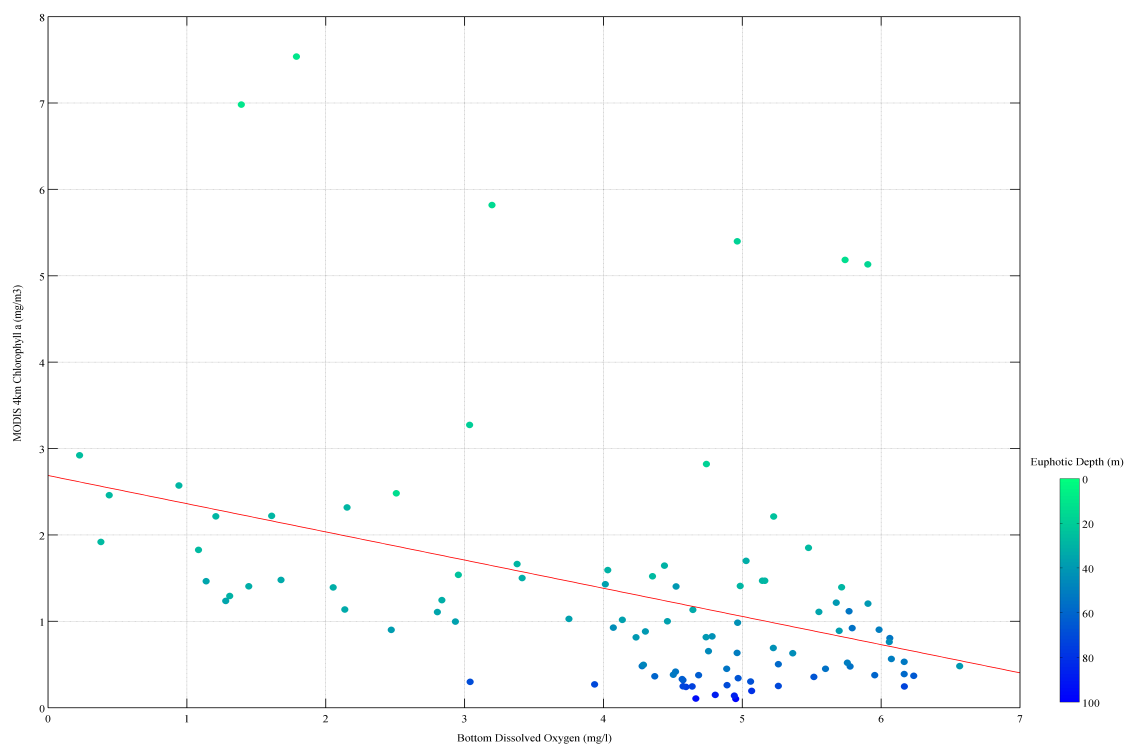


Figure C.2 Continued

Figure C.3 MODIS and SeaWiFS Chl *a* and CDOM versus SEAMAP Bottom Dissolved Oxygen on Texas Shelf. The first two scatterplots show Chl *a* concentrations ( $\text{mg m}^{-3}$ ) from MODIS 4km and SeaWiFS 9km satellites. Both plots show a slightly negative linear relationship between the two variables indicated by the red line. Hypoxic locations are indicated by the maroon color and occur with higher values of Chl *a*. The bottom two panels graph the weak positive relationship between CDOM and bottom dissolved oxygen MODIS 4km and SeaWiFS 9km products. The red line shows the resulting linear model. Data points have a narrow range for lower bottom dissolved oxygen values and a wider range in both Chl *a* and CDOM as the dissolved oxygen increases.



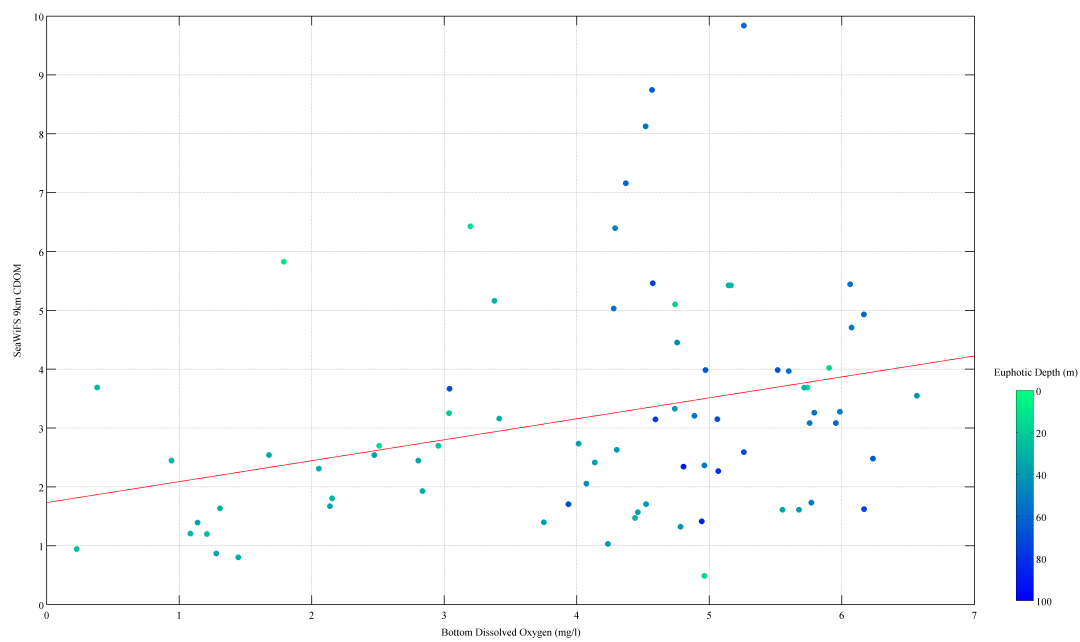
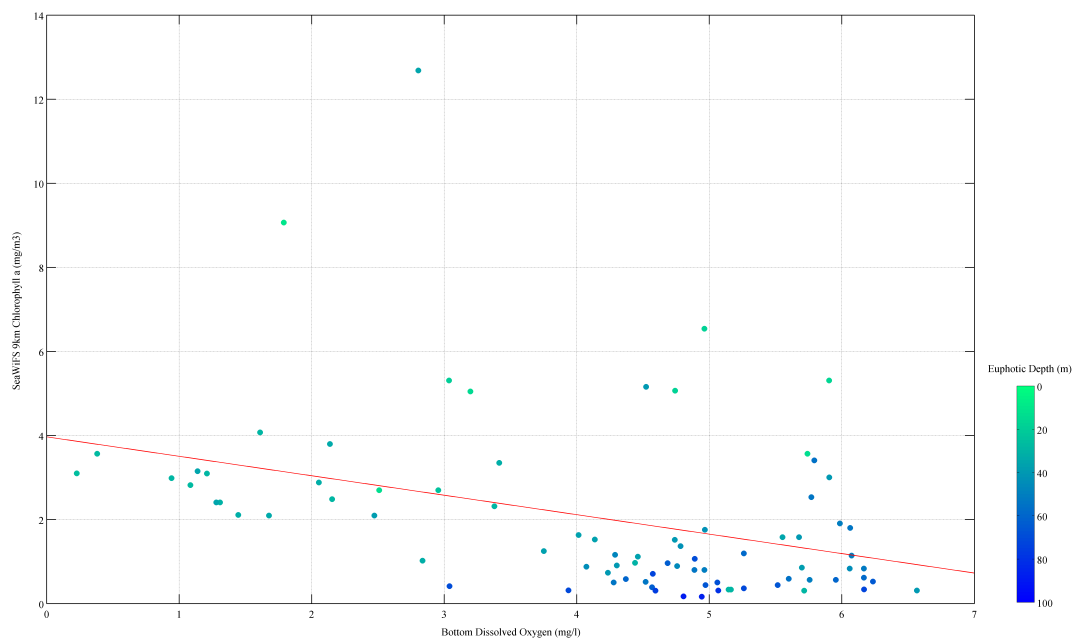


Figure C.3 Continued

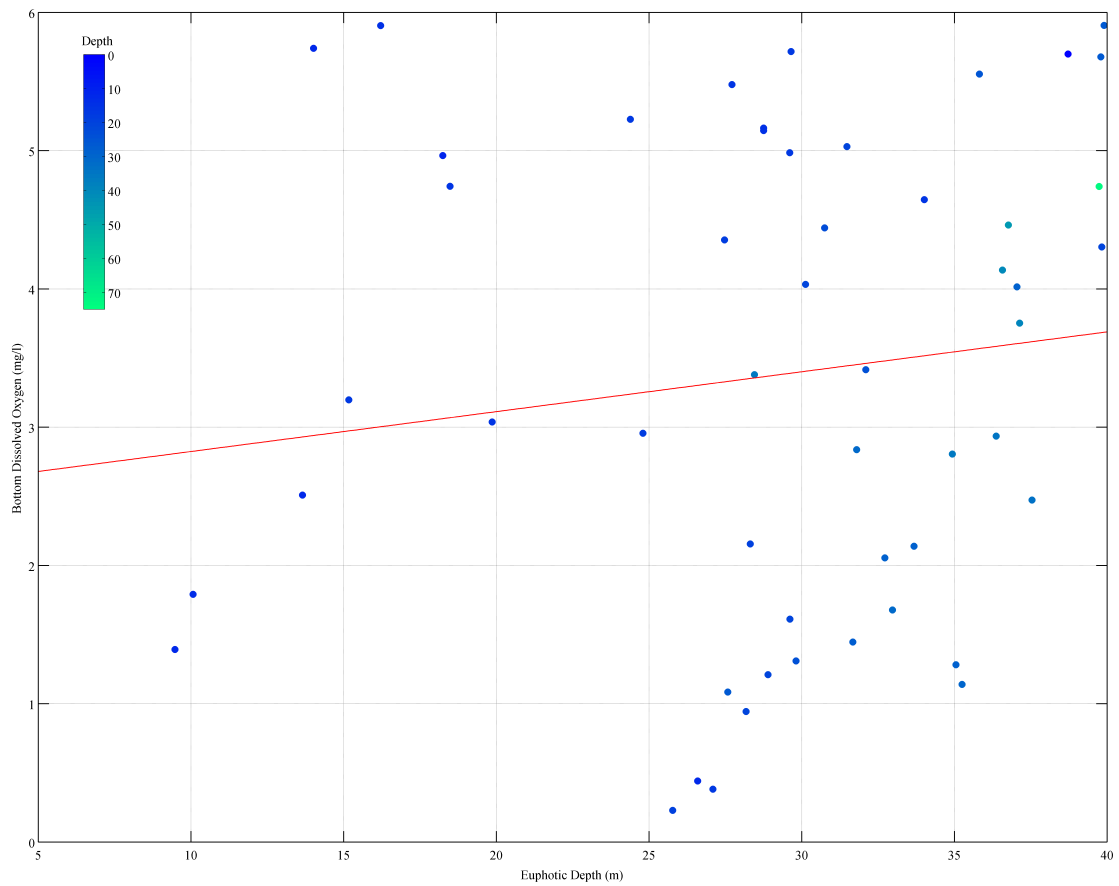


Figure C.4 MODIS 4km Euphotic Depth versus SEAMAP Dissolved Oxygen for 2008. The scatterplot shows MODIS 4km euphotic depth versus bottom dissolved oxygen values on the Texas shelf in 2008. The points are colored by bottom dissolved oxygen values with hypoxic locations plotted in maroon. The red line indicates the direction and strength of the linear relationship between the two variables. The strength of the relationship is weak ( $r = 0.131$ ) due to the variability between deeper euphotic depths and higher bottom dissolved oxygen values.

**APPENDIX D**

**EDUCATION AND OUTREACH CONSIDERATIONS FOR GULF OF**

**MEXICO COASTAL RESEARCH**

## **D.1 Geosciences in the K-12 Educational System**

### *D.1.1 National and State Geosciences Education*

Increasing student exposure to the field of geosciences in the K-12 grade levels is a national educational concern. According to the American Geological Institute Status of the Geoscience Workforce Report, over half of Texas science teachers (~56%) hold an Earth Science certification, but only 6.3% have an Earth Science teaching assignment (Gonzales and Keane 2010). Geosciences are introduced in the 6<sup>th</sup> – 8<sup>th</sup> grade state standards and are recently, but slowly, emerging in the 9<sup>th</sup> – 12<sup>th</sup> elective curriculum for the state of Texas. In the 6<sup>th</sup> – 8<sup>th</sup> curriculum, geosciences is considered an integrative curriculum and not taught year-round. In Texas, geosciences were recently designated as a primary science in 8<sup>th</sup> grade. Less than 20% of all 7<sup>th</sup> and 8<sup>th</sup> grade students electively enroll in a geosciences course (Gonzales and Keane 2010). Gonzales and Keane (2010) also tracked percentages of 9<sup>th</sup> grade students enrolled in earth sciences, which averaged 8.33% from 1996 – 2000, but dropped significantly to 2% from 2003 – 2004.

Opportunities to study in a geosciences field improve as students enter undergraduate programs. Both major Texas University state-systems, Texas A&M and the University of Texas, offer undergraduate and graduate degrees in all geosciences fields. Despite increased course offerings at the University-level, the numbers of degrees earned in the geosciences are significantly lower than other major science degrees, such as life or physical sciences (Gonzales and Keane 2010). To address this growing concern

in K-12 grade levels, there is a need to integrate University-level geosciences programs with the local community K-12 schools.

#### *D.1.2 Programs and Objectives*

As a result of my research, I have developed two effective curriculum-based programs for bringing oceans into the classrooms as a way to increase elementary and middle school student geosciences knowledge. These two programs provide an opportunity for students to interact with scientists and perform oceanographic experiments and provide science lessons (curriculum), equipment, and samples for teachers. Each program provides an opportunity to engage with the public to promote ocean stewardship and make people aware of coastal hazards affecting their local oceans.

### **D.2 Considerations for Program Development**

#### *D.2.1 Initial Program Development*

When first approaching K-12 education curriculum development, it is important to define the type and purpose of the program. These programs integrate academic research into classrooms and the science curriculum. Researchers, teachers, and students benefit from integrating academic research into K-12 schools. Researchers learn how to better communicate scientific research and results to a broader audience. Teachers are able to expand their curriculum by increasing the numbers of lesson plans, supplementing laboratory experiments, and introducing real-world scientific examples to supplement

weak state geosciences criteria. Students are exposed to real-world science opportunities that otherwise would not be experienced until later, if at all, during their education.

Two common integrations of research into grade school classrooms are by lecturing and by working directly with teachers to develop either a complete curriculum, or individual lesson plans. Curriculum development is more time-consuming and hands-on for both the researcher and teacher, but has longer lasting benefit for the teacher and is a way to impact more students across grade levels and schools. Our efforts presented here combine both lecturing and curriculum development.

In 2008, I developed two programs and implemented each in middle school (5<sup>th</sup> and 6<sup>th</sup> grade) classrooms from 2008 to 2011. The first was a pilot program to test a curriculum based on a field-based oceanography training cruise in the Galapagos Islands. The second shifted from an open ocean focus to coastal waters, partnering with researchers in the TAMU MCH project. The programs were designed to accomplish the following goals:

1. Introduce elementary and middle school students to opportunities in the geosciences, especially oceanography,
2. Assist teachers by providing an inquiry-based and interdisciplinary geosciences curriculum, and
3. Connect the public with TAMU oceanographers to promote the importance of geosciences and ocean stewardship.

#### *D.2.2 Program Design Considerations*

The design of both programs is an important consideration to continuing the longevity of each and to assess the program impacts for students, teachers, and researchers. It was important that each program has a high teacher and student impact and that it will be maintained in the classrooms regardless of the presence of a geoscientist. The first consideration in developing the curriculum portion of each program was deciding upon a learning theory on which to base the lessons. A constructivist approach was selected as the initial learning theory to be incorporated in the curriculum program design. This approach is a primary technique used when developing national teaching standards and embraces both structured and open inquiry learning (Jonassen 1999). With structured inquiry learning, the teacher or scientist provides background knowledge and a question, while students design a procedure to test the question ([http://www.temple.edu/CETP/temple\\_teach/CM-struc.html](http://www.temple.edu/CETP/temple_teach/CM-struc.html)). Open inquiry allows the students to be the scientists. Students independently apply the scientific method by developing a scientific question, procedures, and experiment based on their understanding and classroom knowledge on a topic (Jonassen 1999). Both approaches challenge students to design, implement, and answer a scientific question, which challenges students to apply new knowledge and not just memorize scientific facts.

#### *D.2.3 Addressing Texas Essential Knowledge and Skills for Science (TEKS)*

An important consideration for each curriculum development was addressing Texas Essential Knowledge and Skills (TEKS) tests established by the Texas Education Agency ([www.tea.state.us](http://www.tea.state.us)). The science curriculum in Texas schools is designed to

teach TEKS based on grade level. The science topics taught in middle school are interdisciplinary, but the content focus is on the physical sciences ([ritter.tea.state.tx.us](http://ritter.tea.state.tx.us)). Many of the TEKS include recurring themes that are related to mathematics, sciences, and technology at each grade level tested. My focus is on scientific investigation and reasoning, which is one of the main goals of the 6<sup>th</sup> grade TEKS exam.

The Texas Education Agency emphasizes that students should have a strong understanding of why scientific investigations are important and are able to design and perform a scientific study. The design and implementation includes posing a research question, collecting observations and data, analyzing data, and deriving a conclusion ([ritter.tea.state.tx.us](http://ritter.tea.state.tx.us)). Specific skills in this TEKS include knowing when to use equipment to determine a specific measurement, formulating testable hypotheses, collecting data, constructing tables and graphs, and analyzing the data for patterns.

### **D.3 Program Descriptions and Impacts**

#### *D.3.1 Program Overview*

The first program was built as part of a graduate oceanographic training cruise to the Galapagos Island and the second focused on Gulf of Mexico coastal oceanographic research. The two programs were designed with three phases: pre-cruise, cruise, and post-cruise. Each phase involves some level of interaction between researchers, teachers, and students. The first phase, *pre-cruise*, introduces background knowledge relevant to the oceanographic cruise mission for the teachers and students.

The second phase, *cruise*, focuses on student interactions with researchers while the researchers are at-sea and is possible using video and Internet technologies, such as Skype and interactive teacher-student-parent data portals established for individual schools. The *cruise* phase allows for more independent learning than the first phase. Students are encouraged to conduct independent research within the context of the oceanographic studies. This involves asking questions of researchers and directing a portion of the scientific research virtually by interacting with researchers. Based on knowledge of the system and viewing the data, students can contribute to the cruise sampling design by requesting additional water collection at sites they are interested in while the researchers are at sea. The second phase also provides an opportunity for students to share experiences with others beyond the classroom, such as with parents or friends.

The last phase, *post-cruise*, is the inquiry-based level of the program. Based on previously acquired knowledge in the first two phases, students examine samples brought back from the cruise. The geosciences curriculum is also developed in this phase between the researchers and teachers. Examples of curriculum include teaching the hydrologic cycle and principles on climate change using data collected during the second phase. A primary goal of the third phase called longevity, is a curriculum independent of a geoscientist in the classroom.

#### *D.3.2 Program Classroom Selection*

The opportunity and assistance in designing the curriculum resulted from my involvement as a NSF GK-12 Graduate Fellow in the Partnership for Environmental and Rural Health (PEER, [peer.tamu.edu](http://peer.tamu.edu)) program. In this program, I was assigned as a *Resident Scientist* to a classroom at Stephen F. Austin Middle School (SFA) in Bryan, Texas. A *Resident Scientist* is the graduate student designation given as part of the NSF GK-12 program. The *Resident Scientist* is a science subject expert and is placed in a science classroom. At SFA, I primarily worked alongside Mr. Naveen Cunha, a 6th grade science teacher and Director of the Odyssey Academy at SFA, a math, science and technology magnet school within the school.

Each program was implemented for two cohorts, each with approximately 80 students. An added, and unintended benefit to the program was the fact that many of the students had never traveled to a seacoast. Because many students had never traveled to the ocean, we were able to gauge student understanding of an environment that could not be recreated or modeled in the classroom. We were also able to establish a baseline to assess student attitudes toward oceanography and assess progress in testing learning pertinent to the Texas state geosciences testing standards.

A second benefit from working with the 6<sup>th</sup> grade classroom was the Odyssey Academy's participation in an Apple®-sponsored Texas Technology Immersion Project (TIP). Participation in TIP provides each student with a laptop for the school year. The accessibility to online programs, data portals, and the Internet allowed each student to participate outside of the classroom. Technology accessibility also aided in expanding the content of each program by adding follow-up lessons, such as independent research

projects, to the original curriculum. Readily-available technology outside the classroom helped to increase communication with the research scientists during the second phase, and allowed students to share their experiences with a broader audience, such as parents and friends.

The second program was first initiated in a different grade level and classroom. Selection for the second class was based on the intentions of exposing younger students to oceanography as a science, explaining why studying the Gulf of Mexico is important, and showing how human activities can impact the coastal ocean environment. A 5<sup>th</sup> grade classroom at St. Joseph's Catholic School in Bryan, Texas was selected for this program.

#### **D.4 The First Program: *Galapagos Islands – A Virtual Trip of a Lifetime!***

The first program coincided with a graduate-level course requiring a 3-week graduate student oceanographic training cruise to the equatorial Pacific and the Galapagos Islands. Graduate students in the class were encouraged to participate in the education program by contributing curriculum and lesson plan ideas based on their individual graduate research and by communicating with the middle school students during the cruise. Additionally, the cruise was conducted alongside scientists in the Ecuadorian Navy (INOCAR), who were also willing to participate as contributing researchers by communicating and working with SFA students to collect samples for analysis in the classrooms and to teach students about global ocean circulation and climate change in the equatorial Pacific Ocean, and the history of Ecuador and the Galapagos Islands.

#### *D.4.1 Phase 1: Pre-Cruise*

The *pre-cruise* phase focused on the teacher and scientist teaching the classroom about the oceanographic region of interest. The first phase started with presentations to 6<sup>th</sup> graders about oceanographic research and the general physical and biological oceanography in the equatorial Pacific, such as El Nino oscillations, climate change, and marine mammal distributions around the Galapagos Islands. Three graduate students, including myself, gave presentations. The students conducted investigative scientific experiments to study water density, the hydrologic cycle, and the role of salinity in oceanography. Under my guidance as the *Resident Scientist*, students learned how to design and conduct basic oceanographic surveys, plan a research cruise, and measure oceanographic parameters, such as counting phytoplankton and measuring salinity. They were able to do this with the accessibility of technology (e.g. individual laptops and Internet) and by interacting with the guest presenters. Students learned the importance of the scientific method in geosciences research by formulating a scientific hypothesis (e.g. Does pressure increase with depth?) to investigate the role of density in the ocean. School students developed scientific experiments to send with the graduate students to test their hypotheses during the second phase of the program. For example, one experiment was sending different materials mostly comprised of air, such as Styrofoam, to test how pressure and density change with depth.

The trip also coincided with curriculum lessons in the social sciences about South American culture and economies. In social sciences, the resident scientist and teachers

interacted to construct additions to the curriculum materials to teach students about historical, political, and economic culture of Ecuador and the Galapagos Islands. One example involved small-group student projects, in which each group was assigned a different area of Ecuador (e.g. rural or urban) and had to compare their area with Bryan, Texas.

#### *D.4.2 Phase 2: Cruise*

The *cruise* phase relied on communication between researchers and students. This phase incorporated the constructivist and inquiry-based approaches by having students develop laboratory experiments to test the questions introduced by by researchers in the first phase. The primary questions posed to students focused on the role of density and salinity in ocean circulation and on biological productivity around the Galapagos Islands.

From the time the graduate students left College Station and landed in Ecuador, graduate and middle school students communicated using their laptops either from the classroom or their homes. The graduate students shared exploratory data from past INOCAR research cruises and compiled blogs, video, and digital photo albums while exploring Ecuador. Graduate students also led interviews between the middle school students and Ecuadorian scientists to expose the students to the cultural, scientific, and historical relevance of the Galapagos Islands. The real-time communication between SFA and TAMU students even included students' parents, who viewed the videos and posted comments and questions to the science blogs.

Graduate students communicated via satellite with the classroom and provided lesson on data collection at sea. Examples included showing middle school students how

to collect water samples from a CTD profiler, collect biological samples from captured squid, and how to measure biological productivity in the surface waters. Occasionally, cruise tracks, CTD data files, and updates of student density experiments were compiled and sent to Mr. Cunha at SFA. Because of availability of the individual laptops, students were able to actively track the ship's location each day, watch data being collected, and monitor the progress of their experiments. This activity was tracked by Mr. Cunha, who maintained a real-time Google Earth map that students added different layers of information (e.g. cruise tracks, graphs, and data summaries) too each day of the cruise.

#### *D.4.3 Phase 3: Post-Cruise*

The *post-cruise* phase started when the scientists returned to the TAMU. The *post-cruise* phase combined elements from the first two phases and required students to complete their investigation of the scientific method. The first segment of this phase involved three presentations by graduate students who participated on the cruise. Presentations included cruise experiences, data results, and observations of the oceanographic environment.

The second segment of this phase was more student-driven and involved more inquiry-based experimental learning than the first phase. Students concluded their experiments on relating pressure and density to depth by examining samples brought back from the cruise, including shrunken Styrofoam cups that had been exposed to high pressure so the students could examine the effects of increased density on physical objects. Students also used CTD profiles to create graphs of density versus depth to test

their original hypotheses. Curriculum lessons addressing the TEKS discussed previously, such as calculating mean, median, and mode with cruise data, were taught by Mr. Cunha and myself. Additional lessons included students compare samples of phytoplankton from different locations around the Galapagos to make inferences about the levels of biological productivity in upwelling versus downwelling waters and to estimate phytoplankton abundance at different locations. Classroom experiments also learning to measure salinity using different methods (e.g. hydrometers versus evaporation). Exploratory lessons included counting plankton to determine abundance and species diversity phytoplankton at different sites to compare against results produced by the Ecuadorian scientists. A few student projects resulting from these lessons included scientific reports about the ocean productivity around the Galapagos Islands, including building food webs to represent the role of plankton in the oceans, and hydrography of waters around the Galapagos Islands, open ocean between the Islands and Ecuador, and the coastal waters on the Ecuadorian shelf. Many of these reports were displayed around the school and students were given opportunities to share their reports with other science classrooms at SFA.

#### ***D.5 Oceanographers-In-Training: Monitoring Hypoxia From the Classroom***

Gulf of Mexico hypoxia is a nationally recognized environmental issue in coastal and agricultural state politics. By including political context, another avenue of outreach was provided by incorporating social sciences into the program. Because of the national

importance of monitoring Gulf of Mexico hypoxia and the interdisciplinary science necessary to understand the issue, this project provided an opportunity to add curriculum elements and classroom resources in the social sciences, engineering, and mathematics. The program provided the opportunity to expand student horizons by teaching the relevance of coastal oceans to everyday lives.

#### *D.5.1 Phase 1: Pre-Cruise*

Prior to a cruise in April 2009, I developed classroom curricula for both classrooms. Dr. DiMarco visited the 5<sup>th</sup> grade classroom teachers and provided background about hypoxia as a coastal hazard and why hypoxia is a national concern. I presented the same information to the SFA 6<sup>th</sup> grade classroom. In the hypoxia program, students were given the opportunity to observe oceanographic equipment used in the project and to witness classroom demonstrations on measuring dissolved oxygen in water. To conclude the phase, students were presented a wall map to track Gulf of Mexico hypoxia with the scientists during the second phase.

#### *D.5.2 Phase 2: Cruise*

Phase 2 focused on classroom tracking the ship's location and scientists' data, including hypoxic locations in the Gulf of Mexico. As with the first program, students and researchers communicated via email between the ship and the classroom. The classroom downloaded data to add to their map, located the areas of hypoxia, and read blogs posted by various scientists. Students read emails and blogs about life aboard a research vessel and the type of work conducted by oceanographers. The emails and blogs

also included information, such as the difficulties associated with working in the natural environment, (e.g. rough sea-state) through a series of photographs, videos, and blogs posted by members of the scientific party and the ship's crew.

#### *D.5.3 Phase 3: Post-Cruise*

The last phase included scientific experiments and classroom presentations by researchers in the classroom similar to the inquiry-based approach employed during the first program. The 5<sup>th</sup> grade classroom *post-cruise* activities were not as inquiry-based as the 6<sup>th</sup> grade activities. The 5<sup>th</sup> grade activities primarily focused on presentations by the researchers. Presentations included data results from the cruise, the hypoxic area estimate for the Gulf of Mexico and how the area compared to previous years. Each 5<sup>th</sup> grade student was rewarded with an *Oceanographer-In-Training* certificate.

The second part of this phase focused primarily on the 6<sup>th</sup> grade inquiry-based student analysis of samples. This program was also implemented after the first program, so students had prior knowledge of how to analyze oceanographic water samples to measure salinity and phytoplankton. The curriculum included lessons on analyzing water samples, measuring salinity, and counting phytoplankton. The students then developed scientific questions (e.g. Do the depth profiles for temperature or salinity differ between the two locations?) to compare and contrast water samples collected in an equatorial ocean versus from a semi-enclosed sea. In addition, both the 5<sup>th</sup> and 6<sup>th</sup> grade students analyzed sediment samples for grain size and composition. The samples were also analyzed to compare changes in composition between hypoxic and oxygenated sites.

The 6<sup>th</sup> grade students used observations collected from water sample analyses (e.g. phytoplankton and zooplankton abundance and diversity, salinity and temperature profiles) to draw conclusions about productivity in coastal waters and about the type of coastal sediments in the Gulf of Mexico and compared their results to the researcher results to determine their measurement accuracy.

#### *D.5.4 Program Adaptation for 6<sup>th</sup> Grade Classroom*

Laboratory experiments were developed with on-line components that required students to research information on the Internet. The research was similar to the type of research in the first program and specifically was designed for the 6<sup>th</sup> grade SFA students. The 6<sup>th</sup> grade students built upon previous skills learned in the first program by learning to measure dissolved oxygen concentrations in the water

Examples of TEKS not covered by the first program include quantitative reasoning, patterns, geometry and spatial reasoning, and probability and statistics. Students researched historical area estimates of hypoxia in the northwestern Gulf of Mexico and compared present-day estimates to historical averages to investigate how hypoxia area has changed. The same type of analysis, including descriptive statistics for mean and standard deviation, were calculated for bottom dissolved oxygen values collected at CTD stations during the cruise. Further analysis of coastal samples, such as salinity, allowed students to practice multiplication and division skills to evaluate ratios and rates in the coastal ocean, which is also a 6<sup>th</sup> grade mathematics TEK.

Gulf of Mexico hypoxia also allowed teachers at SFA to teach non-science Texas state standards. The primary focus for social science TEKS is the study of people, places, and societies of the contemporary world. Hypoxia provides a context for understanding how an ocean hazard affects coastal populations. Students were able to research how coastal hypoxia impacts local ecosystems and economies for different locations and cultures worldwide.

Studying hypoxia and the results from students' scientific analyses were also incorporated into the teaching of English TEKS. Teachers were able to use the program to teach students' how to construct expository or procedural texts and to develop a research plan, in which students had to determine and locate relevant literature sources describing coastal hypoxia in the Gulf of Mexico. Research planning also progressed into synthesizing information, including recording and visualizing data, to deliver final reports of their findings. These last two examples are specific skills and tasks outlined in the English 6<sup>th</sup> grade TEKS.

## **D.6 Program Assessments**

### *D.6.1 Introduction*

Assessing impact was completed using two different methods: student involvement and NSF GK-12 PEER science surveys. The student involvement was an unexpected measure of program success, because students matriculated to the next grade moving schools in the process. The second assessment was derived from analyzing the

response of students to surveys developed by principal investigators in the NSF GK-12 PEER program.

#### *D.6.2 Student Involvement Assessment*

Students participated more than one year. Five St. Joseph's 5<sup>th</sup> graders attended the Odyssey Academy at SFA the following year. From their involvement in the second program and excitement for conducting a similar, advanced program, each student assisted Mr. Cunha and myself with teaching these programs. The students from St. Joseph's led their new laboratory groups in completing the advanced experiments designed specifically for 6<sup>th</sup> grade, based on their previous knowledge from completing the 5<sup>th</sup> grade program. Advanced experiments included measuring oxygen, salinity, and plankton in the open ocean and coastal samples, and creating graphs and time-series of coastal oxygen concentrations in the Gulf of Mexico. Participation in consecutive years showed the value for this of programs in establishing learning recognition for students and connectivity between science TEKS for teachers, essentially enabling both groups to build and expand upon previous knowledge using current and relevant geosciences fieldwork (coastal oceanography).

#### *D.6.3 NSF GK-12 PEER Survey Design*

Surveys were conducted at the start and end of the year to assess the impact to a *Resident Scientist* in the classroom. The students' responses were extrapolated to be a valuable, but indirect, assessment of the benefits of having a geoscientist in the classroom

and experiencing general science from the perspective of an oceanographer. The resident scientist and teachers did not develop the assessment.

The survey was constructed as a Likert scale (1 to 5) (<http://core.ecu.edu/psyc/wuenschk/StatHelp/Likert.htm>) and designed to ask questions in two major categories: Beliefs About Science and Interest in Science ([peer.tamu.edu](http://peer.tamu.edu)). The Likert scale and table of questions can be seen in Tables D.1 and D.2.

In each year, students were given the survey at the beginning of the school year to complete in early September and then given the same survey during the last week of the school year, typically in late April or early May. These results will herein be referred to as ‘Pre’ and ‘Post’ results respectively. Each survey was assigned a unique ID code to maintain anonymity. Undergraduates in the NSF GK-12 PEER program completed data entry. Data were queried for only student surveys from Mr. Cunha’s class in 2008 and 2009. Quality control and assurance included the following considerations and database adjustments:

- Removal of survey values outside the Likert scale, such as 50 or 4.1,
- Removal of responses that did not include both ‘Pre’ and ‘Post’ responses for each unique ID,
- Coded database for gender (0 = male, 1 = female), year (2008, 2009), test (0 = Pre, 1 = Post), and
- Removal of incomplete or missing values in any category.

To determine the impact of oceanography lessons introduced throughout the year, only a select number of questions (highlighted red in table D.2) were selected for

statistical analysis. The questions provided a baseline for determining if inquiry-based learning examples, such as providing new types of laboratory equipment specific to oceanographic studies or computer interactions with scientists, affect student learning. Additionally, questions were selected to construct a baseline about gender-specific attitudes toward science and furthering secondary science education, such as pursuing college. The responses for the selected questions were analyzed separately by year, except for Q.28, in which responses for years were combined and only gender was analyzed independently. For this question, it was not important to consider the years independently, because I was only interested in the gender response.

Sequences of unbalanced ANOVA tests were conducted in MATLAB to investigate the responses by year, gender, and test (pre or post). The test design, mean, variance, F-statistic, and p-value for each test were recorded. Interactive effects among the three variables listed were also included for a subset of the questions (table D.2) selected for analysis. Interactive effects determine if the response variable is dependent on the interactions of two or more explanatory variables combined (e.g. Does the score of the student depend on gender and year –  $score*gender*year$ ).

#### *D.6.4 NSF GK-12 PEER Survey Results*

The results will be discussed as each appears in Table D.3 to D.6. The first question, Q.14, gages student attitudes towards using computers in the classroom. There was a significant difference between 2008 and 2009 (p-value < 0.01) pre and post responses. The results were likely attributed to improvement of the programs between

Year 2008 and 2009. Results also indicate that students enjoy using computers for scientific experiments and activities, meaning that computer technologies can be useful in the science classroom for improving student interest in science.

In comparing gender versus test score pre and post survey scores, there was no significant difference between male and female scores. The post-test scores for males were lower than the pre-test scores indicating a potential gender bias, although this was not explored further. The standard deviation of these scores show responses were still in the 'Agree' and 'Strongly Agree' range. Additional three-way ANOVA tests supported these results, indicating a significant change ( $p\text{-value} < 0.05$ ) between score responses in 2008 and 2009, but no relationship between gender, score, or interactions between *gender\*score\*year* ( $p\text{-value} > 0.05$ ).

The next question, Q.16, assessed student attitude with using science equipment. Results from the two-way ANOVA tests show significance for test scores in 2008 with a one-point Likert scale increase in post response mean ( $p\text{-value} = 0.04$ ) and interaction of *gender\*test* in 2009 ( $p\text{-value} = 0.02$ ). Survey scores in 2009 were not significantly different in Likert rank, with both years ranging from 'Agree' to 'Strongly Agree'. Results indicate students responded positively to using science equipment in the classroom.

The significance of the interaction between gender and test in 2009 shows a gender effect in the classroom. Educational studies on learning emphasize gender effects, which are important for determining the learning styles appropriate in the classroom, the design of inquiry-based activities, and to expose students to the geosciences (Kimmons et

al. 2011; Lewis and Baker 2009). The *gender\*test* interaction in this survey question shows female scores to increase for pre to post survey responses. The increase shifts Likert scale response from 'Agree' to the 'Strongly Agree' level. The variance in the female scores is also smaller than the male post response, which remains at the 'Agree' level. This result may imply that female students could have responded quickly to learning how to use equipment or had greater interest in the types of equipment brought in for the lessons. More so, this result may have a direction relation to having a female resident scientist, who is teaching lessons and guiding students through the lesson rather than the classroom teacher, who was male.

At this grade level, students are starting to mature as independent thinkers and tend to form relationships with teachers. Increased interest was supported by the students' interactions with the female resident scientist. However, at this time, there is not enough evidence in the survey data to confirm a definite conclusion for a gender effect. The mean values and statistical results do show that female and male students have a strong affinity toward using scientific equipment in the classroom and such equipment, including computers. The strong, positive response support including science equipment in oceanographic education and outreach programs.

The next questions (Q.26) evaluated student attitudes toward science by comparing likeness to science compared to their other classes (table D.5). Results showed a decrease in 2008 between male and female responses in survey responses, but the decrease was not significant ( $p\text{-value} > 0.05$ ). Likert scale responses ranged from 'Agree' to 'Uncertain' about science as their favorite class. In 2009, there was a

significant difference ( $p\text{-value} = 0.02$ ) between the pre and post scores. These results imply a positive attitude towards science and that there are differences in student personalities, which is useful to designing educational programs. Programs, such as these, should attempt to integrate the different subject (e.g. mathematics and social studies) with science to appeal the range of student interest.

Responses for Q.28 address the broad application of integrating speciality programs into the curriculum by gaging student interest in college. Survey responses revealed that students are genuinely interested in attending college (table D.6). Even though there were no statistically significant results ( $p\text{-value} < 0.05$ ), the responses were in the ‘Strongly Agree’ range with small variances of  $< 1$  point between gender and in test responses. This emphasizes that exposure to science careers in fields such as oceanography at the middle school level may have an influence on the subjects that students would be interested in learning more about in college.

## **D.7 Conclusions and Future Directions**

The main focus of these outreach programs was to expose land-locked student to the ocean and connect students to the geosciences field. Though specific standard education assessments were not applied with these outreach developments, the quality of reports created by the students and their enthusiastic attitudes while participating in each program demonstrated that these partnerships are valuable in improving geosciences education in K-12 schools.

In addition, results from the NSF GK-12 PEER survey provided information for continuing to develop future education and outreach programs. The main conclusions for development are computers and specialized laboratory equipment impact students' learning. Introducing these technologies can greatly improve motivation for completing coursework and test performance. Introducing specialized equipment not generally accessible in middle school classrooms aids inquiry-based activities.

Another important consideration resulting from the survey analysis was the consideration for developing interdisciplinary components in oceanographic education and outreach programs. Concepts in oceanography, such as fisheries or impacts of oil spills on the economy, are not limited to being taught in science class, but can be integrated to lessons for social sciences and mathematics classes as well. Integrating interdisciplinary programs across many types of classrooms and grade levels will further help introduce oceanography and promote ocean stewardship by educating the public to make informed future decisions about the oceans.

The implementation of the programs in the 5<sup>th</sup> grade classroom provided an example of how a resident scientist, or graduate student, is not necessarily required for the program to be successful. Program implementation and success can be obtained with scientists working with teachers only to review the scientific experiments. Engagement in the classroom with students can be limited to introduction of the scientific problem and cruise objectives with one classroom presentation and a follow-up conclusion presentation after the cruise. Engagement during the *cruise* phase is the simplest interaction in each program, as it does not require additional in-classroom time and can be

done online. Therefore, the programs can be scaled according to the time available for program implementation for both the scientists and teachers.

Partnerships between K-12 classrooms and Universities provide invaluable opportunities to expose younger generations to geosciences. These partnerships expand and improve the resources for teaching geosciences by alleviating pressures teachers are experiencing with state mandates on earth sciences and the inability to find funds to support inquiry-based activities in the classrooms. Combining laboratory science with the Internet provides a means for exposing students to science outside of their classroom and, more importantly allows students to explore the world. Incorporating these types of programs into the state curricula may engage younger generations in environmental stewardship in pursuing science beyond the classroom.

Table D.1 Likert Scale for NSF GK-12 PEER Surveys

<b>Likert Scale</b>	
<i>Score</i>	<i>Scale</i>
1	Strongly Disagree
2	Disagree
3	Uncertain
4	Agree
5	Strongly Agree

Table D.2 NSF GK-12 PEER Survey Questions.

<b>NSF GK-12 PEER Program Student Survey</b>	
<i>Beliefs About Science</i>	
1. I enjoy science class.	
2. I think I could be a good scientist.	
3. I like to find answers to questions by doing experiments.	
4. I get to do experiments in my science class.	
D. Being a scientist would be exciting.	
6. Science is difficult for me.	
7. I like to use the science book to learn science.	
8. Science is useful in everyday life.	
9. Studying hard in science is not cool.	
10. Scientists help make our lives better.	
11. Being a scientist would be boring.	
12. I want to take more science classes.	
<i>Interest in Science</i>	
13. I think science is important only at school.	
<b>14. I like to use computers to learn about science.</b>	
1D. Science tests make me nervous.	
<b>16. I like to use science equipment to study science.</b>	
17. I usually don't try my best in science class.	
18. The things we study in science are not useful to me in daily living.	
19. I like to work in a small group in science class.	
20. Science activities are boring.	
21. Finishing high school is very important to me.	
22. I get better grades than most of my classmates in school.	
23. I always give my best effort on my school homework.	
24. I like being in school.	
2D. My family cares about the grades I get in school.	
<b>26. I like science more than all other subjects in school.</b>	
27. My friends and I compete for the highest test scores in science class.	
<b>28. I will definitely go to college someday.</b>	
<i>Open-Ended Questions</i>	
29. List five words that describe a scientist.	
30. What are three things scientists do when they are doing science?	
31. Do you think you could become a scientist? Why?	

*\*Questions in red indicate selected questions analyzed in Section D.4*


Table D.3 ANOVA Results for NSF GK-12 PEER Survey Question 14.

Q14. I like to use computers to learn about science.				PRE		POST		ANOVA RESULTS		
2008	YEAR			Mean	Variance	Mean	Variance	F-Statistic	p-value	Design
	Mean	Variance								
GENDER	Male	4.27	0.89	4.24	0.99	4.29	0.81	0.32	0.57	Gender
	Female	4.18	0.67	4.19	0.32	4.16	1.06	0.06	0.8	Gender*Test

Q14. I like to use computers to learn about science.				PRE		POST		ANOVA RESULTS		
2009	YEAR			Mean	Variance	Mean	Variance	F-Statistic	p-value	Design
	Mean	Variance								
GENDER	Male	4.57	0.39	4.77	0.24	4.37	0.48	0.43	0.51	Gender
	Female	4.48	0.86	4.55	0.35	4.41	1.4	0.84	0.36	Gender*Test

Table D.3 Continued

Q14. I like to use computers to learn about science.				PRE		POST		ANOVA RESULTS		
		YEAR		<i>Mean</i>	<i>Variance</i>	<i>Mean</i>	<i>Variance</i>	<i>F-Statistic</i>	<i>p-value</i>	<i>Design</i>
		<i>Mean</i>	<i>Variance</i>							
YEAR	2008	4.23	0.8	4.22	0.72	4.68	0.29	1.43	0.23	<i>Test</i>
	2009	4.54 	0.57	4.24	0.89	4.39	0.81	2.26	0.13	<i>Year*Test</i>



Q14. I like to use computers to learn about science.				PRE		POST		ANOVA RESULTS		
		GENDER		<i>Mean</i>	<i>Variance</i>	<i>Mean</i>	<i>Variance</i>	<i>F-Statistic</i>	<i>p-value</i>	<i>Design</i>
		<i>Mean</i>	<i>Variance</i>							
GENDER	Male	4.41	0.68	4.49	0.71	4.33	0.65	0.69	0.41	<i>Gender</i>
	Female	4.32	0.77	4.35	0.36	4.28	1.2	0.14	0.71	<i>Gender*Test</i>

Table D.4 ANOVA Results for NSF GK-12 PEER Survey Question 16.

Q16. I like to use science equipment...				PRE		POST		ANOVA RESULTS		
2008		GENDER		Mean	Variance	Mean	Variance	F-Statistic	p-value	Design
		Mean	Variance	4.18	0.76	4.47 ↑	0.59	4.15	0.04	Test
GENDER	Male	4.39	0.86	4.27	0.95	4.51	0.76	1.42	0.24	Gender
	Female	4.22	0.41	4.04	0.44	4.4	0.33	0.12	0.74	Gender*Test

Q16. I like to use science equipment...				PRE		POST		ANOVA RESULTS		
2009		GENDER		Mean	Variance	Mean	Variance	F-Statistic	p-value	Design
		Mean	Variance	4.37	0.52	4.39	0.53	0.02	0.9	Test
GENDER	Male	4.37	0.47	4.49	0.32	4.26 ↓	0.61	0.01	0.91	Gender
	Female	4.39	0.61	4.18	0.82	4.59 ↑	0.35	5.39	0.02	Gender*Test

Table D.5 ANOVA Results for NSF GK-12 PEER Survey Question 26.

Q26. I like science ...				PRE		POST		ANOVA RESULTS		
2008		GENDER		Mean	Variance	Mean	Variance	F-Statistic	p-value	Design
		Mean	Variance	3.42	1.36	3.28	1.23	0.56	0.46	Test
GENDER	Male	3.5	1.34	3.6	1.27	3.15 	1.42	3.56	0.06	Gender
	Female	3.12	1.15	3.4	1.43	3.08 	0.91	0.12	0.73	Gender*Test


Q26. I like science ...				PRE		POST		ANOVA RESULTS		
2009		GENDER		Mean	Variance	Mean	Variance	F-Statistic	p-value	Design
		Mean	Variance	3.73	1.42	3.18 	1.48	5.53	0.02	Test
GENDER	Male	3.49	1.57	3.79	1.56	3.18	1.42	0.11	0.74	Gender
	Female	3.4	1.47	3.62	1.25	3.19	1.66	0.16	0.69	Gender*Test

Table D.6 ANOVA Results for NSF GK-12 PEER Survey Question 28.

<b>Q.28 I will definitely go to college someday.</b>				<b>PRE</b>		<b>POST</b>		<b>ANOVA RESULTS</b>		
		<b>GENDER</b>		<i>Mean</i>	<i>Variance</i>	<i>Mean</i>	<i>Variance</i>	<i>F-Statistic</i>	<i>p-value</i>	<i>Design</i>
		<i>Mean</i>	<i>Variance</i>	4.64	0.6	4.62	0.67	0.02	0.88	<i>Test</i>
<b>GENDER</b>	<i>Male</i>	4.62	0.73	4.66	0.68	4.59	0.8	0.03	0.86	<i>Gender</i>
	<i>Female</i>	4.65	0.47	4.62	0.49	4.68	0.48	0.23	0.63	<i>Gender*Test</i>

**APPENDIX E**

**THIS APPENDIX HAS BEEN SUBMITTED AS A SUPPLEMENTARY  
DOCUMENT**